Polymorphism in Precipitation Processes

Polymorphism in Precipitation Processes

Proefschrift

ter verkrijging van de graad van doctor
aan de Technische Universiteit Delft,
op gezag van de Rector Magnificus prof.dr ir J.T. Fokema
voorzitter van het College van Promoties,
in het openbaar te verdedigen op dinsdag 11 oktober 2005 om 15.30 uur

door

Cornelis Petrus Marcus ROELANDS

scheikundig ingenieur
geboren te 's-Hertogenbosch

Dit proefschrift is goedgekeurd door de promotor:

Prof. dr ir P.J. Jansens

Toegevoegd promotor: Dr ir H.J.M. Kramer

Samenstelling promotiecommissie:

Rector Magnificus,	voorzitter
Prof. dr ir P.J. Jansens,	Technische Universiteit Delft, promotor
Dr ir H.J.M. Kramer,	Technische Universiteit Delft, toegevoegd promotor
Prof. Dr-Ing. M. Kind,	Universität Karlsruhe, Duitsland
Prof. dr ir L.A.M. van der Wielen	Technische Universiteit Delft
Prof. dr H.J. Heeres	Rijks Universiteit Groningen
Dr ir J. Derksen	Technische Universiteit Delft
Dr R.M. Geertman	Organon, Oss
Prof. dr ir G.J. Witkamp	Technische Universiteit Delft, reservelid

Dr ir J.H. ter Horst en dr ir H.J.M. Kramer hebben als begeleiders in belangrijke mate aan de totstandkoming van dit proefschrift bijgedragen.

The research presented in this thesis was financially supported by NWO, Akzo Nobel, Bayer, BASF, DSM.

Cover design: Prilly Haroen (SEM picture created by Paul Durville)

ISBN 90-9019815-6

Printed by Febodruk BV, Enschede.

Voor Marloes,
Ruben en Veerle

Table of contents

Summary

Polymorphism in precipitation processes

Mark Roelands

Polymorphic compounds can precipitate in more than one crystal lattice having different properties. At a certain pressure and temperature only one of these structures is thermodynamically stable while the other structures are metastable. The formation of metastable phases may be kinetically favoured, usually followed by transformation into a more stable phase. This was noticed over a century ago when Ostwald formulated his rule of stages.

Apart from metastable crystalline phases a metastable amorphous phase may be observed, as is often the case for ionic compounds. For molecular compounds such amorphous phases are rarely reported, while sometimes a liquid-liquid separation is encountered, resulting in the formation of two liquid phases that are metastable with respect to the crystalline phase.

Precipitation processes offer the opportunity to create very high driving forces and hence the formation of less stable phases may be promoted. The high supersaturation ratio results in rapid primary nucleation according to either a homogeneous or a heterogeneous mechanism. Nucleation is a strongly non-linear function of the supersaturation ratio and of the interfacial energy. Therefore, by varying these parameters the formation of the different polymorphs may be manipulated. An introduction to nucleation and to polymorphism during precipitation is provided in **Chapter 1**.

In precipitation processes the supersaturation can be created by reaction, by pH-shift or by anti-solvent addition. All of these methods require mixing of fluids. In this project a special set-up is designed and constructed aimed at achieving complete and fast mixing. Part of the design is a computational fluid dynamics study on mixing in a wide-angle Y-mixer as described in **Chapter 2**. From this study it was concluded that mixing in a plain Y-mixer would be insufficiently fast to achieve a homogeneous supersaturation ratio in the outflow tube. To overcome this problem a high-intensity static mixer was successfully implemented in the experimental set-up.

In the mixer-tubular reactor set-up the molecular model compound Ethylene Diamine Tetra Acetic acid (H_4EDTA) is precipitated according to a pH-shift mechanism under steady state conditions. In **Chapter 3** measurements are presented of the stationary nucleation rate as a function of supersaturation. Fitting the measured data following classical nucleation theory indicates that the process proceeds according to a heterogeneous nucleation mechanism.

The experimentally determined nucleation rate for H_4EDTA is compared to rates for other molecular and ionic precipitating compounds, described in a number of studies. Commonly employed experimental methods are discussed in **Chapter 4**. From the experimentally determined nucleation rates the probable mechanism, homogeneous or heterogeneous, is derived and compared to the nucleation mechanism that could be expected theoretically. Although for some compounds theoretically homogeneous nucleation is achievable, evidence of such a mechanism is only found for two ionic compounds. For the other studies a heterogeneous mechanism is more likely. Reasons why experimental measurement of homogeneous nucleation from solution is rarely observed are given.

The formation of polymorphs is studied for the anti-solvent precipitation of L-Histidine. In **Chapter 5** is described how the polymorphic fraction of the metastable form B could be increased by raising the supersaturation and the ethanol volume fraction. In a process model the competitive nucleation and growth rates are manipulated to simulate the experimental findings. Varying the relative interfacial energy and relative step free energy proved to be effective to bring experiments and simulation into agreement.

The formation of another polymorphic compound, L-Glutamic acid, is investigated in **Chapter 6**. In a series of pH-shift precipitation experiments the supersaturation ratio is varied and next the effect of post-stirring of the pre-mixed solutions is studied. Evidence is found that in non-stirred solutions a liquid-liquid separation takes place, resulting in the formation of droplets of a highly metastable phase followed by nucleation of the stable beta phase from these droplets. By post-stirring the solution the metastable alpha phase forms directly from the solution, possibly by heterogeneous nucleation from the stirrer surface.

In this thesis precipitation processes are studied that are characterized by the rapid creation of a very high supersaturation ratio by mixing. Under these conditions, rather than the thermodynamically stable phase, a metastable phase may be formed due to a higher nucleation

and growth rate for the metastable phase compared to the stable phase. The metastable phase can be crystalline but also the formation of a metastable liquid appears possible. The formation of a highly metastable liquid phase that rapidly transforms in more stable crystalline phase may be common but often unnoticed.

To direct the precipitation process towards the desired phase the nucleation work of the polymorphs should be varied, aiming for a relatively higher nucleation rate for the desired phase. This may be achieved by varying the supersaturation ratio while another possibility may be manipulation of the interfacial energy, possibly by introducing a heterogeneous surface area (template) that selectively lowers the nucleation work for the desired phase.

Samenvatting

Polymorfie in precipitatie processen

Mark Roelands

Polymorfie is het verschijnsel dat verbindingen kunnen precipiteren in meerdere kristalstructuren die weer verschillende eigenschappen hebben. Slechts één van deze fasen structuren is thermodynamisch stabiel terwijl de andere structuren metastabiel zijn. De vorming van de metastabiele fase kan echter kinetisch voordeliger zijn. Deze wordt gewoonlijk gevolgd door een transformatie naar de stabielere fase. Dit verschijnsel is meer dan een eeuw geleden opgetekend door Ostwald toen hij zijn stappenregel formuleerde.

Naast metastabiele kristallijne fasen worden ook wel metastabiele amorfe fasen waargenomen, in het bijzonder voor verbindingen opgebouwd uit ionen (zouten). Voor moleculaire verbindingen worden amorfe fasen echter zelden gerapporteerd. Wel wordt soms ontmenging waargenomen waarbij twee vloeistoffasen ontstaan die weer metastabiel zijn ten opzichte van de kristallijne fase.

Precipitatie-processen bieden de mogelijkheid om een zeer hoge drijvende kracht te creëren onder welke condities de vorming van metastabiele fasen wordt begunstigd. De hoge oververzadiging resulteert in zeer snelle primaire kiemvorming volgens een homogeen dan wel heterogeen mechanisme. Kiemvorming als proces wordt gekenmerkt door een sterk niet-lineaire afhankelijkheid van de oververzadiging en van de oppervlaktespanning. Door deze parameters te variëren kan de vorming van verschillende polymorfen mogelijk worden gemanipuleerd. De verschijnselen kiemvorming en polymorfie tijdens precipitatie-processen worden ingeleid in **Hoofdstuk 1**.

De oververzadiging voor precipitatie-processen kan worden gecreëerd door middel van een chemische reactie, pH verschuiving of door een anti-solvent toe te voegen. Voor alledrie de methodes is menging van vloeistoffen vereist. Voor dit project is een speciale opstelling ontworpen en gebouwd met als doel het bereiken van zeer snelle volledige menging. Als onderdeel van het ontwerp is een computational fluid dynamics studie uitgevoerd van de menging in een Y-menger met een brede inlaathoek. Deze studie wordt beschreven in **Hoofdstuk 2.** Een

van de belangrijkste conclusies van deze studie was dat de menging in de Y-menger onvoldoende snel zou verlopen om een homogene oververzadiging in de uitstroombuis te creëren. Om dit probleem te ondervangen, is daarom met succes een statische menger ingebouwd in de uitstroombuis, resulterend in intensieve menging.

De opstelling bestaande uit een menger-buisreactor is vervolgens gebruikt om de moleculare verbinding Ethylene Diamine Tetra Azijnzuur (H_4EDTA) onder steady-state condities te precipiteren door het aanzuren van een oplossing in water van het natrium-zout van deze verbinding. In **Hoofdstuk 3** worden metingen gepresenteerd van de stationaire kiemvormingssnelheid als functie van de oververzadiging. Het toetsen van de metingen aan de klassieke kiemvormingstheorie leverde sterke aanwijzingen op dat het proces verloopt volgens een heterogeen kiemvormingsmechanisme.

Vervolgens is de proefondervindelijk bepaalde kiemvormingssnelheid voor H_4EDTA vergeleken met in de literatuur beschreven metingen aan een aantal zouten en moleculaire verbindingen. In **Hoofdstuk 4** worden de toegepaste experimentele technieken bediscussieerd. De experimenteel bepaalde kiemvormingssnelheden worden gebruikt om het vermoedelijke mechanisme (homogeen of heterogeen) af te leiden en deze worden vergeleken met het mechanisme dat verwacht mag worden op grond van de theorie. Ofschoon voor sommige verbindingen in theorie een homogeen kiemvormingsmechanisme mogelijk is, wordt het bewijs voor zo'n mechanisme slechts gevonden voor twee zouten. Voor de andere metingen is een heterogeen kiemvormingsmechanisme waarschijnlijker. Het hoofdstuk wordt afgesloten met een aantal verklaringen waarom een homogeen kiemvormingsmechanisme zelden experimenteel wordt waargenomen.

De vorming van polymorfe kristallen tijdens anti-solvent precipitatie van L-Histidine wordt beschreven in **Hoofdstuk 5**. Het aandeel van de metastabiele polymorfe fase B in de gevormde kristallen kan worden verhoogd door de oververzadiging en de volumefractie ethanol in het oplosmiddelmengsel te verhogen. Om de experimentele resultaten te verklaren, zijn in een procesmodel de kiemvormings- en groei snelheden van de verschillende polymorfen gemanipuleerd. Overeenstemming tussen simulaties en experimentele resultaten kan worden verkregen door relatieve oppervlaktespanning te variëren.

In **Hoofdstuk 6** wordt de vorming onderzocht van de polymorfen van een andere verbinding: L-Glutaminezuur. Deze verbinding wordt geprecipiteerd door het aanzuren van een oplossing in water van het natrium-zout waarbij de oververzadiging wordt gevarieerd. In een

vervolgstap wordt het effect van naroeren van de voorgemengde oplossingen onderzocht. Er zijn sterke aanwijzingen dat in niet-nageroerde oplossingen ontmenging optreedt, resulterend in de vorming van druppels van een zeer metastabiele fase. Deze druppels transformeren vervolgens naar de stabiele kristallijne beta fase. Wanneer wel nageroerd wordt, kiemt de metastabiele kristallijne alfa fase rechtstreeks vanuit de oplossing, mogelijk vanaf het oppervlak van de roerder volgens een heterogeen kiemvormingsmechanisme.

De precipitatie-processen die worden beschreven in dit proefschrift worden gekenmerkt door de vorming van een zeer hoge overzadiging door snelle menging. Onder deze omstandigheden is het veelal niet de thermodynamisch stabiele fase maar de metastabiele fase die het snelst kiemt en groeit. De metastabiele fase kan kristallijn zijn maar ook een vloeibare fase lijkt mogelijk. Het is niet ondenkbaar dat de vorming van zeer metastabiele druppels die snel overgaan naar een meer stabiele kristallijne fase vaker voorkomt maar zelden wordt opgemerkt.

Om tijdens precipitatie de gewenste polymorfe fase te vormen, dient de kiemvormingsarbeid gemanipuleerd te worden met als doel een hogere kiemvormingssnelheid voor de gewenste polymorf. Dit kan mogelijk bereikt worden door de oververzadiging te variëren. Een andere mogelijke stuurparameter is de oppervlaktespanning. Door een heterogeen kiemoppervlak (‘template’) te introduceren kan mogelijk de kiemvormingsarbeid selectief worden verlaagd voor de gewenste fase.

Chapter 1

Introduction to polymorphism in precipitation processes

Polymorphism is the phenomenon that molecules of a compound are able to form more than one crystal structure. These structures possess different properties that are of considerable interest to industry, for example, the solubility and hence bio-availability of pharmaceuticals. Only one of the polymorphic structures is thermodynamically stable but the formation of a metastable structure may be kinetically favoured eventually followed by transformation to the stable structure. To relieve the high supersaturation that is generally created in precipitation processes molecules may follow different polymorphic pathways for nucleation and growth. Apart from the formation of a metastable crystalline phase evidence exists that also a highly metastable liquid-liquid separation may occur. Control over the formation of polymorphs therefore requires control over their relative nucleation rates. Guidelines are presented to achieve control over the polymorphic pathways in precipitation processes.

1.1 Incentive for research on polymorphism in precipitation

The phenomenon of a compound being able to crystallize in more than one crystal lattice is called polymorphism. Polymorphs are found among many molecular and ionic compounds. For example, the two polymorphs of the amino acid L-Glutamic Acid are shown in figure 1.1. For the ionic compound Barium Fluoride two polymorphs are known that are shown in figure 1.2 (Kolar 1986).
The significance of polymorphism lies in the fact that polymorphs possess different product properties because of their difference in crystal structures. Examples of properties that can be structure-dependent are solubility and dissolution rate, density, stability, melting point, colour and morphology. Often these properties are related to the performance of the compound in its application. The bioavailability of pharmaceutical compounds, colour shade of pigments and stability of explosives illustrate this.

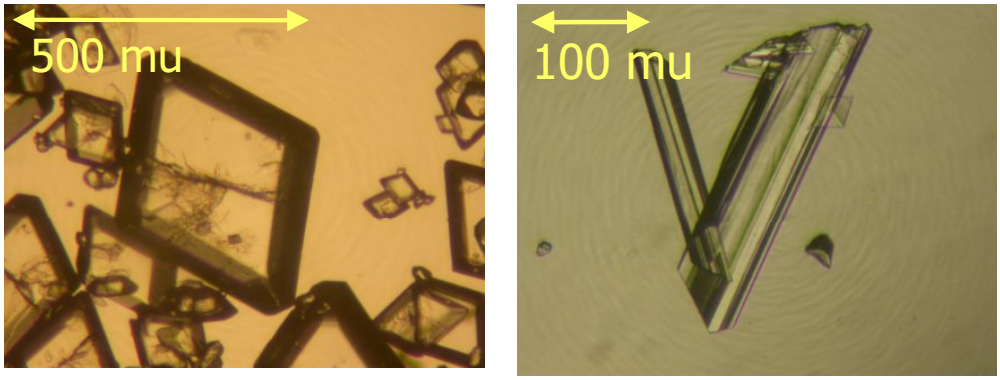

Figure 1.1 Polymorphs of L-Glutamic Acid. Left: prismatic crystal of the metastable alpha phase, right: platelet-shaped crystal of the stable beta phase.

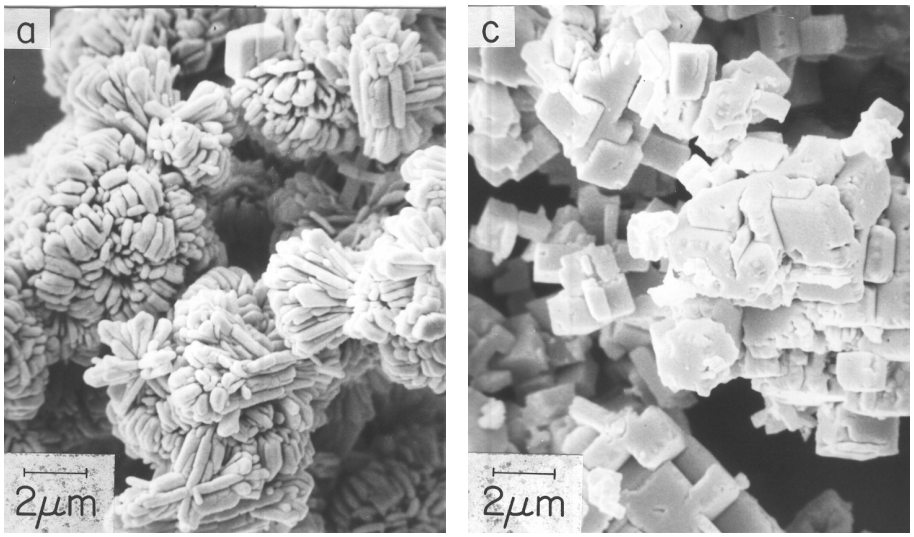

Figure 1.2 Polymorphs of Barium Fluoride. Left: stacked crystal of the metastable phase II, right: cubic crystal of stable phase I (Kolar 1986).

The protease inhibitor Ritonavir had been on the market since 1996 in a formulation containing the compound in ethanol/water based solution. Two years after market introduction a more stable polymorph of this compound appeared that was previously unknown. The solubility of the more stable form in the hydroalcoholic formulation was more than a factor four lower than that of the less stable form. Because the compound was not bioavailable in the solid-state, this phenomenon

forced the company to withdraw their product from the market (Bauer 2001). In manufacturing the metastable poymorph was obtained again by application of a seeding procedure (Chemburkar 2000).

Colour polymorphs present particularly nice examples. Copper-Phtalocyanine can form at least five polymorphs: α, β, γ, δ, ε (Löbbert 2000). The metastable polymorph α and the stable polymorph β are used as blue pigments and are produced in large quantities. The colour of the polymorphs varies from reddish blue (α) to greenish blue (β). Hao and Iqbal (1997) give the example of a red pigment where the β-phase in paint formulation is more yellowish compared to the α-phase. Another example of colour polymorphs is the compound appropriately called ROY after the steadily increasing number of Red, Orange and Yellow coloured polymorphs that were prepared by Stephenson et al (1995), by Stowell et al (1998) and by Yu (2000a, 2000b, 2002). Small differences in the conformation of the ROY-molecule in the crystal lattice are considered to be responsible for the difference in colour. Figure 1.3 shows six different colour polymorphs of ROY.

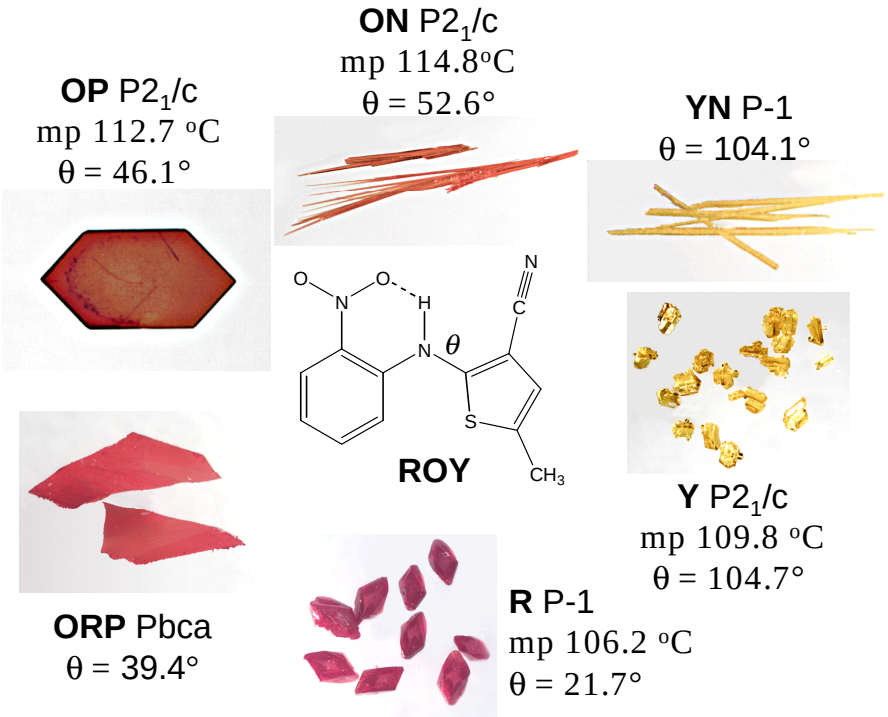

Figure 1.3 Example of colour polymorphs: polymorphs of ROY (Yu 2000).

McCrone (2000, 2001) presented a true war-story regarding the detonation-stability of HMX-polymorphs. HMX was formed as a ~10 % reaction by-product during production of RDX explosives during World War II. When cooling crystallization of the solution proceeded too fast, the less stable polymorph II of HMX formed, while during slow cooling the more stable polymorph I was obtained. Detonation stability was tested by hitting a crystal with a hammer. If this crystal detonated rapidly the less stable polymorph had been formed.

In many chemical, pharmaceutical and food processing industries polymorphism is encountered in precipitation processes. This type of processes is commonly employed to separate a desired product molecule from its solution in the form of crystals with a high yield and preferably a reasonable purity. The term precipitation is reserved for fast crystallization processes, taking place at a high level of supersaturation generally created by mixing. The two mainly employed processes are either reactive crystallization by mixing two solutions of well-soluble compounds that react into a product with a very low solubility or anti-solvent crystallization by mixing of a solution of a well-soluble compound with an anti-solvent, thus lowering the solubility in the mixed solvent. An example of the first type of process is the precipitation of L-Glutamic Acid by mixing of a solution containing Sodium L-Glutamate with diluted Sulfuric Acid. An example of the second type of process is the precipitation of L-Histidine from an aqueous solution with ethanol as anti-solvent.

In industrial practice the selective formation of only one polymorph during precipitation is desired because of the structure-specific properties of the polymorphs. Control over the formation of the desired polymorphic structure requires understanding of the precipitation mechanism. For all precipitation processes the main product properties, structure, morphology and crystal size distribution, are determined by the primary processes nucleation and growth and by the secondary processes agglomeration, attrition, Ostwald ripening and transformation.

In the polymorph control strategy the nucleation process plays an important role because at this stage the foundation for the crystal lattice is laid. Nucleation proceeds as a strongly non-linear function of supersaturation according to either a primary homogeneous or a primary heterogeneous mechanism. Control over polymorph formation therefore starts with control over the nucleation mechanism, and this requires the creation of a homogeneous level of supersaturation by instantaneous mixing. Furthermore, growth of the crystals and subsequent processes like transformation of one polymorph into another have to be taken into account.

1.2 Precipitation kinetics

1.2.1 Driving force for crystallization

The driving force for a crystallization process is the difference in Gibbs free energy between the actual condition of the system and its equilibrium condition. For a one-component crystal in liquid solution under isothermal and isobaric conditions the supersaturation $\Delta\mu$ is defined as $\Delta\mu=\mu_s-\mu_c$ with μ_s chemical potential of a molecule in solution and μ_c chemical potential of a molecule in the bulk of the crystal phase. When $\Delta\mu>0$ the system is supersaturated and nucleation and growth of the crystals is possible. The driving force can be rewritten as $\Delta\mu=kT\ln S$ with $k=1.38\cdot10^{-23}$ [J K^{-1}] the Boltzmann constant and T [K] the absolute temperature.

In this equation the supersaturation ratio for a molecular compound denoted by $S_{a,i}=a_{0,i}/a_{e,i}$ [-] with $a_{0,i}$ actual activity in solution and $a_{e,i}$ equilibrium activity in solution. The activity for a compound in solution denoted by i is defined as $a_i=\gamma_i x_i$ with γ_i activity coefficient [-] and x_i molar fraction [-]. It is common practice to use the concentration c_i [mol m^{-3}] instead of x_i. A further simplification is to use the concentration based supersaturation ratio $S_{c,i}=c_{0,i}/c_{e,i}$ [-] with $c_{0,i}$ actual concentration in solution and $c_{e,i}$ equilibrium concentration in solution. This is allowed for well soluble salts where $\gamma_{0,i}\approx\gamma_{e,i}$. For ionic compounds, like $BaSO_4$, the definition for the supersaturation ratio is the product of the activities or concentrations of the ions i^+ an j^- according to $S_{a,ij}=(a_{0,i}^{+}\ a_{0,j}^{-})/(a_{0,i}^{+}a_{e,j}^{-})$ or $S_{c,ij}=(c_{0,i}^{+}c_{0,j}^{-})/(c_{e,i}^{+}c_{e,j}^{-})$. For a more elaborate derivation is referred to Kashchiev and Van Rosmalen (2003).

For poorly soluble salts the activity based supersaturation ratio $S_{a,i}$ should be used. For a solution at equilibrium the activity coefficient γ_i can be calculated as a function of the ionic strength according to Debye-Hückel, Bromley, Electrolyte-NRTL (Chen), Pitzer, or Helgeson (Bromley 1973, Rafal et al 1994, Pitzer 1991). For the calculation of the activity coefficient under non-equilibrium conditions the use of these equations may cause large errors because the parameters in these equations are generally determined under equilibrium conditions.

1.2.2 Nucleation theory

In this study the classical nucleation theory (CNT) was followed as described and adapted by Kashchiev (1999). Solute molecules collide with each other at a certain frequency due to Brownian motion. After the

creation of a driving force for precipitation, these collisions lead with certain efficiency to the formation of clusters of solute molecules. This is a dynamic process and molecules will attach and detach successively. The driving force for the creation of clusters is the decrease in chemical potential by molecules leaving the solution while forming a cluster due to the decrease in Gibbs free energy between the two bulk phases. However, a penalty has to be paid for creating an interface between the cluster and its surrounding solution.

The work of formation of an n-sized cluster W [J] can be approximated by:

$$W(n) = -nkT \ln S + \gamma A_c(n) \tag{1.1}$$

with interfacial energy γ[J m^{-2}] and cluster surface area $A_c(n)$ [m^2]. The work of formation of a cluster will at first increase with increasing number of molecules until a maximum is reached. At this point the flux of solute molecules attaching to the cluster f^* equals the flux of molecules detaching from the cluster g^*. From this size up, the cluster size will increase with every molecule that attaches and the work of formation will decrease with n. The cluster with the maximum work of formation also called nucleation work W^* is called the nucleus n^*.

For spherical clusters the surface area $A_c(n)=(36\pi v_0^2)^{1/3} n^{2/3}$ with $v_0=M/\rho_c N_a$ [m^3] the molecular volume with M [kg mol^{-1}] molecular weight, ρ_c [kg m^{-3}] crystal density and N_a [mol^{-1}] Avogadro's number. The interfacial energy γ [J m^{-2}] is a weighed average over all crystal faces.

Nielsen and Söhnel (1971) and Söhnel (1982, 1983) observed a linear relationship between the experimentally measured interfacial energy γ and the logarithm of the bulk solubility c_e for 58 compounds. Bennema and Söhnel (1990) confirmed this relationship theoretically. Mersmann (1990) derived the following relationship between the interfacial energy and the natural logarithm of the bulk solubility of the compound c_e [mol m^{-3}]:

$$\gamma = \beta kT \frac{1}{v_0^{2/3}} \ln \frac{1}{v_0 c_e} \tag{1.2}$$

For spherical clusters the shape factor β=0.514.

For spheres the nucleus size n^* and the nucleation work W^* can be derived from the condition $dW/dn=0$ for $n=n^*$ using equation (1.1):

$$n^* = \frac{32\pi v_0^{\,2}\gamma^3}{3(kT)^3 \ln^3 S}$$
$$W^* = \frac{16\pi v_0^{\,2}\gamma^3}{3(kT)^2 \ln^2 S} = \tfrac{1}{2} n^* kT \ln S \qquad (1.3)$$

Nucleus size and nucleation work depend on two main parameters: the externally controlled supersaturation and the interfacial energy.

The CNT assumes that the density and the interfacial energy of the spherical cluster are equal to the ρ and γ for macroscopically large crystals. For small clusters this seems unlikely. Furthermore, simulations by Ten Wolde and Frenkel (1999) suggest that the shape of small nuclei may be irregular or platelet shaped. However, independent of their morphology, nuclei are assumed to have the same crystal lattice as bulk crystals of the compound because ρ and γ are the same. The implication of this assumption is that the crystal lattice is fixed at the beginning of the precipitation process.

1.2.3 Homogeneous nucleation

The stationary nucleation rate J [m^{-3} s^{-1}] is defined as the time-independent frequency of transformation of the nucleus into the smallest supernucleus according to the following equation:

$$J = zf^*C^* \qquad (1.4)$$

With z Zeldovich factor [-], f^* attachment frequency [s^{-1}] and C^* concentration of nuclei [m^{-3}]. The Zeldovich factor corrects for the fact that not all supenuclei grow out to macroscopically large sizes. The attachment frequency is the product of the incoming flux j^* of monomers to the nucleus surface and the nucleus area A^*. For homogeneous nucleation (HON) the concentration of nuclei can be approximated with a Boltzmann-type of formula $C^*=C_0\exp(-W^*/kT)$. The concentration of nucleation sites C_0 is equal to the molecular volume $1/v_0$ because the nucleus can be formed anywhere in the supersaturated solution.

Now the homogeneous nucleation rate J can be rewritten according to:

$$J = zf^* C_0 \exp\left(-\frac{W^*}{kT}\right) = A\exp\left(-\frac{B}{\ln^2 S}\right) = A\exp\left(-\frac{16\pi v_0^2\gamma^3}{3(kT)^3 \ln^2 S}\right) \qquad (1.5)$$

In this equation A [m^{-3} s^{-1}] is a kinetic parameter and B [-] the parameter in the exponent. The kinetic parameter A can be estimated from the attachment frequency f^* for two mechanisms: for volume-diffusion control and for interface-transfer control. It can be expressed for spheres as a function of bulk properties: interfacial energy γ, molecular volume ν_0, diffusion coefficient D [m^{-2} s^{-1}] and bulk concentration c_0 [m^{-3}]:

$$A_D = \left(\frac{kT}{\nu_0^{\,2}\gamma}\right)^{1/2} Dc_0 \ln S$$
$$A_I = \left(\frac{4\pi}{3\nu_0}\right)^{1/3} \left(\frac{\gamma}{kT}\right)^{1/2} Dc_0 \qquad (1.6)$$

A slightly different equation is given by Mersmann (2001):

$$J = (3/2)\left(\frac{\gamma}{kT}\right)^{1/2} \nu_0 D c_0^{\,7/3} \exp\left(-\frac{16\pi\nu_0^{\,2}\gamma^3}{3(kT)^3 \ln^2 S}\right) \qquad (1.7)$$

In this equation the pre-exponential kinetic parameter is a function of the actual concentration to the power 7/3. For an evaluation of the use of these equations see Kashchiev and Van Rosmalen (2003).

1.2.4 Heterogeneous nucleation

For nucleation in the presence of a heterogeneous surface area two additional interfaces are created apart from the interface between the cluster and the solution: one between the heterogeneous surface and the solution and one between the heterogeneous surface and the cluster. The interplay between the different interfacial energies results in an effective interfacial energy γ_{eff}. For 3D heterogeneous nucleation the effective interfacial energy $\gamma_{eff}<\gamma$ so W^* for HEN can be substantially smaller than W^* for HON. In the presence of such a foreign substrate heterogeneous nucleation will start at a lower supersaturation level compared to homogeneous nucleation in a clean solution. In practice even in filtered or distilled solvents a large number of heterogeneous particles are present. In figure 1.4 3D HON, 3D HEN and 2D HEN are schematically represented.

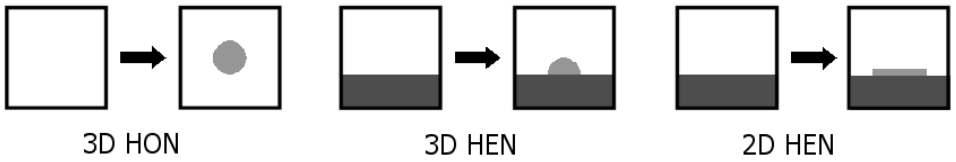

Figure 1.4 Schematic representation of 3D homogeneous nucleation, 3D heterogeneous nucleation and 2D heterogeneous nucleation.

Furthermore, C_0 the concentration of nucleation sites is proportional to the concentration of heterogeneous particles $C_{0,HEN}$ that is much smaller than $1/v_0$ for HON and therefore the kinetic parameter for HEN A_{HEN} is much smaller than the kinetic parameter for HON A_{HON}. Typically A_{HEN}~10^{15}-10^{25} [m^{-3} s^{-1}] and A_{HON}~10^{35} [m^{-3} s^{-1}].

Schubert and Mersmann (1996) studied the homogeneous and heterogeneous nucleation rate of Barium Sulphate by offering defined quantities of heterogeneous particles of SiO_2, TiO_2 and ZrO_2. For high supersaturation the HON-rate exceeded the HEN-rate. For low supersaturation the HEN-rate increased proportionally with the increasing concentration of heterogeneous particles.

1.2.5 Prediction of the nucleation mechanism

Mersmann (1996, 2001) developed a way of plotting the rates for HON and for HEN as a function of the dimensionless driving force $\Delta c/c_c=(c_0-c_e)/c_c$ [-] and of the dimensionless solubility c_e/c_c [-] with $c_c=1/v_0$ [m^{-3}] the 'concentration' of the compound in the crystal. For a compound with known solubility and defined experimental supersaturation ratio, the position in the plot predicts whether nucleation will proceed according to a homogeneous or a heterogeneous mechanism.

Using the dimensionless variables the supersaturation ratio in equation (1.5) for the nucleation rate J then becomes $S=(\Delta c/c_{c+}c_e/c_c)/(c_e/c_c)$ for molecular compounds and $S=[(\Delta c/c_{c+}c_e/c_c)/(c_e/c_c)]^2$ for ionic compounds. In the expression for the interfacial energy (1.2) the logarithmic term can be expressed as $1/(c_e v_0)=(c_e/c_c)$. For HON the expression for the actual concentration c_0 in the pre-exponential kinetic parameter A in equation (1.6) becomes $c_0=(\Delta c/c_{c+}c_e/c_c)c_c$.

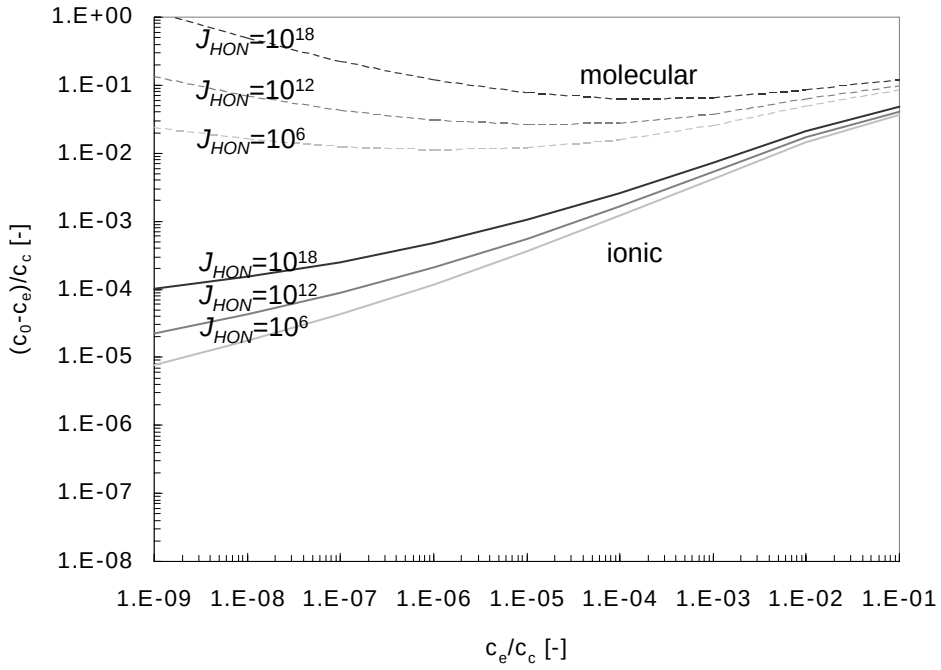

Figure 1.5 Homogeneous nucleation rates for J_{HON} =10^6, 10^{12} and 10^{18} [m^{-3} s^{-1}] for molecular compounds and for ionic compounds as a function of dimensionless driving force and dimensionless solubility.

In figure 1.5 the homogeneous nucleation J_{HON}=10^6, 10^{12} and 10^{18} [m^{-3} s^{-1}] are plotted for molecular compounds and for ionic compounds as a function of dimensionless driving force and dimensionless solubility. The different position of these lines for molecular compounds versus ionic compounds is caused by higher values for S for the ionic compound following from the concentration product in the definition $S_{c,ij}=(c_{0,i}^{+}c_{0,j}^{-})/(c_{e,i}^{+}c_{e,j}^{-})$ for ionic compounds compared to the definition $S_{c,i}=c_{0,i}/c_{e,i}$ for molecular compounds.

In figure 1.6 for molecular compounds HON-rates are compared to HEN-rates. For heterogeneous nucleation an arbitrarily chosen value of the pre-exponential parameter $A_{HEN} \sim 10^{20}$ [m^{-3} s^{-1}] is used while a reduction of the interfacial energy $\gamma_{eff}=0.4\gamma$, 0.5γ and 0.6γ seems reasonable. It can be observed that for HEN compared to HON a lower driving force is needed to achieve an equal nucleation rate of $1 \cdot 10^{12}$ [m^{-3} s^{-1}] but when the driving force is sufficiently increased HON will outnumber HEN.

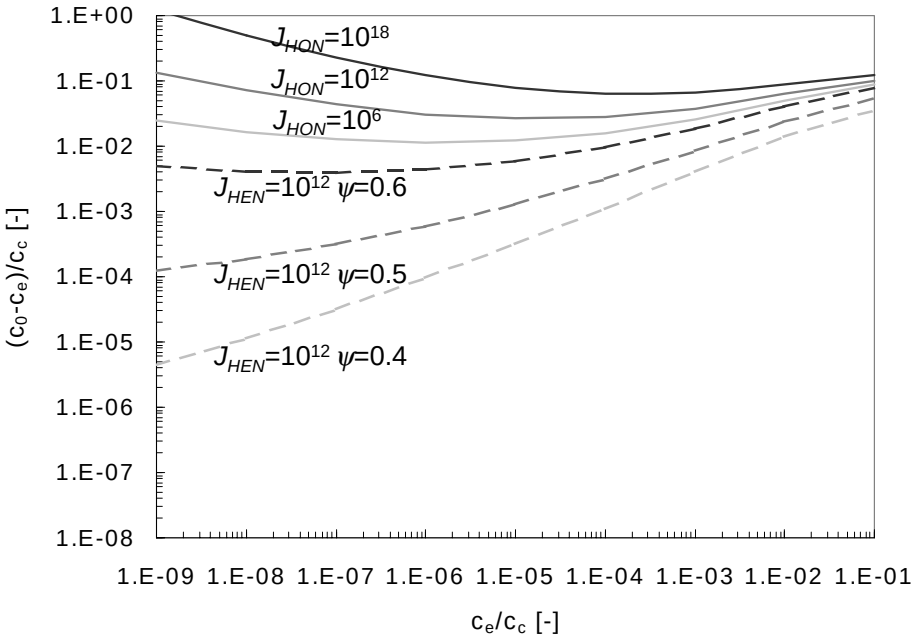

Figure 1.6 Homogeneous nucleation rates J_{HON} $=10^6$, 10^{12} and 10^{18} [m^{-3} s^{-1}] and heterogeneous nucleation rates J_{HEN} $=10^{12}$ [m^{-3} s^{-1}] for molecular compounds as a function of dimensionless driving force and dimensionless solubility. For HEN $A_{HEN}=10^{20}$ [m^{-3} s^{-1}] and $\gamma_{eff}=0.4\gamma$, 0.5γ and 0.6γ [J m^{-2}].

1.2.6 Two-step nucleation mechanism

In a number of studies on the crystallization of proteins the phenomenon is described that after creation of supersaturation a liquid-liquid separation takes place. An overview of theoretical and experimental developments was given by Schüth (2001b). Ten Wolde and Frenkel (1997) did numerical simulations of homogeneous crystal nucleation for globular proteins. A mechanism of crystal nucleation whereby the density fluctuation precedes the structure fluctuation was suggested.

Haas and Drenth (1999) and Drenth (2005) prepared supersaturated solutions of the protein Lysozyme by addition of a sodium chloride solution. Nucleation could take place according to two mechanisms. When the solution temperature was above the critical temperature for liquid-liquid separation, nucleation would take place according to the classical nucleation theory by impingement of single molecules. When the solution temperature was below the critical temperature for liquid-liquid separation the formation of metastable droplets was observed. The presence of a metastable droplet reduced the induction time for Lysozyme crystals. Crystallization was assumed to take place from the droplets by rearrangement of the molecules.

Galkin and Vekilov (2000) and Vekilov (2004) measured nucleation rates for Lysozyme crystals above the critical temperature for liquid-liquid separation. Near this temperature the formation of metastable droplets of the concentrated phase was kinetically favoured over the nucleation of thermodynamically more stable crystals. Nucleation of the crystal lattice was considered to be a structure fluctuation, superposed on density fluctuation. The high viscosity of the liquid of the metastable droplet, however, could arrest rearrangement of the crystals into a crystal lattice.

Biscans (1993) observed for Lysozyme a decrease of the induction time with increasing supersaturation while the precipitate changed from tetragonal crystals to an amorphous precipitate.

Knezic et al (2004) measured induction times for the formation of Lysozyme crystals in electrodynamically levitated droplets. From their measurements the authors conclude that there were two random processes that occurred inside a drop: fluctuation of the size of the clusters as a function of supersaturation with a Gaussian distribution and the randomly distributed time needed for the clusters to rearrange themselves into a crystalline nucleus.

For relatively small molecules the mechanism of liquid-liquid separation of the supersaturated solution is referred to as oiling-out. Two liquid phases are formed, one rich in solute and one poor. These phases are assumed to be thermodynamically metastable with respect to the formation of a crystalline phase from the supersaturated solution but their formation is kinetically favoured. The liquid phases co-exist in equilibrium with each other, so the chemical potential and hence the supersaturation of the solute would be equal in each phase. However, the interfacial energy calculated as a function of bulk the solubility according to equation (1.2) would be lower for the concentrated phase

and hence the nucleation work for the formation of a crystal from this phase.

Lafferrère et al (2003, 2004a, 2004b) studied cooling crystallization of a polymorphic pharmaceutical compound in a 15 w% solution in 3:2 volume ratio Ethanol/water mixed solvent. In quiescent medium the formation of droplets was observed when the solution separated into two coexisting liquid phases of different composition and density. Using turbidity measurements the cloud point and the clarify point were detected. Furthermore, when the composition of the liquid phases was measured, a solute rich phase and a solute poor phase were observed.

Bonnett et al (2003) carried out cooling crystallization of a 50 w% solution of a molecular compound in a water/Methanol mixed solvent (15/85 w%). Initially a liquid-liquid separation was observed with droplets increasing in size by coalescence, followed by crystallization. The crystals grew at the expense of the droplets via the continuous phase by a solution mediated mechanism. The composition of the two liquid phases was measured and these were found to consist of a solute rich phase of 70 w% and of a solute poor phase of 7 w%.

Kim et al (2003) described the anti-solvent crystallization of a polymorphic pharmaceutical compound 'A' from an approximately 25 w% solution in Ethyl-acetate with Cyclohexane as anti-solvent. When the anti-solvent was rapidly added in a 1:5 volume ratio Ethyl-acetate/Cyclohexane oiling-out was observed followed by crystallization into a product with poor properties. To overcome this problem a more polar solvent system was applied: Ethanol as the solvent and water as the anti-solvent. Slow addition was applied of the anti-solvent in a 2:1 volume ratio of Ethanol/water while in an early stage of the addition the solution was seeded with the desired polymorph.

Grön and Roberts (2001) supercooled an 80 w% aqueous solution of Citric acid and observed an increase in turbidity while at the same time the concentration in solution, monitored by ATR-IR spectroscopy, did not change. This was considered an indication that oiling-out took place before actual crystallization of Citric acid.

Chattopadhyay et al (2005) studied the cooling crystallization of a 3.6 M aqueous solution of Glycine by SAXS. Their results indicated that Glycine molecules existed as dimers in the supersaturated solution. A two-step nucleation mechanism was proposed consisting of the formation of liquid like clusters in the supersaturated solution followed by reorganization of the liquid-like clusters.

The experiments where liquid-liquid separation was observed have in common that this phenomenon took place in highly supersaturated solutions. For small molecules these solutions were concentrated as well. When a driving force is imposed on such a system the arrangement of solute molecules into a crystal lattice may be taking place more slowly compared to demixing resulting in the formation of two liquid phases. These phases are thermodynamically metastable compared to the formation of a solid phase from solution. Re-arrangement of the solute molecules into a crystalline phase within droplets of the metastable solute-rich phase can be arrested by the high viscosity in this phase.

1.2.7 Crystal growth rates

The crystal growth process is generally divided into two separate steps that can be assumed to take place in series (Nielsen 1984, Kashchiev 2001, Mersmann 2001):

a. Diffusion of the molecules from the bulk solution towards the crystal surface through the diffusion boundary layer.
b. Surface integration of the molecule into the crystal lattice. This step involves surface diffusion and partial or total desolvation before integration into the lattice.

When growth is limited by diffusion from the bulk, the growth rate can be expressed as a linear function of the difference between bulk solution concentration and equilibrium concentration according to:

$$G_D = k_d \nu_0 (c_0 - c_e) \tag{1.8}$$

With: k_d [m s^{-1}] mass transfer coefficient and ν_0 [m^3] the molecular volume. For mass transfer to suspended crystals in agitated solution the mass transfer coefficient can be related to the Sherwood number:

$$Sh = \frac{k_d L}{D} = 2 + 0.66 Re^{1/2} Sc^{1/3} \tag{1.9}$$

With: L [m] crystal diameter, $Re = \rho u_s L / \eta$ the Reynolds number and $Sc = \eta / \rho D$ the Schmidt number, with u_s [m s^{-1}] particle slip velocity, ρ [kg m^{-3}] solution density and η [kg m^{-1} s^{-1}] solution viscosity. For very small particles (0.1 to 10 μm) the suspended phase tends to move with no slip along with the circulating fluid. In this case the effect of convective transport can be neglected and $Sh = k_d L / D = 2$.

For surface integration three types of crystal surfaces can be observed as a function of increasing supersaturation. First, for a molecularly very smooth crystal surface the attachment of new molecules is very difficult. Roughness is provided by the presence of step and kink sites. Steps at the crystal face are provided by screw-dislocations where spiral growth takes place. The growth rate perpendicular to the surface G [m s^{-1}] can be expressed as:

$$G_{BCF} = \frac{d_0 v_s}{\beta R^*} = \left(\frac{a_0 D c_e kT}{\beta d_0 \kappa} \right) (S-1) \ln S \tag{1.10}$$

With: d_0 [m] the molecular diameter, $v_s = a_0 D(c_0 - c_e)$ [m s^{-1}] velocity of step propagation, a_0 [m^2] the area of a molecule in the monolayer, β=19 [-] a numerical factor, $R^* = a_0 \kappa / \Delta\mu$ [m] radius of a 2D nucleus, with κ [J m^{-2}] the step free energy which is related to the interfacial energy by $\kappa = k_s d_0 \gamma$ with k_s [-] a shape factor. For low supersaturation where $\ln S \approx S-1$, the growth rate equation becomes quadratic $G_{BCF} \sim (S-1)^2$.

Secondly, when the surface is molecularly smooth, the rate of growth is limited by the creation of new steps at the surface. A mechanism to create these steps is 2D nucleation followed by layer growth. The nucleation mechanism can be mononuclear or polynuclear. For the mononuclear mechanism the growth rate perpendicular to the surface can be described as a function of supersaturation according to:

$$G_{MN} = d_0 A_{cr} J_{2D} = d_0 A_{cr} A_0 S \exp\left(-\frac{\pi a_0 \kappa^2}{(kT)^2 \ln S} \right) \tag{1.11}$$

In this equation A_{cr} [m^2] is the area of the crystal face and J_{2D} [m^{-2} s^{-1}] is the equation for the 2D nucleation rate of a compound on its own substrate under the assumption of disk-shaped nuclei with A_0 [m^{-3} s^{-1}] the pre-exponential kinetic parameter.

For the polynuclear mechanism the growth rate perpendicular to the surface can be described as a function of the 2D nucleation rate J_{2D} of a compound on its own substrate under the assumption of disk-shaped nuclei with lateral velocity v_s [m s^{-1}]:

$$G_{PN} = d_0 \left(\tfrac{1}{3} \pi v_s^{\,2} J_{2D} \right)^{1/3} = d_0 \left(\tfrac{1}{3} \pi a_0 D c_e \right)^{2/3} A_0^{\,1/3} (S-1)^{2/3} S^{1/3} \exp\left(\frac{\pi a_0 \kappa^2}{3(kT)^2 \ln S} \right) \tag{1.12}$$

Finally, when a crystal surface is rough on molecular scale, growth is continuous. For molecular compounds the surface becomes rough when the step free energy κ becomes equal to zero at the roughening temperature T_R. When a solute molecule arrives at the surface it is immediately integrated. For rough growth crystal faces tend to become rounded. For salts kinetic roughening is observed when the activation energy required for the formation of a two-dimensional critical nucleus becomes of the order kT. During kinetic roughening the step free energy is still non-zero.

For rough growth of a surface the growth rate depends on the difference between the flux of growth units from the bulk that impinges on a growth position in the crystal surface f_s [s^{-1}] and the flux of growth units that leaves the surface g_s [s^{-1}]:

$$G_{RG} = d_0\left(f_s - g_s\right) = a_0 D c_e \left(S - 1\right) \tag{1.13}$$

Rough growth is a linear function of the supersaturation ratio.

1.2.8 Secondary processes

The crystals that are formed by nucleation and growth can become subject to a number of secondary processes:

a. Aggregation / agglomeration: the particles collide with each other and form clusters, in the case of aggregation they are bound by physical forces, while in the case of agglomeration the crystals are chemically cemented together by growth of a crystalline bridge. For agglomeration to take place it is necessary that the solution is supersaturated. A subdivision is made between perikinetic agglomeration due to Brownian motion of the particles and orthokinetic agglomeration where the particles agglomerate due to shear induced by laminar or turbulent flow.
b. Attrition: crystals that have grown into a sufficiently large size (approximately 50 mu) may collide with each other or with the equipment (stirrers). During such a collision fragments may break off from the larger crystals and in a supersaturated solution these fragments may grow out and act as a source of nuclei. This process is referred to as secondary nucleation in contrast to primary nucleation that happens from a clear solution.
c. Ostwald-ripening: small particles, in the size range below 1 micron, have a relatively large surface area compared to larger crystals and because of their strongly curved surface they possess a larger solubility. In a suspension of particles with a

wide size distribution the smaller particles will re-dissolve while the larger particles will grow. The effect of size on particle solubility can be shown using the Gibbs-Thomson equation:

$$\ln \frac{c(r)}{c_e} = \frac{\beta v_0 \gamma}{rkT} \tag{1.14}$$

With: $c(r)$ [mol m^{-3}] the solubility of a particle with particle radius r [m] and β a surface shape factor.

For Barium Sulphate Judat and Kind (2004) observed the aggregation of primary particles with a size of 10 nm into aggregates of 100 nm followed by re-alignment of these particles, resulting in large secondary particles with an apparent single crystal XRPD pattern. Pujol et al (2004) observed a similar ordered aggregation process for primary particles of Cobalt Oxalate Dihydrate.

During the precipitation of Barium Sulphate Peukert and Schwarzer (2005) added positively charged Barium ions in excess to the reacting solutions. At the surface of the primary particles the Barium ions adsorbed and a repulsive double-layer formed that stabilized the primary particles while preventing them from aggregation.

Dispersing agents such as surfactants have been frequently applied to inhibit agglomeration. Johnson and Prud'homme (2003a, 2003b) applied block-copolymers with a hydrophobic and a hydrophilic part during the precipitation of β-Carotene to stabilize the suspension of primary particles by completely covering the particles with a shell of block-copolymers.

Jongen et al (2000) precipitated Copper Oxalate in the presence of a polymeric additive. Attachment of the surfactant to specific surfaces of the primary particles prevented these from randomly aggregating but allowed aggregation of the particles with the same orientation.

1.2.9 Competitive rates controlling product properties

The properties of a precipitated product depend on the competition between the rates of nucleation, of growth and of agglomeration. The main property that is affected by these processes is the particle size distribution but also the morphology may change. In a batch precipitation process, after the creation of the driving force, nucleation, growth and agglomeration take place simultaneously. These processes have in common that they are all a function of the supersaturation ratio that decreases rapidly due to growth of the crystals. This results first in

a decrease of the nucleation rate because this is a very strong function of supersaturation, followed by a decrease in the growth rate. Because of the decrease in supersaturation the growth mechanism may change as well, for example from 2D nucleation to spiral growth.

Because of the initial high nucleation rate many small crystals are formed. Agglomeration of these small crystals continues until there is no supersaturation left to bridge the crystals together while attrition of the larger crystals continues without supersaturation. Ostwald ripening of the smaller crystals starts when the overall concentration of the bulk drops below their solubility.

1.2.10 Creation of supersaturation by mixing

Up till now it was assumed that the driving force could be created instantaneously, that mixing was indefinitely fast. To create a driving force in precipitation generally two types of mixing processes are applied:

a. Mixing of solutions of compounds that react with each other to form a new compound with a very low solubility.
b. Mixing of a solution of the compound that is to be precipitated with an anti-solvent. The anti-solvent is completely miscible with the solvent but the solubility of the solute in the mixed solvent is drastically lowered.

Baldyga and Bourne (1999) developed a model to describe turbulent mixing consisting of sequential steps, starting at the initial segregation scale of the flows with macro-mixing to distribute the solutions, followed by meso-mixing reducing the scale of segregation down to the Kolmogorov-scale, and further by micro-mixing in the dissipating eddies towards the Bachelor-scale. Finally, at the latter scale mixing proceeds towards molecular level by diffusion. The model is illustrated by figure 1.7. In their model the characteristic times for mixing scale inversely with mixing intensity.

In precipitation processes the mixing intensity is often insufficient to create complete homogenisation of the solutions before the crystals start to nucleate. When mixing of the solutions goes slowly compared to nucleation and growth, the supersaturation level will vary in space and in time within the equipment. This was for example demonstrated by Hollander (2002) who modelled the distribution of supersaturation in time and space during agglomeration of Calcium Oxalate crystals in a stirred vessel using a Large Eddy Simulation technique. Because the nucleation rate is a strongly non-linear function of the supersaturation level large variations exist and to a lesser extent this applies to growth of the nuclei and to agglomeration of the crystals as well. Because of

these reasons, control over the particle size distribution in a stirred tank reactor is notoriously difficult to achieve and the effect of changes in reactant concentrations, in equipment geometry, in flow rates are hard to predict.

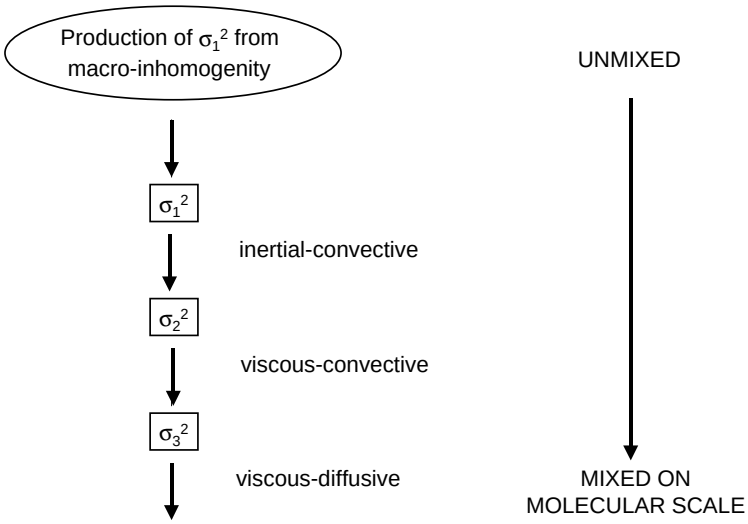

Figure 1.7 Schematic representation of macro-, meso- and micromixing (Baldyga and Bourne 1999).

In tubular reactors under turbulent flow conditions more control over the mixing conditions can be achieved. In continuous precipitation processes the supersaturation will decrease with the length of the tube. In such devices the average particle size was observed to decrease with increasing supersaturation ratio by O'Hern (1964) for the reactive crystallization of Barium Sulphate and by Rivera and Randolph (1978) for the continuous anti-solvent precipitation of PentaErytritol Tetra Nitrate. The decrease in mean particle size was attributed to an increased nucleation rate, resulting in a larger number of particles.

Studies in mixer-tube reactor geometries on the effect of the mixing intensity on the precipitation kinetics were carried out by Tosun (1988) and by Schwarzer and Peukert (2002) for Barium Sulphate and by Manth and Mignon (1996) for Strontium Sulphate. Generally, a decrease in particle size with increasing mixing intensity was observed. It is assumed that with increasing mixing intensity, a relatively larger volume is well mixed, resulting in more nuclei. Haberkorn et al (2003) precipitated Alumina and the organic pigment Quinacridone in a Y-mixer

geometry. Slices of the outflow jet were chopped within milliseconds after mixing and cryogenically quenched. TEM observation revealed that at micro level the solutions were segregated while at the interfaces precipitation had started.

Kim et al (2002) reported the precipitation of a pigment in a miniaturized laminar flow reactor with diameter of 0.1 mm. A product with a narrower distribution was obtained compared to the conventional batch process. The average size of the pigment particles decreased from 600 to 100 nm while the colour performance improved. Continuous operation for hours without scaling was reported.

Computational Fluid Dynamics is a commonly used tool to simulate mixing of flows by solving the Reynolds-averaged Navier-Stokes equations (Baldyga and Bourne 1999). In combination with population balance modelling this technique was used to study precipitation of inorganic compounds. For this type of calculations the geometry is divided into a grids consisting of many small cells. For each cell the momentum, continuity, mass and population balances have to be solved.

Seckler et al (1995) and Van Leeuwen (1998) simulated precipitation of respectively amorphous Calcium Phosphate and Barium Sulphate for steady-state flow conditions in a flat rectangular reactor while Wei and Garside (1997) carried out a CFD study for the precipitation of Barium Sulphate in a concentric tubular reactor geometry. Over each cell an averaged value for the supersaturation with an averaged fluctuation was assumed. Choi et al (2005) simulated the precipitation of the molecular compound HMX from solution in acetone with water as anti-solvent. Over each cell an averaged value for the supersaturation with an averaged fluctuation was assumed.

In precipitation models the nucleation rate is calculated as a strongly non-ideal function of supersaturation. When CFD is applied to simulate precipitation values for supersaturation are used that are both volume-averaged over the grid cell and time-averaged. If the grid resolution is sufficiently refined, the fluids may in reality not have mixed completely within a cell volume. The precipitation rate that is calculated over the whole grid cell volume may be overestimated because precipitation is taking place only in part of the cell. Furthermore, because of the time-averaged supersaturation and time-averaged fluctuation the overall nucleation rate may be underestimated compared to reality where large variations of the supersaturation with time may result in strongly varying nucleation rates. To overcome this problem a sub-grid scale model for mixing within the cell can be used.

Baldyga and Orchiuch (2001) and Marchisio and Fox (2002) introduced probability density functions (PDF) to account for the fluctuating supersaturation for each cell. Following this approach the precipitation of Barium Sulphate in a concentric tubular mixer-reactor geometry was modelled.

To simulate precipitation of Barium Sulphate in a tee-mixer Schwarzer (2005) applied a DNS model to solve the whole flow field in combination with a micro-mixing model to account for diffusion towards molecular scale. Lagrangian particle tracking was applied to obtain the specific power input of volume elements along their path through the mixer. Local values for specific power input and for concentration were introduced in a population balance model to calculate the precipitation kinetics.

It is evident that in all cases CFD simulation of precipitation requires reliable kinetic rate equations because of the strongly non-linear relationship between nucleation rate and supersaturation ratio. Nucleation rate measurements are generally carried out in experimental set-ups consisting of a mixing-tee and a tubular reactor and therefore the kinetics may be 'pollluted' by mixing effects.

1.2.11 Nucleation rate measurements

It would be beneficial to both scientists and engineers if precipitation kinetics were better known. Especially the number of experimental studies on nucleation rates is small because it is difficult to measure at high supersaturation level under well-mixed conditions. In the book by the working party on crystallization of the EFCE on nucleation and growth measurements Garside, Mersmann and Nyvlt (2002) described a method to measure the nucleation rate in precipitating systems. Schüth (2001a) recommended the use of tubular reactors to study nucleation rates for precipitating compounds. These experiments are notoriously difficult because they rely on a number of requirements that are not easily fulfilled:

a. Reactant solutions are completely pre-mixed before nucleation starts.
b. Over the length of the tube only nucleation and growth take place.
c. Over the length of the tube the decrease of the supersaturation is known.
d. All particles present are individually counted, including the smallest.

e. Secondary processes like agglomeration can be compensated for in the particle number measurement.

Most studies concerned inorganic compounds such as Barium Sulphate (Nielsen 1961, 1964, 1967, 1969, Mohanty 1988, Angerhöfer 1994, Schubert 1996) and Alumina (Eble 2000) while a few studies regarding organic compounds such as Benzoic Acid (Stahl 2001), Salicylic Acid (Blandin 2001), L-Asparagine Monohydrate and Lovostatin (Mahajan and Kirwan 1993, 1994) could be found. In these studies typically the increase in the crystal number concentration as a function of the supersaturation was measured. From a plot of this nucleation rate versus supersaturation according to equation (1.5), the kinetic pre-exponential parameter A and the parameter in the exponent B were estimated while from the latter parameter a value for the interfacial energy was calculated. In some studies (Nielsen, Angerhoefer, Schubert, Mahajan and Kirwan) the slope of the plot of the nucleation rate ($\ln J$ versus $1/\ln^2 S$) increased abruptly with increasing supersaturation S. It was concluded that the slope change was caused by a shift in the dominant nucleation mechanism from heterogeneous to homogeneous.

Furthermore, in precipitation studies it is common practice to measure the induction time t_{ind} [s] defined as the time elapsed between the moment that supersaturation is created and the moment that crystals are observed (Verdoes et al 1992). The induction time depends not only on the nucleation rate but also on the growth rate of the crystals, on the applied observation technique and on its detection limit. For stationary nucleation of spherical crystals using a technique based on volume change, e.g. desupersaturation, the induction time is given by the following equation:

$$t_{ind} = \left(\frac{3(1+d)\alpha_v}{4\pi J G^d} \right)^{1/(1+d)} = \left(\frac{3\alpha_v}{\pi J G^3} \right)^{1/4} \qquad (1.15)$$

With $d=3$ the dimensionality of growth and α_v the detectable volume fraction of the new crystalline phase formed in the solution.
Several researchers observed experimental induction times shorter than 100 ms using different techniques. Nielsen (1967, 1969) film-recorded the turbidity in a continuous-flow cell to detect the induction time for the precipitation of Barium Sulphate. Schüth (2001a) applied a stopped-flow cell and used Synchrotron XRD to detect the same compound. Rieger (1997) abruptly quenched the precipitation of Calcium Carbonate and Boehmite (γ-Alumina) and used Small Angle X-ray Scattering (SAXS) to detect whether crystals had formed. Judat and Kind (2004) used the same fast quench in combination with TEM for Barium Sulphate.

Mahajan and Kirwan (1993, 1994) used a rapid quench followed by microscopic detection for two organic compounds.

1.3 Polymorphism

1.3.1 Definition

A large number of compounds show polymorphism, the ability to crystallize in more than one crystal structure. Haleblian and McCrone (1969) classified a system as polymorphic when two polymorphs, that are different in crystal structure, are identical in the liquid and vapour states. Furthermore, the solid phases possess different melting points. Polymorphism is found among many organic and inorganic compounds. For example, for the amino acid Glycine three polymorphs are known (Towler 2004). Another example is the inorganic compound Cobalt Hydroxide for which Gaunand (2002) reported two polymorphs with different colours, a blue coloured metastable amorphous phase and a pink coloured stable phase. The racemic compound Nimodipine poses another example (Grunenberg et al 1995, Grunenberg and Wirges 1999). The compound has two modifications: form II crystallizes as a conglomerate (both enantiomers in one crystal lattice) and is stable between absolute zero and approximately 90°C while form I crystallizes as a racemic compound (each crystal structure consists of one only enantiomer) and is the stable form for higher temperature.

Many compounds crystallize in a lattice containing solvent molecules. These structures are called solvates and hydrates in the case that the solvent is water. This phenomenon is sometimes referred to as pseudo-polymorphism. Magnesium Sulphate is an example of a compound able to form hydrates including a metastable one: $.1H_2O$, $.7H_2O$(I), $.7H_2O$(II) and $.12H_2O$ (Himawan 2005). Furthermore, for Calcium Carbonate are reported: an amorphous phase, three polymorphs (Vaterite, Calcite and Aragonite) and two hydrates ($.6H_2O$ and $.1H_2O$) (Brecevic 1989, 1993, Kralj and Brecevic 1995, Kabasci 1996, Sawada 1998).

Recently books by Bernstein (2001), by Byrn et al (1999) and by Brittain (1999) were published on the subject of polymorphism and reviews by Bernstein et al (1999) and by Caira (1998). An older review was written by Haleblian and by McCrone (1969). McCrone (1965) stated that for every compound polymorphs could be found, provided sufficient effort was spend on preparation and analysis. Rodriguez-Spong et al (2004) and Rodriguez-Hornedo and Murphy (1999) reviewed the kinetics of polymorphism. These studies concerned mostly polymorphism from a pharmaceutical perspective because both

polymorphism and the formation of solvates are especially widespread among pharmaceutical compounds. Henck et al (1995) found that over 50% of the compounds in the European Pharmacopeia show polymorphism and/or solvate formation. Identification and analysis of polymorphs was subject of reviews by Bugay (2001), Giron (1995) and Threllfall (1995).

The significance of polymorphism lies in the fact that polymorphs possess different product properties because they crystallize in different structures. Examples of properties that are structure-dependent are melting point, solubility and dissolution rate, density, stability, colour and morphology. Often these properties are related to the performance of the compound in its application. Control over desired performance properties requires therefore control over the formation of the desired polymorphic structure. Many parameters influence the formation of polymorphs: temperature, pressure, supersaturation, solvent, seeding, additives. Understanding of the precipitation mechanism is required with special attention to the primary processes of nucleation and growth and the secondary process of transformation.

1.3.2 Thermodynamics of polymorphism

In polymorphic systems compounds are able to crystallize in a number of structures that have different lattice free energies. The structure with the lowest free energy at a given pressure and temperature is the stable polymorph. All other structures that have higher free energies are metastable polymorphs. In an energy versus temperature (E/T) diagram, Haleblian and McCrone (1969), Burger and Ramberger (1979a) and Grünenberg et al (1995) depicted the change of the Gibbs free energy $G=H-TS$ as a function of temperature T, with H and S the change of respectively the enthalpy and the entropy of the system. At absolute zero the entropy term disappears and the Gibbs free energy becomes equal to the enthalpy term. At this point the most stable polymorph has the lowest enthalpy.

In figure 1.8 the Gibbs free energies and enthalpies are shown for a dimorphic system with numerals I and II indicating the polymorphs and subscript 'm' the liquid state. The points where the Gibbs free energy lines of the two polymorphs cross the Gibbs free energy line of the liquid state indicate the melting points mp_I and mp_{II}. In this figure form I is the high-melting polymorph. The point where the lines of the Gibbs free energies of the two polymorphs cross each other is the transition point $tp_{I/II}$. This point lies below the melting points, which is characteristic for an enantiotropic system. In this figure form II is the stable form below the transition point. Above the transition point form I is the stable from. When a sample of polymorph II is heated, for example in a Differential Scanning Calorimeter (DSC), it may transform up from the transition point into form I.

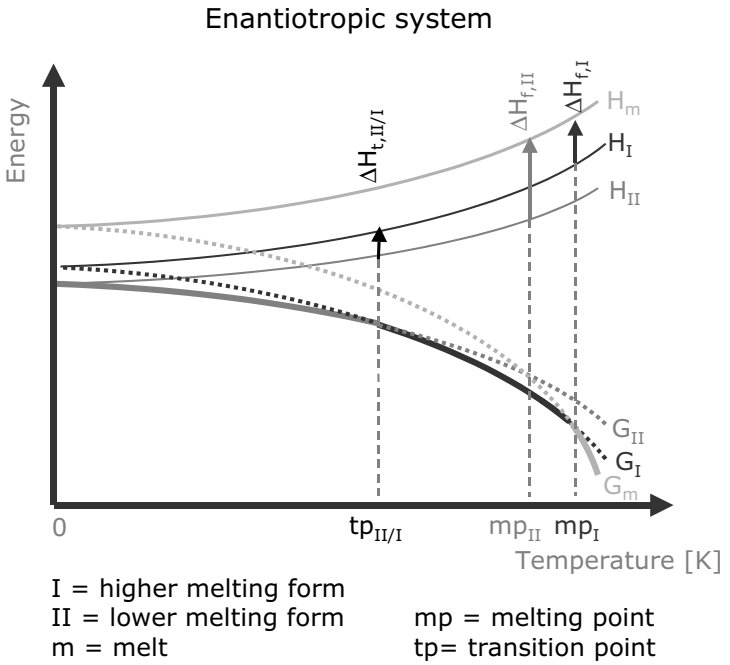

Figure 1.8 E/T diagram for an enantiotropic system.

In figure 1.9 the E/T diagram is shown for a monotropic system. In this figure the lines for the Gibbs free energies of the two polymorphs do not cross below their melting points. In this figure form I is the stable polymorph over the whole temperature range from absolute zero until its melting point.

The polymorphic forms differ in melting point, heat of fusion, entropy of fusion, density and heat capacity. Burger and Ramberger (1979b) derived a number of rules based on measurement of these properties to construct the E/T diagrams in order to check whether the system is enantiotropic or monotropic. In a Van 't Hoff diagram solubility lines can be plotted as a function of 1/T. Polymorphic forms differ in solubility because this property is directly proportional to the Gibbs free energy. If the lines cross below the melting point the system is enantiotropic.

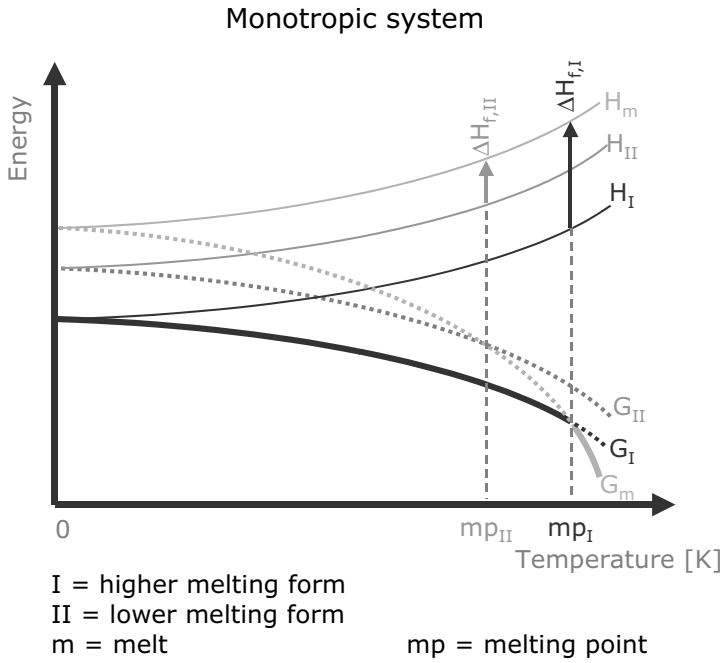

Figure 1.9 E/T diagram for a monotropic system.

1.3.3 Simultaneous formation of polymorphs

When a driving force for crystallization is imposed on a solution of a polymorphic compound, the system tends to minimize its free energy. Theoretically a maximal decrease is achieved by crystallization of the most stable polymorph. However, if a less stable state can be reached faster because its kinetics are faster, the system may crystallize into this less stable polymorph first. Later this less stable polymorph may transform into the more stable one. This phenomenon of formation of the kinetically controlled polymorph over the thermodynamically favored form was noted by Ostwald (1897) in his rule of stages: "when leaving a

metastable state, a given chemical system does not seek out the most stable state, rather the nearest metastable one that can be reached without loss of free energy". Threllfall (2003) and Nyvlt (1995) recently wrote papers on Ostwald's rule of stages. It is noted that Ostwald's rule is based on observation and is not a physical law.

An experimental example of Ostwald's rule is the initial formation of the metastable alpha polymorph of L-Glutamic Acid by cooling crystallization followed by its transformation to the stable beta form as observed by Kitamura (1989), by Black and Davey (1986), by Garti and Zour (1997) and by Cashell (2003a, 2003b). Ono et al (2004a) followed the formation and transformation as a function of time and temperature using an in-situ Raman spectroscopic technique. In a second paper Ono et al (2004b) modelled the transformation using a population balance model.

Bernstein (1999) and Rodriguez-Spong et al (2004) explained the Ostwald's rule of stages by assuming that the work of formation for nuclei of the metastable phase is lower than that for nuclei of the stable phase. In equation (1.6) for spherical nuclei it is assumed that they have the same properties as bulk crystals: solubility, density and interfacial energy. For different polymorphs these properties are different. The work of formation for a stable polymorph I should be larger than the work of formation for a metastable polymorph II, and the following condition has to be fulfilled:

$$\frac{v_{0,I}^2 \gamma_i^3}{\ln^2 S_I} > \frac{v_{0,II}^2 \gamma_{II}^3}{\ln^2 S_{II}} \tag{1.16}$$

Because of the difference in solubility the polymorphs are experiencing a different driving force S. For bulk crystals $S_I > S_{II}$ because $c_{e,I} < c_{e,II}$. In case of a monotropic system the stable form has the highest density, while for enantiotropic systems the stable form can be either denser or less dense than the metastable form, depending on the temperature. When the interfacial energy is estimated according to equation (1.2) as a function of bulk solubility, γ_I is likely to be higher than γ_{II}. The main parameter responsible for a lower work of formation of the metastable polymorph is the interfacial energy γ_{II} that has to be sufficiently lower in order to compensate for the lower S_{II}. The lower interfacial energy for the metastable form reflects that this crystal form has the structure that is closest in energy and arrangement to the molecules in solution.

Ter Horst (2002) expressed competitive nucleation rates as a function of driving force and of the interfacial energy. The ratio of the nucleation

rates $\alpha = J_I/(J_I+J_{II})$ could be varied by varying the ratio of the interfacial energy for low levels of the supersaturation ratio. For very high supersaturation, when the exponential term in equation (1.5) became equal to one, the ratio of the nucleation rates depended on the ratio of the pre-exponential kinetic parameters only. It is noted that the value for A depended on the interfacial energy and molecular volume as well but their value was found to be only slightly different for the polymorphs. This work implicates that it would be possible to change the relative nucleation rates of polymorphs by choosing the appropriate interfacial energy (solvent composition) and supersaturation ratio.

The polymorphic form that is actually obtained may not only depend on competitive nucleation rates but also on competitive growth rates. Gutzow and Toshev (1968) and Cardew and Davey (1982) considered the effect of competing nucleation and growth rates to explain Ostwald's rule of stages. Because of its lower solubility, the supersaturation ratio for the stable polymorph is higher than the supersaturation for the metastable polymorph $S_I > S_{II}$. Analogue to the previously described competitive nucleation rates, this would favour the growth rate of the stable polymorph. Furthermore, in the case of growth by either the spiral mechanism or by the 2D nucleation mechanism, the specific edge energy of the metastable polymorph has to be sufficiently lower than that of the stable polymorph $\kappa_{II} < \kappa_{I,}$ to compensate for the higher driving force that the stable form experiences compared to that of the metastable form.

When the nucleation and growth mechanism are equal, there are indications that when the growth rate of the metastable polymorph is larger than that of the stable polymorph, the nucleation rate of the metastable polymorph is larger than that of the stable polymorph as well. Kitamura and Ishizu (2000) observed for L-Glutamic acid that the growth rate of the metastable alpha was higher than that of the stable beta phase. The measurements were carried out on single crystals in a flowing solution at low supersaturation ratio. Furthermore, the measured growth rate data fitted with a 2D nucleation mechanism.

For the case where two or more polymorphs are obtained in the same experiment Bernstein et al (1999) introduced the term concomitant polymorphs. A possible pathway for concomitant polymorphism is simultaneous nucleation and growth of the polymorphs at comparable rates as described in this paragraph. Alternatively, concomitant polymorphs may be explained by the initial formation of a metastable form, followed by transformation into a more stable form with both processes taking place on the same time-scale.

The driving force for this transformation is the difference in free energy between the different polymorphs. If the difference is small, the metastable form can appear to be the stable one until a more stable polymorph crystallizes. It is not always known beforehand whether a crystalline phase of a compound is the stable polymorph or not. In literature there are a number of examples of structures that were thought to be stable, but later turned out to be metastable when a more stable phase emerged. Woodard and McCrone (1975), Dunitz and Bernstein (1995) and Bernstein and Henck (1998) mentioned several examples of these so called disappearing polymorphs. Among these is Xylitol, considered to be a liquid only until in 1941 or 1942 a phase crystallized with a melting point of 61°C while later a phase with a melting point of 94°C crystallized. Subsequent attempts to prepare the lower melting form were unsuccessful.

During the last few years a number of companies emerged that offer polymorph screening facilities to pharmaceutical companies to discover unknown polymorphs, solvates and salts of new compounds that can be protected by patents. Polymorph screening includes a multitude of crystallization conditions, usually carried out in parallel in a miniaturized set-up. Companies that offer these services include Avantium (Amsterdam, The Netherlands), TransForm (Massachusetts, USA) and SSCI (West-Lafayette, Indiana, USA). Morisette et al (2004) and Gardner et al (2004) wrote review papers on polymorph screening. Examples were given by Peterson et al (2003) who prepared three polymorphs and a trihydrate of Acetaminophen (Paracetamol) while Morisette et al (2003) described three polymorphs, a hydrate and a solvate of Ritonavir. One polymorph and the solvates of this compound were previously unknown. Chyall et al (2002) and Hilden (2003) described a polymorph screening technology by crystallization in capillary space.

1.3.4 Transformation of polymorphs

Transformation of a less stable polymorph into a more stable polymorph takes place either by a solution mediated mechanism or by a solid-solid mechanism. For solution mediated transformation Cardew and Davey (1985, 1986) and Sato (1993) identified two mechanisms that could control the transformation rate: either the dissolution rate of the metastable polymorph is limiting or the growth rate of the stable polymorph. If during transformation the solute concentration remains at the solubility level of the metastable polymorph, the growth of the stable one is limiting. If the solute concentration drops immediately to the solubility level of the stable polymorph the dissolution rate of the

metastable one is limiting. To identify which mechanism prevails the polymorphic composition of the slurry has to be followed in time in combination with the concentration of the solute in the solution.

For example, the solution mediated transformation of the metastable α polymorph of the molecular compound L-Glutamic acid (L-Glu) into the stable β polymorph was studied by Davey and Black (1986), by Kitamura (1989), by Garti and Zour (1997) and by Cashell et al (2003a, 2003b). In all cases the aqueous suspension was stirred in a tank reactor. It was concluded that the slow growth rate of the stable beta form was the limiting step for the transformation. Ono et al (2004) followed the transformation of L-Glu using in-situ Raman spectroscopy following the approach described by Wang et al (2000) for the transformation of the steroid Progesterone.

Ferrari et al (2003) found that the transformation rate of the metastable β polymorph of Glycine to the stable α polymorph in water-ethanol mixed solvent was limited by the slow dissolution rate of the metastable β polymorph. The transformation accelerated by increasing the mixing intensity (when the experimental scale was decreased). It was concluded that increased attrition of the metastable polymorph created additional surface area which facilitated the rate-limiting dissolution process.

In the case of a true solid-solid transition the crystal lattice transforms into a different arrangement, for example when the temperature is raised. A review on this subject was written by Dunitz (1995). Davey et al (1993, 1994) reported the solid-solid transformation of crystals of the metastable polymorph I of Terephtalic Acid when these were heated up. Microscopically a spontaneous change in shape was observed between a temperature of 75 and 100°C. Davey concluded that twinning of the crystals of the metastable phase I of this compound inhibited the solid-solid transformation into the more stable phase II. Another example was given by Arsic et al (2003) who observed microscopically the initial formation of metastable cubes of Cesium Bromide that within seconds to minutes transformed into rough, grainy cubes.

Sometimes a polymorphic transformation may appear to be solid-state but proves to be solution-mediated when studied in detail. For example, Davey et al (1991) and Van Driel et al (1994) studied the transformation of phase III to phase IV of Ammonium Nitrate. Propagation of a transition front consisting of a solution layer throughout a single crystal was observed with the metastable phase III at the dissolving side of this front and the stable phase IV at the growing side. Ito et al (2005)

applied AFM to observe the propagating front during solution mediated transformation of the alpha phase of Glycine into the gamma phase.

Transformation of polymorphs by a HEN mechanism

A transformation process has to start with nucleation of the stable phase. If the nuclei of the stable phase are not formed at the beginning of the (batch) precipitation process, when the supersaturation for nucleation is very high, it has to be assumed that these nuclei form later. When the solute concentration is reduced to the level of solubility of the metastable phase II, the supersaturation for the stable I phase is determined by the solubility difference between the polymorphs $\Delta c = c_{e,II} - c_{e,I}$ with $c_{e,II} > c_{e,I}$. When the supersaturation is small, it seems likely that nuclei of the stable phase form according to a HEN mechanism.

In literature there are a number of indications that the surface of the metastable polymorph may promote the formation of nuclei of the stable polymorph. Nucleation of a more stable phase on the surface of a less stable phase may take place according to an epitaxial mechanism in which close values of the lattice parameters between the solid forms results in oriented growth of the crystals of the newly formed phase or by a strictly heterogeneous mechanism resulting in randomly oriented crystals. In both cases the effective interfacial energy and therefore the supersaturation for nucleation to occur are lowered by the presence of the substrate. Nucleation of a stable phase near or on the surface of the metastable phase may be further promoted by a locally higher solute concentration near the dissolving surface of the metastable phase.

An example of the surface of one polymorph acting as a substrate for oriented growth of another polymorph was given by Stoica (2005a, 2005b) who observed microscopically the epitaxial formation of the stable polymorph of a steroid at the surface of the metastable form. When the solution was supersaturated for both polymorphs simultaneous growth of both polymorphic forms was observed. Boerrigter et al (2002) observed the opposite: the nucleation of the metastable polymorph on the surface of the stable polymorph of the same steroid, followed by solution-mediated transformation of the metastable polymorph propagating through the metastable crystal.

Boistelle and Rinaudo (1981) reported an epitaxial relationship between the anhydrous and the monohydrate phases during a recrystallization study of Diuric Acid from aqueous solution. The new phase grew on the substrate followed by phase transformation of the parent crystal according to a solution mediated mechanism. Rodriguez-Hornedo et al (1992) observed heterogeneous nucleation of the monohydrate phase of

Theophylline on a substrate of anhydrous crystals with the new phase growing epitaxially on the parent crystal.

Sudo et al (1991) described how a supersaturated solution of Cimetidine in Isopropanol was seeded with crystals of either the metastable polymorph A or the stable polymorph B. For a supersaturation ratio S_A<2.0 the phase corresponding to the seed phase grew. However, for high S_A>3.6, the metastable phase A nucleated heterogeneously on the surface of the seeds of phase B and subsequently the phase A crystals were growing.

For L-Glutamic Acid Ferrari and Davey (2004) and Cashell et al (2003a, 2003b) observed the growth of needle-shaped crystals of the stable β polymorph growing from the metastable α polymorph. From molecular simulation Ferrari and Davey concluded that the dimensional fit between the lattices was poor in both cases. Cashell found that the lattice of the stable β polymorph propagated inside prismatic crystals that from the outside appeared to be the metastable α polymorph. It was concluded that β crystals had nucleated in an earlier stage on the surface of α crystals and that these were later overgrown by the faster growing α crystals.

Furthermore, Ferrari and Davey (2004) studied the effect of mixing intensity on the transformation of L-Glutamic acid by scaling down the experiment. The authors concluded that increased attrition of the metastable α polymorph resulted in more α surface area available for nucleation of the stable β polymorph. Interestingly, Cashell et al (2004) found the opposite: stirring a suspension of metastable α crystals inhibited the transformation process because disruption of the α surfaces was believed to prevent nucleation of the β phase.

In the case of 2,6-Dihydroxy Benzoic acid Davey et al (2002) found that increasing the mixing intensity by scaling-down accelerated the transformation rate. The slow nucleation rate of the stable polymorph was thought to be rate limiting. Microscopic images of crystals of the dissolving metastable polymorph showed that the surface was covered with presumably needle-shaped crystals of the stable polymorph. No epitaxially favourable fit between faces of the two polymorphs was found and therefore it was concluded that surface nucleation of the stable polymorph was driven by the higher supersaturation at the dissolving interface. Attrition due to mixing was assumed to be an effective way to distribute these surface nuclei to create additional surface area for growth of the stable polymorph.

From these experiments it may be possible to derive two mechanisms. First, the crystal surface of the metastable polymorph itself may act as a substrate for 3D HEN of the stable polymorph proceeding either epitaxially or 'randomly'. It seems likely that initially the metastable polymorph is neither growing nor dissolving but is in equilibrium with the solution. Secondly, when the crystal of the metastable polymorph is dissolving the concentration of the solute near the surface may be sufficiently high to initiate 3D HEN of the stable polymorph from solution. In both cases, after nucleation of the more stable polymorph, the transformation takes further place according to a solution-mediated mechanism with the stable polymorph growing at the expense of the dissolving metastable polymorph.

Transformation from an amorphous phase

For some compounds initially the formation of an amorphous phase is observed after creation of a supersaturated solution. Interest in amorphous phases follows from their specific properties, for example the solubility of the amorphous phase is larger than that of the crystalline phases (Hancock and Zografi 1997). Commonly reported procedures to prepare amorphous forms include quenching of a melt and quenching of a solution followed by freeze-drying (Yu 2001). When the resulting amorphous form is heated sometimes a solid-state transformation into a new crystalline phase is observed. Examples of such methods are given for the crystallization of polymorphs from the melt of Indomethacin by Andronis and Zografi (2000) and of D-Mannitol and D-Sorbitol by Yu (2003).

Examples of the formation of amorphous phases are especially common among inorganic, poorly soluble, compounds like Calcium Carbonate, Calcium Phosphate, Alumina, Cobalt Hydroxide and Iron Hydroxide.

Kabasci (1996), Brecevic (1989) and Sawada (1998) precipitated Calcium Carbonate from aqueous solutions of Calcium Chloride and Sodium Carbonate for different concentration and temperature. Within seconds an amorphous phase was formed that transformed on a scale of minutes to Vaterite and next on a scale of hours to Calcite (low temperature) or Aragonite (high temperature). On a scale of days the Sawada observed how Aragonite further transformed to Calcite.

To explain the formation of the amorphous phase and subsequent transformation into the crystalline phases Kabasci discussed several models, comparing simultaneous and sequential kinetics. The model with simultaneous nucleation at different rates of all phases was preferred by the author. The high nucleation rate for the initially

dominant amorphous phase was explained by a significantly lower interfacial energy and hence nucleation work compared to that of the crystalline phases. However, following this approach the nucleation rate of the stable Calcite phase was predicted to be higher than that of the less stable Vaterite and Aragonite phases. This was blamed to the insufficiently accurate estimate of the interfacial energy as a function of bulk solubility using the equation according to Mersmann (1990).

Using small-angle X-Ray scattering Bolze (2002, 2004) and Pontoni (2003) observed that from a supersaturated solution of Calcium Carbonate within 10 ms after mixing first primary particles of an amorphous phase nucleated with size ~19nm followed by aggregation within seconds. During aggregation the size of the primary particles did not change. Over a time period of 50 minutes, the bulk suspension transformed into Vaterite, the least stable polymorph of Calcium Carbonate while at the surfaces of the measurement cell HEN and growth of Calcite was observed.

Brecevic (1987) described the formation of an amorphous phase of Calcium Phosphate from aqueous solutions of Calcium Chloride Sodium Phosphate at pH~7. The proposed mechanism started with homogeneous nucleation, followed by aggregation of primary particles into spheres. These spheres subsequently agglomerated to chain-like structures.

Sato (1984) described the precipitation of Alumina from aqueous solutions of Aluminium Chloride and Sodium Hydroxide. First a gelatinous amorphous Aluminium Hydroxide was obtained that transformed into Pseudo-Boehmite (a poorly crystallized oxyhydroxide similar to Boehmite) by aging. Over time in contact with aqueous solution at low pH Gibbsite formed while at high pH Bayerite was obtained.

Eble (2000) precipitated Alumina from aqueous solutions of Sodium Aluminate and Sulphuric Acid at a temperature of 75°C. At constant pH=9 with increasing concentration from 0.05 to 1 [kmol m^{-3}] the Boehmite fraction in the product increased from 15 to 40% while the Bayerite fraction decreased from 50 to 5% and overall crystallinity decreased from 65 to 45%. With increasing pH from 7 to 12 more Bayerite was obtained while the Boehmite fraction decreased to zero.

Rieger et al (2002) and Haberkorn (2003) precipitated the pigment Quinacridone and Alumina in a Y-mixer geometry and studied by SAXS. Within 10 and 40 milliseconds after mixing samples were cryogenically quenched (shock frozen) and the samples were studied using TEM. In

the case of Quinacridone particles could be observed after 40 ms and for Alumina after 10 ms. Dehydration of the precipitated Alumina occurred even under cryogenic conditions. A scheme was proposed for particle formation: first a droplet-like structure was formed due to mixing, followed by formation of nanoparticles within the droplet structure, these particles later transformed into respectively thin Quinacridon and Psudoboehmite platelets.

Rousseaux (2002) prepared an amorphous alumina gel from aqueous solutions of Sodium Aluminate and Aluminium Sulphate. When this gel was transferred into an alkaline solution at approximately 75°C aging took place according to a simultaneous two-step mechanism consisting of rapid structural rearrangement and slow Ostwald-ripening. The resulting product consisted always of Pseudo-Boehmite. This was blamed to the presence of Sulphate ions acting as a chemical glue, suppressing dissolution and hence further polymorphic transformation of the particles.

Gaunand (2002) precipitated Cobalt Hydroxide fro aqueous solutions of Cobalt Sulphate and Sodium Hydroxide in a double jet stirred crystallizer. The blue amorphous α form precipitated first followed by transformation into the more stable crystalline β form. The transformation rate was limited by the dissolution rate of the metastable α form that was hindered by adhering Sulphate ions.

Sugimoto (1996, 1998) precipitated a highly condensed Iron (III) Hydroxide gel from aqueous solutions of Iron (III) Chloride and Sodium Hydroxide. A two-step solution mediated transformation to β-FeOOH and next to α-Fe_2O_3 (Hematite) was observed.

Mintova (1999) prepared zeolite A from an Aluminosilicate solution and Tetra Methyl Ammonium template. Initially amorphous gel particles with a size of 40-80 nm were obtained. After a time period of several days at room temperature nucleation and growth of single crystals of zeolite with size 10-30 nm could be observed in the gel particles by TEM. When the transformation was completed after seven days a zeolite A crystal with a size of 40-80 nm had been formed according to a solution mediated mechanism.

The number of publications on the formation of amorphous phases of organic compounds from solution is surprisingly small. Stagner and Guillory (1979) reported the preparation of an amorphous form of Iopanoic Acid from a solution of Sodium Iopanate with diluted acid. In the same paper two polymorphs of this compound were reported.

The formation of an amorphous phase may be considered in two ways. First, the amorphous phase may be considered as a truly metastable phase consisting of randomly oriented solute molecules, nucleated by an aggregation mecheanism according to the classical nucleation theory. The transformation to a more stable phase takes place either by a solution mediated or solid-solid mechanism, similar to the description in the previous paragraphs.

Secondly, it may be allowed to consider the formation of an amorphous phase from solution as a liquid-liquid phase split, with the solute-rich phase having such a high viscosity that it becomes effectively solid. From this solute-rich phase, possibly at the interface with the solute-poor phase, a truly crystalline phase may nucleate and subsequently grow, while the solute-rich phase dissolves again.

1.3.5 Factors influencing the formation of polymorphs

In industrial processes the formation of the desired polymorphs has to be controlled and therefore such a process should be robust and reproducible. Kitamura (2004) differentiated between primary and secondary factors controlling polymorphic crystallization. Primary factors include supersaturation, temperature, stirring rate and addition rate while secondary factors included solvent, seeds and additives.

Supersaturation

With increasing supersaturation the rates of nucleation and growth are likely to increase, but the increase may be different for different polymorphic forms. Beckmann (1999) studied the anti-solvent crystallization of Abecarnil from iso-propyl acetate with hexane as anti-solvent. At low supersaturation predominantly the stable C-form was obtained while at high supersaturation the occurrence of the metastable B-form increased. This is in line with Ostwald's rule of stages. Toth (2005) studied the anti-solvent crystallization of Glycine from aqueous solution with ethanol as anti-solvent. At low supersaturation the more stable α-form was obtained, while with increasing supersaturation first only the less stable β-form was observed and for even higher supersaturation a mixture of α and β.

Mixing intensity

Haselhuhn and Kind (2003) studied the effect of mixing on the formation of the Monohydrate (COM) and the Dihydrate (COD) of Calcium Oxalate in a Y-mixer set-up. With increased mixing intensity Haselhuhn observed

an increase of the polymorphic fraction from completely stable COM to completely metastable COD. Füredi-Milhofer et al (1990) precipitated Calcium Oxalate in a batch vessel with different modes of stirring. In unstirred solutions mostly the stable form COM was found while in solution stirred with an overhead stirred the fraction of the metastable Trihydrate (COT) increased. When a magnetic stirrer was used, or an overhead stirrer with glass beads, predominantly COT was formed.

Kabasci (1996) applied two types of mixing chambers, a low intensity tee-mixer and a high-intensity vortex-mixer, during the precipitation of Calcium Carbonate at high supersaturation. The mixing intensity in the vortex mixer is higher than in the tee-mixer. With both types of mixers first an amorphous phase was made that was introduced into a stirred vessel. Within minutes the amorphous phase recrystallized into a mixture of Vaterite and Calcite. When the vortex mixer was used Vaterite was predominantly formed after recrystallization, while use of the tee-mixer resulted in mostly Calcite.

Addition rate

The anti-solvent crystallization of a thiazole-derivative (BPT) was studied by Kitamura (2002, 2003). Water was added to a solution of the compound BPT in Methanol. When the addition rate was low, a mixture of the metastable polymorph D and the metastable hemi-hydrate (BH) was formed. When the addition rate was increased the fraction BH increased. It was concluded that with a higher addition rate a larger quantity of water became available, promoting the formation of the hemi-hydrate at the expense of form D.

Kim et al (2003) reported the anti-solvent crystallization of the anhydrous and hydrated phase of L-Ornithine-L-Aspartate (LOLA) from aqueous solution with methanol as anti-solvent. When methanol was added to the aqueous solution the phase of LOLA that was obtained depended only on the temperature, for T>60°C the anhydrous phase and for T<50°C the hydrate was formed. When the aqueous solution was added to methanol always the anhydrous phase was obtained even at T<50°C. This may be attributed to the high local supersaturation in a methanolic environment when the water activity is low.

Seeding

Seeds can be intentionally added to direct the crystallization of a polymorphic system towards a desired polymorph. Seeding can be considered as a special case of heterogeneous nucleation with nuclei consisting of the desired polymorph. For effective and reproducible

seeding, seeds with a sufficiently large surface area have to be prepared (Beckmann 2000). Chemburkar et al (2000) described how a robust process was developed to prepare the metastable polymorph of Ritonavir using seeds of this form. Donnet et al (2005) prepared seeds from the filtrate (<0.2 μm) of slurries of Calcite, Vaterite and Aragonite to direct the formation of the polymorphs of Calcium Carbonate.

Recently, attempts were described to prepare heterogeneous templates to nucleate a desired polymorph. Aizenberg et al (1999) described how the templated crystallization of Calcite from solution on Self-Assembled Monolayers always started with one specific crystal surface of the Calcite crystal from the template. Mitchell et al (2001) reported the epitaxial nucleation of a new polymorph of the compound ROY from a single crystal Pimelic Acid substrate. Price et al (2005) used libraries of polymer heteronuclei to prepare polymorphs of different compounds such as Acetaminophen and ROY. The methodology was aimed at discovery and selective production of crystalline polymorphs.

Green (DuPont 2003) patented the use of a template nucleation device for industrial purpose. In this device the template surface is attached to an ultrasound horn. After nucleation and growth of the crystals at the template surface, ultrasound is applied to remove them from the surface. To overcome the problem of limited surface area for templated nucleation, Küther and Bartz (1998) prepared templates for Calcite on gold colloids that were suspended in the solution.

Zaccaro (2001) et al and Garetz et al (2002) reported a novel type of physical seeding in highly concentrated aqueous solutions of Glycine (3.7-3.9 M). Polarized laser light pulses were used to nucleate polymorphs of Glycine as a function of the polarization direction. When linearly polarized light was used the γ polymorph was obtained while for circularly polarized light the α polymorph was formed. The explanation for this phenomenon was the presumed alignment in the solution of the building blocks for the nuclei under influence of the laser light pulses. Differently polarized light induced a different alignment of the molecules in the solution. This alignment promoted the nucleation of the polymorph in which the lattice mostly resembled the alignment of the molecules in the solution.

Solvents

Solvents influence the precipitation process primarily by the solubility of the solute and the resulting supersaturation ratio and interfacial energy. Interaction between solvent and solute molecules may promote or

inhibit the formation of structures that are specific for the crystal lattices of the different polymorphs.

An example is the speciation in solution, for example the formation of dimers. Gracin and Rasmuson (2004) assumed that the building blocks for the different polymorphs p-Aminobenzoic acid (p-ABA) were different. The metastable polymorph was built from solute dimers while the stable polymorph was built from single molecules. In the case of p-ABA in apolar solutions dimers were dominant in the solution, while only in strongly polar solvents like water and Ethyl-Acetate the molecular form of p-ABA was present.

Sato et al (1985) followed the polymorphic transition of Stearic Acid polymorphs B (low temperature stable) and C (high temperature stable) in apolar and polar solvents at different temperatures. The C to B transition was faster in polar solvents than in non-polar solvents because of the formation of dimers in non-polar solvents with a poor fit into the crystal lattice of form B.

Blagden et al (1998a, 2001) and Khoshkhoo and Anwar (1993) reported how the use of different solvents influenced the formation of the four polymorphs of Suphathiazole. The least stable polymorph I was obtained from n-Propanol, the less stable polymorphs II and III from Nitromethane and from aqueous Ammonia while the most stable polymorph formed in water. Interactions between solute and solvent molecules in the solution were assumed to inhibit or promote the formation of the specific crystal lattices.

Kitamura et al (1994) prepared L-Histidine form mixed solvent solutions by cooling crystallization. L-Histidine is a rigid molecule. With increasing ethanol fraction (increasing supersaturation ratio) the proportion of the metastable B polymorph increased while for low ethanol fractions a mixture of the stable polymorph A and the metastable polymorph B was obtained. The higher polymorphic fraction of form B for high ethanol fraction could be explained from the experimentally observed higher growth rate of the B form under these conditions. Kitamura (2004) proposed that the solvent could influence the concentration of conformers in solution and therefore the formation of conformational polymorphs.

Maruyma and Ooshima (2000) crystallized the polymorphs of Taltirelin Tetrahydrate from water-Methanol mixtures by cooling. The conformation of the solute in solution was assumed to determine the polymorph that formed: in solvent with low Methanol fraction the α conformer should dominate while in the solvent with high Methanol

fraction the β conformer would. These assumptions were based on the increase of the growth rates of the stable β phase with increasing concentration of Methanol while that of the metastable α phase decreased.

Additives

Additives may be deliberately used in crystallization processes to block the growth of specific or all surfaces of a crystal (Weissbruch et al 1995). In the case that only specific surfaces are blocked, the surfaces which growth is not inhibited continue to grow, resulting in a different morphology of the crystal compared to the non-inhibited situation. In the case of polymorphs, the specific inhibition of the growth of crystals of a more stable phase may slow down or even inhibit the transformation of a metastable phase. For L-Glutamic Acid, for example, it was found by Kitamura and Ishizu (1998) that a small quantity of 0.5 mole % L-Phenylalanine was effective in suppressing the formation of the stable β polymorph. At the same time growth of the metastable α polymorph was retarded as well. The D-isomer of Phenylalanine was found to be ineffective.

Cashell et al (2005) studied the stabilization of the metastable α polymorph of L-Glutamic Acid by L-Phenylalanine and by L-Tyrosine. In a low 1:30 molar ratio L-Tyr/L-Glu in solution minute quantities were incorporate in the α crystals. In a high 1:6 molar ratio the uptake became significant and the morphology of the α crystal changed. It was assumed that the additives disrupted the formation of the crystal surfaces of polymorph α that could act as template for HEN of crystals the stable polymorph β.

Davey et al (1997) selected four additives that resembled the L-Glutamic Acid conformer in the β polymorph. The additives were added in a quantity of 10 mole% to a solution of L-Glutamic Acid that was cooling crystallized at 38°C. All additives were found to retard the formation of the metastable α polymorph somewhat. The subsequent transformation was retarded with varying effect, with the Trimesic Acid being the most effective additive. After transformation the morphology of the β crystals was less elongated while their size had decreased. In the absence of stirring, the transformation was further retarded in the presence of this additive with no sign of the β polymorph after several weeks.

Another example was given by Blagden et al (1998b) for the cooling crystallization of Sulphathiazole from aqueous solution in the presence of an increasing quantity of a reaction by-product. Without additives

after 24 hours only the most stable phase IV is normally obtained by a crystallization-recrystallization mechanism. With increasing impurity concentration of 0.5-1.0 mole% less stable forms III and II are obtained and ultimately only the least stable phase I is stabilized at a concentration of 1 mole%.

Kitamura (2001) found that Magnesium ions that were built into the crystal lattice of Calcite crystals suppressed the transformation of Vaterite to Calcite by inhibiting the growth of the Calcite crystals. In the field of biomineralization many studies are done to find out how organisms are able to direct nucleation and growth of the desired polymorphs of inorganic compounds like Calcium Carbonate (Dove, De Yoreo, Weiner 2003).

A special case is when the solute itself is a source of a growth modifier. This was for example the case for the crystallization of α-Lactose Monohydrate from aqueous solutions. In solution the β-isomer of α-lactose was formed by when isomerisation. The growth in one direction of the crystals was blocked by the adhering β-isomer, resulting in a truncated morphology ('tomahawk') due to unidirectional growth (Visser and Bennema 1983, Raghavan et al 2000).

Glycine posed another example of self-poisoning. Towler et al (2004) assumed different building blocks for the different polymorphs. The main motiv in the lattice of the metastable polymorph α consisted of dimers while the more stable polymorph γ was built from single molecules. In aqueous solution with pH around the iso-electric point of the amino acid, dimers were dominant, resulting in the formation of the metastable polymorph α. In more acidic or more alkali solutions also Glycine molecules with a dissociated or associated proton were present in a significant amount. These were assumed to inhibit the growth of the less stable polymorph α, and instead the thermodynamically more stable but kinetically less favoured polymorph γ was able to form.

1.4 Scope and outline

Polymorphism is of great interest to many industries because polymorphs have different properties due to their difference in crystal structure. Many polymorphs are produced during precipitation, which is a fast crystallization process due to the high supersaturation created by mixing of two reacting solutions or of a solution with an anti-solvent.

In general, control over the main properties of precipitated products, structure, shape and crystal size distribution, is desired. This requires

control over the kinetics of the precipitation process: the primary processes nucleation and growth, and secondary processes agglomeration, attrition, ripening and transformation.

This work focuses on nucleation kinetics because the nucleation rate is a strongly non-linear function of supersaturation. Variations in supersaturation may have a large effect on the relative nucleation rates of different polymorphs.

For good nucleation rate measurements the mixing intensity should be sufficient to mix two solutions completely before nucleation begins in order to guarantee that the precipitation process starts at a constant supersaturation level.

Nucleation rate measurements of a monomorphic compound under well-defined mixing conditions can be compared to estimates for the nucleation rate according to the classical nucleation theory in order to determine whether the mechanism is either homogeneous or heterogeneous.

Relative nucleation and growth rates may be derived from a study of the polymorphic composition of a precipitate as a function of supersaturation. Compared to the nucleation of monomorphic compounds, the mechanism is more complicated because two or more polymorphs are competing for the depletion of the supersaturation with different nucleation and growth rates. Furthermore, a less stable polymorph may transform into a more stable phase by a solution mediated mechanism.

In this project a special set-up is designed and constructed aimed at achieving complete and fast mixing. Part of the design is a computational fluid dynamics study on mixing in a wide-angle Y-mixer, described in **chapter 2**.

In this set-up precipitation of the molecular model compound Ethylene Diamine Tetra Acetic acid (H_4EDTA) according to a pH-shift process under steady state conditions is investigated in **chapter 3**. The stationary nucleation rate is measured and plotted as a function of supersaturation. From the plot the kinetic parameter and the interfacial energy in the nucleation rate equation are derived. These values are compared to estimates based on the classical nucleation theory to elucidate whether the nucleation proceeds according to a homogeneous or a heterogeneous mechanism.

This experimental study on nucleation rate measurements is evaluated in the context of similar experimental studies on nucleation rates for both ionic compounds and for molecular compounds, as described in **chapter 4**. Although for some compounds theoretically homogeneous nucleation is achievable, indications for such a mechanism are only found for two ionic compounds. For the other studies a heterogeneous mechanism is more likely. Reasons why experimental measurement of homogeneous nucleation from solution is rarely observed are given.

The anti-solvent precipitation of L-Histidine from aqueous solution with ethanol as anti-solvent is studied and the effect of increasing supersaturation on the polymorphic composition is measured. A process simulation of the effect of competitive nucleation and growth rates on the polymorphic fraction during precipitation is presented in **chapter 5**.

Furthermore, to study the pH-shift precipitation of the polymorphs of the model compound L-Glutamic acid the mixing device is used as a pre-mixer to build-up supersaturation instantaneously. The competitive nucleation and growth of the polymorphs as a function of supersaturation and of post-stirring the sampled solutions is studied in **chapter 6**. A mechanism is proposed to explain the experimental findings.

1.5 References

Aizenberg, J.; A.J. Black, G.M. Whitesides, Nature 398 (1999) 495
Andronis, V.; G. Zografi, J. Non-Cryst. Solids 271 (2000) 236
Angerhöfer, M., Untersuchung zur Kinetik der Fällungskrustallisation von Bariumsulfat, Thesis, Technische Universität München (1994)
Arsic, J.; I.C. Reynhout, W.J.O. van Enckevort, E. Vlieg, J. Cryst. Growth 253 (2003) 472

Baldyga, J.; J.R. Bourne, Turbulent Mixing and Chemical Reactions, Wiley, Chichester (1999)
Baldyga, J.; W. Orchiuch, Chem. Eng. Sci. 56 (2001) 2435
Bauer, J.; S. Spanton, R. Henry, J. Quick, W. Dziki, W. Porter, J. Morris, Pharm. Res. 18 (2001) 859
Beckmann, W., J. Cryst. Growth 198/199 (1999) 1307
Beckmann, W., Org. Process Res. Dev. 4 (2000) 372
Bennema P.; O. Söhnel, J. Cryst. Growth 102 (1990) 547
Bernstein, J.; J.-O. Henck, Crystal Engineering 1 (1998) 119
Bernstein, J.; R.J. Davey, J.-O. Henck, Angew. Chem. Int. Ed. 38 (1999) 3440

Bernstein, J. Polymorphism in Molecular Crystals, Oxford University Press (2002)
Black, S.N.; R.J. Davey, J. Cryst. Growth 90 (1988) 136
Blagden, N.; R.J. Davey, H.F. Lieberman, L. Williams, R. Payne, R. Roberts, R. Rowe, R. Docherty, J. Chem. Soc. 94 (1998) 1035
Blagden, N.; R.J. Davey, R. Rowe, R. Roberts, Int. J. Pharm. 172 (1998) 169
Blagden, N., Powder Technol. 121 (2001) 46
Blandin, A.F.; D. Mangin, V. Vallet, J.P. Klein, J.M. Bossoutrot, Chem. Eng. J. 81 (2001) 91
Boerrigter, S.X.M.; C.J.M. van den Hoogenhof, H. Meekes, P. Bennema, E. Vlieg, P.J.C.M van Hoof, J. Phys. Chem. B 106 (2002) 4725
Boistelle, R.; C. Rinaudo, J. Cryst. Growth 53 (1981) 1
Bolze, J.; B. Peng, N. Dingenouts, P. Panine, T. Narayanan, M. Ballauff, Langmuir 18 (2002) 8364
Bolze, J.; D. Pontoni, M. Ballauff, T. Narayanan, H. Cölfen, J. Coll. Interface Sci. 277 (2004) 84
Bonnett, P.E.; K.J. Carpenter, S. Dawson, R.J. Davey, Chem. Commun. (2003) 698
Brecevic, Lj.; V. Hlady, H. Füredi-Milhofer, Colloids and Surfaces 28 (1987) 301
Brecevic, Lj.; A.E. Nielsen, J. Cryst. Growth 98 (1989) 504
Brecevic, Lj.; A.E. Nielsen, Acta Chim. Scand. 47 (1993) 668
Brittain, H.G., Polymorphism in Pharmaceutical Solids, Marcel Dekker Inc., New York (1999)
Bromley, L.A., AIChE J. 19 (1973) 313
Bugay, D.E., Advanced Drug Delivery Reviews 48 (2001) 43
Burger, A.; R. Ramberger, Mikrochim. ACTA [Wien] II (1979) 259
Burger, A.; R. Ramberger, Mikrochim. ACTA [Wien] II (1979) 273
Byrn, S.R.; R.R. Pfeiffer, J.G. Stowell, Solid-State Chemistry of Drugs, Second Edition, SSCI Inc., West Lafayette, Indiana (1999)

Caira, M.R., Topics in Current Chemistry 198 (1998) 164
Cardew, P.T.; R.J. Davey, North Western Branch Papers No. 2, IChemE (1982) 1.1
Cardew, P.T.; R.J. Davey, Proc. R. Soc. Lond. A 398 (1985) 415
Cashell, C.; D. Corcoran, B.K. Hodnett, Chem. Comm. (2003) 374
Cashell, C.; D. Sutton, D. Corcoran, B.K. Hodnett, Cryst. Growth Des. 3 (2003) 869
Cashell, C.; D. Corcoran, B.K. Hodnett, J. Cryst. Growth 273 (2004) 258
Cashell, C.; D. Corcoran, B.K. Hodnett, Cryst. Growth Des. 5 (2005)
Chattopadhyay, S.; D. Erdemir, J.M.B. Evans, J. Ilavsky, H. Amenitsch, C.U. Segre, A.S. Myerson, Cryst. Growth Des. 5 (2005) 523
Chemburkar, S.R. et al, Org. Process. Res. Dev. 4 (2000) 413
Choi, Y.J.; S.-T. Chung, M. Oh, H.-S. Kim, Cryst. Growth Des. 5 (2005)

Chyall, L.J.; J.M. Tower, D.A. Coates, T.L. Houston, S.L. Childs, Cryst. Growth Des. 2 (2002) 505

Davey, R.J.; P.T. Cardew, J. Cryst. Growth, 79 (1986) 648
Davey, R.J.; A.J. Ruddick, P.D. Guy, B. Mitchell, S.J. Maginn, L.A. Polywka, J. Phys. D 24 (1991) 176
Davey, R.J. et al, Nature 366 (1993) 248
Davey, R.J. et al, Mol.Cryst. Liq. Cryst. 242 (1994) 79
Davey, R.J.; N. Blagden, G.D. Potts, R. Docherty, J. Am. Chem. Soc 119 (1997) 1767
Davey, R.J.; N. Blagden, S. Righini, H. Alison, E.S. Ferrari, J. Phys. Chem. B 106 (2002) 1954
Donnet, M.; P. Bowen, N. Jongen, J. Lemaître, H. Hofmann, Langmuir 21 (2005) 100
Dove, P.; J.J. de Yoreo, S. Weiner, Biomineralization 54 (2003)
Drenth, J., Cryst. Growth Des., accepted for publication (2005)
Driel, C.A. van, A.E.D.M. van der Heijden, S. De Boer, G.M. van Rosmalen, J. Cryst. Growth, 141 (1994) 404
Dunitz, J.D.; J. Bernstein, Acc. Chem. Res. 28 (1995) 193

Eble, A., Precipitation of nanoscale crystals with particular reference to interfacial energy, Technische Universität München (2000)

Ferrari, E.S.; R.J. Davey, W.I. Cross, A.L. Gillon, C.S. Towler, Cryst. Growth Des. 3 (2003) 53
Ferrari, E.S.; R.J. Davey, Cryst. Growth Des. 4 (2004) 1061
Füredi-Milhofer, H.; V. Babić-Ivančić, Lj. Brečević, N. Filipović-Vinceković, D. Kralj, Lj. Komunjer, M. Marković, D. Škrtić, Colloids and Surfaces 48 (1990) 219

Galkin, O.; P.G. Vekilov, J. Am. Chem. Soc. 122 (2000) 156
Gardner, R. et al, Computers and Chemical Engineering 28 (2004) 943
Garetz, B.A.; J. Matic, A.S. Myerson, Physical Review Letters 89 (2002) 175501-1
Garside, J.; A. Mersmann, J. Nyvlt, Measurement of crystal growth and nucleation rates, EFCE Working Party on Crystallization, IchemE, Rugby, 2002
Garti, N.; H. Zour, J. Cryst. Growth 172 (1997) 486
Gaunand, A.; W.L. Lim, Powder Technology 128 (2002) 332
Giron, D., Thermochim. Acta 248 (1995) 1
Gracin, S.; Å.C. Rasmuson, Cryst. Growth Des. 4 (2004) 1013
Green, D.A., Apparatus and process used in growing crystals, patent WO03084631 (2003)
Grön, H.; K.J. Roberts, J. Phys. Chem. B 105 (2001) 10723

Grunenberg, A.; J.-O. Henck, H.W. Siesler, Int. J. Pharm. 129 (1996) 147
Grunenberg, A.; H.-P. Wirges, Industrial Crystallization (1999) 1
Gutzow, I.; S. Toschev, Kristall u. Technik 3 (1968) 485

Haas, C.; J. Drenth, J. Cryst. Growth 196 (1999) 388
Haberkorn, H.; D. Franke, Th. Frechen, W. Goesele, J. Rieger, J. Colloid Interface Sci. 259 (2003) 112
Haleblian, J.; W. McCrone, J. Pharm. Sci. 58 (1969) 911
Hancock, B.C.; G. Zografi, J. Pharm. Sci 86 (1997) 1
Hao, Z.; A. Iqbal, Chemical Society Reviews 26 (1997) 203
Haselhuhn, F.; M. Kind, Chem. Eng. Technol. 26 (2003) 3
Henck, J.-O.; U.J. Griesser, A. Burger, Pharm. Ind. 59 (1997) 165
Hilden, J.L. et al., Cryst. Growth Des. 3 (2003) 921
Himawan, C., PhD Thesis, Delft University of Technology, (2005)
Horst, J. ter; H.K.M Kramer, P.J. Jansens, Cryst. Growth Des. 2 (2002) 351

Ito, A.; M. Yamanobe-Hada, H. Shindo, J. Cryst. Growth 275 (2005) 1691

Johnson, B.K.; R.K. Prud'homme, Physical Review Letters 91 (2003) 118302
Johnson, B.K.; R.K. Prud'homme, Aust. J. Chem 56 (2003) 1021
Jongen, N.; P. Bowen, J. Lemaître, J.C. Valmalette, H. Hofman, J. Colloid Interface Sci. 226 (2000) 189
Judat, B.; M. Kind, J. Colloid Interface Sci. 269 (2004) 341

Kabasci, S.; W. Althaus, P.-M. Weinspach, Trans IchemE 74 (1996) 765
Kashchiev, D. Nucleation Basic Theory with Applications, Butterworth Oxford (1999)
Kashchiev, D.; G.M. van Rosmalen, Cryst. Res. Technol. 38 (2003) 555
Khoshkhoo, S.; J. Anwar, J. Phys. D 26 (1993) B90
Kim, Y. et al, Ind. Eng. Chem. Res. 42 (2003) 883
Kim, H.; K. Saitmacher, L. Unverdorben, Ch. Wille, Macromol. Symp. 187 (2002) 631
Kim, S.; C. Wei, S. Kiang, Organic Process Research & Development 7 (2003) 997
Kitamura, M., J. Cryst. Growth 96 (1989) 541
Kitamura, M.; H. Furukawa, M. Asaeda, J. Cryst. Growth 141 (1994) 193
Kitamura, M.; T. Ishizu, J. Cryst. Growth 192 (1998) 225
Kitamura, M.; T. Ishizu, J. Cryst. Growth 209 (2000) 138
Kitamura, M., J. Colloid Interface Sci. 236 (2001) 318
Kitamura, M.; K. Nakamura, J. Cryst. Growth 236 (2002) 676
Kitamura, M.; K. Nakamura, J. Chem. Eng. Japan 35 (2002) 1116

Kitamura, M.; M. Sugimoto, J. Cryst. Growth 257 (2003) 177
Kitamura, M., Cryst. Growth Des. 4 (2004) 1153
Knezic, D.; J. Zaccaro, A.S. Myerson, J. Phys. Chem. B 108 (2004) 10672
Kolar, Z.; J.J.M. Binsma, B. Subotić, J. Cryst. Growth 76 (1986) 408
Kralj, D.; Lj. Brečević, Colloids and Surfaces 96 (1995) 287
Küther, J.; R. Seshadri, W. Tremel, Angew. Chem. Int. Ed. 37 (1998) 3044

Lafferrère, L.; C. Hoff, S. Veesler, Eng. Life Sci. 3 (2003) 127
Lafferrère, L.; C. Hoff, S. Veesler, Cryst. Growth Des. 4 (2004a) 1175
Lafferrère, L.; C. Hoff, S. Veesler, J. Cryst. Growth 269 (2004b) 550
Leeuwen, M.L.J. van, Precipitation and mixing, Thesis, Delft University of Technology (1998)
Löbbert, G., Phthalocyanines, Chapter in Ullmann's Encyclopedia of Industrial Chemistry, Wiley, New York (2002)

Mahajan, A.J.; D.J. Kirwan, J. Phys. D 26 (1993) B176
Mahajan, A.J.; D.J. Kirwan, J. Cryst. Growth 144 (1994) 281
Manth, T.; D. Mignon, H. Offerman, Chem. Eng. Sci. 51 (1996) 2571
Marchisio, D.L.; A.A. Barresi, M. Garbero, AICheE Journal 48 (2002) 2039
Maruyma, S.; H. Ooshima, J. Cryst. Growth 212 (2000) 239
McCrone, W.C., Polymorphism, Chapter 8 in Physics and chemistry of the organic solid state, Wiley, New York (1965)
McCrone, W.C., International Laboratory (2000) 26
McCrone, W.C., Microscope 49 (2001) 47
Mersmann, A., J. Cryst. Growth 102 (1990) 841
Mersmann, A., IchemE (1996) 812
Mersmann, A., Crystallization Technology Handbook, Marcel Dekker Inc., New York (2001)
Mintova, S.; N.H. Olson, V. Valtchev, T. Bein, Science 283 (1999) 958
Mitchell, C. A.; L. Yu, M.D. Ward, J. Am. Chem. Soc. 123 (2001) 10830
Mohanty, R.; S. Bhandarkar, B. Zuromski, R. Brown, J. Estrin, AIChE J. 34 (1988) 2063
Morisette, S.L. et al, PNAS 100 (2003) 2180
Morisette, S.L. et al, Adv. Drug Deliv. Rev. 56 (2004) 275

Nielsen, A.E., Acta Chem. Scand. 15 (1961) 441
Nielsen, A.E., Kinetics of Precipitation, Pergamon, Oxford (1964)
Nielsen, A.E., Crystal Growth: Proceedings ICCG-1, H.S. Peiser ed.; Pergamon, Oxford (1967) 419
Nielsen, A.E., Kristall un. Techniek 4 (1969) 17
Nielsen, A.E.; O. Söhnel, J. Cryst. Growth 11 (1971) 233
Nielsen, A.E., J. Cryst. Growth 67 (1984) 289

Nyvlt, J., Cryst. Res. Technol. 30 (1995) 443

O'Hern, H.A.; F.E. Rush Jr., I&EC Fundamentals 2 (1963) 267
Ono, T.; H.J.M. Kramer, J.H. ter Horst, P.J. Jansens, Cryst. Growth Des. 4 (2004) 1161
Ono, T.; J.H. ter Horst, P.J. Jansens, Cryst. Growth Des. 4 (2004) 465
Ostwald, W., Zeitschrift f. Physik. Chemie XXII (1897) 19

Peterson, M.L.; D. McIlroy, P. Shaw, J.P. Mustonen, M. Oliveira, Ö. Almarsson, Cryst. Growth Des. 3 (2003) 761
Peukert W.; H.-C. Schwarzer, F. Stenger, Chem. Eng. Processing 44 (2005) 245
Pitzer, K.S. Activity coefficinets in electrolyte solutions, 2nd ed., CRC Press, Boca Raton (Fl) (1991)
Pontoni, D.; J. Bolze, N. Dingenouts, T. Narayanan, M. Ballauff, J. Phys. Chem. B 107 (2003) 5123
Price, C.P.; A.L. Grzesiak, A.J. Matzger, J. Am. Chem. Soc. (2005)
Pujol, O.; P. Bowen, P.A. Stadelmann, H. Hofman, J. Phys. Chem B accepted for publication (2005)

Rafal, M.; J.W. Berthold, N.C. Scrivner, S.L. Grise, Models for electrolyte solutions in Sandler, S.I. (editor), Models for thermodynamic and phase equilibria calculations, Marcel Dekker, New York (1994)
Raghavan S.L. et al, J. Phys. Chem. B 104 (2000) 12256
Rieger, J.; E. Hädicke, I.U. Rau, D. Boeckh, Temside Surf. Det. 34 (1997) 6
Rieger, J.; D. Franke, T. Frechen, H. Haberkorn, W. Goesele, in Proc. of the 9th Int. Workshop on Ind. Cryst. (BIWIC) (Ed: J. Ulrich), Halle (2002)
Rivera, T.; A.D. Randolph, Ind. Eng. Chem. Process Des. Dev. 17 (1978) 182
Rodriguez-Hornedo, N.; D. Lechuga-Ballesteros, H.-J. Wu, Int J. Pharm. 85 (1992) 149
Rodriguez-Hornedo, N.; D. Murphy, J. Pharm. Sci. 88 (1999) 651
Rodriguez-Spong, B.; C.P. Price, A. Jayasankar, A.J. Matzger, N. Rodriguez-Hornedo, Adv. Drug Deliv. Rev. 56 (2004) 241
Rousseaux, J.M.; P. Weisbecker, H. Muhr, E. Plasari, Ind. Eng. Chem. Res. 41 (2002) 6059

Sato, K.; K. Suzuki, M. Okada, J. Cryst. Growth 72 (1985) 699
Sato, K., J. Phys. D: Appl. Phys. 26 (1993) B77
Sato, T., Ind. Crystallization 84 (1984) 385
Sawada, K., Mechanism of Crystal Growth of Ionic Crystals in Solution, Chapter 3 in Crystallization Processes, H. Ohtaki (Ed.) Wiley, New York (1998)

Schubert, H.; A. Mersmann, Trans IchemE 74 (1996) 821
Schüth, F.; P. Bussian, P. Ågren, S. Schunk, M. Lindén, Solid State Sciences 3 (2001a) 801
Schüth, F., Current opinion in Solid State & Materials Science 5 (2001b) 389
Schwarzer, H.C.; W. Peukert, Chem. Eng. Technol. 25 (2002) 657
Schwarzer, H.C., personal communication (2005)
Seckler, M.M.; O.S.L. Bruinsma, G.M. van Rosmalen, Chem. Eng. Comm. 135 (1995) 113
Söhnel, O., J. Cryst. Growth 57 (1982) 101
Söhnel, O., J. Cryst. Growth 63 (1983) 174
Stagner, W.C.; J.K. Guillory, J. Pharm. Sci. 68 (1979) 1005
Ståhl, M.; L. Åslund, Å.C. Rasmuson, AIChE J. 47 (2001) 1544
Stephenson, G.A. et al, J. Pharm. Sci. 84 (1995) 1385
Stoica, C.; P. Verwer, H. Meekes, E. Vlieg, P.J.C.M. van Hoof, F. Kaspersen, J. Cryst. Growth 275 (2005) el1727
Stoica, C.; P. Tinnemans, H. Meekes, E. Vlieg, P.J.C.M. van Hoof, F.M. Kaspersen, Cryst. Growth Des. (2005)
Stowell, J.G.; T.B. Borchardt, S.R. Byrn, S. R. Byrn Laboratories, Purdue University (1998) 1
Sudo, S.; K. Sato, Y. Harano, J. Chem. Eng. Japan 24 (1991) 237
Sugimoto, T.; A. Muramatsu, J. Colloid Interface Sci. 184 (1996) 626
Sugimoto, T.; Y. Wang, H. Itoh, A. Muramatsu, Colloids Surfaces A 134 (1998) 265

Ten Wolde, P.R.; D. Frenkel, Science 277 (1997) 1975
Ten Wolde, P.R.; D. Frenkel, Phys. Chem. Chem. Phys. 1 (1999) 2191
Threllfall, T.L., Analyst 120 (1995) 2435
Threllfall, T.L., Org. Process Res. Dev. 7 (2003) 1017
Tosun, G., Proceedings of the 6th European Conference on Mixing, Pavia, Italy 24-26 May, (1988), AIDIC
Tóth, J.; A. Kardos-Fodor, S. Halász-Péterfi, Chem. Eng. Processing 44 (2005) 193
Towler, C.S.; R.J. Davey, R.W.Lancaster, C.J. Price, J. Am. Chem. Soc. 126 (2004) 13347

Vekilov, P.G., Cryst. Growth Des. 4 (2004) 671
Verdoes, D.; D. Kashchiev, G.M. van Rosmalen, J. Cryst. Growth 118 (1992) 401
Visser, R.A.; P. Bennema, Neth. Milk Dairy J. 37 (1983) 109

Wang, F. J.A.; Wachter, F.J. Antosz, K.A. Berglund, Org. Process Res. Dev. 4 (2002) 391
Wei, H.; J. Garside, Trans IchemE 75 (1997) 219

Weissbruch, I.; R. Popovitz-Biro, M. Lahav, L. Leiserowitz, Acta Cryst. B51 (1995) 115
Woordard, G.D.; W.C. McCrone, J. Appl. Cryst. 8 (1975) 342

Yu, L., Adv. Drug Delivery Rev. 48 (2001) 27
Yu, L., J. Phys. Chem. A 106 (2002) 544
Yu, L.; G.A. Stephenson, C.A. Mitchell, C.A. Bunnell, S.V. Snorek, J.J. Bowyer, T.B. Borchardt, J.G. Stowell, S.R. Byrn, J. Am. Chem. Soc. 122 (2000) 585
Yu, L.; S.M. Reutzel-Edens, C.M. Mitchell, Org. Process R&D 4 (2000) 396
Yu, L., Cryst. Growth Des. 3 (2003) 967

Zaccaro, J.; J. Matic, A.S. Myserson, B.A. Garetz, Cryst. Growth Des. 1 (2001) 5

Chapter 2

Analysis of mixing in a typical experimental set-up to measure nucleation rates of precipitation processes

Chem. Eng. Tech. 26 (2003) 296-302

Mixing in a typical experimental set-up to measure nucleation rates in precipitation processes was assessed. To determine these rates as a function of the driving force for concomitant polymorphs, it is necessary to perform these experiments at constant supersaturation. Therefore the mixing time must be shorter than the time for the first nuclei to appear. For fast precipitation processes complete mixing has to be achieved within milliseconds. The mixing performance of a wide angle Y-mixer was studied to see whether this is possible.

An analysis of characteristic mixing times as a function of the average energy dissipation rate showed that turbulent dispersion of the feed streams determined the rate of the mixing process. The characteristic time for turbulent dispersion was of the same order as an arbitrarily set residence time in the Y-mixer. However, CFD simulations of the flow showed large variation in the spatial distribution of the dissipation rate and revealed unsatisfying macromixing.

2.1 Introduction

Polymorphism is of great interest to industry because the polymorphs have different physical properties influencing their performance, e.g. the color of pigments and the solubility of pharmaceuticals. Control over the formation is desired. From the viewpoint of thermodynamics only one polymorph is stable. However, in precipitation the formation of less stable polymorphs may be kinetically favored, according to Ostwald's rule of stages. If the nucleation rates and growth rates are in the same range, and transition is slow, concomitant polymorphs will be observed (Bernstein et al 1999).

In precipitation research nucleation rates are generally measured according to the method developed by Nielsen (1961,1964) for Barium Sulfate. Two flows of reactant solutions are intensively mixed in a mixing tee and nuclei form in the outlet tube. From crystal size distribution (CSD) data of samples from the resulting suspension the nucleation rate is calculated. Angerhöfer (1994) and Schubert and Mersmann (1996) applied this method for Barium Sulfate and Ståhl et al (2001) for Benzoic Acid. Haselhuhn and Kind (2002) used the Nielsen method to study the formation of pseudo-polymorphs of calcium oxalate hydrates as a function of supersaturation. Mahajan and Kirwan (1994) modified the Nielsen-method by varying the residence time in a tube with variable length. The shift in the CSD with residence time was measured and used to calculate nucleation and growth rates for the amino acid Asparagine and a drug Lovostatine.

In these investigations it was assumed that complete mixing of the reactants preceded nucleation and thus that nucleation took place at a constant supersaturation level. However, recent papers indicate that for some compounds this assumption does not hold: precipitation starts before mixing is still completed. This is especially the case for insoluble compounds, precipitating at high supersaturation levels. Schwarzer and Peukert (2002) and Baldyga and Orchiuch (2001) precipitated Barium Sulfate and observed a decrease of the average particle size with increasing mixing intensity indicating the interaction between mixing and nucleation kinetics.

It is the objective of this research program at the Delft University of Technology to measure the competitive nucleation rates of concomitant polymorphs. Mixing of the reactants is crucial to these measurements because the mixing intensity determines the local supersaturation level. A constant supersaturation level must be achieved before nucleation starts. Therefore, this paper presents an assessment of mixing in a typical experimental set-up used to determine nucleation kinetics.

2.2 Nucleation theory

The nucleation rate *J* is represented by the following equation according to the classical nucleation theory:

$$J = A\exp\frac{-4\Gamma^3}{27\ln^2 S} \quad with \quad \Gamma = \frac{\nu_m^{2/3}}{k_B T}\left(\sum_i^{hkl} c_i\gamma_i\right) \tag{2.1}$$

In this equation A is a kinetic parameter and S is supersaturation defined as the ratio of the actual concentration of the compound over its

solubility. Ter Horst et al (2002) define Γ as the dimensionless overall interfacial energy. It contains all unknown parameters γ_i and c_i for all hkl crystal surfaces with γ_i the interfacial energy and c_i a geometrical factor reflecting the surface area. This Γ, rather than its individual parameters, is of great importance in nucleation processes.

Primary nucleation proceeds as a strongly non-linear function of the supersaturation and therefore fluctuations in the supersaturation level due to mixing have a strong effect on the nucleation rate. Polymorphs will be formed at different rates because all three parameters A, Γ and S in equation (1.1) may be different. Polymorphs experience different supersaturation levels at a certain concentration level $c_0 > c^{II}_{eq}$ because the solubility c^{I}_{eq} of the stable polymorph is always lower than the solubility c^{II}_{eq} of the less stable polymorph. Concentration fluctuations may therefore affect the polymorph composition of the precipitate by promoting the formation of either one of the polymorphs.

To measure the nucleation rate of the polymorphs at a fixed composition according to the method described in the introduction, the nucleation process has to take place at a constant value for the supersaturation level. Therefore, mixing should be completed down to molecular scale before nuclei form.

2.3 Time scale analysis

2.3.1 Experimental set-up

Time scale analysis is done for a typical experimental set-up to measure nucleation rates in a precipitation process, shown in figure 2.1. The flows are generated using low-pulse gear pumps. Main components are the wide angle Y-mixer and the precipitation tube. The inner diameter of the tubing D is 3.10^{-3} m. The length of the precipitation tube can be varied from 1 to 2 and to 6 m. The average flow velocity U in the outlet tube is 6 m s^{-1} corresponding to a Reynolds number of $1.8 \cdot 10^4$, with $Re = UD/\nu$ and kinematic viscosity $\nu = 1 \cdot 10^{-6}$ m^2 s^{-1} for water. Under these plug-flow conditions a narrow residence time distribution is expected. At the end of the tube the suspension is quenched into a vessel filled with saturated solution to inhibit further nucleation. From this vessel samples will be collected to determine the crystal size distribution and the polymorph composition.

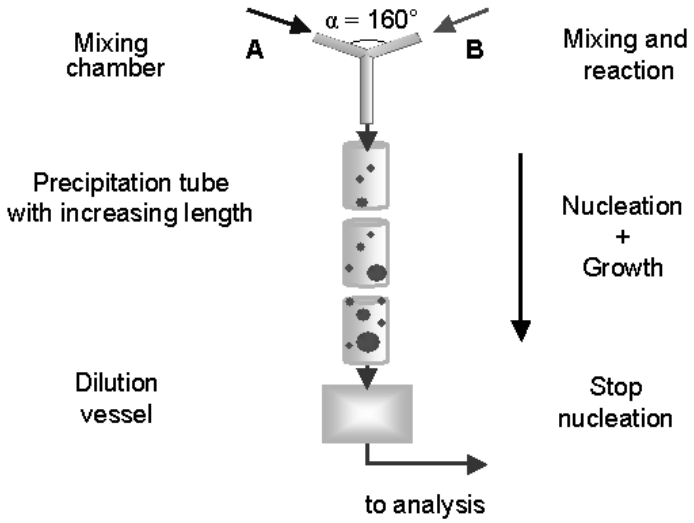

Figure 2.1 Experimental set-up with the wide angle Y-mixer.

2.3.2 Mixing time scales

Nucleation rate measurements at high supersaturation level will be carried out in the wide angle Y-mixer. In this geometry rapid mixing down to molecular scale has to be achieved before nuclei form. However, it is not possible to set this minimum for the mixing time, as the nucleation time is unknown. Direct observation of the nucleation time is not possible due to the small size of the nuclei and the statistical character of the nucleation process. Therefore, in this study the required time for complete mixing is arbitrarily set as the residence time of the reacting mixture flowing through the outlet tube over a length of twelve times its diameter:

$$\tau_r = \frac{12D}{U} \tag{2.2}$$

Initially, in the Y-mixer the opposing reactant flows are completely segregated. Upon impact of the flows the reactants are first dispersed by large eddies then transported by cascading eddies that decay finally towards the scale for molecular diffusion. The time scales that are characteristic for these mixing processes were estimated according to the mechanistic model by Baldyga and Bourne (1999).

Mixing times are written down as a function of the dissipation rate of the turbulent kinetic energy ε. The mean dissipation rate of the turbulent

kinetic energy is calculated from an estimate of the pressure drop over the outlet tube of the Y-mixer according to:

$$\varepsilon = \frac{\phi_v \Delta P}{\rho V} = \frac{2 f U^3}{D} \quad with \quad 4f = 0.316 \mathrm{Re}^{-0.25} \tag{2.3}$$

In this equation ϕ_v is the flow rate, V the volume of the outlet tube and f the friction factor for the tube wall. Under the conditions described above, the mean dissipation rate in the tube ε is of the order of $1 \cdot 10^3$ m^2 s^{-3}.

It must be noted that the pressure drop is calculated for well-developed turbulent flow in the outlet tube. The pressure drop over the actual Y-mixer is expected to be larger and therefore the local energy dissipation rate may be higher. Measurement of the pressure drop over the Y-mixer would improve the estimate of the mean dissipation rate.

First there is the time scale τ_D for turbulent dispersion or macromixing. This time scale takes into account the large-scale mass transfer of the reactants across the turbulent flow, but not molecular diffusion (Shekunov and Baldyga 2001).

$$\tau_D = \frac{L_0^2}{D_T} \tag{2.4}$$

In this equation L_0 is the characteristic dimension of the system, set at half the tube diameter. For the Y-mixer this scale is equal to the length scale of initial segregation. D_T represents turbulent diffusivity, estimated from $D_T = \nu_t / Sc_T$ with turbulent viscosity $\nu_t = C_\mu k^2 / \varepsilon$ with constants $Sc_T = 0.7$ and $C_\mu = 0.09$ (Baldyga and Bourne 1999). The turbulent kinetic energy $k = 3/2 u'^2$ with $u' \approx 1.1$ m s^{-1} the root mean square of the velocity fluctuation estimated from $\varepsilon = u'^3 / L_0$.

Next, there is the time-scale for the disintegration of large eddies to smaller eddies, reducing the size of concentration fluctuations (inertial-convective mixing) (Baldyga and Bourne 1999):

$$\tau_s = \frac{3}{4} \frac{L^{2/3}}{\varepsilon^{1/3}} \tag{2.5}$$

With L the scale of large energy containing eddies being equal to the initial segregation scale for the Y-mixer.

The final size of these eddies is characterized by the Kolmogorov length $\eta_k=(\nu^3/\varepsilon)^{1/4}$. In this case the Kolmogorov length $\eta_k \approx 6\cdot10^{-6}$ m. By the process of viscous-convective mixing these eddies decay and the scale for concentration fluctuations goes from the Kolmogorov scale towards the scale for diffusion or Batchelor scale. This processes is characterized by the engulfment rate E (viscous-convective mixing) (Baldyga and Bourne 1999):

$$\tau_E = \frac{1}{E} = 17.24\left(\frac{\nu}{\varepsilon}\right)^{1/2} \tag{2.6}$$

The Batchelor scale $\eta_B=\eta_k\ Sc^{-1/2}$ with the Schmidt number $Sc=\nu/D_m$, the ratio of the kinematic viscosity over the molecular diffusion coefficient $D_m \approx 1\cdot10^{-9}$ m^2s^{-1}. For low concentrated aqueous solutions the Schmidt number is approximately $1\cdot10^3$ so the Batchelor scale for molecular diffusion is about 30 times smaller ($\eta_B \approx 2\cdot10^{-7}$ m) than the Kolmogorov length scale.

Finally, diffusion of the reactant solutions into each other takes place over the Batchelor length scale (viscous-diffusive mixing):

$$\tau_{diff} = \frac{\eta_B^2}{D_m} \tag{2.7}$$

Table 2.1 shows the calculated characteristic mixing times scaled over the average residence time in the outlet tube over a length of twelve diameters.

Table 2.1 Dimensionless mixing time scales [-].

τ_D/τ_r	τ_s/τ_r	τ_E/τ_r	τ_{diff}/τ_r
0.78	0.17	0.09	0.01

It can be observed that the characteristic time τ_D for turbulent dispersion is comparable to the average residence time. The eddy-disintegration time τ_s and the engulfment time τ_E are one order of magnitude smaller and the time for diffusion τ_{diff} is two orders smaller. This analysis reveals that turbulent dispersion is the rate-determining step for mixing the flows down to the molecular level.

The mechanistic approach to calculate characteristic mixing times requires an average value for the energy dissipation rate. This value was estimated by considering the flow in the outlet tube as a well-developed

turbulent flow. However, the flow pattern in the wide angle Y-mixer, with two jets colliding, is likely to be different. Within the Y-mixer large differences in the distribution of energy dissipation rates are expected. In the following section a method based on computational fluid dynamics is described to estimate characteristic mixing times taking into account these differences.

2.4 Computational Fluid Dynamics simulations

2.4.1 CFD set-up

The flow in the wide angle Y-mixer was simulated with Computational Fluid Dynamics (CFD) using Fluent 6.0.20 software. For the simulations the physical properties of water were used at a pressure of 1 bar and temperature of 300K.

The flow in a wide angle Y-mixer was simulated with three circular channels all having the same diameter of $3 \cdot 10^{-3}$ m. The length of the inlet tubes was $25 \cdot 10^{-3}$ m and the length of the outlet tubes was $35 \cdot 10^{-3}$ m. The angle between the inlet channels was 160°. The average velocity of the flow was 3 m s^{-1} in the two inlet tubes and 6 m s^{-1} in the outlet tube, corresponding with a Reynolds number of $9 \cdot 10^3$ in the inlet tube and $18 \cdot 10^3$ in the outlet tube.

A 3D grid consisting of $144 \cdot 10^3$ cells was defined using Gambit 2.0.4 software representing half the volume of the Y-mixer making use of the symmetry plane dividing all channels in half. The first four cells near the wall with a total thickness of $0.23 \cdot 10^{-3}$ m or 15% of the inner radius were used to represent the boundary layer.

For closure of the Reynolds Averaged Navier-Stokes equations the k-ε model was used. This model assumes isotropic turbulence. The flow near the wall was described by wall functions and adjacent to the wall by the laminar stress-strain relationship. As boundary conditions for the inlet user defined profiles for the velocity, kinetic energy and dissipation were applied. The outlet boundary condition was set as zero gradient.

Macromixing of two non-reacting species A and B by convection and by turbulent diffusion was simulated. The mass fractions of A and B were set at 0.1 for each inlet. Molecular diffusion coefficients for A and B were set at 10^{-9} m^2 s^{-1}. No sub-grid scale model was applied to take into account micromixing within the grid cells. This implies that if in a grid cell both species are present, they are completely mixed.

2.4.2 Macromixing and dissipation rate

The pattern of two impacting flows in the wide angle Y-mixer was expected to result in a distribution of energy dissipations rates and therefore in different mixing times. In figure 2.2 velocity vectors are shown for the center plane through the Y-mixer. The vectors have a length proportional to the velocity at the point of origin of the vector.

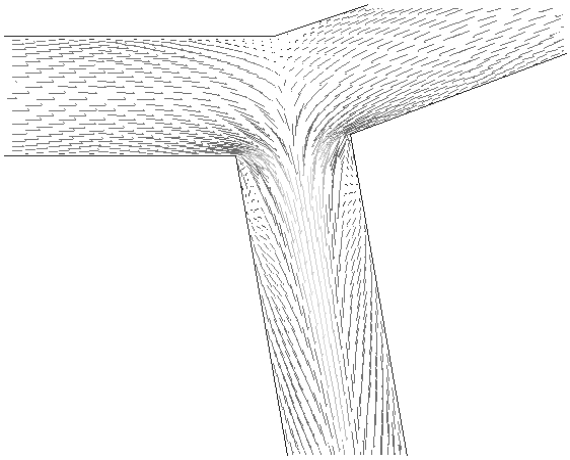

Figure 2.2 Velocity vector plot for the center plane through the wide angle Y-mixer.

High velocities can be observed at the edges of the outlet tube. Directly behind the edges, near the wall, a recirculating flow can be observed. An almost stagnant zone is visible in the top of the Y-mixer. Not all vectors are shown here to enable interpretation of the figure.

In figure 2.3 the contour plot of mass fraction A and B is shown. The wedge-shaped macromixed zone where the species mix can be observed. Directly behind the edges near the wall of the outlet tube the flow is still completely unmixed at macro-level and remains so over a length of several pipe diameters.

Figure 2.4 is a contour plot of the rate of dissipation of turbulent kinetic energy in the center plane of the Y-mixer. A large variation in levels of the dissipation rate exists at the edges between the inlet tubes pipes with the outlet tube. From figure 2.3 it can be observed that in these zones the flows are unmixed at macro scale so the high-energy dissipation rate is not effectively used in these zones for mixing. In the plane where the two flows collide high-energy dissipation rates occur as well but here they coexist with a zone that is, at least at macro scale, well mixed.

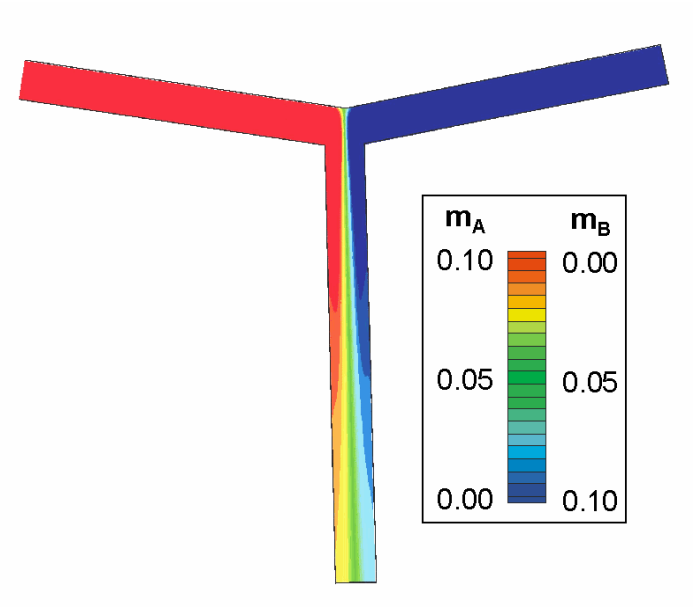

Figure 2.3 Contour plot of the mass fraction of species A and B [-].

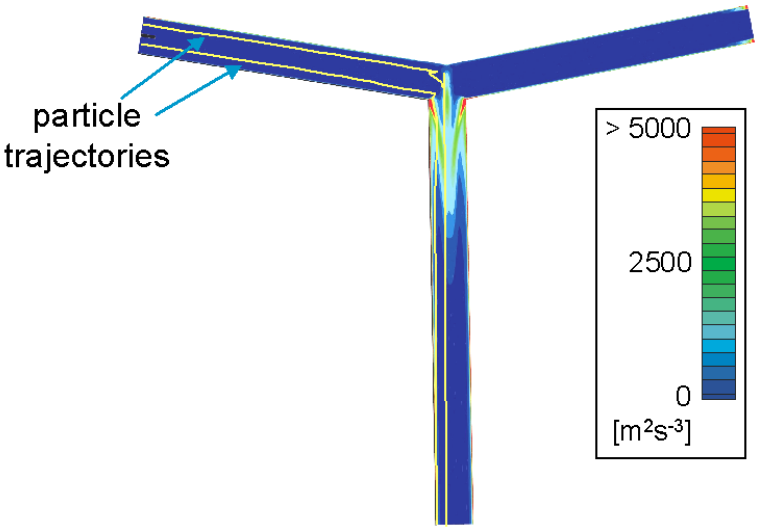

Figure 2.4 Contour plot of the turbulent kinetic energy dissipation rate ε with particle trajectories for two particles.

2.4.3 Mixing times from particle tracking

Particle tracking is used as a computational method to investigate macromixing flow patterns. Inert particles were defined to resemble fluid elements and have no influence on the flow. The trajectories of the fluid elements were followed during their movement with the average flow. Each trajectory was calculated by stepwise integration over discrete time steps. The effect of turbulent velocity fluctuations on the course of the fluid elements was not taken into account.

On their way through the Y-mixer the fluid elements encounter zones with different levels of turbulent energy dissipation and with different concentrations of the species A and B. A total number of 254 fluid elements were followed with their starting positions equally distributed over the inlet plane.

Trajectories for some fluid elements are shown in figure 2.4. For two fluid elements the levels of the energy dissipation rate and of the dimensionless product of the mass fractions of A and B are shown in figure 2.5. The mass fraction product was made dimensionless by dividing it by the product of its mean concentrations in the outlet tube. In these figures a value of 0 for this product means that only one of the species is present, a value of 1 means that both species are present in equal amounts. The mass fraction product is considered here as a measure for macromixing and the energy dissipation rate for micromixing.

The maximum level of energy dissipation experienced by the fluid elements during their way through the wide angle Y-mixer differs up to one order in magnitude, as can be seen in figure 2.5. For the fluid element on the left side, the zone of high-energy dissipation coincides with the zone with a high dimensionless mass fraction product. It is expected that in this zone the reactants mix effectively down to the molecular level.

The fluid element on the right side of figure 2.5 moves first through a zone with a very high rate of energy dissipation. However, in this zone the high energy dissipation rate does not contribute to the mixing because the mass fraction product remains zero, meaning that at macro-level the fluid element is still unmixed.

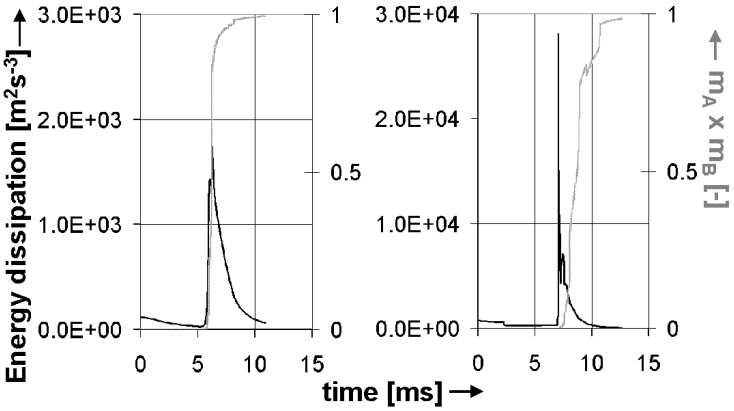

Figure 2.5 Plots of the energy dissipation rate (black line) and mass fraction product (gray line) encountered by two particles on their way through the wide angle Y-mixer.

The contour plots of the distribution of species A and B were used to define a 'residence time for effective macromixing' t_{rm} for the fluid elements on their way through the mixing geometry. The starting point for this time period is the point where the dimensionless mass fraction product exceeds an arbitrarily set value of $1 \cdot 10^{-8}$. Such a value may be used in future to define the supersaturation level. This period ends when a fluid element has left the simulated grid. It is stressed that at the endpoint of the grid mixing of the flows is not necessarily completed. In figure 2.6 these times are shown as a function of the starting positions of the fluid elements in the inlet plane.

The fluid elements starting near the wall have slightly longer residence times than those starting in the center. This is to be expected as the fluid elements follow the average flow velocities that are a bit lower near the wall compared to those in the center. Remarkable is that the macromixing residence times for the elements released in the top zone of the tube are about 2-3 times longer than those for elements in the rest of the tube. Their path through the stagnant top-zone of the Y-mixer causes these longer residence times. For our purpose of premixing two feed streams in this geometry before nucleation can take place, these fluid elements are to be considered with caution. If micromixing proceeds within this time period as well, undesired nuclei formation may take place in these elements before the bulk of the flow is mixed.

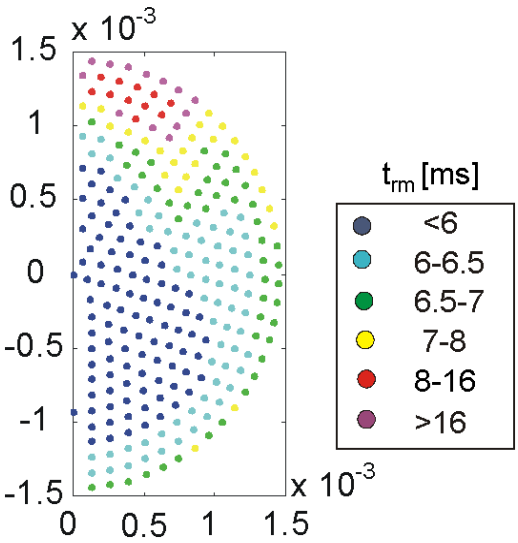

Figure 2.6 Distribution of macromixing residence times of the fluid elements as function of starting position.

The level of the energy dissipation rate encountered by the fluid elements can be followed over the whole residence time for effective macromixing. This was done for two characteristic time scales for mixing: the time scale for turbulent dispersion and for engulfment. For each fluid element these time scales, being functions of the local energy dissipation rate, were averaged over the residence time according to the flowing equation:

$$\bar{\tau}_m = \frac{\int_0^{t_{rm}} \tau_m(\varepsilon) dt}{t_{rm}} \tag{2.8}$$

In figures 2.7 and 2.8 the averaged time scales for turbulent dispersion and for engulfment for the 254 fluid elements are shown versus the macromixing residence time t_{rm}. At the diagonal line the averaged mixing times and the residence times are equal.

In this figure it can be observed that most of the fluid elements have residence times around 7 milliseconds, except the fluid elements caught in the top zone of the Y-mixer which have residence times 2-3 times longer.

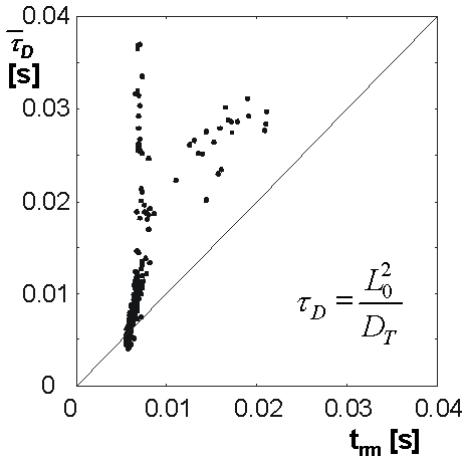

Figure 2.7 Averaged turbulent dispersion time as function of the macromixing residence time for 254 fluid elements.

Most of the points in figure 2.7 lie above the diagonal line, with the averaged turbulent dispersion times being longer than the residence times. This means that most of the fluid elements are not mixed at macroscale when they leave the outlet tube after a length of twelve diameters. This agrees with the contour plots of the mass fractions of the species A and B observed in figure 2.3.

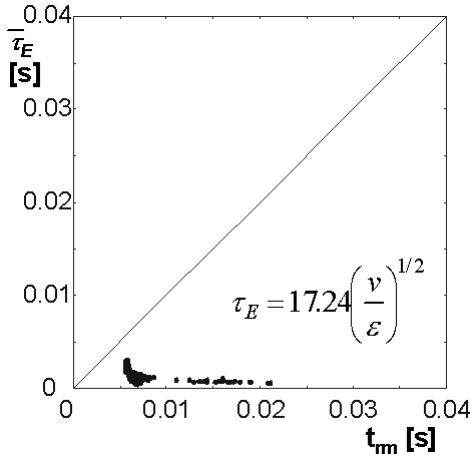

Figure 2.8 Averaged time for engulfment as function of the macromixing residence time for 254 fluid elements.

In figure 2.8 for all points that lie below the diagonal line, the averaged characteristic time for engulfment (micromixing) is smaller than the residence time. This means that mixing at micro scale is not limiting the

overall mixing process over the reference length of the outlet tube of twelve diameters.

2.4.4 Some remarks on the CFD simulations

In this study time-averaged flow simulations were carried out instead of time-dependent simulations because the flow in the wide angle Y-mixer is likely to be steady in time, e.g. non-oscillating. The k-ε turbulence model was selected assuming isotropic turbulence. The Reynolds Stress Model may be selected for flows with anisotropic turbulence, for example swirling flows.

The flow in the boundary layer was described by semi-empirical formulas or wall functions. The alternative to this approach is to resolve the flow in the near wall region down to the wall with modified turbulence models valid in this region and a sufficiently fine grid at the cost of increased computational resources.

Mixing of the non-reacting species A and B was followed at macro level. A typical grid cell is much larger than the length scales for micromixing with a cell dimension of $60 \cdot 10^{-6}$ m while typical Kolmogorov and Batchelor length scales are $6 \cdot 10^{-6}$ m and $0.2 \cdot 10^{-6}$ m respectively. To include micromixing within the grid cells a micromixing model should be introduced.

Particle tracking was carried out for fluid elements that followed trajectories calculated from average flow velocities. The random effect on the path of turbulent velocity fluctuations was not taken into account. Under the assumption that these are up to 15% of the mean velocity, they may have a significant effect on the trajectories. To include the effect of the velocity fluctuations an approach similar to that of Rielly and Marquis (2001) may be followed.

In future work it is tempting to study the effect on macromixing of an alternative turbulence model, of different boundary conditions and of velocity fluctuations on the track of fluid elements. Validation of the CFD simulations may be achieved by comparing the calculated pressure drop with experimental values.

2.5 Discussion

To measure nucleation rates of concomitant polymorphs complete mixing of the reactants creating supersaturation is desired before nucleation starts. The question is whether or not the wide angle Y-mixer

is suitable for this purpose. The time scales from section 3, based on an estimate of the average dissipation rate, do not correspond with the averaged time scale distributions from section 4. From time scale analysis one may conclude that the geometry is suitable, with macromixing being the limiting step. From the CFD simulation however, it follows that macromixing is not completed over a length of the outlet tube of twelve diameters (corresponding with a residence time of approximately $6 \cdot 10^{-3}$ s). Although very high energy dissipation rates are achieved in this Y-mixer, fluid elements moving through this geometry only experience these high rates during very short times and partially also in zones where only one of the species is present.

To improve mixing a few options exist. First, to enhance macromixing in the outlet tube a static mixer can be inserted. This is however a costly improvement because the pressure drop over the wide angle Y-mixer is expected to increase approximately 100 times. Furthermore, there may be small stagnant zones in a static mixer, giving rise to long residence times for fluid where undesired nucleation may occur.

Another way to make the mixing process more efficient is to enlarge the zones where both species are present in combination with a high energy dissipation rate (e.g. the collision plane) while reducing the zones that have high energy dissipation rate but lack either one of the species (downstream the edges between inlet and outlet tubes). This may be achieved by decreasing the angle between the inlet tubes. This may also reduce the stagnant zone in the top of the wide angle Y-mixer. The angle should not be too narrow because the flows should still collide with sufficient impact. The Roughton mixer can be considered as an extreme case of such a mixing device. In this geometry the inlets are mixed with a swirling flow while edges near wall (and stagnant zones) have disappeared. Both alternative geometries are shown in figure 2.9.

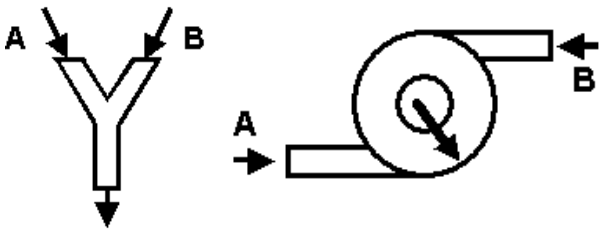

Figure 2.9 Alternative mixers: a. narrow angle Y-mixer and b. Roughton mixer.

These options support the need for additional simulations in combination with experimental validation by comparison with the measured pressure drop over the Y-mixer.

The effect of mixing rate on the average size of precipitates was observed experimentally by Schwarzer and Peukert (2002) and by Baldyga and Orchiuch (2001) for Barium Sulfate and by Manth and Mognon (1996) for Strontium Sulfate. By increasing the Reynolds number to a sufficiently large value the CSD does not change anymore. It may be concluded that up from these values the effect of mixing on the formation of the crystals has disappeared. It is not clear yet whether the increase of the mixing intensity results in complete premixing of the reactants before nuclei form or that some kind of mixing limitation was overcome. These experiments were done with insoluble, rapidly precipitating inorganic compounds. Nucleation may start at the interface between fluid elements of the reacting species before these are completely mixed.

Rieger et al (2002) analyzed precipitates of Boehmite and an organic pigment shortly after mixing. Cryo-TEM images showed two-phase liquid regions shortly ($1 \cdot 10^{-2}$ s) after mixing. The authors found that nucleation had taken place at the interface between the regions. If this behavior applies to all precipitates, the method proposed in this paper to separate in time and place the creation of supersaturation (chemical reaction) from nucleation (physical reaction) may be not possible. However, this phenomenon may be limited to very rapidly precipitating (very insoluble) compounds. In-line measurement of the composition of reaction mixtures and of the processes taking place directly after mixing the reactants may give more answers.

2.6 Conclusions

The measurement of nucleation rates of concomitant polymorphs requires that complete mixing precedes nucleation. This means that the time scale for mixing must be smaller than the time scale for nucleation. Two analyses were performed to verify whether this condition was met in a wide angle Y-mixer. First mixing time scales were estimated as a function of the average dissipation rate of turbulent kinetic energy. These times were compared to the residence time for the flow through the outlet tube. The time for turbulent dispersion (macromixing) was the rate-determining step being of the same order as the residence time. Therefore, mixing was complete over a length of the outflow tube equal to twelve times its diameter.

However, CFD simulations of the mixing process in the wide angle Y-mixer revealed large spatial differences in energy dissipation rate. There were zones observed with high energy dissipation rates where no mixing occurred because either one of the species was lacking. By means of

particle tracking two averaged characteristic mixing times were calculated and compared to effective residence times for macromixing. From the simulations it followed that turbulent dispersion was not complete at the end of the outlet tube. Macromixing may be improved by introducing a static mixer in this tube.

2.7 Acknowledgements

The authors wish to thank Aimée Tan for her contribution and are grateful to Akzo Nobel, BASF, Bayer and DSM for their support. This project is part of the M3 program of the Delft University of Technology.

2.8 References

Angerhöfer, M., Untersuchung zur Kinetik der Fällungskrustallisation von Bariumsulfat, Thesis, Technische Universität München (1994)

Baldyga, J.; J.R. Bourne, Turbulent Mixing and Chemical Reactions, Wiley, Chichester (1999)

Baldyga,J.; W. Orchiuch, Chem. Eng. Sci. 56 (2001) 2435

Bernstein, J.; R.J. Davey, J.O. Henck, Angew. Chem. Int. Ed. 38 (1999) 3440

Haselhuhn, F.; M. Kind, in Proc. of the 15th Int. Symp. on Ind. Cryst. (Ed: A. Chianese), AIDIC, Milano (2002)

Horst, J.H. ter; H.J.M. Kramer, P.J. Jansens, Cryst. Growth Des. 2 (2002) 351

Mahajan, A.M.; D.J. Kirwan, J. Cryst. Growth 144 (1994) 281

Manth, Th.; D. Mignon, H. Offermann, Chem. Eng. Sci. 51 (1996) 2571

Nielsen, A.E., Acta Chem. Scand. 15 (1961) 441

Nielsen, A.E., Kinetics of Precipitation, Pergamon, Oxford (1964)

Rieger, J.; D. Franke, T. Frechen, H. Haberkorn, W. Goesele, in Proc. of the 9th Int. Workshop on Ind. Cryst.(BIWIC) (Ed: J. Ulrich), Halle (2002)

Rielly, C.D.; A.J. Marquis, Chem. Eng. Sci. 56 (2001) 2475

Schubert, H.; A. Mersmann, Trans IChemE 74A (1996) 821

Schwarzer, H.C.; W. Peukert, Chem. Eng. Technol. 25 (2002) 657

Shekunov, B.Yu.; J. Baldyga, P. York, Chem. Eng. Sci. 56 (2001) 2421

Ståhl, M.; B.L. Åslund, Å C. Rasmuson AIChE J. 47 (2001) 1544

2.9 List of symbols

A	[m^{-3} s^{-1}]	pre-exponential kinetic parameter
c_i	[-]	geometrical factor for surface area
c_{eq}	[moles kg^{-1}]	solubility per kg solvent
D	[m]	tube diameter

D_m	[m^2 s^{-1}]	molecular diffusion coefficient
D_T	[m^2 s^{-1}]	turbulent diffusion coefficient
E	[s^{-1}]	engulfment rate
f	[-]	friction factor
G	[m s^{-1}]	growth rate
J	[m^{-3} s^{-1}]	nucleation rate
k	[m^2 s^{-2}]	turbulent kinetic energy
k_B	[J K^{-1}]	Boltzmann constant
L_0	[m]	initial length scale for turbulence
P	[N m^{-2}]	pressure
Re	[-]	Reynolds number
S	[-]	supersaturation
Sc	[-]	Schmidt number
Sc_T	[-]	turbulent Schmidt number
T	[K]	temperature
t_{rm}	[s]	residence time for effective macromixing
u	[m s^{-1}]	average flow velocity
u'	[m s^{-1}]	mean root square of the turbulent velocity fluctuation
V	[m^3]	volume
Γ	[-]	dimensionless overall interfacial energy
γ_i	[N m^{-2}]	interfacial energy
ε	[m^2 s^{-3}]	energy dissipation rate [W kg^{-1}]
ϕ_v	[m^3 s^{-1}]	flow rate
η_B	[m]	Batchelor length scale
η_k	[m]	Kolmogorov length scale
ν	[m^2 s^{-1}]	kinematic viscosity
ν_m	[m^3]	molecular volume
ν_T	[m^2 s^{-1}]	turbulent viscosity
ρ	[kg m^{-3}]	density
τ_D	[s]	time scale for turbulent dispersion
τ_{diff}	[s]	time scale for molecular diffusion
τ_E	[s]	time scale for engulfment
τ_r	[s]	mean residence time
τ_s	[s]	time scale for disintegration of large eddies

Chapter 3

Development of an experimental method to measure nucleation rates in reactive precipitation

Cryst. Growth Des. 4 (2004) 921-928

Measurement of the stationary nucleation rate as a function of supersaturation in reactive precipitation requires that nucleation and growth of the crystals to an observable size take place under well-controlled hydrodynamic conditions and at a constant supersaturation. An experimental method was chosen that is based on the measurement of the increase of the particle concentration with increase of the residence time in a precipitation tube. This method was applied to measure the nucleation rate for the pH-shift precipitation of the molecular compound H_4EDTA. The parameters A and B in the classical nucleation theory equation were derived from the measured nucleation rates. A value of $A=(5.7\pm1.0)\cdot10^{15}$ $m^{-3}s^{-1}$ was found for the intercept with the ordinate and a value of $B=(3.3\pm2.0)\cdot10^{2}$ for the slope. The estimated value for parameter A is lower than the theoretical value of $A_{HON}=10^{33}$ $m^{-3}s^{-1}$ for homogeneous nucleation. Using the experimentally determined value for B the interfacial energy is found to be $\gamma=21\pm9$ mJ m^{-2} compared to a theoretical value of $\gamma_{HON}=38$ mJ m^{-2} based on bulk properties. The experimentally obtained values for A and γ indicate heterogeneous nucleation.

3.1 Introduction

For precipitation processes it is generally hard to control crystal properties such as polymorphic structure, crystal morphology and crystal size distribution. Regulating authorities and customer demands put increasingly severe restrictions on these properties. In batch vessels that are typically applied large variations in the level of driving force occur both in space and in time. This was for instance, illustrated by Van Leeuwen (1998) for the precipitation of $BaSO_4$ at the inlets in stirred vessels. The strongly non-linear dependence of the nucleation rate on supersaturation combined with the large variations in this supersaturation explains the difficulty in achieving control over crystal

properties. Furthermore, scale-up of this type of processes requires considerable experimental effort as the change in the nucleation rate is virtually impossible to predict. The first step towards control over the properties of precipitated materials is to obtain control over the primary nucleation process. This requires reliable measurements of nucleation rates as a function of an unchanging local supersaturation.

In this study the nucleation rate of an organic model compound as a function of supersaturation is measured. In a Y-shaped mixing chamber two solutions of the sodium salt of EDTA and of diluted sulfuric acid are rapidly mixed. The neutralization reaction is assumed to take place instantaneously. The mixing performance of the mixing chamber was discussed by Roelands (2003). Because the reaction product H_4EDTA has a very low solubility a large driving force for precipitation is created. In the outlet tube of the Y-shaped mixing chamber crystals nucleate and grow in the turbulently flowing solution. The precipitating mixture was diluted to stop further nucleation and the particle number concentration was measured. Because conversion in the tube remained low ~1% the driving force was constant over the length of the tube. This enabled measurement of the stationary nucleation rate. From the increase in the particle number concentration at the end of the tube with increasing residence time the nucleation rate was calculated. This was done for three different levels of the supersaturation ratio. The results were fitted against the classical nucleation theory in order to determine the parameters in the nucleation rate equation.

3.2 Theory

3.2.1 Classical nucleation theory

A recent review paper Kashchiev and Van Rosmalen (2003) evaluates the classical nucleation theory (CNT) for precipitation from solution. In supersaturated solutions primary nucleation takes place according to either a homogeneous or a heterogeneous mechanism. In pure solutions consisting of solvent and solute molecules only, homogeneous nucleation (HON) occurs when solute molecules form a cluster that exceeds the critical nucleus size. Heterogeneous nucleation (HEN) takes place in solutions that contain foreign substrates that provide active centers for nucleation.

The driving force for nucleation of a molecular compound is defined as the difference in chemical potential between a molecule in solution and in the bulk of the crystal phase:

$$\Delta\mu = \mu_s - \mu_c = kT \ln S \tag{3.1}$$

The supersaturation ratio is defined as the ratio of the actual activity in solution of the crystallizing compound over the equilibrium activity according to $S_a = a_0/a^*$. It is assumed that under equilibrium conditions the activity for the solid crystal phase is equal to the activity of the solute in solution. For sufficiently dilute solutions where the activity coefficient is close to one conform to the asymmetric convention and for very low supersaturations where actual and equilibrium concentration are almost equal it is common practice to define the supersaturation ratio using experimentally measurable concentrations. The supersaturation ratio is then equal to the ratio of the concentration of the dissolved molecular compound over the solubility: $S_c = c_0/c^*$. Precipitation usually takes place at high supersaturation so the use of the definition S_a based on activities is recommended. The CNT describes the nucleation rate as a function of the supersaturation according to equation (3.2).

$$J = AS\exp\left(-\frac{B}{\ln^2 S}\right) \tag{3.2}$$

A straight line can be obtained when measurements of the nucleation rate at different levels of supersaturation under isothermal conditions are plotted according to:

$$\ln\ J/S = \ln A - \frac{B}{\ln^2 S} \tag{3.3}$$

The pre-exponential kinetic parameter A follows from the intercept of the line with the ordinate while the slope of the line delivers the parameter B. The value of the pre-exponential kinetic parameter A gives information whether the nucleation occurs homogeneously or heterogeneously. The pre-exponential parameter A is calculated as the product of the Zeldovich-factor, equilibrium attachment frequency and the concentration of nucleation sites. For homogeneous nucleation the concentration of nucleation sites is taken to be the inverse molecular volume of the crystalline compound since a nucleus can be formed anywhere in the solution.

According to Kashchiev and Van Rosmalen (2003) A_{HON} has a value in the order of 10^{30}-10^{35} for homogeneous nucleation. For heterogeneous nucleation A_{HEN} is related to the number of heterogeneous nucleation sites and has a value in the range of 10^{15}-10^{25}. For homogeneous nucleation of spherical nuclei the parameter A_{HON} is given by the following two equations for volume-diffusion or surface-integration

control, that are respectively approximately and strictly independent of S:

$$A_{HON,D} = \left(\frac{kT}{\nu^2\gamma}\right)^{1/2} DC_e \ln S \tag{3.4a}$$

$$A_{HON.I} = \left(\frac{4\pi}{3\nu}\right)^{1/3} \left(\frac{\gamma}{kT}\right)^{1/2} DC_e \tag{3.4b}$$

The exponential factor B incorporates the effect of the interfacial energy between crystal and solution. The interfacial energy can be estimated from the experimentally determined value for B if a value for the shape factor is assumed. Assuming spherical nuclei again the following relationship is obeyed:

$$B = \frac{16\pi}{3} \frac{\nu^2 {\gamma_{eff}}^3}{(kT)^3} \tag{3.5}$$

This measured value for γ_{eff} can be compared to an estimate γ_{HON} based on bulk properties of the crystal where also the nuclei are assumed to have a spherical shape (β=0.514):

$$\gamma_{HON} = \beta kT \frac{1}{\nu^{2/3}} \ln \frac{1}{\nu C_e} \tag{3.6}$$

In case of heterogeneous nucleation the effective interfacial energy γ_{eff} is used that takes into account the interfacial energies between substrate and solution and between cluster and substrate as well as the interfacial energy between cluster and solution. For the heterogeneous mechanism to be dominant the term in the exponent B_{HEN} should be smaller than B_{HON} because the pre-exponential term $A_{HEN} << A_{HON}$. This implies that $\gamma_{eff} < \gamma_{HON}$.

Furthermore, the estimate of parameter B can be used to calculate the nucleation work according to equation (3.7) and the nucleus size according to the Gibbs-Thomson equation (3.8):

$$\frac{W^*}{kT} = \frac{B}{\ln^2 S} \tag{3.7}$$

$$n^* = \frac{2B}{\ln^3 S} \tag{3.8}$$

3.2.2 Development of the experimental method

Nielsen (1961, 1964, 1967, 1969) adapted a stopped-flow type technique to measure chemical reaction rates for precipitation kinetics. A good overview of this approach to measure nucleation rates is given by Garside et al (2001). Two flows of reactant solutions are mixed in a mixing-tee. After mixing the concentration of the reaction product exceeds the solubility so the driving force for precipitation is created. In the tube the molecules of the supersaturated compound will cluster into nuclei that start to grow. At the end of the tube the number of particles could be counted directly using a microscope.

This method was followed mainly for ionic crystals: Mohanty (1988), Angerhoefer (1994) and Schubert (1996) for Barium Sulfate, Eble (2000) for Alumina, Andrieu (1999) for Uranium Oxalate, Salvatori (2002) for Barium Carbonate and Sellami (1999) for Calcium Carbonate. Molecular crystals of Benzoic Acid were studied by Stahl (2001) and of Salicylic Acid by Blandin (2001). In these cases the reacting suspension of particles was quenched in an excess volume of saturated solution in order to stop further nucleation while preventing re-dissolution of the crystals. From the quenched suspension samples were taken to measure the particle number concentration.

A point of attention of this method is that in practice a detection limit exists for the particles depending on the measurement technique that is applied. Particles that are smaller than this limit remain undetected and this causes an underestimate again. Schubert (1996) described a method to grow these undersize particles into an observable range at a low supersaturation level in order to prevent further nucleation. However, in this case agglomeration took place as well and this reduced the effective number of particles being counted.

For correct measurements constant supersaturation has to be created instantaneously in a rapid mixing device. However, for very rapidly precipitating systems nucleation may be so fast that nuclei will already form at the interface between fluid elements of the two solutions while these are being mixed. Within this boundary layer a concentration profile exists due to diffusion so the nucleation process takes place at non-stationary supersaturation levels. For precipitation of Barium Sulfate from a tee-mixer Schwarzer and Peukert (2002) observed a decrease in particle size and an increase in number of particles with increasing Reynolds-number (mixing intensity). Manth and Mignon (1996) observed a similar change in CSD with Reynolds-number for Strontium Sulfate. Haberkorn et al (2003) found for very rapidly precipitating systems like Alumina and the pigment Quinacridone that

upon mixing at first a liquid-liquid phase split occurred with nucleation of amorphous solid at the interface followed by a transition to crystalline phase. For such compounds and conditions the measured nucleation rates will not be free of the effect of mixing because of the variations in the supersaturation.

Furthermore, when after nucleation the crystals start to grow they are consuming supersaturation so over the length of the tube the supersaturation will decrease. This results in a rapid decrease of the nucleation rate with position in the tube. To account for this reduction Nielsen (1961) originally defined the measured nucleation rate as the particles number concentration divided by induction time. The induction time is the time required to observe particles after creation of supersaturation. The induction time is inversely proportional to the nucleation and to the crystal growth rate according to $t_{ind} \sim (JG^3)^{-1/4}$ (Kashchiev and Van Rosmalen 2003). Experimentally, with increasing supersaturation, a decrease in induction time was observed proportional to the decrease in nucleation rate.

For low concentrations the induction time was measured in the stagnant mixture (stopped-flow) while for high concentrations it was measured while the mixture was still flowing (continuous-flow). According to Nielsen (1967, 1969) the crystal growth mechanism is diffusion-limited. Turbulent mixing will improve diffusion and therefore enhance the growth rate. Because the growth rates are different in a turbulently flowing mixture compared to the stagnant mixture the induction time measurements are likely to be influenced by the mixing conditions.

Nielsen (1967, 1969) later defined the number of particles observed as the integral of the nucleation rate from the moment the flows were mixed until the induction time. It was assumed that over this time period the nucleation rate had become zero because supersaturation decreased due to growth of the nuclei. In the calculation of the nucleation rate a model for diffusion-controlled crystal growth was included to take this decrease in supersaturation into account.

Angerhoefer (1994), Schubert (1996), Eble (2000), Andrieu (1999), Sellami (1999) and Salvatori (2002) precipitated ionic crystals in a plug-flow type tube reactor. Their method has the advantage that all crystals nucleate and grow under identical flow conditions. The mixture coming from the tube was rapidly diluted to prevent further nucleation. The nucleation rate was defined as the measured particle number concentration divided by a characteristic residence time for the flow in the tube. The rate of depletion of supersaturation over the length of the

tube is unknown but the decrease in nucleation rate may be large. Because nucleation may be restricted to the first part of the tube the use of the residence time over the whole tube to calculate the nucleation rate may result in an underestimation of the nucleation rate.

Ståhl (2001) and Blandin (2001) precipitated molecular crystals in a plug-flow type tube reactor. The parameters for nucleation and growth were derived by fitting measured Crystal Size Distributions to a precipitation model based on population balances including nucleation and growth and sometimes secondary processes like agglomeration.

Mahajan (1993, 1994) described an approach based on stationary nucleation and growth rates in a plug-flow type tube reactor. A prerequisite of this method is a constant supersaturation level over the length of the tube. Figure 3.1 shows schematically the principle of this method. With increasing residence time in the tube (length of the tube) the particle concentration increases linearly. The nucleation rate is the slope of a straight line fitted through the particle concentration versus residence time.

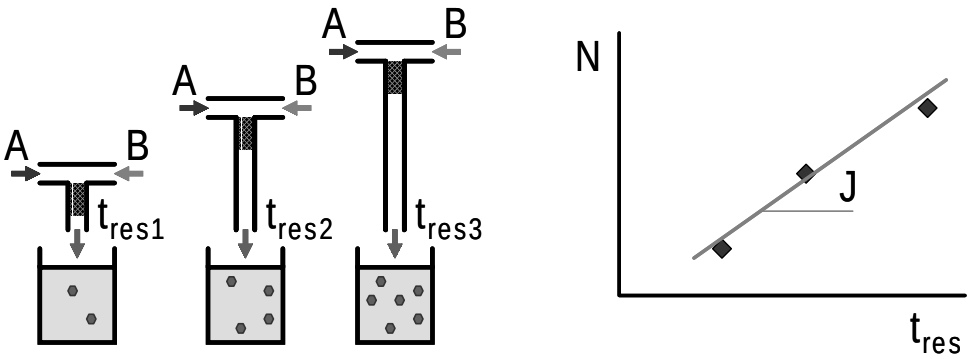

Figure 3.1 Schematic representation of the method applied to measure nucleation rates based on incremental increase of the particle concentration with residence time.

These methods are restricted to an operating window formed by on the one hand mixing and reaction times and on the other hand the range of supersaturation. In figure 3.2 the operating window of the method is shown. The induction time decreases with increasing supersaturation. The lower limit for the experiments is formed by the time required to mix the reactants completely. During this time period no nucleation is allowed. The upper limit is formed by the experimental residence time in the tube. This should be sufficiently long for the nuclei to grow towards an observable size.

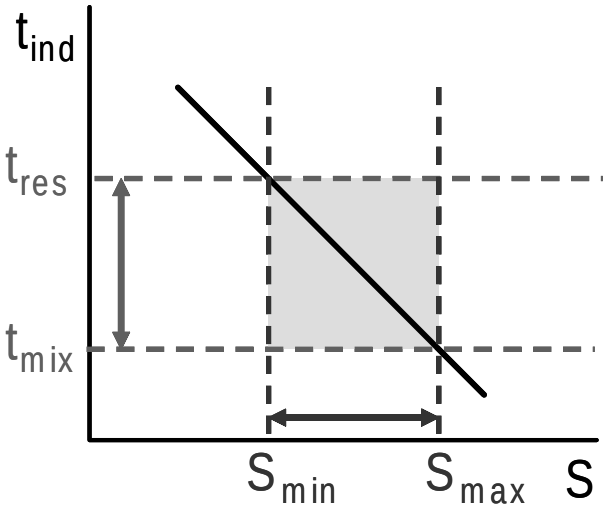

Figure 3.2 The experimental method is limited by the induction time which is a function of the supersaturation, the time required to achieve complete mixing of the reactants and the residence time in the tube.

In this study the method described by Mahajan (1993, 1994) was in general followed because nucleation and growth take place under well-defined flow conditions. Furthermore, the measurement of the increase in the particle number concentration with residence time in the tube allows the calculation of the stationary nucleation rate without the use of a complex precipitation model. However, this is only allowed when the supersaturation ratio remains approximately constant over the whole residence time in the tube.

3.3 Experimental procedure

3.3.1 Model compound

In this study H_4EDTA ($C_{10}H_{16}N_4O_8$) was used as model compound. This food additive and sequestrant is non-toxic, biodegradable and relatively cheap. H_4EDTA was precipitated from aqueous solutions of Tetra Sodium EDTA and diluted Sulfuric Acid according to the following equation:

$$EDTA^{4-}(aq) + 4\,H^{+}(aq) + 4\,Na^{+}(aq) + 2\,SO_4^{2-}(aq) \Leftrightarrow$$
$$H_4EDTA(aq) + 4\,Na^{+}(aq) + 2\,SO_4^{2-}(aq) \Leftrightarrow$$
$$H_4EDTA(s)\downarrow + 4\,Na^{+}(aq) + 2\,SO_4^{2-}(aq)$$

It is assumed that the H_4EDTA molecule is the building block in crystallization. In solution between pH-values of 1 and 3 the H_4EDTA-species is present in the form of a Zwitter-ion. With the speciation software package Streamanalyzer (OLI Systems, Morris Plains, New Jersey) it was possible to estimate the fraction of the molecules present in solution as H_4EDTA-species. Equilibrium speciation in solution is calculated using the Helgeson equation of state. Activity coefficients were calculated using an equation that includes a Debye-Hückel and a Bromley-Zemaitis term. This enabled the calculation of the activity at equilibrium. For the actual activity the solid species H_4EDTA was excluded from the simulation under the assumption that speciation under non-equilibrium conditions is equal to speciation under equilibrium conditions. The results for the actual and equilibrium activities of the H_4EDTA-species were combined to calculate the supersaturation ratio S_a.

Figure 3.3 shows the speciation in a 0.01 molal solution of Tetra Sodium EDTA as a function of increasing Sulfuric Acid concentration for the initial and the equilibrium state. The simulation in the initial state, without H_4EDTA-crystals, shows that the maximum fraction of EDTA present in the form of the H_4EDTA-species in solution is approximately 40%. From the simulation at the equilibrium state it can be observed that at equimolar ratio Sulfuric Acid/EDTA the solubility for EDTA (dashed line) is strongly dependent on Sulfuric Acid concentration. This is due to incomplete dissociation of the Hydrogen Sulfate ions at this pH-level. Therefore it was decided to carry out the experiments at a higher Sulfuric Acid to EDTA molar ratio of 2.4:1 because under these conditions the solubility of EDTA depends less on small variations in reactant ratio. This would improve the stability of the suspension samples quenched in saturated solution. Because of the lower solubility for EDTA at the corresponding pH level of 2.0 the driving force is also larger compared to the equimolar situation at pH=2.9.

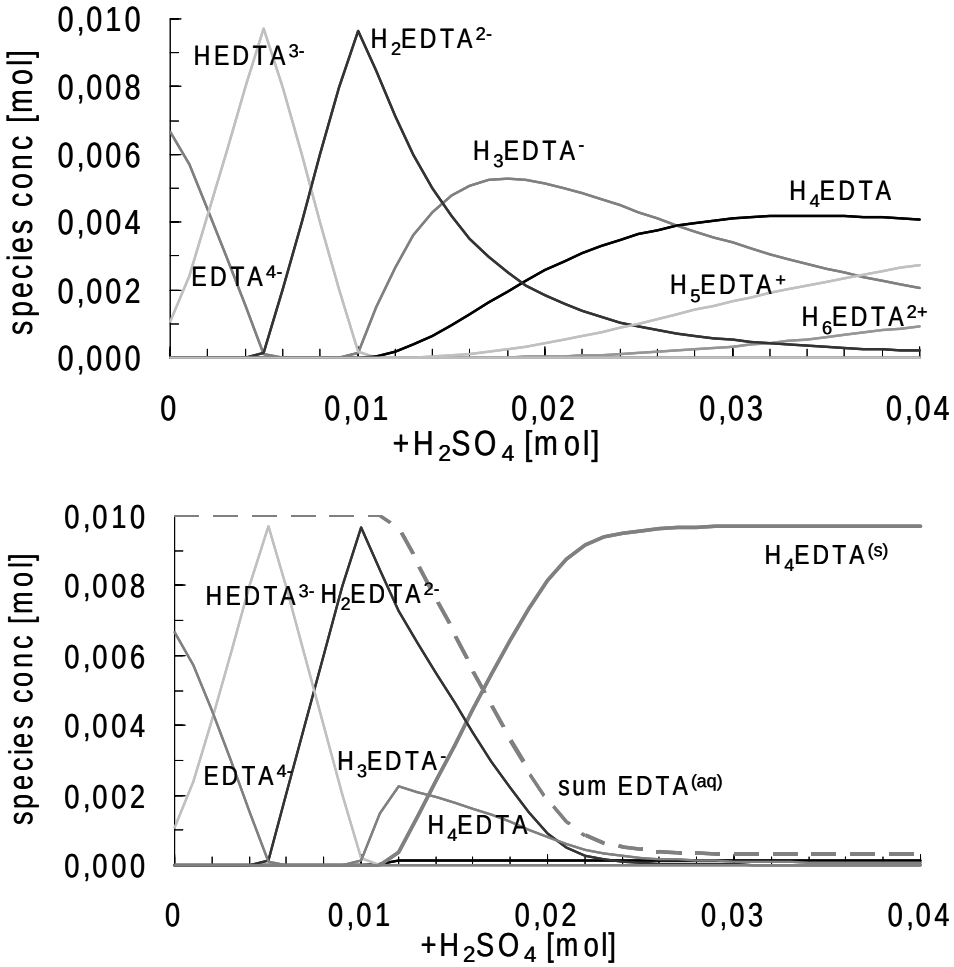

Figure 3.3 Speciation in a 0.01 molal solution of Tetra Sodium EDTA as a function of the Sulfuric Acid added calculated with Streamanalyzer software. Top: without solids. Bottom: with solids. The dashed line represents the overall solubility of H_4EDTA.

For the experiments an aqueous solution of Sodium EDTA was prepared by dissolving Tetra Sodium EDTA.$4H_2O$ crystals (Sigma-Aldrich, Steinheim, Germany) in ultra pure water (Elga systems, conductivity 18MΩ). After 24 hours the solution was filtered over a 0.22 μm filter (Millipore, Molsheim, France). Sulfuric Acid 95-98% (Baker, Deventer, Netherlands) was diluted with ultra pure water and filtered over a 0.22 μm filter as well. Five aqueous solutions of Tetra Sodium EDTA with concentrations between 0.074 and 0.106 molal were prepared. Diluted Sulfuric Acid solutions in an excess molar ratio 2.4:1 were added with concentrations of in the range of 0.17 to 0.25 molal H_2SO_4. The

corresponding values for the supersaturation ratio based on the activities of the H_4EDTA species as calculated with the Streamanalyzer software varied from $S_{a=}1.1 \cdot 10^2$ to $1.7 \cdot 10^2$ while the values based on overall concentrations c_0 and c^* were in the range of $S_c=1.0 \cdot 10^2$ to $1.7 \cdot 10^2$. In this case the difference between S_a and S_c values was small because the calculated fraction of the H_4EDTA-species at the actual concentration was almost identical to the fraction at equilibrium. In this paper the activity based values for the supersaturation were used.

3.3.2 Experimental set-up

From two storage vessels aqueous solutions were pumped through a wide-angle Y-mixer (160° between inlets) with both inlets and outlet having the same internal diameter of 3 mm. The symmetric construction of the wide-angle Y-mixer required equal mass flow rates. From the Computational Fluid Dynamics study of the mixing behavior in this geometry by Roelands (2003) it was concluded that mixing would be insufficiently fast in this device. Therefore in the study presented in this paper a static mixer (SMX Sulzer, Winterthur, Swiss) was implemented in the outflow tube of the wide angle Y-mixer directly after the mixing point. It was assumed that nucleation would only start after the solutions had passed the static mixer with a residence time of 3.5 ms. Both the Y-mixer with static mixer and without this device were tested.

To create stable and equal flow rates low-pulse MAAG gear pumps (MAAG, Zürich, Swiss) were applied in combination with pulsation dampeners. The flows were controlled using a feed-forward type of control based on the signal from Coriolis-type mass-flow meters (Emerson, Rijswijk, Netherlands). Signals were processed through the Fieldpoint system in a Labview program with PID controllers. The flow rate was set at 0.6 kg min^{-1} for each pump. The variation in the logged flow rate was approximately 1 percent. The tube diameter was 3 mm so the Reynolds number in the tube was approximately 8500 for water. Under these conditions fully developed turbulent plug-flow may be assumed. Four different tube lengths of 0.5, 1, 2 and 6 m were used with additional 0.2 m for the sampling hose. At a flow velocity of 2.8 m s^{-1} the average residence times in the tubes were 0.25, 0.43, 0.78 and 2.2 s.

3.3.3 Sampling and measurement

Solutions saturated with respect to H_4EDTA were prepared by dissolving H_4EDTA crystals (Sigma-Aldrich, Steinheim, Germany) in a solution with Sodium Sulfate concentrations corresponding to the mixture of Tetra Sodium EDTA and Sulfuric Acid solutions. The pH was adjusted to 2.0

using 1 molal Sulfuric Acid. After 24 hours of stirring using a magnetic stirrer the suspension was filtered over a 0.22 μm filter. For each particle number measurement a sample of the flow of approximately 3 g was collected manually in a beaker filled with 150 g saturated solution. The exact sample mass was determined by weighing the beaker glass before and after the sample was added.

The ratio of sample to quench was determined by repeating the particle number concentration after 30 minutes. For the range of supersaturations used in this study this number remained constant with time for a ratio of 1:50 so this ratio was further used. This time period of 30 minutes was sufficient to process the samples in the particle counter. For a smaller ratio of 1:10 the number increased with time indicating that the suspension was not sufficiently diluted to prevent additional nucleation.

The particle number concentration of the diluted suspension was measured using a Pamas PMT2100 particle counter (Pamas, Rutesheim, Germany) in combination with an HCB50-50 sensor. This instrument works according to the principle of obscuration of a laser beam by particles flowing between a laser and a photo diode. The instrument was calibrated by the manufacturer for a size range of 1-200 μm using spherical latex particles for a constant suspension flow rate of 25 ml min^{-1}. From previous experiments the shape of H_4EDA crystals was known to be rod-like and not spherical so this might introduce an error in the crystal size distribution. However, in this study only the number concentration was considered. The maximum acceptable particle number concentration for this type of measurement is $2.4 \cdot 10^4$ ml^{-1} with 6% error due to coincidence. Typical particle concentrations are in the order of 10 ml^{-1} for ultra pure water and 10^2-10^3 ml^{-1} for saturated solutions filtered over a 0.22 μm filter. From each sample of quenched suspension the number of particles was counted three times for 10 ml each time. The particle number concentrations in the samples were corrected for the particle concentration in the saturated solution.

After starting the flows through the mixer it took less than 10s to reach the set value. During the next one or two minutes the number of rpm of the gear pumps slowly and gradually increased while the flow rates remained constant. The rpm increase is presumably caused by an increase in the pressure drop over the tube due to scaling on the tube walls. After the maximum number of rpm of the pump was reached, the flow rate could not be maintained. The time period available to take samples was therefore in the order of minutes.

To find out whether scaling would influence the nucleation rate measurements its effect on the particle number concentration and on the level of supersaturation were studied. Suspension samples were collected at different time intervals: t=20, 40 and 60s. Both the particle number concentration and the particle density of the samples were found to be identical for all time intervals. Furthermore, the EDTA-concentrations of the feed flow entering the Y-mixer and of the flow exiting the tube were measured by titration. If the scale layer would deplete supersaturation, a significant drop in concentration would be expected.

However, the EDTA-concentration of three samples taken at different time intervals: t=20, 40 and 60s remained constant at the expected level of effectively half the concentration of the feed flow entering the Y-mixer. The mass of the crystals leaving the tube was less than 1% of the EDTA supplied in solution. It therefore can be concluded that the supersaturation over the length of the tube remained constant. Finally, because the stainless steel pipes applied in this study had a rather rough inner wall surface, the precipitate was compared to crystals obtained using smoother PFA-polymer tubing. In both cases scaling was observed. Both the particle number concentration and the particle density were identical. From these observations it was concluded that scaling at the tube wall did not influence the measured precipitation kinetics.

3.4 Results

3.4.1 Solubility measurement

The solubility of H_4EDTA at the iso-electrical point pH=2.8 was measured as a function of the concentration of Sodium Sulfate in the background. This is shown in figure 3.4. H_4EDTA crystals were dissolved in solutions of Sodium Sulfate and after 24 hours of stirring the suspensions were filtered. The EDTA concentration in the solutions was determined by potentiometric titration with a solution of Ferric Chloride. The results are shown in figure 3.4. An increase in solubility was observed from $1.2 \cdot 10^{-3}$ molal for pure water to $5 \cdot 10^{-3}$ molal for 0.2 molal Sodium Sulfate. The solubility of H_4EDTA under these conditions was also calculated using Streamanalyzer software. Good agreement between measured and calculated solubility was found in the range from 0 to 0.2 molal Sodium Sulfate. The experiments described in this paper were carried out at a lower pH of 2.0 because of the improved stability of the sample suspensions. A solubility for H_4EDTA of about $0.5 \cdot 10^{-3}$

molal sufficiently independent of the Sodium Sulfate concentration was both calculated and experimentally observed.

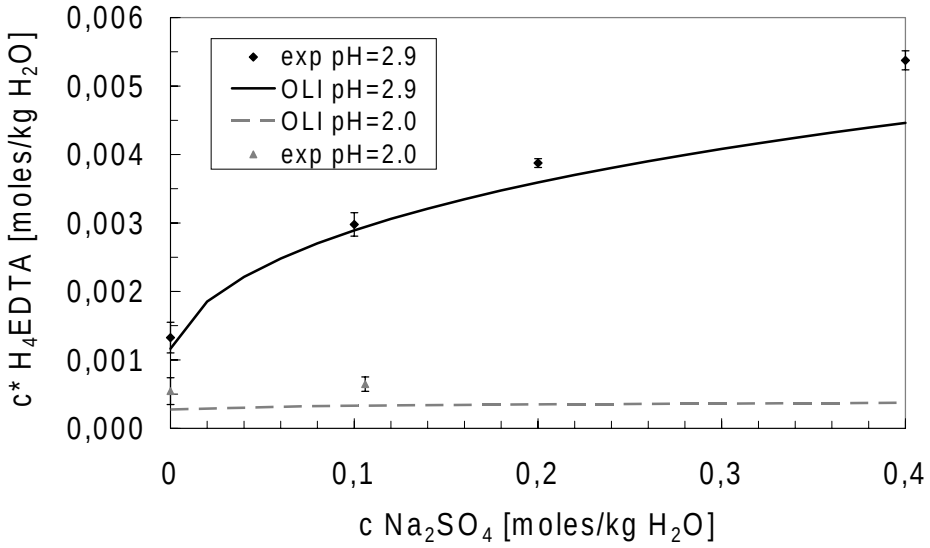

Figure 3.4 Solubility of H_4EDTA in water as a function of Sodium Sulfate concentration and of pH. The markers represent measured data at pH=2.9 and at pH=2.0, the lines represent calculations with Streamanalyzer software for pH=2.9.

3.4.2 Mixing effects

The wide-angle Y-mixer was tested both with static mixer in the outlet tube and without this device for the precipitation of H_4EDTA. For $S=1.6\cdot10^2$ and $\tau=2.2$ s a large increase was observed in the particle concentration from $7\cdot10^4$ to $4\cdot10^6$ ml^{-1} upon using when the static mixer. The effect of an increase in flow rate and therefore in mixing intensity was tested for the mixing chamber combined with static mixer. Figure 3.5 shows the resulting particle number concentration versus the Reynolds number of the flow in the outlet. The experiment was done for $S=1.3\cdot10^2$ and $\tau=2.2$ s. A change in Reynolds number from 6500 to 9000 did not result in a significant change in the number of particles. It can be concluded that the mixing chamber with static mixer is sufficiently effective to mix the reactants preceding nucleation at Reynolds number above 6500.

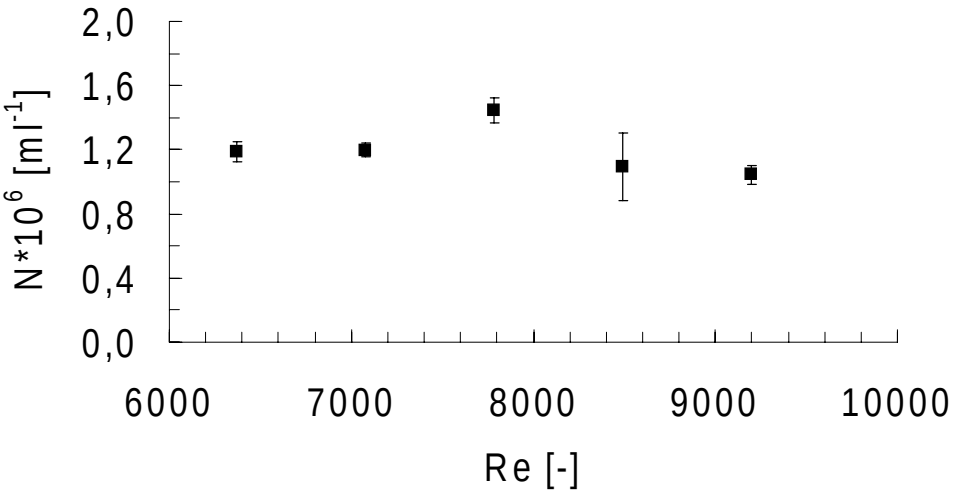

Figure 3.5 Particle concentration as a function of the Reynolds number of the flow in the outlet tube with $S=1.3\cdot10^2$. Error bars represent standard deviations for the measurements.

3.4.3 Nucleation rate measurements

The nucleation rate was determined for five different initial concentration levels: 0.036, 0.041, 0.042, 0.051 and 0.053 molal EDTA in the reaction mixture with corresponding supersaturation ratios of $S_a=1.1\cdot10^2$, $1.3\cdot10^2$, $1.6\cdot10^2$ and $1.7\cdot10^2$. For each value of the supersaturation ratio the particle number concentration was measured at three different residence times and for each residence time multiple measurements were carried out. Figure 3.6 shows the measured particle densities for $S=1.7\cdot10^2$ at three different residence times $t=0.25$, 0.43 and 0.78 s. An increase in number and in size of the crystals with residence time can be observed. The conversion was calculated to be less than 1% assuming spherical particles. From this calculation it was concluded that the supersaturation remained sufficiently constant over the length of the tube to justify the assumption of a stationary nucleation rate. The largest particles are in the range of 3 μm. Under the assumption that the largest particles nucleated directly after the static mixer the overall growth rate can be estimated to be in the order of a few micrometers per second. Stahl (2001), Blandin (2001) and Mahajan (1993, 1994) observed growth rates of the same order of magnitude.

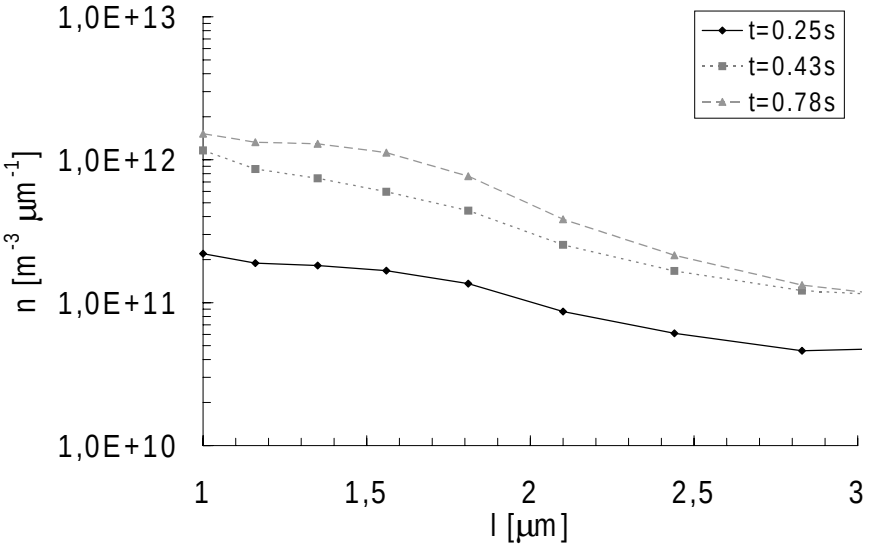

Figure 3.6 Particle density [m^{-3} μm^{-1}] for samples formed at $S=1.7\cdot10^2$ at three different residence times after dilution 50 times in saturated solution.

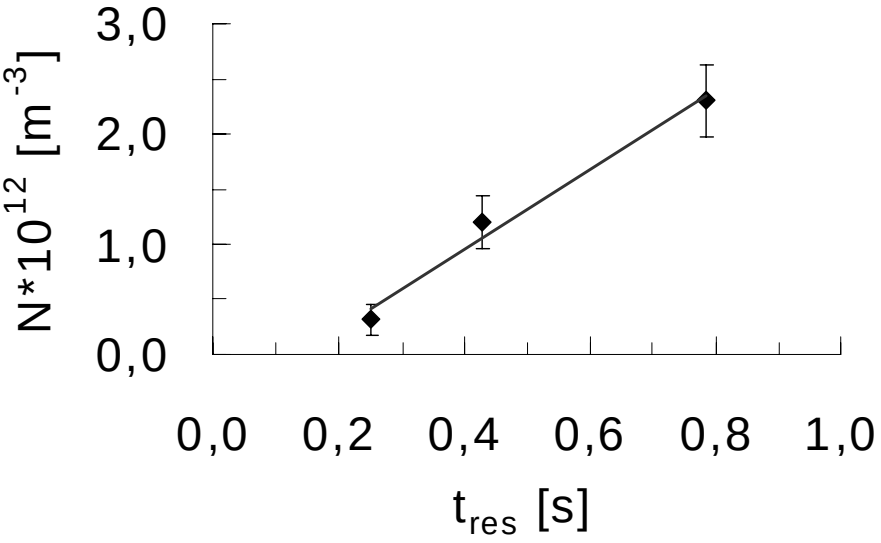

Figure 3.7 Increase in particle concentration with residence time for supersaturation $S=1.7\cdot10^2$. The corresponding nucleation rate is $J=3.9\cdot10^{12}$ m^{-3} s^{-1}. The error bars represent standard deviations.

In figure 3.7 the total number of particles is plotted versus residence times for $S=1.7\cdot10^2$. An increase in the particle number concentration with increasing residence time is observed. The nucleation rate was estimated from the slope of a straight line through these points according to $J=\Delta N/\Delta\tau$. For $S=1.7\cdot10^2$ a value of $J=(3.9\pm0.9)\cdot10^{12}$ $m^{-3}s^{-1}$ was found. Table 3.1 contains the particle number concentration values for the different residence times at all supersaturation ratios. Table 3.2 shows the nucleation rate for all supersaturations used. An increase in nucleation rate with increasing supersaturation ratio is observed.

Table 3.1 Particle number concentration versus residence time in the precipitation tube with standard deviation and number of measurements for five levels of supersaturation.

C_0 [molal]	t [s]	N [m^{-3}]	
0.037	0.43	$0.09\pm0.03\cdot10^{12}$	(n=4)
	0.78	$0.15\pm0.03\cdot10^{12}$	(n=8)
	2.2	$0.53\pm0.23\cdot10^{12}$	(n=9)
0.041	0.43	$0.12\pm0.06\cdot10^{12}$	(n=6)
	0.78	$0.21\pm0.11\cdot10^{12}$	(n=6)
	2.2	$1.6\pm0.4\cdot10^{12}$	(n=6)
0.042	0.43	$0.20\pm0.07\cdot10^{12}$	(n=6)
	0.78	$0.37\pm0.03\cdot10^{12}$	(n=6)
	2.2	$1.1\pm0.2\cdot10^{12}$	(n=3)
0.051	0.43	$0.6\pm0.6\cdot10^{12}$	(n=4)
	0.78	$1.2\pm0.5\cdot10^{12}$	(n=4)
	2.2	$3.5\pm0.8\cdot10^{12}$	(n=8)
0.053	0.25	$0.32\pm0.15\cdot10^{12}$	(n=6)
	0.43	$1.2\pm0.2\cdot10^{12}$	(n=4)
	0.78	$2.3\pm0.3\cdot10^{12}$	(n=6)

Table 3.2 Nucleation rates versus supersaturation ratios.

C_0 [molal]	S [-]	J [$m^{-3}s^{-1}$]
0.037	$1.1\cdot10^2$	$0.23\pm0.11\cdot10^{12}$
0.041	$1.3\cdot10^2$	$0.67\pm0.20\cdot10^{12}$
0.042	$1.3\cdot10^2$	$0.49\pm0.12\cdot10^{12}$
0.051	$1.6\cdot10^2$	$1.6\pm0.9\cdot10^{12}$
0.053	$1.7\cdot10^2$	$3.9\pm0.9\cdot10^{12}$

In figure 3.8 the natural logarithm of the nucleation rate divided by the supersaturation ratio $\ln(J/S)$ is plotted versus one over the square of the natural logarithm of the supersaturation level $1/\ln^2 S$ according to equation (3.3). From this plot the parameters in equation (3.1) were derived. For the intercept a value of $A=(5.7\pm1.0)\cdot10^{15}$ $m^{-3}s^{-1}$ was estimated and for the slope a value of $B=(3.4\pm2.0)\cdot10^2$. The experimental value for parameter A is much lower than the theoretical

value of approximately $A_{HON}=10^{33}$ $m^{-3}s^{-1}$ for homogeneous nucleation. This is an indication that nucleation of H_4EDTA under these experimental conditions is heterogeneous. The value for A_{HON} was calculated using equation (3.4a) and (3.4b) with molecular volume $\nu=3.8\cdot10^{-28}$ m^3, equilibrium solubility $C_e=2.0\cdot10^{23}$ molecules m^{-3}, diffusion coefficient $D=1.5\cdot10^{-9}$ m^2s^{-1}, interfacial energy calculated according to equation (3.6) $\gamma_{HON}=38$ mJ m^{-2} and supersaturation $S=1.3\cdot10^2$.

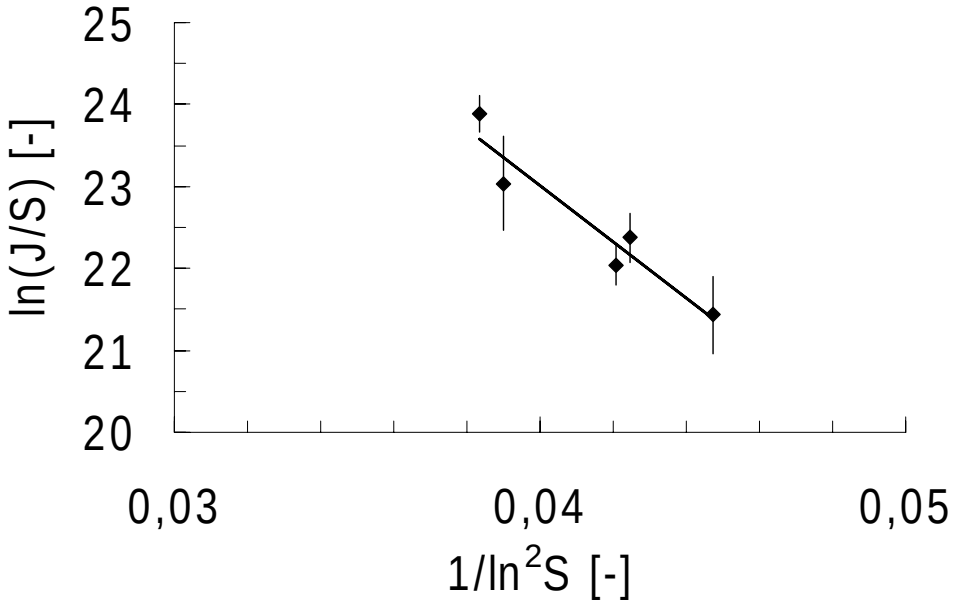

Figure 3.8 Plot of the nucleation rate $\ln(J/S)$ versus supersaturation $1/\ln^2 S$ with nucleation rate J expressed in [m^{-3} s^{-1}]. The error bars represent standard deviations.

From the value for parameter B the interfacial energy of the nucleus was estimated under the assumption of spherical nuclei. A value of $\gamma_{eff}=21\pm9$ mJ m^{-2} was found, compared to a value of $\gamma_{HON}=38$ mJ m^{-2} based on bulk properties according to equation (3.6). This is another indication for heterogeneous nucleation.

Table 3.3 Nucleus size and nucleation work versus supersaturation ratio calculated from equation (3.7) and (3.8) with $B=3.3\cdot10^2$ [-].

S [-]	n* [-]	W*/kT [-]
$1.1\cdot10^2$	6.4	15.2
$1.3\cdot10^2$	6.0	14.4
$1.3\cdot10^2$	5.9	14.3
$1.6\cdot10^2$	5.2	13.3
$1.7\cdot10^2$	5.1	13.0

Furthermore, in table 3.3 the calculated nucleus size n^* and nucleation work W^* are shown versus supersaturation. The calculated value of the interfacial energy γ_{HON} is used. The nucleus size is small, consisting of five to six molecules only.

3.5 Discussion

In figure 3.9 a straight line was plotted through the measured data for the nucleation rate $\ln(J/S)$ versus supersaturation $1/\ln^2 S$. More data points would be desirable to study whether there is a change in the slope and in the intercept of the line. Such a transition with increasing supersaturation is generally attributed to the change from heterogeneous nucleation to homogeneous nucleation. This change in the slope and in the intercept is observed for Barium Sulfate (Nielsen 1961, 1964, Mohanty 1988, Angerhöfer 1994, Schubert 1996), for Uranium Oxalate (Andrieu 1999), for Calcium Carbonate (Sellami 1999), and for Asparagine and for Lovostatin (Mahajan 1993, 1994).

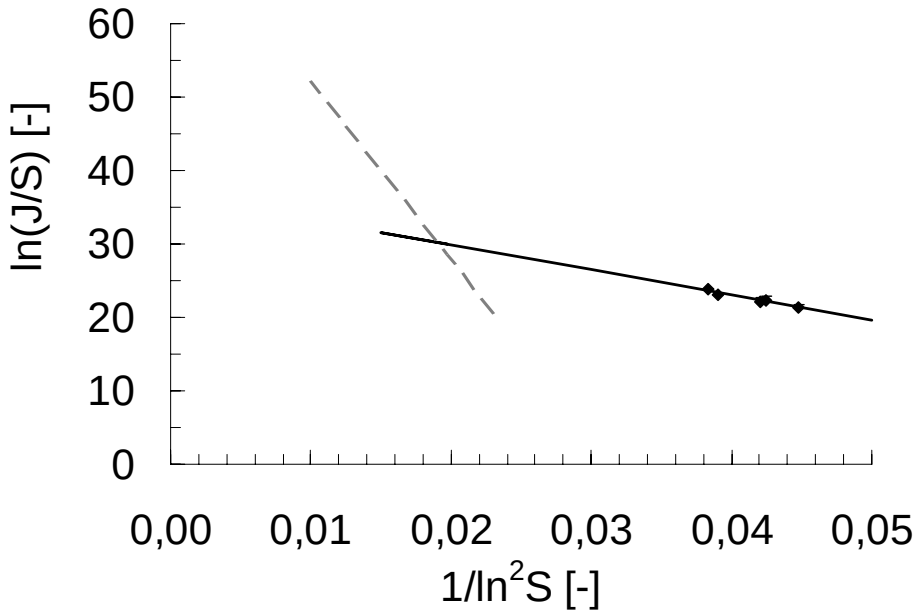

Figure 3.9 Experimental and theoretical nucleation rates versus supersaturation with nucleation rate J expressed in [m^{-3} s^{-1}]. The solid line represents the experimentally found nucleation rate with $A=5.7\cdot10^{15}$ $m^{-3}s^{-1}$ and $B=3.3\cdot10^{2}$ extrapolated from experimental data. The dashed line represents the theoretically predicted homogeneous nucleation rate with $A_{HON}=2.0\cdot10^{33}$ $m^{-3}s^{-1}$ and $B_{HON}= 2.4\cdot10^{3}$.

The theoretical homogeneous nucleation rate versus supersaturation according to equation (3.3) was plotted in the same figure as a dashed line. The parameters A an B were calculated to be $A_{HON}=2.0\cdot10^{33}$ $m^{-3}s^{-1}$ according to equation (3.4b) and $B_{HON}=2.4\cdot10^{3}$ according to equation (3.5) with the calculated interfacial energy γ_{HON} according to equation (3.7) to replace γ_{eff} in equation (3.7). The experimental line and the theoretical line intersect at the point at $\ln(J/S)=30$ and $S=1.4\cdot10^{3}$. This corresponds to a tenfold increase in actual supersaturation ratio compared to the experimental range and a nucleation rate J of about 10^{16} $m^{-3}s^{-1}$ that has increased by an order of four compared to the experimentally observed nucleation rates.

The method presented in this study is suitable to measure the heterogeneous nucleation rate of the molecular compound H_4EDTA. Application of a rapid mixing device and choosing a suitable range of initial concentrations ensures that mixing is completed before nucleation takes place. Conversion over the length of the tube is limited (~1%) so the supersaturation ratio can be assumed constant over the entire tube. A linear increase in particle number with residence time was observed. The particle number concentration of the samples that were diluted in saturated solution remained constant over sufficient time to perform the measurement.

The kinetic parameters that were derived from the nucleation rate measurements were attributed to heterogeneous nucleation. The question arises whether it is possible to measure homogeneous nucleation rates as well using this experimental method. Figure 3.9 indicates experiments at higher supersaturation. This would also result in faster nucleation, possibly before mixing is completed. If this is the case it may be desirable to accelerate mixing of the liquids by increasing the mixing intensity. Ultrasound may be applied to break up the liquid layers to enhance the mixing process. To ensure the supersaturation remains constant over the tube, its length may have to be shortened in order to decrease the residence time. To achieve sample stability dilution with a larger volume of saturated solution may be desired. Furthermore, it would be of interest to measure kinetic data for a different compound, in particular by anti-solvent precipitation to study the effect of the co-solvent on the interfacial energy.

3.6 Conclusion

Several methods exist to measure nucleation rates as a function of supersaturation in reactive precipitation. These methods differ in the way how the supersaturation is created by mixing, how crystals nucleate

and grow and how the particle number concentration is measured. In the selected experimental method a mixing tee with tube reactor was applied to precipitate the molecular compound H_4EDTA by a pH-shift process under well-defined flow conditions. Stationary nucleation rates were derived from the increase in particle concentration with incremental residence time in the tube reactor under the condition that the decrease of the supersaturation over the length time of the tube remained restricted to a few percent.

From a plot of the nucleation rates versus supersaturation ratio according to the classical nucleation theory the kinetic parameters in the nucleation rate expression were derived. For H_4EDTA for a range of supersaturation ratios of $1.1 \cdot 10^2$-$1.7 \cdot 10^2$ values of $A=(5.7 \pm 1.0) \cdot 10^{15}$ $m^{-3}s^{-1}$ and $B=(3.3 \pm 2.0) \cdot 10^2$ were found. This estimated value for parameter A is much lower than the theoretical value of $A_{HON}=10^{33}$ $m^{-3}s^{-1}$ for homogeneous nucleation. This is an indication that nucleation of H_4EDTA under the experimental conditions is heterogeneous. From the value for parameter B the interfacial energy of the nucleus was calculated under the assumption of spherical nuclei. A value of $\gamma=21 \pm 9$ mJ m^{-2} was found compared to a value of $\gamma_{HON}=38$ mJ m^{-2} calculated from bulk properties. This is another indication for heterogeneous nucleation.

3.7 Acknowledgements

The authors thank Akzo Nobel, BASF, Bayer and DSM for their support to this project. Furthermore, the helpful discussions with Dimo Kashchiev and Gerda van Rosmalen were highly appreciated.

3.8 References

Andrieu, M.; E. Plasari, P. Baron, in Proceedings of the 14th International Symposium on Industrial Crystallization, IChemE Cambridge (1999)

Angerhöfer, M., Untersuchung zur Kinetik der Fällungskrustallisation von Bariumsulfat, Thesis, Technische Universität München (1994)

Blandin, A.F.; D. Mangin, V. Nallet, J.P.Klein, J.M. Bossoutrot, Chem. Eng. J. 81 (2001) 91

Eble, A., Precipitation of nanoscale crystals with particular reference to interfacial energy; Thesis; Technische Universität München (2000)

Garside, J.; A. Mersmann, J. Nyvlt, Measurement of crystal growth and nucleation rates, EFCE Working Party on Crystallization, IChemE, Rugby (2002)

Haberkorn, H.; D. Franke, Th. Frechen, W. Goesele; J. Rieger, Coll. Interface Sci. 259 (2003) 112
Kashchiev, D.; G.M. van Rosmalen, Cryst. Res. & Technology 38 (2003) 555
Leeuwen, van M.L.J., Precipitation and mixing, Thesis, Delft University of Technology (1998)
Mahajan, A.M.; D.J. Kirwan, Phys D: Appl. Phys. 26 (1993) B176
Mahajan, A.M.; D.J. Kirwan, J. Cryst. Growth 144 (1994) 281
Manth, Th.; D. Mignon, H. Offermann, Chem. Eng. Sci. 51 (1996) 2571
Mohanty, R.; S. Bhandarkar, B. Zuromski, R. Brown, J. Estrin, AIChE J. 34 (1988) 2063
Nielsen, A.E., Acta Chem. Scand. 15 (1961) 441
Nielsen, A.E., Kinetics of precipitation, Pergamon, Oxford (1964)
Nielsen, A.E., Crystal Growth: Proceedings ICCG-1, H.S. Peiser ed.; Pergamon, Oxford (1967) 419
Nielsen, A.E., Kristall un. Technik 4 (1969) 17
Roelands, C.P.M.; J.J. Derksen, J.H. ter Horst, H.J.M Kramer, P.J. Jansens, Chem. Eng. Technol. 26 (2003) 296
Salvatori, F.; H. Muhr, E. Plasari, J.M. Bossoutrot, Powder Technol. 128 (2002) 114
Schubert, H.; A. Mersamann, Trans IChemE 74A (1996) 821
Schwarzer, H.C.; W. Peukert, Chem. Eng. Technol. 25 (2002) 657
Sellami, J.; N. Frikha, H. Muhr, E. Plasari, in Proceedings of the 14th International Symposium on Industrial Crystallization, IChemE Cambridge (1999)
Ståhl, M.; B.L. Åslund, Å.C. Rasmuson, AIChE J. 47 (2001) 1544

3.9 List of symbols

A	$[m^{-3}\ s^{-1}]$	pre-exponential kinetic parameter of nucleation
a	[molal]	activity
B	[-]	exponent parameter
c	$[mol\ m^{-3}]$ or [molal]	concentration
C_e	$[m^{-3}]$	molecular equilibrium concentration
D	$[m^2\ s^{-1}]$	diffusion coefficient
J	$[m^{-3}\ s^{-1}]$	nucleation rate
k	$[J\ K^{-1}]$	Boltzmann constant
N	$[m^{-3}]$	particle number concentration
n^*	[-]	nucleus size
S	[-]	supersaturation ratio
T	[K]	temperature
t_{ind}	[s]	induction time

t_{mix}	[s]	mixing time
t_{res}	[s]	residence time
W*	[J]	nucleation work
γ	[J m^{-2}]	interfacial energy
ν	[m^3]	molecular volume

Chapter 4

Analysis of nucleation in precipitation processes

For precipitation processes measurement of the nucleation rate as a function of supersaturation is difficult because the formation of the precipitate is fast and often hard to control due to the high supersaturation.

For a number of studies on both ionic and molecular precipitating compounds the experimental methods are discussed. From the experimentally determined nucleation rates the probable nucleation mechanism, homogeneous or heterogeneous, is derived and compared to the theoretically expected mechanism.

For all ionic compounds and for one molecular compound considered in this work, theoretically homogeneous nucleation is achievable. However, only for two ionic compounds, Barium Sulphate and Boehmite, the measurements possibly indicated a homogeneous nucleation mechanism. For the other studies, including all molecular compounds, a heterogeneous mechanism was more likely.

The difference between theoretically expected and experimentally observed mechanism may be explained by the use of less suitable experimental methods and measurement techniques but also by secondary processes, like agglomeration and transformation, taking place in the precipitated suspension.

Based on these findings an experimental procedure is suggested to standardize and to improve nucleation rate measurements in precipitation.

4.1 Introduction

Precipitation is widely applied to produce particles that have specific performance properties. Examples of these properties are colour for pigments, stability for explosives, porosity for catalyst carriers and solubility for pharmaceuticals. These performance properties are a function of the powder properties of the precipitate: crystal structure,

morphology and crystal size distribution (CSD). Control over performance properties requires control over powder properties. These powder properties in turn are determined by the precipitation kinetics: the primary processes nucleation and growth, followed by the secondary processes agglomeration, attrition, transformation and ripening.

The process that dominates precipitation is primary nucleation causing the formation of new crystals. Primary nucleation occurs either homogeneously by molecules assembling directly from solution or heterogeneously where the formation of nuclei is facilitated by a foreign substrate. The nucleation rate determines the number of particles that can precipitate and therefore the distribution of the surface area created to consume supersaturation by crystal growth. This has a large effect on the final CSD of the product. Furthermore, if the compound is able to crystallize in more than one crystal lattice (polymorphism), the competitive nucleation rates of the polymorphs may be controlled by the supersaturation ratio.

The driving force for precipitation is created by the mixing of two liquids, either two reactant solutions for reactive precipitation or a solution and a completely miscible anti-solvent for anti-solvent precipitation. Because the solubility of the precipitated product is low, the supersaturation is usually high. During (batch) precipitation the level of the supersaturation ration may vary strongly with the location in the vessel as well as with time. Primary nucleation proceeds as a strongly non-linear function of supersaturation. Because of the large supersaturation variation in space and in time the nucleation rate undergoes large variations as well. Because of this reason it is often difficult to control precipitation processes and therefore to control the properties of the products. Design of precipitation processes or prediction of the effect of changes to the process like dosing rate, geometry and mixing rate is difficult too.

To facilitate control and design, experiments have to be carried out to measure the nucleation rate as a function of supersaturation under well-controlled hydrodynamic conditions. A prerequisite for these experiments is that the reactants are premixed instantaneously to exclude the effect of variation in supersaturation from the measurements. The nucleation rate measurements as a function of supersaturation ratio can be fitted according to the classical nucleation theory (CNT) to derive whether the primary nucleation mechanism is homogeneous or heterogeneous.

In a previous study Roelands et al (2004) described nucleation rate measurements of a molecular compound, Ethylene Diamine Tetra

Carboxylic Acid (H_4EDTA), as a function of supersaturation ratio. Fitting these measurements according to the CNT indicated a heterogeneous mechanism. The number of comparable studies on primary nucleation from solution as a function of supersaturation ratio under well-controlled conditions is, however, small while the methods differ. This may be due to the fact that it is impossible to exclude the effect of mixing or to separate nucleation kinetics from other processes taking place simultaneously, like growth and agglomeration.

The objective of this study is to compare and to analyse the methods to measure nucleation rates while the advantages and disadvantages of each method will be summarized. The measured data will be fitted according to the CNT in order to derive the primary nucleation mechanism: homogeneous or heterogeneous. A good method is both fast and simple while accurate and reliable measurements are to be used in nucleation studies as well as in precipitation process design.

4.2 Prediction of nucleation rates according to the Classical Nucleation Theory

4.2.1 Driving force for nucleation

The driving force for a crystallization process is the difference in free Gibbs energy between the actual condition of the system and its equilibrium condition. For a one-component crystal in liquid solution under isothermal and isobaric conditions the supersaturation $\Delta\mu$ is defined as:

$$\Delta\mu = \mu_s - \mu_c \tag{4.1}$$

with μ_s and μ_c the chemical potentials of a molecule in solution and in the bulk of the crystal phase. When $\Delta\mu>0$ the system is supersaturated and nucleation and growth of the crystals is possible. The driving force can be rewritten as:

$$\Delta\mu = kT \ln S \tag{4.2}$$

with k [J K^{-1}] the Boltzmann constant and T [K] absolute temperature.

In this equation the supersaturation ratio for a molecular compound denoted by i $S_{a,i}=a_{0,i}/a_{e,i}$ [-] with $a_{0,i}$ actual activity in solution and $a_{e,i}$ equilibrium activity in solution. The activity for a compound in solution denoted by i is defined as $a_i=\gamma_i x_i$ with γ_i activity coefficient [-] and x_i molar fraction [-]. It is common practice to use the concentration c_i [mol m^{-3}] instead of x_i. A further simplification is to use the concentration

based supersaturation ratio $S_{c,i}=c_{0,i}/c_{e,i}$ [-] with $c_{0,i}$ actual concentration in solution and $c_{e,i}$ equilibrium concentration in solution. This is allowed for well soluble salts where $\gamma_{0,i}\approx\gamma_{e,i}$. For ionic compounds, like $BaSO_4$, the definition for the supersaturation ratio is the product of the activities or concentrations of the ions i^+ an j^- according to $S_{a,ij}=(a_{0,i}{}^{+}a_{0,j}{}^{-})/(a_{0,i}{}^{+}a_{e,j}{}^{-})$ or $S_{c,ij}=(c_{0,i}{}^{+}c_{0,j}{}^{-})/(c_{e,i}{}^{+}c_{e,j}{}^{-})$. For a more elaborate derivation it is referred to Kashchiev and Van Rosmalen (2003).

For poorly soluble salts the activity based supersaturation ratio $S_{a,i}$ should be used. For a solution at equilibrium the activity coefficient γ_i can be calculated as a function of the ionic strength according to Debye-Hückel, Bromley, Electrolyte-NRTL (Chen), Pitzer, or Helgeson (Bromley 1973, Rafal 1994, Pitzer 1991). For the calculation of the activity coefficient under non-equilibrium conditions the use of these equations may cause large errors because the parameters in these equations are generally determined under equilibrium conditions.

4.2.2 Homogeneous nucleation (HON)

In this study the classical nucleation theory (CNT) was followed as described by Kashchiev (2001). Solute molecules impinge on each other at a certain frequency due to Brownian motion. After the creation of a driving force for precipitation, these collisions take place with certain efficiency resulting in the formation of clusters of solute molecules. This is a dynamic process and molecules will attach and detach successively. The driving force for the creation of clusters is the difference in chemical potential between crystal bulk and solution. However, a penalty has to be paid for creating an interface between the cluster and its surrounding solution.

The work of formation of an n-sized cluster can be expressed as:

$$W(n)=-nkT\ln S+\gamma A_c(n) \tag{4.3}$$

with interfacial energy γ [J m^{-2}] and cluster surface area $A_c(n)$ [m^2].

The work of formation of a cluster will at first increase with increasing number of molecules until a maximum is reached. Up from this size the work of formation will decrease with n. This cluster with critical size n^* is called the nucleus and W^* is the nucleation work.

For spherical clusters the surface area $A_c(n)=(36\pi v_0{}^2)^{1/3}n^{2/3}$ with $v_0=M/\rho_c N_a$ [m^3] the molecular volume with M [kg mol^{-1}] molecular weight, ρ_c [kg m^{-3}] crystal density and N_a [mol^{-1}] Avogadro's number.

The interfacial energy γ [J m^{-2}] is a weighed average over all crystal faces.

Söhnel and Nielsen (1982) observed a linear relationship between the experimentally measured interfacial energy γ and the logarithm of the bulk solubility c_e for 58 compounds. Bennema and Söhnel (1990) confirmed this relationship theoretically. Mersmann (1990) derived the following relationship between the interfacial energy and the natural logarithm of the bulk solubility of the compound c_e [mol m^{-3}]:

$$\gamma = \beta kT \frac{1}{v_0^{2/3}} \ln \frac{1}{v_0 c_e} \tag{4.4}$$

For spherical clusters the shape factor β=0.514.

For a spherical nucleus the critical size n^* and the nucleation work W^* can be derived from the condition $dW/dn=0$ for $n=n^*$ using equation (4.3):

$$n^* = \frac{32\pi v_0^{\,2}\gamma^3}{3(kT)^3 \ln^3 S} \tag{4.5}$$

$$W^* = \frac{16\pi v_0^{\,2}\gamma^3}{3(kT)^2 \ln^2 S} = \tfrac{1}{2} n^* kT \ln S$$

The first equation is known as the Gibbs-Thomson equation. The critical nucleus size and the nucleation work depend on two main parameters: the externally controlled supersaturation and the interfacial energy between crystal and solution.

The CNT assumes that the density and the interfacial energy of the spherical cluster are equal to the ρ and γ for macroscopically large crystals. For small clusters this seems unlikely. Furthermore, simulations by Ten Wolde (1997) and experimental observations on proteins by Yau and Vekilov (2000) suggest that the shape of small nuclei may be irregular or platelet shaped. However, independent of their morphology, nuclei are assumed to have the same crystal lattice as bulk crystals of the compound because ρ and γ are the same. The implication of this assumption is that the crystal lattice is fixed at the beginning of the precipitation process.

The stationary nucleation rate J [m^{-3} s^{-1}] is defined as the time-independent frequency of transformation of the nuclei into the smallest supernuclei according to the following equation:

$$J = zf^{*}C^{*} \tag{4.6}$$

With z the Zeldovich factor [-], f^* attachment frequency [s^{-1}] and C^* equilibrium concentration of nuclei [m^{-3}]. The Zeldovich factor corrects for the fact that not all supenuclei grow out to macroscopically large sizes. The attachment frequency is the product of the incoming flux j^* of monomers to the nucleus surface and the nucleus area A^*. In this work it is assumed that the stickyness factor is equal to one. For homogeneous nucleation (HON) the equilibrium concentration of nuclei can be approximated with a Boltzmann-type of formula $C^*=C_0\exp(-W^*/kT)$. The concentration of nucleation sites C_0 is equal to the molecular volume $1/\nu_0$ because the nucleus can be formed anywhere in the supersaturated solution.

Now the nucleation rate J can be rewritten according to:

$$J = zf^{*}C_0 \exp\left(-\frac{W^{*}}{kT}\right) = A\exp\left(-\frac{B}{\ln^2 S}\right) = A\exp\left(-\frac{16\pi\nu_0^2\gamma^3}{3(kT)^3\ln^2 S}\right) \tag{4.7}$$

In this equation A [m^{-3} s^{-1}] is a kinetic parameter and B [-] the parameter in the exponent. The kinetic parameter for homogenous nucleation A_{HON} can be estimated from the attachment frequency f^* for two mechanisms: for volume-diffusion control and for interface-transfer control. It can be expressed as a function of bulk properties: interfacial energy γ, molecular volume ν_0, diffusion coefficient D [m^{-2} s^{-1}] and bulk concentration c_0 [m^{-3}]:

$$A_{HON,D} = \left(\frac{kT}{\nu_0^{\,2}\gamma}\right)^{1/2} Dc_0 \ln S$$
$$A_{HON,I} = \left(\frac{4\pi}{3\nu_0}\right)^{1/3}\left(\frac{\gamma}{kT}\right)^{1/2} Dc_0 \tag{4.8}$$

4.2.3 Heterogeneous nucleation (HEN)

In the presence of a heterogeneous surface area in the supersaturated solution the apparent interfacial energy decreases because the creation of a crystal-particle interface is energetically favourable over the creation of a crystal-solution interface. In the presence of a foreign substrate the nucleation work is smaller and heterogeneous nucleation will start at a lower supersaturation level compared to homogeneous

nucleation in a clean solution. In practice even in filtered or destilled solvents a large number of heterogeneous particles are present.

For 3D heterogeneous nucleation the effective interfacial energy $\gamma_{eff}=\psi\gamma$ with $0<\psi<1$ so B can be substantially smaller than that for HON. Furthermore, the kinetic parameter A_{HEN} is proportional to the concentration of heterogeneous particles C_a that is much smaller than $1/\nu_0$ in HON and therefore $A_{HEN}<<A_{HON}$. Typically $A_{HON}\sim10^{35}$ [m^{-3} s^{-1}] and $A_{HEN}\sim10^{15}$-10^{25} [m^{-3} s^{-1}].

The nature of the nucleation mechanism in a precipitation experiment, HON or HEN, can be determined from a plot of the measured nucleation rate J versus supersaturation $1/\ln^2 S$ according to equation (4.7). In the case of HON the values for the pre-exponential parameter A_{exp} and that of the interfacial energy γ_{exp}, derived from B_{exp} through equation (4.9), should have the same order of magnitude as the theoretical values calculated according to equations (4.8) and (4.4). In the case of HEN the experimental values A_{exp} and γ_{exp} should be considerably lower than the theoretical values.

4.2.4 Plot of rates for HON of molecular and ionic compounds

Mersmann (1996, 2001) developed a way of plotting the rates for HON and for HEN as a function of dimensionless driving force $\Delta c/c_c=(c_0-c_e)/c_c$ [-] and of dimensionless solubility c_e/c_c [-] with $c_c=1/\nu_0$ [m^{-3}] the 'concentration' of the compound in the crystal. For a compound with known solubility and defined experimental supersaturation ratio, the position in the plot predicts whether nucleation will proceed according to a homogeneous or a heterogeneous mechanism.

Using the dimensionless variables the supersaturation ratio in equation (4.7) for the nucleation rate J then becomes $S=(\Delta c/c_c+c_e/c_c)/(c_e/c_c)$ for molecular compounds and $S=[(\Delta c/c_c+c_e/c_c)/(c_e/c_c)]^2$ for ionic compounds. In the expression for the interfacial energy (4.4) the logarithmic term can be expressed as $1/(c_e\nu_0)=(c_c/c_e)$. For HON the expression for the actual concentration c_0 in the pre-exponential kinetic parameter A in equation (4.8) becomes $c_0=(\Delta c/c_c+c_e/c_c)c_c$.

In figure 4.1 the rates for $J_{HON}=10^6$, 10^{12} and 10^{18} [m^{-3} s^{-1}] are plotted for molecular compounds and for ionic compounds as a function of dimensionless driving force and dimensionless solubility. The different position of these lines for molecular compounds versus ionic compounds is caused by higher values for S for the ionic compound following from the concentration product in the definition $S_{c,ij}=(c_{0,i}^{+}c_{0,j}^{-})/(c_{e,i}^{+}c_{e,j}^{-})$ for ionic compounds compared to the definition $S_{c,i}=c_{0,i}/c_{e,i}$ for molecular compounds. The apparent minimum for molecular compounds is due to the mathematical formulation.

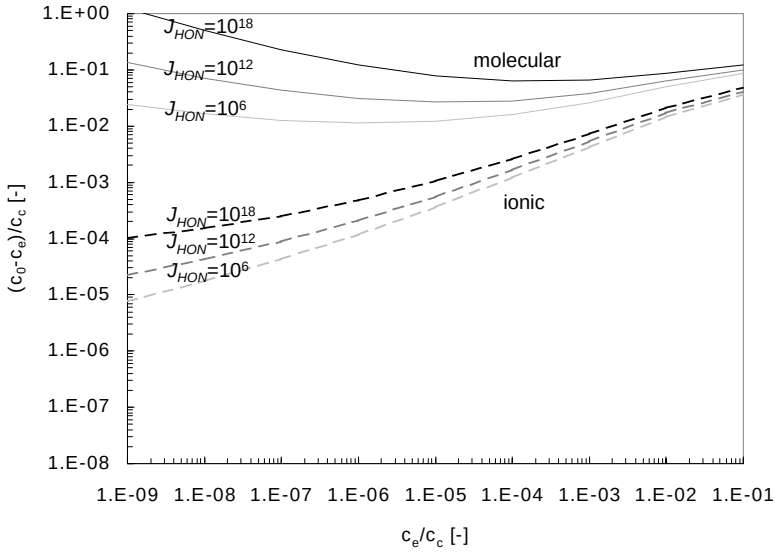

Figure 4.1 Rates for J_{HON} [m^{-3} s^{-1}] for molecular compounds and for ionic compounds as a function of the dimensionless solubility c_e/c_c [-] and dimensionless supersaturation $(c_0-c_e)/c_c$ [-].

4.2.5 Crystal growth

The crystal growth process is generally divided into two separate steps that can be assumed to take place in series:

a. Diffusion of the molecules from the bulk solution towards the crystal surface through the diffusion boundary layer.
b. Surface integration of the molecule into the crystal lattice. This step involves surface diffusion and partial or total desolvation before integration into the lattice.

When growth is limited by diffusion from the bulk, the growth rate G [m s^{-1}] can be expressed as a linear function of the difference between bulk solution concentration and equilibrium concentration.

For surface integration three types of crystal surfaces can be observed as a function of increasing supersaturation. First, for a molecularly very smooth crystal surface the attachment of new molecules is very difficult. Roughness is provided by the presence of step and kink sites. Steps at the crystal face are provided by screw-dislocations where spiral growth takes place. For low supersaturation where the growth rate equation becomes a quadratic function of the supersaturation ratio.

Secondly, when the surface is molecularly smooth, the rate of growth is limited by the creation of new steps at the surface. A mechanism to create these steps is 2D nucleation followed by layer growth. The nucleation mechanism can be mononuclear or polynuclear.

Finally, when a crystal surface is rough on molecular scale, growth is continuous. For molecular compounds the surface becomes rough when the step free energy becomes equal to zero at the roughening temperature T_R. When a solute molecule arrives at the surface it is immediately integrated. For rough growth crystal faces tend to become rounded. For salts kinetic roughening is observed when the activation energy required for the formation of a two-dimensional critical nucleus becomes of the order kT. During kinetic roughening the step free energy is still non-zero. Rough growth is a linear function of the supersaturation ratio.

4.2.6 Induction time

In precipitation studies it is common practice to measure the induction time t_{ind} [s] defined as the time elapsed between the moment that supersaturation is created and the moment that crystals are observed. The method depends not only on the nucleation rate but also on the growth rate of the crystals, on the applied observation technique and its detection limit. For stationary nucleation of spherical crystals using visual observation (a volume-based technique) the induction time is given by the following equation:

$$t_{ind} = \left(\frac{3\alpha_v}{\pi J G^3} \right)^{1/4} \tag{4.9}$$

with α_v the detectable volume fraction of the new crystalline phase formed in the solution.

4.3 Evaluation of experimental methods

4.3.1 General classification of methods to measure nucleation rates

In literature a number of methods are described to measure nucleation rates in precipitation processes. Because precipitation is a fast process supersaturation has to be created instantaneously. A pre-mixer is used to ensure complete and rapid pre-mixing of the solutions. The use of a tube reactor under turbulent flow conditions has the advantage that a sample with a narrow residence time distribution is obtained because back-mixing is reduced. All methods are based on counting of the number of crystals that nucleated over the length of the tube reactor during a defined time-period. In a review paper by Schüth (2001) and in the book by the EFCE-working party on crystallization by Garside, Mersmann and Nyvlt (2002) these methods were recommended for precipitating systems.

In this paragraph the methods will be classified and the differences will be highlighted. The main difference between the methods is the rate of depletion of supersaturation due to growth of the nuclei within the precipitation tube. This is explained in figures 4.2 and 4.3 where two extreme situations are depicted.

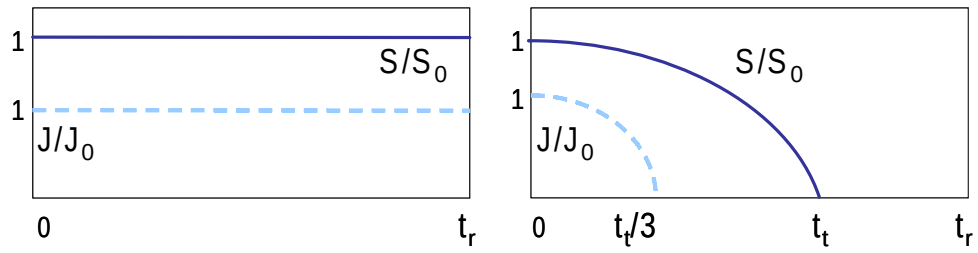

Figure 4.2 Left: constant S and J profile. Right: decreasing S and J profile.

If the desupersaturation proceeds relatively slowly the supersaturation and therefore the nucleation rate remain approximately constant over the length of the tube. At the end of this tube the solution is still supersaturated so a sample is rapidly quenched in a saturated solution in order to reduce the supersaturation and to inhibit additional nucleation. The nucleation rate follows now from the particle number concentration and from the residence time of the sample within the tube: $J=N/t_r$.

Furthermore, in figure 4.4 the differential method is depicted for the case where the supersaturation and the nucleation rate remain approximately constant over the length of the tube. The nucleation rate now follows from the increase in the particle number concentration with increasing residence time in the tube: $J=\Delta N/(\Delta V \Delta t_r)$.

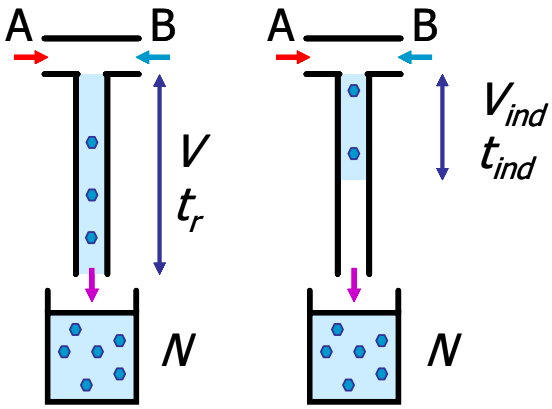

Figure 4.3 Left: method 2 with $J=N/(V_n t_r)$ suitable for constant S and J profile. Right: method 1 with $J=N/(V_{ind} t_{ind})$ and method 4 with CSD/PBM fitting suitable for decreasing S and J profile.

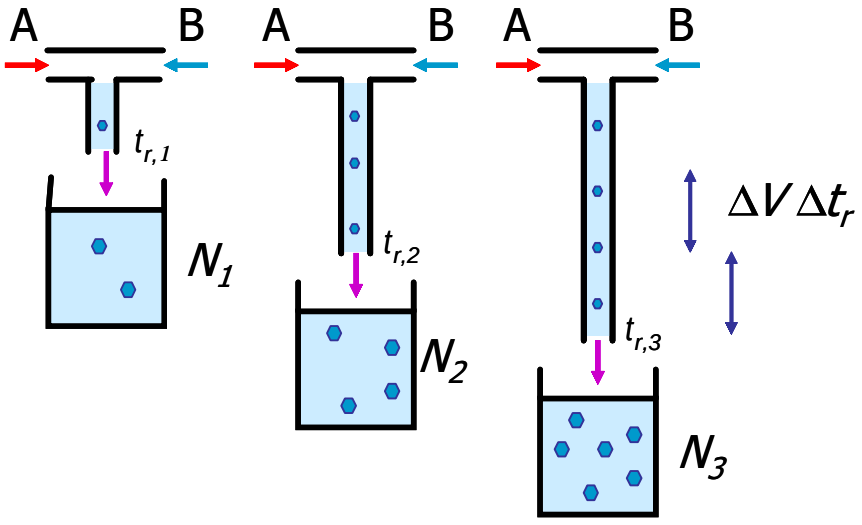

Figure 4.4 Method 3 with $J=\Delta N/(\Delta V \Delta t_r)$ suitable for constant S and J profile.

If the desupersaturation proceeds rapidly, because many nuclei form that grow rapidly, only in the first section of the tube the

supersaturation is sufficiently high for nucleation to take place. In the remaining part of the tube the previously formed nuclei only grow while consuming the remaining supersaturation and no additional nuclei form. The nucleation rate follows from the particle number concentration of a sample taken at the end of the tube and from the actual time for nucleation in the tube: $J=N/t_t$. This actual time is defined as the length of the tube to the point where the nucleation rate drops below an arbitrarily value where it has become insignificant. In a simplified approach this actual time is estimated from the observed induction time t_{ind}, that includes both nucleation and growth rates.

A more laborious but more correct approach is to use a population balance model (PBM) that includes both nucleation and growth rates as a function of supersaturation. The progress of the CSD is calculated over the length of the tube. By fitting the CSD measured at the end of the tube with model predicted CSD the parameters in the nucleation and growth rate equations can be obtained.

4.3.2 Rapidly decreasing supersaturation and nucleation rate over the length of the tube

Nielsen (1961, 1964, 1967, 1969) pioneered the measurement of nucleation rates for the precipitation of Barium Sulphate by mixing aqueous solutions of Barium Chloride and of Sulphuric Acid. This work was partially duplicated and partially extended by Mohanty and Estrin (1988). The nucleation rate was defined as the particle number concentration N_p [m^{-3}] divided by the half-life time t_t, for which the solution had become depleted ($S/S_0=1$) due to growth of the nuclei. From estimates of the growth rate, the half-life time t_t was conveniently approximated by the induction time t_{ind} [s] while the time for which the nucleation rate had become negligible was $t_{ind}/3$. This resulted in the following definition for the nucleation rate: $J=3N_p/t_{ind}$.

Three kinds of experiments were carried out to determine the induction time dependent on the supersaturation. For low supersaturation when precipitation was slow, the solutions were mixed in a stirred vessel. The induction time was measured as the time period between introducing the solutions in the stirred vessel and the moment that crystals could be detected. For intermediate and high supersaturation a tee-mixer device with a transparent outlet tube was applied. For intermediate S stopped-flow experiments and for high S continuous-flow experiments were carried out. In the former case the induction time was defined as the time period between stopping the flows and the moment that crystals could be detected inside the tube. In the latter case the induction time

was calculated from the length of the tube to the point where crystals could be observed divided by the solution velocity in the tube.

Blandin (2001) precipitated Salicylic acid from an aqueous solution of Sodium Salicylate and diluted Sulfuric Acid while Stahl (2001) precipitated Benzoic Acid from an aqueous solution of Sodium Benzoate and diluted Hydrochloric Acid. In both cases a mixing device in combination with a tube reactor was used while the CSD was measured at the outlet of the tube. A population balance model including nucleation and growth kinetic equations was used to estimate the CSD at the end of the tube. By fitting the experimental CSD with the estimated value the kinetic constants were obtained.

It is noted that this method has the advantage that it is suitable for systems that consume supersaturation in the tube very rapidly. It is not necessary that the supersaturation remains constant over the length of the outlet tube. A disadvantage is that estimation of the nucleation kinetics is more complicated because the model includes growth kinetics as well. Furthermore, it is noted that Stahl applied the previously described induction time method too.

4.3.3 Constant supersaturation and nucleation rate over the length of the tube

Angerhoefer (1994) and Schubert (1996) measured nucleation rates for Barium Sulphate precipitated from aqueous solution of Barium Hydroxide with diluted Sulphuric Acid while Eble (2000) prepared γ-Alumina (Boehmite) by mixing aqueous solutions of Sodium Aluminate with diluted Sulphuric Acid. A tee-mixer was used to pre-mix the solutions while nucleation and growth of the crystals took place in a tube reactor. The reacting mixture was quenched in a larger volume of saturated solution to stop further nucleation. The nucleation rate was defined as $J=N/(V_n t_r)$ with N the observed number of particles, V_n [m^3] the total volume fed through the tube and t_r [s] the residence time in this tube.

This method was also applied by Salvatori (2000) for Barium Carbonate from aqueous solutions of Barium Hydroxide and Sodium Carbonate and by Sellami (2000) for Calcium Carbonate from aqueous solutions of Calcium Chloride and Sodium Carbonate. Instead of the tube residence time t_r the total injection time t_n was used and instead of the volume fed through the tube V_n, the volume of the tube V_r was used. This makes no difference for the value of the nucleation rate that is obtained.

It is noted that for very rapidly precipitating compounds, that nucleate only in the first part of the outlet tube, these methods may underestimate the nucleation rate because either the tube residence time t_r will be too large compared to the actual time for nucleation t_t or the tube volume V_r will be too large compared to the actual fraction of the tube volume for nucleation V_t.

Mahajan (1993, 1994) used the differential method to measure the nucleation rates for the precipitation of Asparagine from water with 2-Propanol as anti-solvent and for Lovostatin from Methanol with water as anti-solvent. For the measurements on Asparagine in the tee-mixer a stopped-flow approach was followed while for Lovostatin a continuous-flow approach was applied. Roelands (2004) applied the latter method for the pH-shift precipitation of Ethylene Diamine Tetra Acetic Acid from an aqueous solution of Tetra Sodium EDTA and diluted Sulfuric Acid.

A mixer device and tube reactors with increasing length (residence time) were applied. At the outlet of the tube samples of the reacting mixture were quenched in saturated solution to stop further nucleation. The nucleation rate was defined as the increase of the particle number concentration with increasing residence time (tube length) according to $J=\Delta N_p/\Delta t_r$. It is noted that this method is only suitable when the supersaturation over the additional tube length remains approximately constant so nucleation and growth rates remain constant as well.

Kinetic data from Nielsen were used by Orchiuch and Baldyga (2001) and by Marchisio and Fox (2001) in CFD simulation of Barium Sulphate precipitation in tubular reactors. This kind of studies would clearly benefit from the availability of reliable kinetic data.

4.3.4 Comparison of experimental methods

The methods described in literature to measure nucleation rates do not only vary in measurement principle, but also in experimental set-up and in analytical instruments. The main differences are summarized in the following section while in appendix I the experimental methods are compared more in detail.

Hydrodynamic conditions in nucleation rate measurements

The mixing chambers used in these studies were usually tee-mixers. Mahajan and Roelands inserted a turbulence grid and a static mixer in the outflow tube just after the mixing point to improve mixing. Nielsen, Sellami and Salvatori used a Hartridge-Roughton vortex mixer for which a higher mixing intensity was expected compared to the basic tee-

mixer. Under the flow conditions applied in the experiments tee- and vortex mixers have a residence time in the order of ms. Blandin used a mixing-tee with a spherical mixing chamber with residence time of approximately 15% of the residence time in the outlet tube.

The diameter of the tube reactor was generally a few mm and the length was typically between ~ 1 and 50 cm so the residence time was in the order of 1-100 ms. Turbulent plug-flow in the tube was desired to assure that all crystals of a sample at the end of the tube had the same residence time. From experimental flow rates and tube diameter the Reynolds-number in the outlet tube was calculated: $Re=\rho u d/\eta$ [-] with u [m s^{-1}] flow velocity, d [m] tube diameter and ρ [kg m^{-3}] and η [kg m^{-1} s^{-1}] respectively density and viscosity of the solution (properties of water assumed). In a straight tube laminar flow becomes turbulent flow for $Re>3.3\cdot10^3$. In all experiments except for those by Mahajan and by Blandin turbulent plug-flow conditions in the outlet tube were expected because the Reynolds number was larger than this value.

The effect of mixing intensity on the precipitation was tested for Benzoic Acid by Stahl who observed no effect on the CSD of reducing the Reynolds-number from $1\cdot10^4$ to $6\cdot10^3$. Neither did Blandin for the precipitation of Salicylic Acid by reducing the Reynolds-number from $3\cdot10^3$ to $2\cdot10^3$. For these experimental conditions such rather small reductions is of the mixing intensity had no effect on the precipitation process.

It is noted that in some experiments for conditions where precipitation proceeded slowly (low supersaturation) the residence time in the tubes was not sufficiently long to obtain crystals that were large enough to be observed. For the precipitation of Barium Sulphate at low supersaturation, with induction time over one second Nielsen applied a stirred beaker. Mahajan did the same for the anti-solvent precipitation of Asparagine and of Lovostatin. However, in this study these experiments are discarded because only measurements in the tee-mixer set-up are considered.

Sample collection and particle counting

For the experiments that took place with slowly decreasing supersaturation over the length of the tube, for example those by Roelands for H_4EDTA, it was necessary to dilute suspension samples at the outlet in a larger volume of saturated solution to stop further nucleation. Quenching is usually not desired because the precipitated crystals may dissolve when the solution becomes undersaturated, Ostwald-ripening may take place and secondary processes like

agglomeration may occur. For some particle counting techniques quenching has the advantage that the suspension is already pre-diluted.

For the experiments with rapidly decreasing supersaturation over the length of the tube, for example those by Nielsen for Barium Sulphate and those by Stahl for Benzoic Acid, no quench was required because at the outlet of the tube the solution was already saturated. In this case, however, it was generally necessary to reduce the high suspension density of the samples before particle counting could be applied. Stahl added a dispersant and applied ultrasound to the Benzoic Acid suspension sample before counting. Nielsen added a peptising agent to the Barium Sulphate sample when these threatened to coagulate while Mohanty collected the Barium Sulphate sample in a ten times larger volume of gelatine solution.

A particle counting technique that measures the number-based crystal size distribution (CSD) is preferred. Stahl applied electro-zone sensing while Angerhöefer, Schubert, Mahajan and Roelands used laser obscuration. It is noted that these techniques are usually calibrated with spherical particles. When non-spherical crystals are measured, the actual CSD may deviate from the measured CSD, although the particle number concentration should not be affected. Nielsen, Mohanty and Blandin applied microscopy and counted the crystals from the images. Blandin applied image analysis software that enabled automatic characterization.

The derivation of the number-based CSD from the volume-based CSD is not recommended because the number of large particles may be overestimated. Sellami and Salvatori used laser diffraction measure the volume-based CSD. For submicron particles, however, no technique was available to measure the number-based CSD and therefore Eble used Quasi Elastic Light Scattering measuring the volume-based CSD of Boehmite. Eble observed a bimodal distribution and concluded that this was due to agglomeration. Knowing the size of the primary particles the number of primary particles in the agglomerates was estimated. A similar approach was followed by Salvatori for Barium Carbonate.

Miscellaneous

Most studies were carried out at or near room temperature, in the range 293-303 K. One exception was the work by Eble on Boehmite that was done at 348K. Furthermore, in all studies pure chemicals and solvents were used with the exception of the experiments by Sellami who precipitated Calcium Carbonate in the presence of Citrate ions. This additive was expected to inhibit crystal growth.

Furthermore, different equations for the supersaturation ratio and for the nucleation rate were applied to derive the kinetic parameters in the nucleation rate equation from the measured data. In appendix II the differences in the applied supersaturation and equation are summarized.

4.4 Measurements of the nucleation rate as a function of supersaturation ratio

4.4.1 Approach

Part of this study is to derive the kinetic parameters in the nucleation rate equation from experimental measurements of the nucleation rate as a function of the supersaturation ratio. The experimentally obtained values are to be compared with theoretical values for HON in order to find out whether the measurements were carried out on a system nucleating according to a HEN or a HON mechanism.

The following approach was followed for all studies:

a. Prediction: the experimental conditions were recalculated into dimensionless driving force and dimensionless solubility. From their position in the iso-rates plot the nucleation mechanism, HON or HEN, was predicted.
b. Fit: the experimental data on J versus S were all plotted and the same nucleation rate equation $J=A\exp(-B/\ln^2 S)$ was fitted.
c. Comparison: the values derived from experimental data for the kinetic parameter A_{exp} and the interfacial energy γ_{exp} were compared to values A_{HON} and γ_{HON} estimated from the CNT.

4.4.2 Prediction of the nucleation mechanism: HON or HEN?

For the studies considered in this review the experimentally applied ranges of the dimensionless solubility c_e/c_c and the dimensionless driving force $\Delta c/c_c$ were plotted together with the rates for HON of $1\cdot10^6$, $1\cdot10^{12}$ and $1\cdot10^{18}$ [m^{-3} s^{-1}] and for HEN of $1\cdot10^{12}$ [m^{-3} s^{-1}] in figures 4.5a and 4.5b The rates for HEN were plotted for three values of the parameter $\Psi=\gamma_{eff}/\gamma_{HON}=0.4$, 0.5 and 0.6 while the value for the pre-exponential parameter A_{HEN} was 10^{20} [m^{-3} s^{-1}]. With decreasing value of Ψ a smaller driving force $\Delta c/c_c$ is needed to achieve the same rate for HEN.

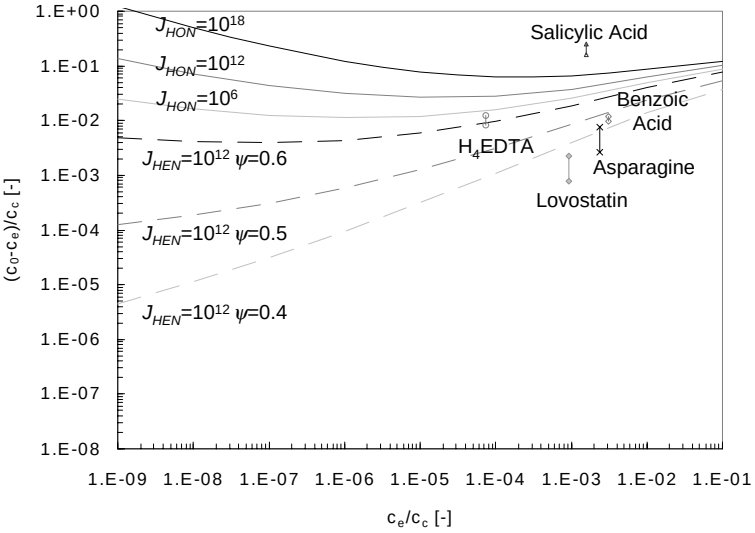

Figure 4.5a Rates for J_{HON} and for J_{HEN} [m^{-3} s^{-1}] of molecular compounds as a function of the dimensionless solubility c_e/c_c [-] and dimensionless supersaturation $(c_0-c_e)/c_c$ [-]. For the experimental conditions of the studies considered in this paper their position is shown.

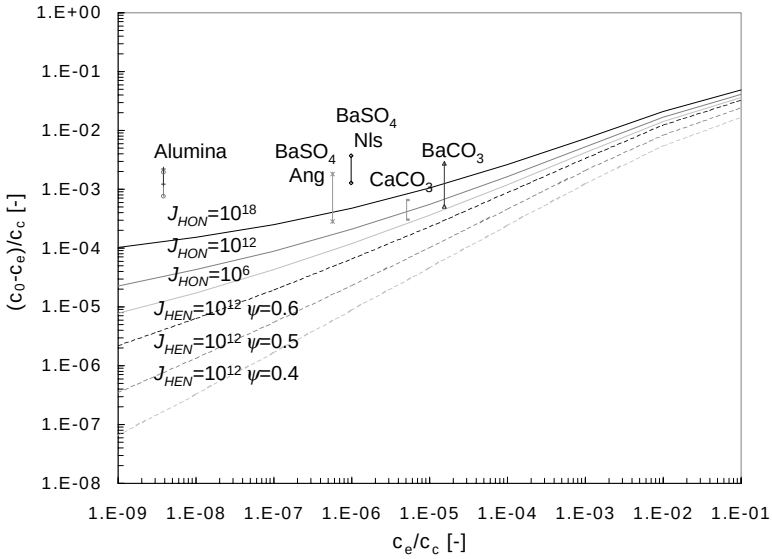

Figure 4.5b Rates for J_{HON} and for J_{HEN} [m^{-3} s^{-1}] of ionic compounds as a function of the dimensionless solubility c_e/c_c [-] and of the dimensionless supersaturation $(c_0-c_e)/c_c$ [-]. For the experimental conditions of the studies considered in this paper their position is shown.

It can be observed that for the ionic compounds c_e/c_c and $\Delta c/c_c$ are lower than those for the molecular compounds. For the ionic compounds HON-rates should be measured. Especially for Boehmite (Eble) and Barium Sulphate (Nielsen) high HON rates are expected. For most molecular compounds a HEN mechanism is predicted while only for Salicylic acid (Blandin) HON may be expected.

4.4.3 Pre-processing of experimental data

This study includes data from a series of papers on experimentally measured nucleation rates over a wide range of supersaturation ratio values. The measurements were done for the precipitation of both ionic and molecular compounds. Different experimental methods were applied using different experimental set-ups and particle counting techniques. Furthermore, different equations for the supersaturation ratio and for the nucleation rate were applied. For comparison it was sometimes necessary to recalculate the original experimental data (see appendix III).

Furthermore, for verification, the original nucleation rate measurements from the literature were plotted as a function of the supersaturation in the same way as was done in the original papers. Next, the originally employed equation for the nucleation rate was fitted in order to derive the kinetic parameter and the interfacial energy. The values that were obtained by reproduction were compared to the values originally obtained by the authors. It was verified that in all cases the pre-exponential kinetic parameter and the interfacial energy had (approximately) the same order of magnitude for both reproduced and as the original data. In appendix IV the results of the reproduction of the original figures are evaluated.

4.4.4 Fit of the measured nucleation rate as a function of supersaturation with the nucleation rate equation according to the CNT

The experimental values for $\ln J_{exp}$ were plotted versus supersaturation ratio ($1/\ln^2 S$) and a linear function was fitted through the data points. The intercept with the abscissa was the value for $\ln A_{exp}$ while the slope gave a value for B_{exp}. From the value for the slope B_{exp} the interfacial energy γ_{exp} was estimated. The experimental values were compared to theoretical values A_{HON} and B_{HON} estimated according to the CNT.

The approach is illustrated for the measurements by Roelands for the molecular compound H_4EDTA. In figure 4.6 the position of the experimentally measured nucleation rate J_{exp} (straight line) lies above that of corresponding theoretical HON-rate for the same value of S. At the same time the slope B_{exp} of the experimental line was smaller than that of the theoretical line (B_{HON}). Both observations are an indication that for the measurements on H_4EDTA nucleation proceeded probably according to a HEN mechanism.

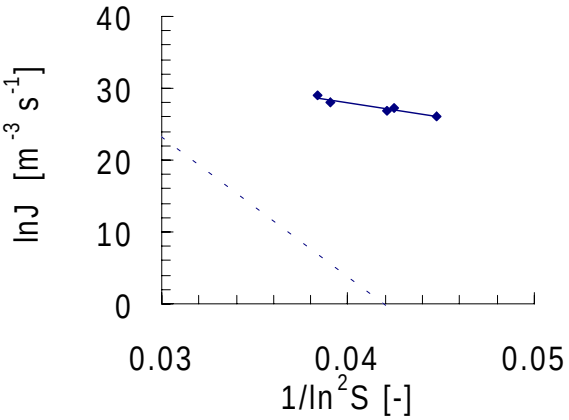

Figure 4.6 Plot of nucleation rate measurements versus supersaturation for H4EDTA (Roelands 2004) with dashed line representing nucleation rate calculated according to the CNT.

4.4.5 Comparison between experimental and theoretical values

In table 4.1 experimental values are shown for A_{exp} and γ_{exp} together with theoretical values for A_{HON} and γ_{HON}. The order of magnitude difference between A_{exp} and A_{HON} is calculated as $\Delta n = \log(A_{exp}/A_{HON})$ and this value is added to facilitate comparison together with the ratio $\gamma_{exp}/\gamma_{HON}$. The upper half of the table from 'Nielsen' to 'Salvatori' contains data for ionic compounds while the lower part, from 'Mahajan' to 'Stahl' contains data for molecular compounds.

Table 4.1 Comparison between experimentally and theoretically obtained values for the kinetic parameter A [m^{-3} s^{-1}] and interfacial energy γ [J m^{-2}].

Paper	A_{exp} [m^{-3} s^{-1}]	A_{HON} [m^{-3} s^{-1}]	Δn [-]	γ_{exp} [J m^{-2}]	γ_{HON} [J m^{-2}]	$\gamma_{exp}/\gamma_{HON}$ [-]	HON /HEN
Nielsen t_{ind}	$3 \cdot 10^{38}$	$3 \cdot 10^{35}$	+3	173	148	1.2	HON
Mohanty t_{ind}	$2 \cdot 10^{44}$	$6 \cdot 10^{35}$	+10	200	149	1.3	*HON*
Mohanty t_{res}	$4 \cdot 10^{37}$	$6 \cdot 10^{35}$	+2	180	149	1.2	HON
Angerhöfer	$5 \cdot 10^{17}$	$2 \cdot 10^{35}$	-18	91	156	0.6	HEN
Schubert	$6 \cdot 10^{18}$	$5 \cdot 10^{34}$	-16	88	156	0.6	HEN
Eble R=3.33	$7 \cdot 10^{30}$	$3 \cdot 10^{36}$	-6	448	464	1.0	HON
Eble R=3.0	$6 \cdot 10^{58}$	$5 \cdot 10^{36}$	+22	702	464	1.5	*HON*
Sellami	$5 \cdot 10^{21}$	$4 \cdot 10^{35}$	-14	89	172	0.5	HEN
Salvatori	$6 \cdot 10^{20}$	$4 \cdot 10^{35}$	-15	54	133	0.4	HEN
Mahajan-Asp	$1 \cdot 10^{11}$	$4 \cdot 10^{35}$	-25	8	42	0.2	HEN
Mahajan-Lov	$5 \cdot 10^{13}$	$5 \cdot 10^{34}$	-21	6	23	0.3	HEN
Roelands	$1 \cdot 10^{19}$	$3 \cdot 10^{35}$	-16	23	38	0.6	HEN
Blandin t_{res}	$1 \cdot 10^{18}$	$9 \cdot 10^{35}$	-18	24	46	0.5	HEN
Stahl t_{res}	$7 \cdot 10^{17}$	$1 \cdot 10^{36}$	-18	13	42	0.3	HEN
Stahl t_{ind}	$2 \cdot 10^{28}$	$1 \cdot 10^{36}$	-8	21	42	0.5	HEN

For all compounds theoretical values for the kinetic parameter are $A_{HON} \sim 10^{35}$ while values for the interfacial energy for ionic compounds are $\gamma_{HON} > 100$ [mJ m^{-2}] and for molecular compounds $\gamma_{HON} < 50$ [mJ m^{-2}]. From table 4.1 it can be observed that experimental values A_{exp} varied between orders 10^{11} and 10^{58}.

When $A_{exp} \sim A_{HON}$ and $\gamma_{exp} \sim \gamma_{HON}$ it was assumed that experimentally a homogeneous nucleation rate was measured. Because of the large variation in nucleation rate measurements an order of magnitude $\Delta n = 6$ difference between A_{exp} and A_{HON} was considered acceptable. At the same time the ratio $\gamma_{exp}/\gamma_{HON}$ should not differ more than a rather arbitrarily set value of 25%. The observation that $A_{exp} << A_{HON}$ and $\gamma_{exp} < \gamma_{HON}$ was a strong indication that nucleation during these measurements took place following a heterogeneous mechanism. When physically incorrect values $A_{exp} >> A_{HON}$ and $\gamma_{exp} >> \gamma_{HON}$ were observed this was an indication of erroneous measurements. In the last column of table 4.1 the resulting mechanism is indicated while italics were used when physically incorrect values were obtained.

For the experiments on ionic compounds it was expected from their position in figure 4.3 that nucleation would proceed according to homogeneous mechanism. However, only for the work on Barium Sulphate by Nielsen and by Mohanty (t_{res}-based) and possibly for the

work on Boehmite by Eble for R=3.3 values for the kinetic parameter A_{exp} were obtained that differed no more than a 10^6 order of magnitude from their theoretical values for A_{HON}. The values for A_{exp} found by Eble for R=3.0 and by Mohanty for t_{ind}-based measurements were much larger than the theoretical values A_{HON}. Experimental factors may have resulted in an overestimate of the number of primary particles and hence in an overestimate of the nucleation rate.

For the experiments on the other ionic compounds experimental values were much lower than theoretical values. This was an indication that heterogeneous nucleation rates were measured. For the experiments on molecular compounds considered in this review HEN was predicted, except for one study on Salicylic Acid, but in table 4.1 for all cases HEN can be observed. For the latter study by Blandin it is noted that the prediction in figure 4.3a is based on incomplete data on the actual experimental concentration c_0 to estimate the dimensionless variables.

Using the values for γ_{exp} as presented in table 4.1 the work of formation W^* divided by kT and the nucleus size n^* were calculated according to equation (4.5). The results are presented in table 4.2.

Table 4.2 Work of formation W*/kT [-] and nucleus size n* [-].

Paper	**Compound**	**W*/kT [-]**	**n* [-]**	**HON/HEN (exp)**
Nielsen	Barium Sulphate	41-56	6-9	HON
Mohanty t_{ind}	Barium Sulphate	57-62	7-8	*HON*
Mohanty t_{res}	Barium Sulphate	42-45	5-6	HON
Angerhöfer	Barium Sulphate	4-8	0.5-1.4	HEN
Schubert	Barium Sulphate	7-12	1.0-2.3	HEN
Eble R=3.33	Boehmite	81-89	6-7	HON
Eble R=3.0	Boehmite	22-25	1.6-2.1	*HON*
Sellami	Calcium Carbonate	6-9	1.3-2.1	HEN
Salvatori	Barium Carbonate	2-4	0.4-1.2	HEN
Mahajan-Asp	Asparagine	2-5	2-15	HEN
Mahajan-Lov	Lovostatin	3-7	2-10	HEN
Roelands	H_4EDTA	15-17	6-7	HEN
Blandin t_{res}	Salicylic Acid	1-2	1.3-2.5	HEN
Stahl t_{res}	Benzoic Acid	6-7	7-10	HEN
Stahl t_{ind}	Benzoic Acid	32-41	40-58	HEN

From this table it can be observed that for a number of experiments the calculated nucleus size becomes as small as 1-2. This was the case for the work by Angerhöefer and Schubert on Barium Sulphate, by Eble on

Boehmite for R=3.0, by Sellami on Calcium Carbonate, by Salvatori on Barium Carbonate and by Blandin on Salicylic Acid. In these cases the nucleation work becomes very small as well. Physically, a nucleus size of one would imply that there is no energy barrier for the formation of a nucleus anymore. This situation is comparable to rough growth for crystal growth.

Interestingly, the observation of very low values of the nucleus size n^* for selected experiments on ionic compounds and on Salicylic Acid coincided with the observation of HEN where HON was expected (except for the experiment by Eble on Boehmite for R=3.0). This coincidence may be explained from the fact that when in an experimental study the number of particles is underestimated, the slope B_{exp} will be too small and therefore the interfacial energy γ_{exp} calculated from equation (4.9) will be too small, resulting in values for the nucleus size and work of formation according to equation (4.5) that are too small as well.

4.5 Further evaluation of nucleation rate measurements

4.5.1 Effect of the applied method to measure the nucleation rate

For rapidly precipitating compounds supersaturation will deplete rapidly over the length of the tube reactor. Because the nucleation rate is a steep function of supersaturation, it will decrease rapidly with decreasing supersaturation as well. In this case only in the first section of the tube, directly after the mixing point, nucleation may effectively take place. The use of the method based on the whole length of the tube: $J=N/t_{res}$ is for these systems not desired because it will result in an underestimate of the actual nucleation rate. In this case either the method based on the induction time $J=3N_p/t_{ind}$ or a population balance model (PBM) that includes nucleation and growth should be used.

This was illustrated by Stahl for the work on Benzoic Acid. In figure 4.7 it can be observed that the use of the method based on t_{ind} resulted in higher values for A_{exp} and γ_{exp} than the method based on t_{res}. It is noted that the value for A_{exp} from the method based on t_{res} agreed well with the value for A_{exp} from the PBM-method as originally applied by Stahl.

The same phenomenon could be observed for the data on Barium Sulphate by Mohanty where the use of the t_{ind}–based method resulted in

a too high and physically incorrect value of the pre-exponential kinetic parameter A_{exp} compared to the use of the t_{res}–based method. Furthermore, the t_{ind}–based values for A_{exp} by Mohanty and by Nielsen differed by a 10^7 order of magnitude in spite of the fact that these experimentally were considered to be identical.

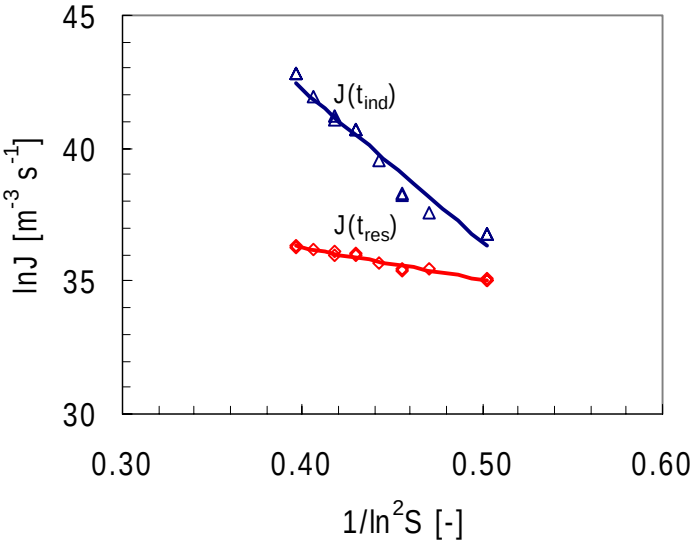

Figure 4.7 Plot of nucleation rate measurements versus supersaturation for Benzoic. Acid (Stahl 2001) for the induction time based method (triangles) and residence time based method (squares).

4.5.2 Observation of a slope change in the plot of ln$J$ versus $1/\ln^2 S$

In his paper on Barium Sulphate Nielsen (1961) observed an abrupt change in slope when the nucleation rate J was plotted as a function of supersaturation $1/\ln^2 S$. This change is slope was attributed to a change in nucleation mechanism from heterogeneous to homogeneous nucleation. This rather abrupt slope change was observed as well by Mohanty for Barium Sulphate and by Mahajan for Asparagine and for Lovostatin. A more gentle change of slope was observed by Stahl for Benzoic Acid, and by Angerhöfer and Schubert for Barium Sulphate, and finally by Sellami for Calcium Carbonate, although hardly present.

In figure 4.8 the nucleation rates for Barium Sulphate measured by Nielsen (1961), by Mohanty and by Angerhöfer are plotted as a function of supersaturation S_c. First, it can be observed that much higher

nucleation rates were measured by Nielsen and Mohanty compared to Angerhöfer although the measurements were done for the same range of S_c. Angerhöfer observed a slope change that was not as steep as Nielsen's. Angerhöfer explained the lower nucleation rates measurements by assuming that the original number of particles had decreased by agglomeration in the sampling beaker. Nielsen and Mohanty did not use such a beaker but collected the samples directly form the tube reactor. Furthermore, for the data by Nielsen and by Mohanty the abrupt slope change was observed at a different value of S_c although the data range was similar.

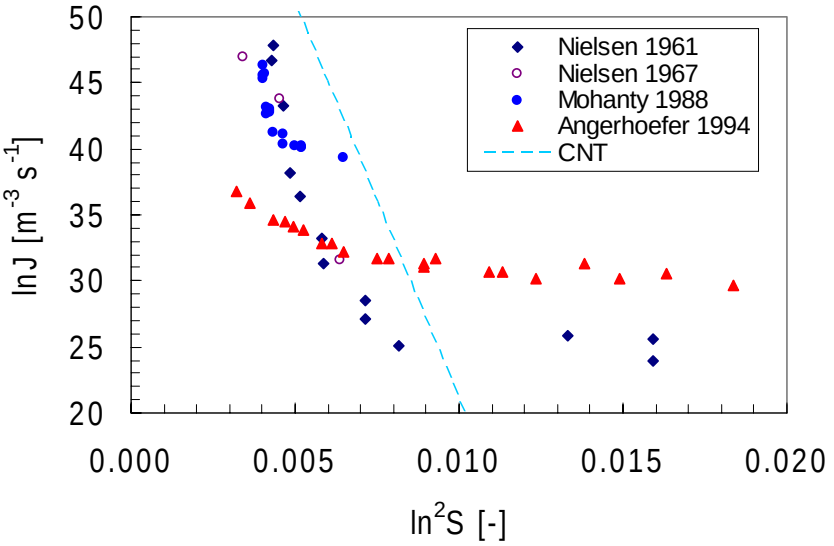

Figure 4.8 Experimental and theoretical nucleation rates for $BaSO_4$ as a function of concentration based supersaturation ratio.

It is noted, however, that the point of change in Nielsen's data, approximately at an induction time of 1 second, coincides with the use of a different set-up. For the experiments at low supersaturation ratio beakers were used and for those at high supersaturation the mixer-tube reactor in either the stopped-flow or the continuous flow mode. Mahajan did the same, switching from a batch set-up for low S to the continuous flow grid mixer for high S.

The observation of a slope change does not necessarily indicate a change in nucleation mechanism, from heterogeneous to homogeneous. It is recommended to calculate the corresponding values of parameters A_{exp} and γ_{exp} that should be in the theoretical HON-range too. In this study

it was intended to compare theoretically predicted values for HON rates with experimentally determined values. Therefore, in the case of experimental data exhibiting an abrupt change of slope, only the data for the left part of the figure, with the steepest slope, were considered because these were assumed to represent HON measurements.

4.5.3 Effect of molecular ratio on Boehmite precipitation

In figure 4.9 the plots of the experimental data by Eble for the ionic compound Boehmite can be observed for molecular ratio $R=[Na[Al(OH)_4]]/[H_2SO_4]=3.0$ (pH=9.3) and $R=3.33$ (pH=10) as straight lines while dashed lines represent the position of theoretical HON rates at corresponding values for S. The theoretical values for HON are larger than the experimentally observed values. Furthermore, for the ratio $R=3.0$ a much steeper slope B_{exp} can be observed compared to that for $R=3.33$ and also compared to that of the theoretical line (B_{HON}).

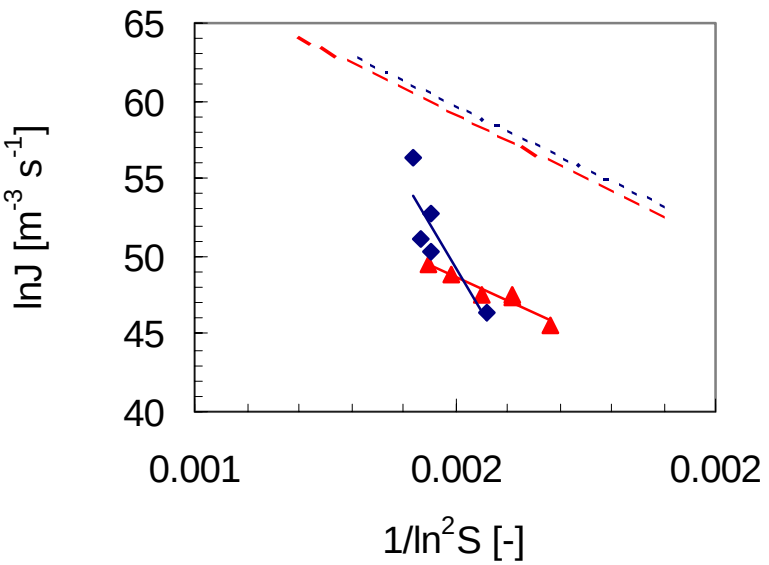

Figure 4.9 Plot of nucleation rate measurements versus supersaturation for Boehmite (Eble 2000) for $R=3.33$ (triangles) and for $R=3.0$ (squares). Dashed lines represent nucleation rates calculated according to the CNT (——:$R=3.33$ and --:$R=3.0$).

Eble calculated a value of $pH_{PZC}=8.9$ for the point of zero charge (PZC) for Boehmite. With increasing distance from this point, a decreasing interfacial energy was predicted, theoretically resulting in lower nucleation work and therefore a higher nucleation rate for $R=3.33$ compared to $R=3.0$. Experimentally, however, the opposite was

observed, a lower nucleation rate for R=3.33 compared to R=3.0. This discrepancy was related to experimental limitations and also to limitations regarding the applicability of the CNT.

4.5.4 Activity-based superaturation ratio versus concentration-based supersaturation ratio

In the theoretical paragraph the difference between the concentration-based supersaturation ratio S_c and activity-based supersaturation ratio S_a was explained. In this study it was attempted to use values of S_c whenever these were available. For the work by Schubert, Eble, Sellami and Salvatori only activity-based supersaturation ratio data were available so these were used. For the experiments on Barium Sulphate Schubert reduced the values of S_c by Angerhöfer by a factor 10-100 when these were recalculated in the form of S_a. In Nielsen's work (1967-1969) the values of S_a were reduced by a factor 10-100 compared to S_c. Furthermore, recently Vicum (2004) applied a Pitzer-equation to calculate S_a from S_c data of Nielsen for Barium Sulphate (1961). Furthermore, in this work S_a was calculated from the same data of Nielsen using the Bromley-Meissner equation available in the OLI Streamanalyzer software.

In figure 4.10 it can be observed that $S_a < S_c$ while with increasing actual concentration of the mixture, even a decreasing value for S_a can be observed. It is noted that for high concentration, at conditions that deviate strongly from equilibrium, the use of models to estimate the activity coefficient that were originally developed for equilibrium conditions may be speculative.

The effect of the use of S_a instead of S_c on the derivation of the parameters A_{exp} and γ_{exp} was studied. In figure 4.11, a plot of the nucleation rate $\ln J$ versus $1/\ln^2 S_c$ and versus $1/\ln^2 S_a$ is shown for measurements on Barium Sulphate. Measured data of $\ln J$ by Nielsen (1961) were plotted versus $1/\ln^2 S_c$ (original paper) and also versus $1/\ln^2 S_a$ as recalculated by Vicum. Furthermore, Nielsen's data for $\ln J$ from the 1967/1969 papers were plotted, both as function of S_c and S_a (both were given in the original paper). The same was done for original data for $\ln J$ using S_c by Angerhöfer and using S_a as recalculated by Schubert. In both cases the lines have shifted to the right because $S_a < S_c$. In table 4.3 the values for A_{exp} and interfacial energy γ_{exp} are compared.

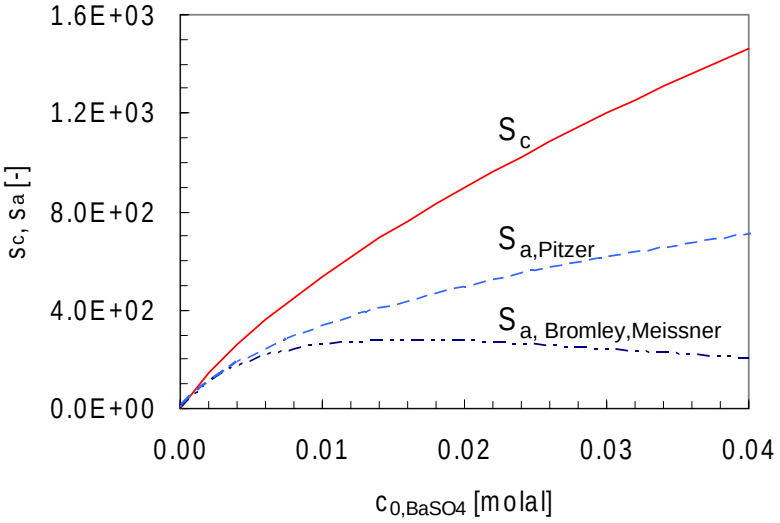

Figure 4.10 Supersaturation ratio for $BaSO_4$ as a function of the actual concentration. Superaturation ratio calculation based on concentration (straight line) and on activity according to Bromley-Meissner and Pitzer method (dashed lines).

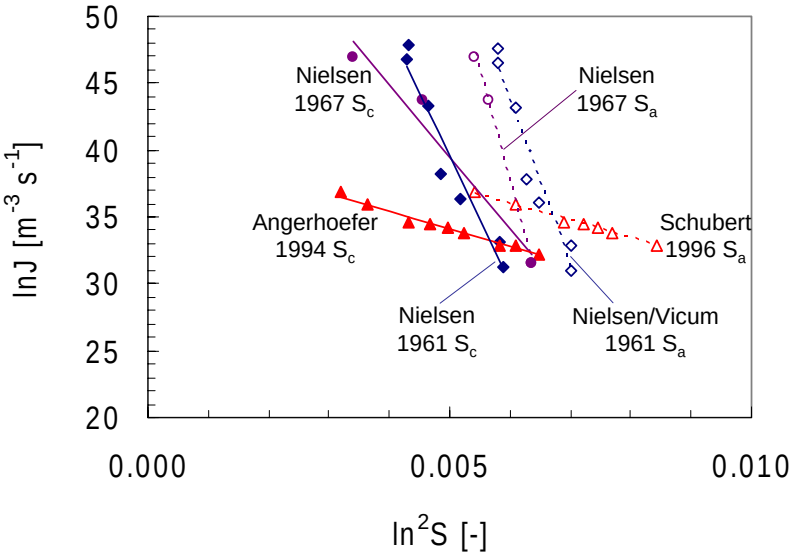

Figure 4.11 Experimental and theoretical nucleation rates for $BaSO_4$ as a function of concentration and activity based supersaturation ratio. Only the data for the higher levels of *S* are considered: ♦ Nielsen 1961, • Nielsen 1967, ▲Angerhöfer 1994.

Table 4.3 Comparison of kinetic parameter A_{exp} and interfacial energy γ_{exp} for Barium Sulphate experiments as a function of concentration-based and activity-based supersaturation ratio.

Paper	$A_{exp}(S_c)$ [$m^{-3}\ s^{-1}$]	$A_{exp}(S_a)$ [$m^{-3}\ s^{-1}$]	$\gamma_{exp}(S_c)$ [$J\ m^{-2}$]	$\gamma_{exp}(S_a)$ [$J\ m^{-2}$]
Nielsen 1961/ Vicum 2003	$3 \cdot 10^{38}$	$2 \cdot 10^{51}$	173	189
Nielsen 1967	$2 \cdot 10^{29}$	$1 \cdot 10^{60}$	143	208
Angerhöfer 1994/ Schubert 1996	$5 \cdot 10^{17}$	$6 \cdot 10^{18}$	91	88

It can be observed for the data of Nielsen (both 1961 and 1967) that the use of S_a instead of S_c resulted in a physically incorrect value for the kinetic parameter A_{exp} and in a steeper slope (higher value for γ_{exp}). This indicated that the models to calculate the activity coefficient γ_i result in an underestimate of the actual activity, resulting in an underestimate of S_a. This shift in value for S results in an overestimate of the intercept A_{exp}. Models to calculate the activity coefficient should be used with caution for conditions that are far from equilibrium (as encountered in precipitation) because their parameters have been determined for equilibrium conditions. For the data by Angerhöfer/Schubert such a large difference between the use of S_a instead of S_c was not encountered but experimental nucleation rates were already lower for these experiments.

4.6. Discussion

4.6.1 Approach

In the previous section predictions of the homogeneous nucleation rate were compared to experimental measurements. For all ionic compounds considered HON was predicted but only for the studies on Barium Sulphate and possibly on Boehmite HON was actually observed. For the other studies on ionic compounds the kinetic parameter and interfacial energy derived from the measurements indicated a HEN mechanism. For two studies on Barium Sulphate and on Boehmite physically incorrect values for these parameters were obtained. Furthermore, for the molecular compounds considered in this work HEN was predicted, except for one study on Salicylic Acid, and in all cases HEN was observed.

An attempt will be made to explain the difference between experiments and theory for the ionic compounds for the situation when HON was predicted and HEN was experimentally observed. In this case the experimental factors have to be identified that could be responsible for

the observation of HEN when in reality the mechanism was HON. Also the observation of physically incorrect values will be considered. The following factors will be considered: the use of a less suitable experimental method, inadequate mixing and the use of a less suitable particle measurement technique. Furthermore, secondary processes will be considered.

4.6.2 Less suitable experimental method

The method that is applied to measure nucleation rates should fit the experimental conditions. For precipitating compounds for which the supersaturation rapidly decreases over the length of the tube, either the method based on the induction time $J=3N_p/t_{ind}$ or on a population balance model (PBM) that includes nucleation and growth should be used. For systems precipitating under the condition that the supersaturation remains constant over the length of the tube, the method based on the whole length of the tube $J=N/t_{res}$ can be applied or the method based on counting the increase of the particle number concentration with increasing residence time (tube length) $J=\Delta N_p/\Delta t_r$. In the case of the work on Barium Sulphate by Angherhöfer and by Schubert, on Barium Carbonate by Salvatori and on Calcium Carbonate by Sellami the method $J=N/t_{res}$ presumed that supersaturation remained constant over the length of the tube. This may not have been the case because for the chosen concentrations these compounds may be expected to precipitate rapidly. For the measurements on Boehmite, Eble indicated that this may have been the cause for the 10^6 order of magnitude underestimate for A_{exp} compared to A_{HON}.

4.6.3 Inadequate mixing

If for very rapidly precipitating compounds the reacting solutions are not instantaneously premixed, nucleation will start in an environment with inhomogeneous local supersaturation. Because of incomplete premixing nucleation is not taking place in the whole volume of the tube, but only at the interface of the reacting solutions. This will result in local nucleation rates that vary widely with the position in the mixing field. Because nucleation is only taking place in a fraction of the volume this may result in an underestimate of the actual nucleation rate and this situation is not desired when nucleation rates are to be measured as a function of (presumably) constant supersaturation.

A high Reynolds number for turbulent flow alone does not guarantee that the reactant solutions are instantaneously and completely pre-mixed after the flows collide in the mixing chambers. Computational Fluid Dynamics (CFD) by Roelands et al indicated that for a wide-angle

Y-mixer (that is very similar to a plain mixing tee) after a length of 12 diameters beyond the collision point, macro-mixing was still not completed and a large variation in supersaturation ratio level in radial direction still existed.

The effect of mixing intensity on precipitation of ionic compounds was studied for Barium Sulphate by Schwarzer and Peukert (2002) and by Judat and Kind (2004) and for Strontium Sulphate by Manth and Mignon (1996). It was found that from a certain mixing intensity (Reynolds number) the CSD remained unchanged. They concluded that from this level pre-mixing was completed before nucleation occurred.

Haberkorn and Rieger (2003) studied the precipitation of Boehmite and Quinacridole in a free jet created by mixing two reactant solutions in a Y-mixer. At a distance of several tube diameters from the outlet slices from the jet were chopped and freeze-quenched. These slices were studied by cryo-TEM and showed that within the slice the solutions were not completely mixed and that at the interfaces between two slabs of solution the precipitation reaction had already started. This study stresses the need for high-intensity mixing as a prerequisite in precipitation research.

For the work on Salicylic Acid by Blandin a tee-mixer with a spherical mixer chamber was applied while for the measurements on Barium Sulphate by Angerhöfer and by Schubert and by Eble on Boehmite a tee-mixer was applied that was slightly modified into a wide-angle Y-mixer with an angle of 160° between the inlet tubes. The mixing intensity in the spherical mixing chamber and also of the Y-mixer may have been insufficient to premix the solution flows completely while at the same time fresh reactants were mixed with already precipitated crystals, resulting in a reduced nucleation rate.

4.6.4 Less suitable particle measurement technique

Direct particle counting is preferred over the derivation of the number-based CSD from a volume-based CSD measurement. The latter method may result in an underestimate of the number of small particles. Salvatori, Sellami and Eble derived the particle number concentration from volume-based CSD measurements using a laser diffraction instrument. Eble observed a bimodal distribution with primary particles with mean size of 0.01 μm and aggregated particles between 1 and 10 μm. The total number of primary crystals was estimated from the total precipitated mass, assuming that the aggregates consisted completely of primary particles with known size. This may have resulted in an overestimate of the number of particles.

Furthermore, particles below the detection limit are not counted at all. This might result in an underestimate of the nucleation rate. For most techniques the detection limit was around a few micron and the maximum size of crystals to be counted between 10 and 100 micron. The method based on counting the increase in the number of particles with increasing residence time may overcome this problem. However, this method can only be applied if the supersaturation ratio can be assumed to be constant over the tube length.

4.6.5 Secondary processes

In studies on precipitation kinetics as evaluated in this chapter, it is the objective to measure the number of primary crystals in order to determine the nucleation mechanism, HON or HEN. However, for some ionic compounds the formation of an amorphous phase may precede the formation of crystalline particles. This phenomenon was observed for example for Calcium Carbonate by Kabasci (1996), by Sawada (1998) and by Bolze (2003) and for Alumina by Sato (1984) and by Haberkorn (2003).

After the formation of an amorphous phase the actual supersaturation for a more stable crystalline phase is significantly lowered compared to the initial conditions, hence nucleation of the crystalline phase is likely to take place at a lower supersaturation and at a lower rate compared to that of the amorphous phase. If the transformation is taking place fast, the observed number of crystals of the more stable phase may be lower than the number of particles of the amorphous phase that was originally present, resulting in a relatively lower nucleation rate for trhe crystalline phase compared to that of the amorphous phase. It is assumed that the amorphous phase nucleates according to the mechanism described in the classical nucleation theory.

It can not be excluded that for the measurements on Boehmite by Eble and on Calcium Carbonate by Sellami, an amorphous phase would have precipitated first depleting the supersaturation. Nucleation of a more stable crystalline phase would then occur from an already partially depleted solution followed by subsequent rapid transformation while the samples were being processed. Eble indicated that the formation of Boehmite occurred to a two-step mechanism with the first step being the formation of the aqueous $Al(OH)_3$ complex. Furthermore, overall crystallinity for measurements at pH=9 was always below 65%, indicating the presence of a significant quantity of XRD amorphous material.

Furthermore, during the precipitation of Barium Sulphate in a tubular reactor Judat and Kind (2004) observed the aggregation of nanocrystallites followed by recrystallization, resulting in larger apparently single crystals. This aggregation/recrystallization process would result in a significantly reduced particle number concentration and an underestimate of the actual nucleation rate, as measured by Nielsen, by Mohanty, by Angerhöfer and by Schubert.

For Barium Sulphate Peukert and Schwarzer (2005) added excess positively charged Barium ions to the reacting solutions. At the surface of the primary particles the Barium ions adsorbed and a repulsive double-layer formed that stabilized the primary particles while preventing them from aggregation. The measured nucleation rate would therefore depend on the concentration of ions in the solution that have the possibility to adsorb to the crystal surface.

Nielsen and Mohanty used solutions of Barium Chloride and Sodium Sulphate while Angerhöfer and Schubert applied solutions of Barium Hydroxide and Sulphuric acid. The ionic strength in the background was much higher for Nielsen and Mohanty compared to Schubert and Angerhöfer. The stronger repulsive double-layerformed for higher ionic strength may have arrested agglomeration, resulting in a much higher particle number concentration found by Nielsen and by Mohanty compared to Schubert and Angerhöfer. Interestingly, Angerhöfer and Schubert explained the much lower number of particles compared to Nielsen and Mohanty by agglomeration in the stirred tank reactor that was used to collect the crystals after the tubular reactor.

It is noteworthy that in this work it was found that only for two ionic compounds, Barium Sulphate and Boehmite, the measurements actually indicated a homogeneous nucleation mechanism. However, the occurrence of the secondary processes aggregation and recrystallization, as reported in studies on these compounds, may influence the measured number of particles and hence the observed nucleation kinetics.

4.6.6 Summary

To measure HON rates it is assumed that the most suitable method is the one that takes into account the depletion of supersaturation over the length of the tube. Mixing should be instantaneous; all mixers are preferred over plain tee-mixers. The particle counting technique should be number-based. Finally, it should be known whether during precipitation of the compound a secondary mechanism may take place. In the following table these possible causes are summarized for the observation of HEN when HON was expected and for the observation of

physically incorrect values of the kinetic parameter. The number of stars indicates how likely the cause is to explain the difference.

Table 4.4 Possible causes to explain disagreement between HON prediction and HEN observation and to explain physically incorrect parameters.

Author	Com-pound	Less suitable method	Inade-quate mixing	Less suitable PMS	Secondary process
Mohanty t_{res}	Barium Sulphate	*	**	*	***
Anger-höfer	Barium Sulphate	***	**	*	***
Schubert	Barium Sulphate	***	**	*	***
Eble	Boehmite	**	**	***	***
Sellami	Calcium Carbonate	**	*	***	***
Salvatori	Barium Carbonate	**	*	***	*
Blandin	Salicylic Acid	*	***	*	*

4.6.7 Recommendations

A number of recommendations can be formulated to improve nucleation rate measurements for a precipitating compound and to propose a 'best practice'.

1. First carry out experiments on small scale with increasing supersaturation ratio. The induction time should decrease until it becomes equal to the mixing time in a beaker (~1 s). This value for the supersaturation ratio can be taken as the starting point for experiments in a fast mixing set-up.
2. Plot the experimental conditions in the form of the dimensionless solubility and the dimensionless driving force in figures 4.3a or 4.3b to tell whether HON or HEN may be expected.
3. The measurements should be not contaminated by mixing effects. It is recommended to verify this by measuring the particle number concentration at the end of the outlet tube with increasing mixing intensity (Reynolds-number).
4. For particles >1 μm a number based particle counting method is preferred. For particles <1 μm only volume-based techniques are available but recalculation of a volume-based CSD into a number-

based CSD may be a source of error. In all cases samples should be observed under a microscope as well to check for agglomeration.

5. Choose the appropriate measurement method.
   a. For conditions where compounds precipitate slowly, with supersaturation that is constant over the length of the tube, the differential method developed by Mahajan is preferred because it does not require that all particles have a size above the detection limit. Polymer tubing is recommended because the tube can be cut off at the desired length. Quenching of the sample requires attention because the precipitate should not dissolve or agglomerate. A further point of attention is to be aware of encrustation at tube walls.
   b. For compounds that precipitate very fast, a method should be used that corrects for desupersaturation over the length of the tube. Growth kinetics should be taken into account. The method based on measurement of the induction time may be used when exact growth kinetics is not known. More elaborate is the use of a method of fitting a population balance model to the experimentally measured CSD.
6. Plot the measured nucleation rates $\ln J$ as a function of supersaturation ratio $1/\ln^2 S$. For low values of S, especially for molecular compounds, the use of S_c instead of S_a will not have a large effect. For ionic compounds precipitating at high driving force the use of S_a may be preferred, but models to estimate the activity coefficient at non-equilibrium conditions, under conditions that deviate strongly from equilibrium, should be considered with caution.
7. Compare the experimentally measured nucleation rates with theoretically predicted rates to find out whether the nucleation mechanism was homogeneous or heterogeneous.

4.7 Conclusions

To predict the nucleation mechanism the experimental conditions for studies on four ionic compounds, Barium Sulphate, Boehmite (γ-Alumina), Calcium Carbonate and Barium Carbonate, and on five molecular compounds, H_4EDTA, Salicylic Acid, Benzoic Acid, Asparagine and Lovostatin, were plotted in a modified version of the so-called Mersmann-plot. In such a plot the rates for homogeneous and heterogeneous nucleation calculated according to the Classical Nucleation Theory (CNT) are plotted as a function of the dimensionless solubility and dimensionless driving force. For all ionic compounds and for the molecular compound Salicylic Acid homogeneous nucleation was predicted.

By fitting nucleation rate measurements versus supersaturation according to: $J=A\exp(-B/\ln^2 S)$ the kinetic parameter A_{exp} and interfacial energy γ_{exp} (from parameter B_{exp}) were calculated. Only for three studies on ionic compounds, two on Barium Sulphate and possibly one on Boehmite, the values for A_{exp} and γ_{exp} agreed approximately with A_{HON} and γ_{HON} confirming that nucleation proceeded according to a homogeneous mechanism. For the other studies it was found that the experimental values were significantly smaller than the theoretical values for HON. This indicated a heterogeneous mechanism. For two studies, on Barium Sulphate and on Boehmite, physically incorrect too high values for A_{exp} and for γ_{exp} were observed. This observation and also the difference between predicted and experimentally observed mechanism and may be explained by the use of a less suitable method, a less suitable volume-based particle counting technique or inadequate mixing. It cannot be excluded that secondary processes like agglomeration, Ostwald-ripening and transformation of a less stable phase to a more stable phase influenced these measurements as well. For most of the molecular compounds the experimental observation of a HEN mechanism this was in line with the prediction of HEN.

Recommendations were given for experimental studies on nucleation rate measurements in precipitation. First the applied method should fit the experimental conditions. For relatively slowly precipitating systems, where the supersaturation remains approximately constant over the length of the tube, a constant nucleation rate over the whole length of the tube is assumed. The differential method based on counting the increase of the number of particles with increasing residence time (tube length) $J=\Delta N_p/\Delta t_r$ is preferred but also the method based the residence time in the tube $J=N/t_r$ may be applied. For very rapidly precipitating compounds, where the supersaturation is depleted over the length of the tube, either the method based on the induction time $J=3N_p/t_{ind}$ or a method based on a population balance model (PBM) that includes nucleation and growth should be used.

Furthermore, it was concluded that the observation of a slope change in the plot of $\ln J$ versus $1/\ln^2 S$ should not always be an indication of a change in nucleation mechanism from heterogeneous to homogeneous. In some cases the change in slope could be attributed to a change in experimental set-up. To check whether homogeneous nucleation was actually observed it is recommended to calculate the values of parameters A_{exp} and γ_{exp} that should be approximately equal to A_{HON} and γ_{HON}.

Finally, the use of activity-based supersaturation ratio instead of concentration-based supersaturation ratio is desired for studies carried out at high supersaturation, but the accuracy of models to predict the activity coefficient at non-equilibrium conditions is questionable because these models were generally developed for equilibrium conditions.

4.8 References

Angerhöfer, M., Untersuchung zur Kinetik der Fällungskrustallisation von Bariumsulfat, Thesis, Technische Universität München (1994)

Bennema P.; O. Söhnel, J. Cryst. Growth 102 (1990) 547

Blandin, A.F.; D. Mangin, V. Vallet, J.P. Klein, J.M. Bossoutrot, Chem. Eng. J. 81 (2001) 91

Bromley, L.A., AIChE J. 19 (1973) 313

Eble, A., Precipitation of nanoscale crystals with particular reference to interfacial energy, Technische Universität München (2000)

Garside, J.; A. Mersmann, J. Nyvlt, Measurement of crystal growth and nucleation rates, EFCE Working Party on Crystallization, IchemE, Rugby, 2002

Haberkorn, H.; D. Franke, Th. Frechen, W. Goesele, J. Rieger, J. Colloid Interface Sci. 259 (2003) 112

Judat, B.; M. Kind, J. Colloid Interface Sci. 269 (2004) 341

Kabasci, S.; W. Althaus, P.-M. Weinspach, Trans IchemE 74 (1996) 765

Kashchiev, D., Nucleation, basic theory with applications, Butterworth, Oxford (2001)

Kashchiev, D.; G.M. van Rosmalen, Cryst. Res. Technol. 38 (2003) 555

Mahajan, A.J.; D.J. Kirwan, J. Phys. D 26 (1993) B176

Mahajan, A.J.; D.J. Kirwan, J. Cryst. Growth 144 (1994) 281

Manth, T.; D. Mignon, H. Offerman, Chem. Eng. Sci. 51 (1996) 2571

Mersmann, A., J. Cryst. Growth 102 (1990) 841

Mersmann, A., IchemE (1996) 812

Mersmann, A., Crystallization Technology Handbook, Marcel Dekker Inc., New York (2001)

Mohanty, R.; S. Bhandarkar, B. Zuromski, R. Brown, J. Estrin, AIChE J. 34 (1988) 2063

Nielsen, A.E., Acta Chem. Scand. 15 (1961) 441

Nielsen, A.E., Kinetics of precipitation, Pergamon, Oxford (1964)

Nielsen, A.E., Crystal Growth: Proceedings ICCG-i, H.S. Peiser ed., Pergamon, Oxford (1967)

Nielsen, A.E., Kristall un. Techniek 4 (1969) 17

Pitzer, K.S., Activity coefficinets in electrolyte solutions, 2nd ed., CRC Press, Boca Raton (Fl) (1991)

Rafal, M.; J.W. Berthold, N.C. Scrivner, S.L. Grise, Models for electrolyte solutions in Sandler, S.I. (editor), Models for thermodynamic and phase equilibria calculations, Marcel Dekker, New York (1994)
Roelands, C.P.M.; R.W. Roestenberg, J.H. ter Horst, H.J.M. Kramer, P.J. Jansens, Cryst. Growth Des. 4 (2004) 921
Salvatori, F.; H. Muhr, E. Plasar, J.M. Bossoutrot, Powder Technol. 128 (2002) 114
Sato, T., Ind. Crystallization 84 (1984) 385
Sawada, K., Mechanism of Crystal Growth of Ionic Crystals in Solution, Chapter 3 in Crystallization Processes, H. Ohtaki (ed.) Wiley, New York (1998)
Schubert, H.; A. Mersmann, Trans IchemE 74 (1996) 821
Schüth, F.; P. Bussian, P. Ågren, S. Schunk, M. Lindén, Solid State Sciences 3 (2001) 801
Schwarzer, H.C.; W. Peukert, Chem. Eng. Technol. 25 (2002) 657
Sellami, J.; N. Frikha, H. Muhr, E. Plasari, in Proceedings of the 14th International Symposium on Industrial Crystallization, IchemE, Cambridge (1999)
Söhnel, O., J. Cryst. Growth 57 (1982) 101
Söhnel, O., J. Cryst. Growth 63 (1983) 174
Ståhl, M.; L. Åslund, Å.C. Rasmuson, AIChE J. 47 (2001) 1544
Vicum, L; M. Mazzotti , J. Baldyga, Chem. Eng. Tech 26 (2004) 325
Ten Wolde, P.R.; D. Frenkel, Science 277 (1997) 1975

Appendix 4.I Comparison of experimental methods to measure nucleation rates

The methods described in literature to measure nucleation rates differ in the experimental set-up: mixing device, tube reactor, sampling method and particle counter. Most studies were carried out at or near room temperature, in the range 293-303K. One exception was the work by Eble on Boehmite that was done at 348K. In Table 4.I.1 the experimental details are summarized.

4.I.1 Mixing chamber

The experimental set-ups that are used for nucleation rate measurements consist of a mixing chamber to premix the reactant solutions rapidly and completely and a tubular reactor that acts as a confined space for nucleation and growth of the precipitate. Often the reacting mixture is quenched in a larger volume solution to stop further nucleation and growth. Samples of the resulting crystal suspension are taken to count the number of particles.

The mixing chambers that are used in these studies are tee-mixers or variations in this theme. The residence times in this type of mixers with given flow rates are in the order of milliseconds. Mahajan and Roelands inserted a turbulence grid and a static mixer in the outflow tube to improve mixing. Nielsen, Sellami and Salvatori used a Hartridge-Roughton type of vortex mixer that presumably had a better mixing performance than a plain tee-mixer. Furthermore, Blandin used a mixing-tee with a spherical mixing chamber. The residence time in this mixing chamber was approximately 15% of the residence time in the outlet tube.

4.I.2 Tube reactor

The outlet tube applied in this type of measurements usually had a diameter of a few millimeters and a length that was typically between ~0.01 and 0.5m. The residence time in the outlet tube was in the order of 1-100 milliseconds. Flow rate data and tube dimensions were used to calculate the Reynolds-number in the outlet tube. In this calculation the Reynolds-number $Re=\rho u d/\eta$ [-] with u [m s^{-1}] flow velocity, d [m] tube diameter and ρ [kg m^{-3}] and η [kg m^{-1} s^{-1}] respectively density and viscosity of the solution. In the calculation of the Reynolds-number the density and viscosity of pure water are assumed. For a Reynolds number

above $3.3 \cdot 10^3$ in a straight tube laminar flow goes over to turbulent flow. In this type of measurements turbulent plug-flow in the tube may be desired to assure that all crystals in a sample at the end of the tube have had the same residence time. The calculated Reynolds-numbers for the experimental set-ups are shown in table 4.I.1.

It can be observed that in all cases except for Mahajan and Blandin the Reynolds number is larger than $3.3 \cdot 10^3$ indicating that in the outlet tube turbulent plug-flow conditions may be assumed.

4.I.3 Sample collection

In most cases the crystal suspension was collected at the outlet tube in a larger volume of solution to stop further nucleation and to dilute the suspension for particle counting. Quenching is a sensitive operation because the precipitate may dissolve when the solution is subsaturated, Ostwald-ripening may take place when the solution is saturated for the larger crystals but subsaturated for the smaller ones, and during mixing secondary processes may take place like agglomeration. Attrition is not very likely because the precipitate is usually small, less than 10 micron. Eble applied a chemical quench to the Boehmite precipitation. A solution of Potassium Fluoride was used to bind unreacted Aluminium ions with Fluoride ions to the very stable Aluminium Fluoride complex. In the case of Nielsen ($BaSO_4$) and of Stahl (Benzoic Acid), the precipitation process was assumed to take place completely inside the outlet tube and therefore the samples were not quenched after leaving the outlet tube. Blandin applied the same method and used iced water for quenching.

In some cases the samples were pre-treated before particle counting was applied.

Stahl added a dispersant to the Benzoic Acid suspension sample and applied ultrasound before counting. Also Nielsen mentioned treatment of the $BaSO_4$ sample before particle counting when these threatened to coagulate. Mohanty collected the $BaSO_4$ sample in a ten times larger volume of gelatine solution.

4.I.4 Particle counting method

In most studies the particles were counted using techniques like electro-zone sensing by Stahl, laser obscuration by Angerhöefer, Schubert, Mahajan and Roelands, and microscopy by Nielsen, Mohanty, Blandin. These techniques give a number-based particle distribution. Laser obscuration and electro-zone sensing are usually calibrated with spherical particles and the CSD of crystals that are not spherical but for

example elongated may be erroneous. However, the number of particles should not be not affected.

Sellami and Salvatori used laser diffraction to measure the volume-based particle distribution while Eble used Quasi Elastic Light Scattering to measure the volume-based particle distribution for submicron particles. The derivation of the number-based particle distribution from the volume-based particle by Sellami, by Salvatori and by Eble may introduce a large error because the number of large particles may be overestimated and these results must be handled with caution.

Regarding particle counting techniques the following aspects have to be taken into account: detection limit, maximum particle density, number of particles counted.

For most techniques the detection limit lies around a few micron and the maximum size of crystals to be counted between 10 and 100 micron. Particles below the minimum size are not counted and this may underestimate the nucleation rate. The method applied by Mahajan and Roelands to determine nucleation rate from the increase of the number of particles with increasing residence time (derivative) may overcome this problem. However, this method may only be applied if the supersaturation ratio decrease with increasing tube length is small.

Eble was able to measure particles below one micron using the QUELS technique. He observed a bimodal distribution and concluded that this was due to agglomeration. Knowing the size of the primary particles he could estimate the number of primary particles in the agglomerates. A similar approach was followed by Salvatori for Barium Carbonate.

In most cases the precipitate suspension had to be diluted with saturated solution. This was usually already taken care of by quenching the suspension to stop the precipitation process. Redissolution and agglomeration of the precipitate should be avoided.

When the particle number concentration is determined by counting of the number of crystals under a microscope there is a risk that the sample is not representative for the product because the sample is too small or the crystals were not distributed evenly within the suspension. Furthermore, a sufficiently large number of crystals should be counted. Blandin applied image analysis software that enabled automatic characterization of a more representative number of crystals but unfortunately no absolute numbers were given.

Table 4.I.1 Overview of type of mixing chamber, the Reynolds number in the outlet tube, the particle measurement technique and the detectable size range.

Paper	Mixing chamber	Reynolds number	Particle measurement	Detection range
Nielsen 1967/69	vortex-mixer	$30 \cdot 10^3$	microscope	>1 μm
Mohanty	tee-mixer	$20 \cdot 10^3$	microscope	>1 μm
Angerhöfer	tee-mixer	$4 \cdot 10^3$	laser obscuration	1.5-20 μm
Schubert	tee-mixer	$7 \cdot 10^3$	laser obscuration	8-200 μm
Eble	tee-mixer	$9 \cdot 10^3$	QUELS	$3.2 \cdot 10^{-3}$-6.54 μm
Sellami	vortex-mixer	$20 \cdot 10^3$	laser diffraction	0.1-100 μm
Salvatori	vortex-mixer	$20 \cdot 10^3$	laser diffraction	0.1-100 μm
Mahajan	tee-mixer with grid	$2 \cdot 10^3$	laser obscuration	2-120 μm
Roelands	tee-mixer / static mixer	$9 \cdot 10^3$	laser obscuration	1-200 μm
Blandin	tee-mixer chamber	$2/3 \cdot 10^3$	microscope	>1 μm
Stahl	tee-mixer	$10 \cdot 10^3$	electro-zone sensing	1.2-19 μm

Appendix 4.II Comparison of methods to derive the kinetic parameters from measured nucleation rates as a function of supersaturation

In Table 4.II.1 for each study that was considered in this paper the experimental compound, the measurement principle, the supersaturation definition and suipersaturation range and the applied nucleation rate equation are summarized.

4.II.1 Nucleation rate equation and supersaturation definition

The supersaturation ratio S is defined for molecular compounds as the ratio of the actual concentration over the equilibrium concentration. It is either based on concentration $S_c=c_0/c_e$ or based on activity $S_a=a_0/a_e$. For ionic compounds that can dissociate and associate it is possible to define the supersaturation ratio only for the active species that is built into the crystal: $S_{i,c}=c_{i,0}/c_{i,e}$. However, little is known about dissociation at the starting point of the precipitation process, at a condition that deviates strongly from equilibrium. One approach is to extrapolate the dissociation from the equilibrium condition. For H_4EDTA dissociation was similar both for the non-equilibrium and for the equilibrium condition.

For molecular compounds Stahl, Blandin and Mahajan used the concentration based definition $S_c=c_0/c_e$. In this study for ionic compounds the definition for the supersaturation ratio is $S_c=(c_0^+c_0^-)/K_{sp,c}$ or $S_a=(a_0^+a_0^-)/K_{sp,a}$ with K_{sp} the solubility product at equilibrium. Some authors used the definition $s=S^{1/2}$, with $s_c=[(c_0^+c_0^-)/K_{sp,c}]^{1/2}$ or $s_a=[(a_0^+a_0^-)/K_{sp,a}]^{1/2} = [\gamma_\pm(c_0^+c_0^-)/K_{sp,a}]^{1/2}$ with the mean activity coefficient $\gamma_\pm$ calculated as a function of ionic strength I. Eble used a somewhat different definition $s_{a,0}=\{\gamma_\pm([Al(OH)_4^-]\cdot([H^+]_{ini}-[OH^-]_{ini}))/K_{sp,a}\}^{1/2}$ to compensate for the initial concentration.

Nielsen used the concentration equation for s_c in his first publication on $BaSO_4$ and so did Mohanty. Later Nielsen used the activity equation s_a with mean activity coefficient $\gamma_\pm$ defined by the Güntelberg equation: $\log\gamma_{\pm,z}=-0.509z^2\sqrt{I}/(1+\sqrt{I})$ with z the ionic valency. Angerhöfer used the similar Debye-Hückel equation for $\log\gamma_\pm=(-(A|z_1z_2|\sqrt{I})/(1+Ba\sqrt{I})$ with a the mean ionic distance. Schubert and Eble used the Davies equation while Schubert, Sellami and Salvatori applied the Bromley equation for $\gamma_\pm$.

For H_4EDTA Roelands calculated the activity coefficient using the Bromley-Meissner equation in the OLI Streamanalyzer software. In these calculations it was observed that for the experimental conditions at dilute concentration the activity coefficient was almost the same both for non-equilibrium and for equilibrium conditions.

In this study the equation $J=A\exp(-B/\ln^2 S)$ is used to estimate values for A and B from plots of the measured nucleation rate J versus supersaturation S. In the work on ionic compounds by Angerhöfer, Schubert and Eble a different nucleation rate equation was used: $J=A's^{7/3}\exp(-B/4\ln^2 s)$ with a different definition for the supersaturation: $s=S^{1/2}$. In this paper all experimental data were refitted according to equation (4.7) in order to obtain values for A and B that were comparable.

Table 4.II.1 Overview of studies considered: author, compound, method, supersaturation ratio definition and experimental range and nucleation rate equation.

Paper	Compound	Method J [m^{-3} s^{-1}]	Supersaturation ratio [-]	Equation J [m^{-3} s^{-1}]
Nielsen 1961	$BaSO_4$	$N/(V_{ind}t_{ind})$	$s_c=10^2$-10^3	-
Nielsen 1967/69	$BaSO_4$, misc. ionic	$N/(V_{ind}t_{ind})$	$s_a=10^2$-10^3 Güntelberg	$A\exp(-B/\ln^2 s)$
Mohanty	$BaSO_4$	$N/(V_{ind}t_{ind})$	$s_c=10^3$	-
Anger-höfer	$BaSO_4$	$N/(V_n t_r)$	s_c, $s_a=10^2$-10^3 Debye-Hückel	$A's^{7/3}\exp(-B/4\ln^2 s)$
Schubert	$BaSO_4$	$N/(V_n t_r)$	$s_a=10^2$-10^3 Davies, Bromley	$A's^{7/3}\exp(-B/4\ln^2 s)$
Eble	AlOOH	$N/(V_n t_r)$	$s_a=10^5$-10^6 Davies	$A's^{7/3}\exp(-B/4\ln^2 s)$
Sellami	$CaCO_3$	$N/(V_t t_n)$	$s_a=10^1$-10^2 Bromley	$A\exp(-B/\ln^2 s)$
Salvatori	$BaCO_3$	$N/(V_t t_n)$	$s_a=10^1$-10^2 Bromley	$A\exp(-B/\ln^2 s)$
Mahajan	Asparagine Lovostatin	$\Delta N/(\Delta V \Delta t_r)$	$S_c=10^0$-10^1	$A\exp(-B/\ln^2 S)$
Roelands	H_4EDTA	$\Delta N/(\Delta V \Delta t_r)$	$S_a=10^2$ Bromley-Meissner	$AS\exp(-B/\ln^2 S)$
Blandin	Salicylic Acid	PBM	$S_c=10^2$	$A\exp(-B/\ln^2 S)$
Stahl	Benzoic Acid	PBM, $N/(V_{ind}t_{ind})$	$S_c=10^0$	$A\exp(-B/\ln^2 S)$

Appendix 4.III Recalculation and reproduction of experimental data

a. Nielsen data presented in 1961 paper: nucleation rate calculated from particle number concentration together with induction time according to $J=3N_p/t_{ind}$.
b. Mohanty: nucleation rate calculated from particle number concentration together with induction time according to $J=3N_p/t_{ind}$. For low $S_c=2\cdot10^3$: $t_{ind}=0.5$ s, for high $S_c=2.7\cdot10^3$: $t_{ind}=0.15$ s. The induction times for the range of S-values in between these limits were interpolated according to a linear function.
c. Eble: two data sets were considered, one for a molar ratio $R=3.33$ and one for a ratio $R=3.0$.
d. Blandin: two data sets were considered, one for high flow rates and one for low flow rates. Because for this study the original population balance model by Blandin et al was not available the nucleation rate was estimated from the particle number concentration and the residence time in the tube according to $J=N/Vt_{res}$.
e. Stahl: two methods were applied, the first was similar to Nielsen's method with $J=3N_p/t_{ind}$, the second was based on a fit of the population balance model CSD with experimental CSD. Because for this study the population balance model of Stahl et al was not available the nucleation rate was the nucleation rate was estimated from the particle number concentration and the residence time in the tube according to $J=N/Vt_{res}$.

It is noted that in the case of an observed change in the slope of the plot of the nucleation rate measurements versus supersaturation ratio, only the data were considered which belonged to the plot with the largest slope (assigned HON).

First the original data were fitted with their original equation, this was done to reproduce the kinetic parameter A or A' and interfacial energy γ.

As an example for this approach the measurements of Eble for the ionic compound Boehmite were replotted as a function of supersaturation. These plots are shown in figure 4.III.1. Next the data for the kinetic parameter A or A' and interfacial energy γ that were obtained by replotting were compared to the original values as given by the authors.

This was, however, not possible for all papers because not always these parameters were given.

The data for the kinetic parameter A or A' and interfacial energy γ obtained by replotting are shown in table 4.III.1 with the original values as given by the authors.

Table 4.III.1 Comparison between replotted and original values for the kinetic parameter A or A' [m^{-3} s^{-1}] and interfacial energy γ [J m^{-2}].

Paper	**Replotted A or A' [m^{-3} s^{-1}]**	**Replotted γ [J m^{-2}]**	**Original A or A' [m^{-3} s^{-1}]**	**Original γ [J m^{-2}]**
Nielsen	$A=1\cdot10^{38}$	120	$A=1\cdot10^{38.5}$	135
Mohanty	-	-	-	-
Angerhöfer	-	-	-	-
Schubert	-	-	-	-
Eble R=3.33	$A'=4\cdot10^{11}$	320	$A'=2\cdot10^{12}$	339
Eble R=3.0	$A'=1\cdot10^{39}$	659	$A'=3\cdot10^{39}$	662
Sellami	$A=5\cdot10^{21}$	56	$A=4\cdot10^{21}$	38
Salvatori	$A=6\cdot10^{20}$	34	$A=7\cdot10^{20}$	34
Mahajan Asp	$A=1\cdot10^{11}$	8	-	6
Mahajan Lov	$A=5\cdot10^{13}$	6	-	2
Roelands	-	-	$A=1\cdot10^{19}$	23
Blandin t_{res}	$A=1\cdot10^{18}$	23	$A=1\cdot10^{18}$	24
Stahl t_{res}	$A=7\cdot10^{17}$	12	$A=3\cdot10^{19}$	14
Stahl t_{ind}	$A=7\cdot10^{27}$	21	$A=10^{30.5}$	-

It can be observed that the values for A or A' and for γ that were obtained by replotting data, agreed well with the values obtained by the authors. This allowed the use of these datasets for the next step.

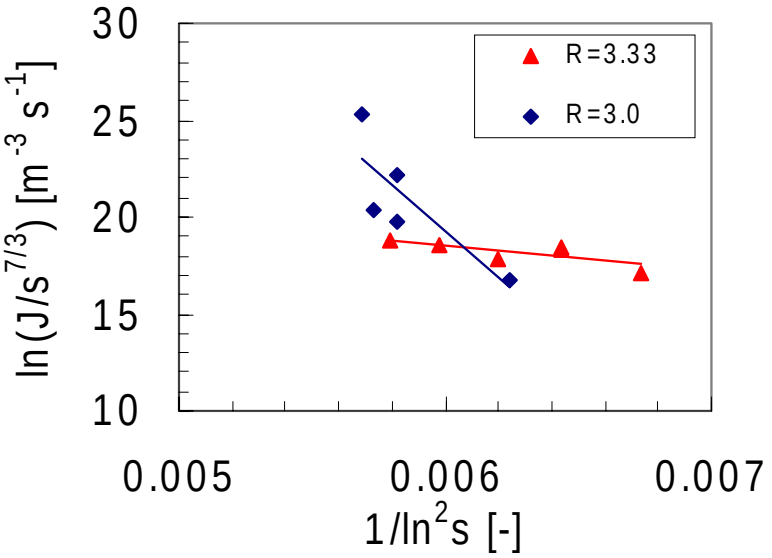

Figure 4.III.1 Reproduction of original data for Boehmite (Eble) for R=3.33 (triangles) and for R=3.0 (squares).

Chapter 5

Anti-solvent crystallization of the polymorphs of L-Histidine as a function of supersaturation ratio and of solvent composition

During the anti-solvent crystallization of L-Histidine from aqueous solution with the anti-solvent ethanol the polymorphic fraction of the metastable polymorph B increased with increasing supersaturation ratio. For supersaturation ratio $S_A \leq 2.0$ a mixture of the stable polymorph A and the metastable polymorph B was obtained, while for high supersaturation $S_A \geq 2.3$ only form B was observed. The supersaturation ratio was increased either by increasing the L-His concentration in the aqueous solution or by increasing the ethanol volume fraction. The induction time for the anti-solvent crystallization was one to several orders of magnitude smaller than the time to transform the metastable polymorph B into stable polymorph A in solution, indicating that both polymorphs formed simultaneously.

Process simulation of the batch anti-solvent crystallization of the polymorphs of L-His was applied to predict the outcome of the competition between heterogeneous nucleation and polynuclear growth rates for both polymorphs. When the interfacial energy was calculated as a function of the solubility only the formation of the stable polymorph A was erroneously predicted. By modifying the relative interfacial energy and the relative step free energy the predicted polymorphic fraction could be directed towards the observed polymorphic fraction.

5.1 Introduction

Polymorphism is of great interest to industry because polymorphs have different physical properties. Control of the formation of the different polymorphic structures during production is desired, especially to avoid concomitant polymorphism because this would result in a product with ill-defined properties. The relative stability of the polymorphs is defined by thermodynamics but the structure that will actually form, depends also on the kinetics, i.e. competitive nucleation and growth rates.

In anti-solvent crystallization a solution of the compound that has to be crystallized is mixed with an anti-solvent. The solubility of the compound in the mixed solvent is lowered compared to that in the original solution and in this way a driving force for crystallization or supersaturation can be created. At the same time, the interfacial energy between solution and crystal will increase. The increase in supersaturation ratio results in a decrease of the nucleation work while the increase of the interfacial energy results in an increase of the nucleation work.

In the case of polymorphism, different polymorphs will have a different solubility in the mixed solvent with the stable polymorph having the lowest solubility. Because of the difference in solubility the driving force towards the forms is different and so is the interfacial energy between the crystals and solution. The contribution of these effects to the reduction of the nucleation work may be different, and therefore the polymorphs may nucleate and grow at different rates. The polymorphic form that is obtained depends on how these competitive rates vary. According to Ostwald's rule of stages, the metastable polymorph forms first, followed by transformation to the more stable polymorph. It is generally known that this rule is not a physical law and that more stable forms can form directly as well.

In literature a number of studies describe the formation of different polymorphs in anti-solvent crystallization processes as a function of supersaturation or as a function of the ratio solution/anti-solvent. Beckmann (1999) studied the anti-solvent crystallization of Abecarnil from iso-propyl acetate with hexane as anti-solvent. At low supersaturation predominantly the stable form C was obtained while at high supersaturation the occurrence of the metastable form B increased. Toth (2003) studied the anti-solvent crystallization of Glycine from aqueous solution with ethanol as anti-solvent. At low supersaturation the more stable α-form, with increasing supersaturation only the less stable β-form and for even higher supersaturation a mixture of α and β was obtained.

The amino acid L-Histidine (L-His) is known to crystallize in a stable form A and a metastable form B [Kitamura 1994]. The stable form A has the orthorhombic space group $P2_12_12_1$ with $Z=4$ molecules in the unit cell [Madden 1972a]. The metastable form B has the monoclinic space group $P2_1$ with $Z=2$ molecules in the unit cell [Madden 1972b]. Figure 5.1 shows the crystal unit cell of both forms. The figure furthermore compares the conformation of the L-his molecule in the crystalline structures. The molecular conformation is quite similar. Experimentally it is determined that form A is the thermodynamically stable form at

room temperature, although the solubility difference of both forms is rather small.

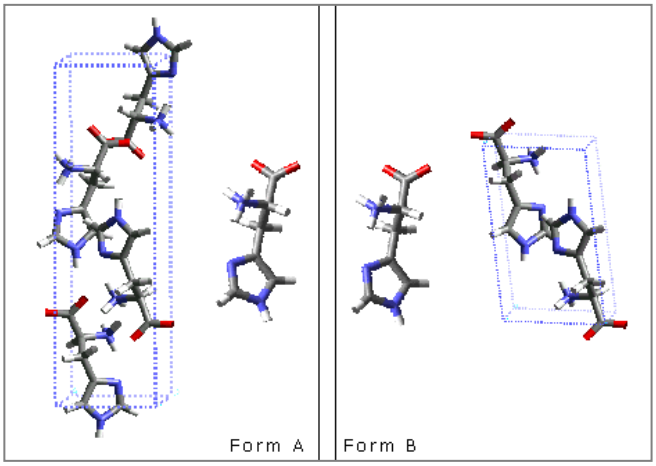

Figure 5.1 The crystal structure of form A (left) and form B (right) of the amino acid L-Histidine. The molecular conformation of both forms is shown next to the crystal structures and it can be seen that the molecular conformation is equal.

Kitamura (1993, 1994) described batch experiments on the formation of the polymorphs of L-Histidine:

a. By rapidly cooling an aqueous solution always a mixture of the stable A-form and the metastable B-form was obtained, followed by transformation to the A-form. It was concluded that the mixture formed because nucleation and growth rates were approximately equal.
b. By rapidly cooling a mixed solvent water-ethanol: for a low ethanol volume fraction a mixture of the stable A-form and the metastable B-form was obtained, while for a high ethanol fraction only the metastable B-form crystallized. Furthermore, for low ethanol fraction approximately equal growth rates for both polymorphs were measured while for high ethanol volume fraction the growth rate for the metastable B-form was higher compared to that of the stable A-from.

Gutzow and Toshev (1967) and Cardew and Davey (1982) defined rules for the conditions of formation of either the stable or the metastable polymorph. The polymorph that nucleates and grows with the highest rates consumes most of the supersaturation and the resulting product consists mainly of this polymorph. Two extreme cases can be defined:

a. Both polymorphs nucleate and grow at approximately similar rates and a mixture of the two polymorphs is initially obtained, also called concomitant polymorphism (Bernstein et al 1999).

b. One of the polymorphs nucleates and/or grows much faster than the other one and this polymorph is obtained.

It is the objective to study the formation of the polymorphs of L-His in anti-solvent crystallization as a function of increasing supersaturation ratio and of increasing interfacial energy. To do so the work by Kitamura (1994) will be extended in two ways:

a. By additional measurements in order to study the formation of polymorphs as function of supersaturation ratio and of ethanol fraction.
b. By population balance modeling of the batch crystallization with competitive nucleation and growth rates of the two polymorphs.

5.2 Precipitation theory

5.2.1 Driving force for anti-solvent crystallization

The driving force for a crystallization process is the difference in free Gibbs energy between the actual condition of the system and its equilibrium condition: $\Delta\mu=\mu_s-\mu_c$ with μ_s and μ_c the chemical potentials in solution and in the bulk of the crystal phase. When $\Delta\mu>0$ the system is supersaturated and nucleation could occur either homogeneously or heterogeneously.

In anti-solvent crystallization the driving force for the process is created by mixing a solution with an anti-solvent. In the resulting mixed solvent the solubility of the solute is decreased. The driving force can be rewritten as $\Delta\mu=kT\ln S_a$ with k [J K^{-1}] the Boltzmann constant and T [K] the absolute temperature. The activity-based supersaturation ratio is defined as $S_a=a_0/a_e$ with a_0 actual activity and a_e equilibrium activity. It is common practice to use the concentration c [mol m^{-3}] instead of x. A further simplification is to use the concentration based supersaturation ratio $S_c=c_0/c_e$ [-] with c_0 actual concentration in solution and c_e equilibrium concentration in solution. This is allowed when $\gamma_0\approx\gamma_e$.

5.2.2 Classical nucleation theory

To estimate the nucleation rates the classical nucleation theory is followed as described by Kashchiev (2001). The stationary rate of nucleation J [m^{-3} s^{-1}] can be described according to the following equation:

$$J = A\exp\left(\frac{-W^*}{kT}\right) \tag{5.1}$$

with: A [m^{-3} s^{-1}] pre-exponential kinetic parameter and W^* [J] the nucleation work.

For homogeneous nucleation (HON) A_{HON} is inversely proportional to the molecular volume ν_0 [m^{-3}]. Assuming spherical nuclei the nucleation work in the exponent is defined as:

$$W^* = -\frac{16\pi\nu_0^2\gamma^3}{3(kT)^2 \ln^2 S} \tag{5.2}$$

with: γ [J m^{-2}] interfacial energy. The nucleus size n^* [-] is defined according to the Gibbs-Thomson equation:

$$n^* = -\frac{32\pi\nu_0^2\gamma^3}{3(kT)^2 \ln^3 S} \tag{5.3}$$

The nucleation work depends on two main parameters: the externally controlled supersaturation ratio and the material surface/solution composition dependent interfacial energy. The interfacial energy γ can be estimated for a spherical nucleus from the bulk solubility c^* and molecular volume ν_0 according to Mersmann (1990):

$$\gamma = 0.514kT\frac{1}{\nu_0^{2/3}}\ln\frac{1}{\nu_0 c_e} \tag{5.4}$$

In practice even in filtered or destilled solvents a large number of particles that can act as template for nucleation are present. For 3D heterogeneous nucleation the effective interfacial energy γ_{eff} for HEN will be reduced by an activity factor $0<\psi<1$ [-] compared to the interfacial energy γ for HON. Because $\gamma_{eff}<\gamma$ the work of formation for HEN is substantially reduced compared to that for HON. Furthermore, for HEN the pre-exponential kinetic parameter A_{HEN} [m^{-3} s^{-1}] becomes inversely proportional to the concentration of heterogeneous particles C_a [m^{-3}] that is much smaller than the molecular volume ν_0. Typically $A_{HEN}\sim10^{15}$-10^{25} [m^{-3} s^{-1}]$<<A_{HON}\sim10^{35}$ [m^{-3} s^{-1}].

5.2.3 Growth mechanism

The crystal growth process is generally divided into two separate steps that can be assumed to take place in series:

a. Diffusion of the molecules from the bulk solution towards the crystal surface through the diffusion boundary layer.

b. Surface integration of the molecule into the crystal lattice. This step involves surface diffusion and partial or total desolvation before integration into the lattice

When growth is limited by diffusion from the bulk, the growth rate can be expressed as a linear function of the difference between bulk solution concentration and equilibrium concentration according to:

$$G_D = k_d \nu_0 (c_0 - c_e) \tag{5.5}$$

with: k_d [m s^{-1}] mass transfer coefficient and ν_0 [m^3] the molecular volume. For mass transfer to suspended crystals in agitated solution the mass transfer coefficient can be related to the Sherwood number:

$$Sh = \frac{k_d L}{D} = 2 + 0.66 Re^{1/2} Sc^{1/3} \tag{5.6}$$

with: L [m] crystal diameter, $Re = \rho u_s L/\eta$ the Reynolds number and $Sc = \eta/\rho D$ the Schmidt number, with u_s [m s^{-1}] particle slip velocity, ρ [kg m^{-3}] solution density and η [kg m^{-1} s^{-1}] solution viscosity. For very small particles (0.1 to 10 μm) the suspended phase tends to move with no slip along with the circulating fluid. In this case the effect of convective transport can be neglected and $Sh = k_d L/D = 2$.

For surface integration three types of crystal surfaces can be observed as a function of increasing supersaturation. First, for a molecularly very smooth crystal surface the attachment of new molecules is very difficult. Roughness is provided by the presence of step and kink sites. Steps at the crystal face are provided by screw-dislocations where spiral growth takes place. The growth rate perpendicular to the surface G [m s^{-1}] can be expressed as:

$$G_{BCF} = \frac{d_0 \nu_s}{\beta R^*} = \left(\frac{a_0 D c_e kT}{\beta d_0 \kappa} \right) (S-1) \ln S \tag{5.7}$$

with: d_0 [m] the molecular diameter, $\nu_s = a_0 D(c_0 - c_e)$ [m s^{-1}] velocity of step propagation, a_0 [m^2] the area of a molecule in the monolayer, $\beta = 19$ [-] a numerical factor, $R^* = a_0 \kappa/\Delta\mu$ [m] radius of a 2D nucleus, with κ [J m^{-2}] the step free energy which is related to the interfacial energy by $\kappa = k_s d_0 \gamma$ with k_s [-] a shape factor. For low supersaturation where $\ln S \approx S-1$, the growth rate equation becomes quadratic $G_{BCF} \sim (S-1)^2$.

Secondly, when the surface is molecularly smooth, the rate of growth is limited by the creation of new steps at the surface. A mechanism to create these steps is 2D nucleation followed by layer growth. The

nucleation mechanism can be mononuclear or polynuclear. For the mononuclear mechanism the growth rate perpendicular to the surface can be described as a function of supersaturation according to:

$$G_{MN} = d_0 A_{cr} J_{2D} = d_0 A_{cr} A_0 S \exp\left(-\frac{\pi a_0 \kappa^2}{(kT)^2 \ln S}\right) \quad (5.8)$$

In this equation A_{cr} [m^2] is the area of the crystal face and J_{2D} [m^{-2} s^{-1}] is the equation for the 2D nucleation rate of a compound on its own substrate under the assumption of disk-shaped nuclei with A_0 [m^{-3} s^{-1}] the pre-exponential kinetic parameter.

For the polynuclear mechanism the growth rate perpendicular to the surface can be described as a function of the 2D nucleation rate J_{2D} of a compound on its own substrate under the assumption of disk-shaped nuclei with lateral velocity v_s [m s^{-1}]:

$$G_{PN} = d_0 (\tfrac{1}{3}\pi {v_s}^2 J_{2D})^{1/3} = d_0 (\tfrac{1}{3}\pi a_0 D c_e)^{2/3} {A_0}^{1/3} (S-1)^{2/3} S^{1/3} \exp\left(\frac{\pi a_0 \kappa^2}{3(kT)^2 \ln S}\right) \quad (5.9)$$

Finally, when a crystal surface is rough on molecular scale, growth is continuous. For molecular compounds the surface becomes rough when the step free energy κ becomes equal to zero at the roughening temperature T_R. When a solute molecule arrives at the surface it is immediately integrated. For rough growth crystal faces tend to become rounded. For salts kinetic roughening is observed when the activation energy required for the formation of a two-dimensional critical nucleus becomes of the order kT. During kinetic roughening the step free energy is still non-zero.

For rough growth of a surface the growth rate depends on the difference between the flux of growth units from the bulk that impinges on a growth position in the crystal surface f_s [s^{-1}] and the flux of growth units that leaves the surface g_s [s^{-1}]:

$$G_{RG} = d_0 (f_s - g_s) = a_0 D c_e (S-1) \quad (5.10)$$

Rough growth is a linear function of the supersaturation ratio.

5.2.4 Induction time

In precipitation studies it is common practice to measure the induction time t_{ind} [s] defined as the time elapsed between the moment that

supersaturation is created and the moment that crystals are observed. The method depends not only on the nucleation rate but also on the growth rate of the crystals, on the applied observation technique and its detection limit. For stationary nucleation of spherical crystals using visual observation (a volume-based technique) the induction time is given by the following equation:

$$t_{ind} = \left(\frac{3\alpha_v}{\pi J G^3} \right)^{1/4} \tag{5.11}$$

with α_v the detectable volume fraction of the new crystalline phase formed in the solution. In the case of the polymorphs of L-His, nucleating and growing at different rates J_i and G_i, the metastable polymorph B is first observed when $J_B G_B^3 > J_A G_A^3$. The induction time should be larger than the time for mixing $t_{ind} > t_m$ to exclude the effect of mixing.

5.2.5 Process simulations of polymorph crystallization

The aim of the population balance based process model is to describe the evolution of the crystal quality in a precipitation process as a result of the nucleation and growth of a polymorphic system. In this way the effects of the evolution of the process conditions like supersaturation and interfacial energy during the process can be taken into account as well as the spatial distribution of these process variables. An example of the use of population balances was given by Ono (2004) who modeled the solution mediated transformation of the polymorphs of L-Glutamic Acid, taking into account the simultaneous dissolution of the metastable polymorph and the growth of the stable polymorph.

In this study the overall effect of competitive nucleation and growth rates of the polymorphs during a batch anti-solvent crystallization process is simulated. For the two polymorphic phases, the time evolution of the crystal size distributions is described with population balances coupled with the component mass balances and the enthalpy balance. Assuming a well-mixed vessel, the population balance equation (PBE) for a batch process is given by:

$$\frac{\partial V(t) n_i(L,t)}{\partial t} = \frac{V(t) \partial G_i(L,t) n_i(L,t)}{\partial L} + B_i(L,t) V(t) - D_i(L,t) V(t) \quad \{i = 1,2\} \tag{5.12}$$

with: n_i is the population density [# μm^{-1} m^{-3}] of polymorph i, B_i and D_i the birth and death functions [# μm^{-1} m^{-3}], V the volume and L the

crystal size [μm]. The initial conditions for the two different classes of population is given by:

$$n_i(L, t=0) = 0 \tag{5.13}$$

while the boundary condition (B.C.) with respect to crystal size for the two PBE's is:

$$n_i(L=0, t) = \frac{J_i(t)}{G_i(L=0, t)}; \quad G_i(L) \geq 0 \ \forall L \tag{5.14}$$

In this paper agglomeration of crystals is neglected and only size independent crystal growth is considered while it is assumed that nuclei formed via the primary nucleation mechanism only taking place at the lower boundary of the size domain. Solvent mediated transformation of the two polymorphs is not considered.

5.3 Experimental

5.3.1 Materials and instrumentation

Solutions of L-His (Fluka Chemie chemical purity ≥99%) were prepared with ultra pure water and pure ethanol (chemical purity ≥99.9%). In a typical batch experiment, the two solutions were poured synchronously into a stirred crystallizer with volume V=0.1 dm3. The mixed solutions were continuously stirred with a magnetic stirrer (300 rpm). A HoloLab Series 5000 Raman spectroscopy (Kaiser Optical System, Inc.) was used to record Raman spectra (NIR excitation radiation at 785 nm).

5.3.2 Preparation of polymorph B

The purchased L-His was found to be pure form A using powder diffraction. To obtain the B-form of L-His, an undersaturated aqueous solution (0.25mol l^{-1}) was prepared by dissolving L-His form A in ultra pure water. This solution was stirred at room temperature during 24 hours using a magnetic stirrer. In a batch set-up to this solution pure ethanol was added to a volume fraction $x_{v,EtOH}$=0.5. After stirring for 5 minutes, crystals were obtained by filtration over a 0.22 μm filter (Millipore). The wet cake was dried immediately in the oven at 323K for 12 h. The dried crystals were identified by XRPD as polymorph B.

5.3.3 Solubility measurement

The solubility of L-His at room temperature (298K) was measured as a function of ethanol volume fraction. Excess amounts of L-His form A and form B were dissolved in 20 ml mixed solvent to saturate the solutions. After 24 h of stirring, the suspensions were filtered over a 0.22 μm filter. The saturated solutions were evaporated at 323K. The weight of the dry L-His sample was used to calculate the solubility.

5.3.4 Polymorphic transformation

The transformation rate of the metastable polymorph B into the stable polymorph A was studied as a function of the ethanol fraction $x_{v,EtOH}$=0.2, 0.3, 0.4 and 0.5. An aqueous solution at 90% of the L-His solubility was prepared. Mixtures were prepared from this aqueous solution by addition of the ethanol in a stirred crystallizer. Samples of the crystals were taken at time intervals of several hours for analysis of their polymorphic composition by Raman spectroscopy.

5.3.5 Anti-solvent crystallization of L-His polymorphs

The formation of L-His polymorphs was studied during crystallization from aqueous solutions with ethanol as anti-solvent. For an ethanol volume fraction $x_{v,EtOH}$=0.3-0.4 the concentration of the L-His aqueous solution was varied from 80%-100% of the solubility in pure water (0.28 mol l^{-1}), for $x_{v,EtOH}$=0.5 from 60%-100% and for $x_{v,EtOH}$=0.6 from 50-60%. Aqueous solutions of L-His were prepared by dissolving L-His in 50ml ultra pure water. The solutions were stirred during 24 hours using a magnetic stirrer.

In a stirred crystallizer pure ethanol was added to the aqueous solution and the mixture was stirred using a magnetic stirrer (300 rpm). Induction times were measured by visual observation. Samples of the crystals were filtered over a 0.22 μm filter. The wet cake was dried in the oven at 323K for 12 h. The resulting dry powders were analyzed by Raman spectroscopy to determine the polymorphic fraction.

5.4 Experimental results

5.4.1 Raman spectroscopy

The Raman spectra of pure form A and form B show some distinct differences. These differences can be used to quantify the polymorphic fraction in samples in mixtures of both polymorphs with unknown

composition. A calibration line for quantitative analysis was constructed using pure A and B to create a binary mixture with known polymorphic fraction. The mixtures were prepared by grinding dry powders. In this way, samples with A-form fraction x_A=0, 10, 20, …, 90, 100 wt % were obtained.

As shown in figure 5.2, the specific A and B peaks overlapped for the binary mixture samples, especially in the range of 200-230 cm^{-1}. It was found that the most accurate calibration line could be obtained using the surface area of the peak in this range while setting the peak in the range of 510-560 cm^{-1} as a reference. Good agreement was found between the actual values and the predicted values given by Raman quantitative analysis. The average error between these two values was 4%, which was considered acceptable.

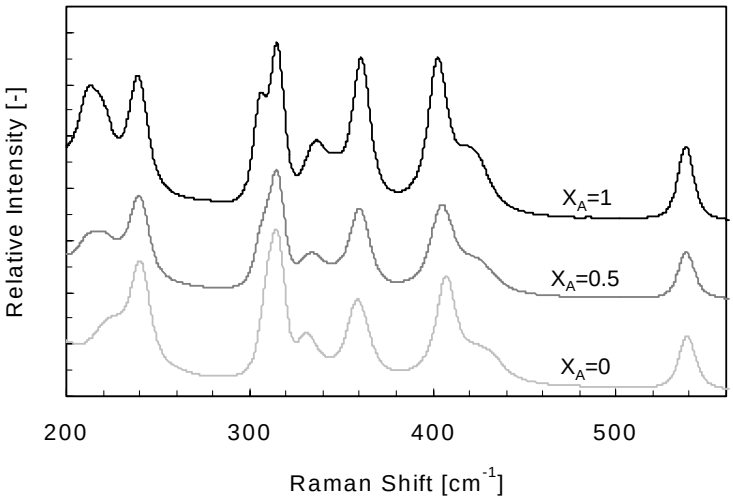

Figure 5.2 Comparison of Raman spectra in range of 200-560 cm^{-1} for the pure polymorphs A and B of L-His and for a mixture of both polymorphs.

5.4.2 Solubility measurements

In this work the solubility of the L-His polymorphs A and B in a water-ethanol mixed solvent was measured as a function of the volume fraction ethanol in the range $x_{v,EtOH}$=0 to 0.8 at a temperature of 298K. The results are shown in figure 5.3 together with the data obtained by Kitamura (1994) at 293K. An overall higher solubility level can be observed for the measurements carried out at the higher temperature. Kitamura observed an increase of the solubility of the polymorphs of L-

His with temperature in pure water. Both at 293K and at 298K the solubility of the stable polymorph A was slightly smaller than that of the metastable polymorph B. For an ethanol volume fraction of $x_{v,EtOH}$=0.6 the solubility of the two polymorphs could not be measured sufficiently accurate to detect a significant difference. Theoretically, the ratio of the solubility of the polymorphs $c_{A,e}/c_{B,e}$ (or more precisely the ratio of the activities $a_{A,e}/a_{B,e}$) should be independent of the composition of the mixed solvent, because this property is determined by the difference in Gibbs free energy between the bulk crystal forms.

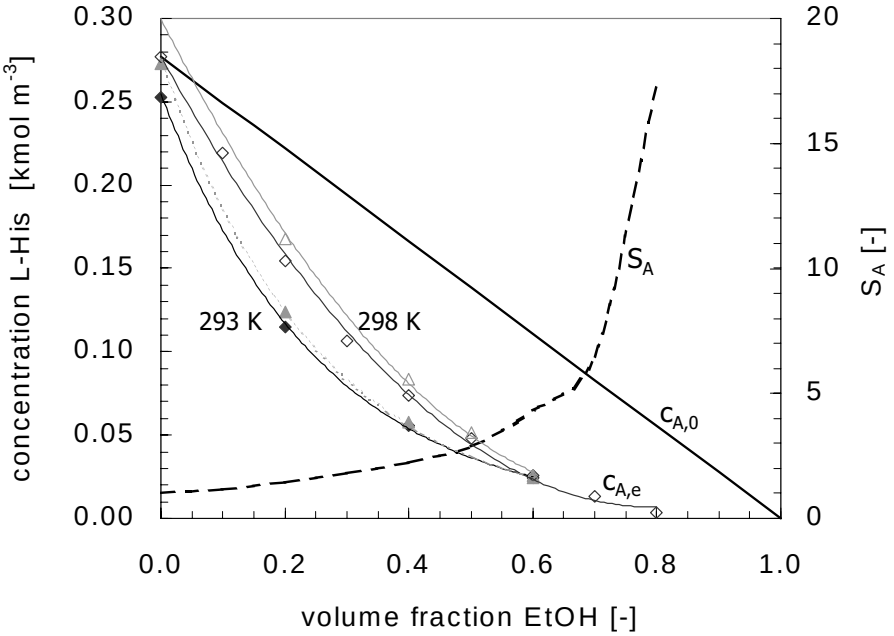

Figure 5.3 Solubility curves for the polymorphs of L-His as a function of ethanol volume. Symbols: ♦: form A, ▲: form B, T=293K [Kitamura 1994], ◊: form A, Δ: form B, T=298K (this work). Lines are given as a guide to the eye. In this figure is shown the working line $c_{A,0}$ (solid line) for form A at 298K as a function of the volume fraction ethanol. The supersaturation S_A (dotted line) is a function of the difference between the working line and the solubility curve $c_{A,e}$.

In figure 5.3 the working line $c_{A,0}$ and the solubility curve $c_{A,e}$ for L-His stable polymorph A are presented as a function of the ethanol volume fraction. The corresponding concentration-based supersaturation ratio $S_A=c_{A,0}/c_{A,e}$ is shown as well. An increase of the supersaturation ratio with increasing ethanol fraction $x_{v,EtOH}$ can be observed. For further increasing values of $x_{v,EtOH}$ the supersaturation ratio will eventually decrease again until for the ethanol volume fraction approaching $x_{v,EtOH}$=1, S_A=0. This

was not depicted in this figure because no reliable solubility measurements were available for high ethanol volume fraction.

5.4.3 Supersaturation ratio calculation: activity versus concentration

The activity coefficients γ_0 and γ_e for actual concentration c_0 and equilibrium concentration c_e for L-His in mixed solvents were determined using COSMOtherm, a Chemical Computational tool to calculate the surface charge density of the electron shell of molecules [Klamt 2004, Eckert 2002]. The objective of this calculation was to investigate whether there would be a difference between the activity based supersaturation ratio and the concentration-based supersaturation ratio.

For the solute L-His the chemical potential was calculated separately for both the charged Zwitter-ion and the uncharged molecule. The effective chemical potential of the L-His in solution was calculated from a Boltzmann-distribution over these two forms of the molecule. This distribution changed with the composition of the mixed solvent. The solvent environment was approached having the electrical properties of a mixture of the more polar water molecule and the less polar ethanol molecule.

In figure 5.4 the activity coefficient is shown as a function of increasing ethanol molar fraction $x_{m,EtOH}$ and of increasing L-His molar fraction $x_{m,L\text{-}His}$. It can be observed that the activity coefficient $\gamma_{L\text{-}His}$ increases with increasing ethanol molar fraction $x_{m,EtOH}$ in the mixed solvent because the polar L-His molecule has less affinity for the less polar solvent ethanol and more for the polar solvent water. For $x_{m,EtOH} \approx 0.2$ a point can be observed where activity coefficient $\gamma_{L\text{-}His} \approx 0.7$ becomes invariant with L-His molar fraction $x_{m,L\text{-}His}$. For this specific mixed solvent the surface charge density of the L-His-molecule is very similar to that of the surrounding mixed solvent and also close to that of the L-His molecule in its reference state (L-His melt $\gamma_{L\text{-}His}=1$). Under these conditions the solution may be considered as a 'diluted melt'. This point corresponds to an ethanol volume fraction $x_{v,EtOH} \approx 0.4$.

In the experiments described in this work $x_{m,EtOH}$ varied from 0.15 to 0.37 and $x_{m,L\text{-}His}$ from 0.0007 to 0.0035 while the molar supersaturation ratio $S_x = x_{0,m,L\text{-}His} / x^*_{m,L\text{-}His}$ varied from 1.4 to 3.1. At these conditions the lines for $\gamma_{L\text{-}His}=0.001$, 0.005 and 0.01 lie closely together. Because the difference in γ_0 and γ^* is always less than 10%, the use of a concentration-based supersaturation ratio in the analysis of the experiments is justified

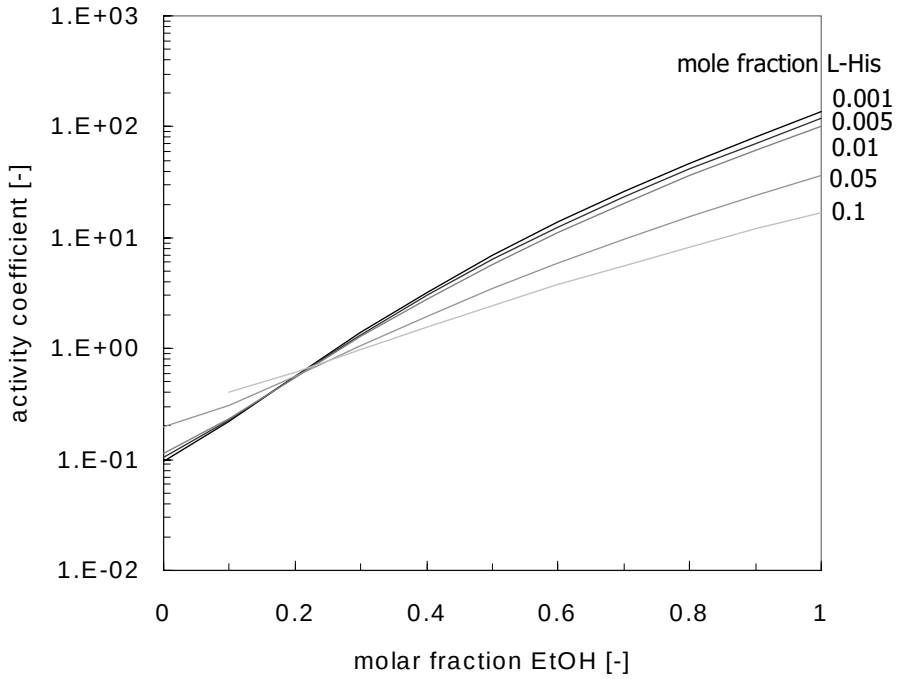

Figure 5.4 Activity coefficients as a function of increasing ethanol molar fraction $x_{m,EtOH}$ for different molar fractions $x_{m,L\text{-}His}$ of L-His as calculated from molecular simulations.

5.4.4 Induction time versus transformation time

Induction times were measured as a function of supersaturation. Induction times varied from one hour for $x_{v,EtOH}$=0.2 to approximately 40 seconds for $x_{v,EtOH}$=0.4. For $x_{v,EtOH}$=0.2 and 0.3 the induction time decreased strongly with increasing supersaturation ratio while for $x_{v,EtOH}$=0.4 no significant difference could be measured with increasing supersaturation. Mixing of the reactants was assumed to have no influence on the experimental results because the shortest induction time of anti-solvent precipitation t_{ind}>40 [s] is much longer than the premixing time in the batch crystallizer t_m~1 [s].

Experimentally the supersaturation ratio was increased either by increasing the concentration of L-His in the aqueous solution while the ethanol volume fraction was kept constant, or by increasing the ethanol volume fraction. In the latter case, the solubility in the mixed solvent decreased, resulting in an increase of the interfacial energy.

Theoretically, an increase in supersaturation ratio results in a decrease of the nucleation work while an increase of the interfacial energy has the opposite effect. Experimentally, with increasing ethanol volume fraction a decrease of the induction time was observed, indicating that the effect of a higher supersaturation ratio outbalanced the effect of the higher interfacial energy.

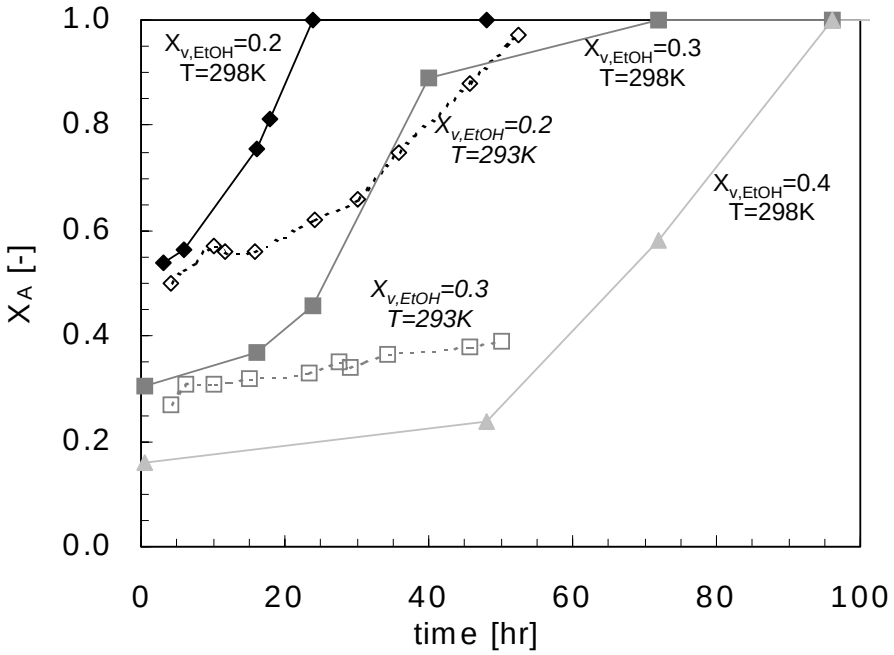

Figure 5.5 Increasing fraction of the stable polymorph A is shown as a function of time. Symbols: ♦: $x_{v,EtOH}$=0.2, ■: $x_{v,EtOH}$=0.3 and ▲: $x_{v,EtOH}$=0.4 at T=298K (this work), ◊: $x_{v,EtOH}$=0.2 and □: $x_{v,EtOH}$=0.3 at T=293K [Kitamura 2001]. Lines are added to guide the eye.

The transformation in a slurry of crystals of polymorphs A and B was followed versus time. In figure 5.5 the increasing fraction of the stable polymorph A is shown as a function of time. The transformation is more rapidly for the more aqueous mixtures. The transformation times are one to several orders of magnitude longer than the induction times. The assumption that when two polymorphs are observed in the same experiment, this is due to concomitant nucleation and growth, seems therefore acceptable. Figure 5.5 includes the results of Kitamura (2001) on transformation at 293K as well. In these experiments the transformation takes place slightly slower. This may be due to the lower solubility of L-His in solution at lower temperature (293 K vs. 298K).

5.4.5 Formation of polymorphs as a function of concentration and ethanol fraction

The concentration-based supersaturation ratio S_A was varied from 1.5 to 2.9. The polymorphic fractions and experimental conditions are shown in table 5.1. In this table the interfacial energy calculated according to equation (5.4) is included as well.

Table 5.1 The ethanol volume fraction $x_{v,EtOH}$, actual concentration c_0 in the mixed solvent, polymorph A equilibrium concentration in the mixed solvent $c_{A,e}$, interfacial energy γ_A, supersaturation ratio $S_A=c_0/c_{A,e}$ and the experimentally obtained polymorphic fraction X_A.

$x_{v,EtOH}$ [-]	c_0 [kmol m^{-3}]	$c_{A,e}$ [mol m^{-3}]	γ_A [mJ m^{-2}]	S_A [-]	X_A [-]
0.3	0.155	0.106	30	1.5	0.47
	0.175			1.6	0.42
	0.194			1.8	0.44
0.4	0.133	0.074	32	1.8	0.24
	0.150			2.0	0.16/0.36
	0.166			2.2	0.10/0.0
0.5	0.083	0.048	35	1.7	0.36
	0.097			2.0	0.25/0.35/0.23
	0.111			2.3	0.0/0.0
	0.125			2.7	0.0/0.0
	0.139			2.9	0.0
0.6	0.052	0.026	39	2.2	0.19
	0.067			2.6	0.0

In figure 5.6 the fraction of the stable polymorph A is shown as a function of the supersaturation ratio S_A and of the interfacial energy γ_A. In this figure from the left bottom corner to the right top corner, with increasing supersaturation ratio and with increasing interfacial energy, the polymorphic fraction A decreases. For low supersaturation ratio $S_A \leq 2.0$ the polymorphic fraction $0.16 < X_A < 0.47$ while for high supersaturation ratio $S_A \geq 2.3$: $X_A = 0$. In the same figure the results by Kitamura for crystallization from mixed solvent at 293K are shown that fit with the new measurements at 298K.

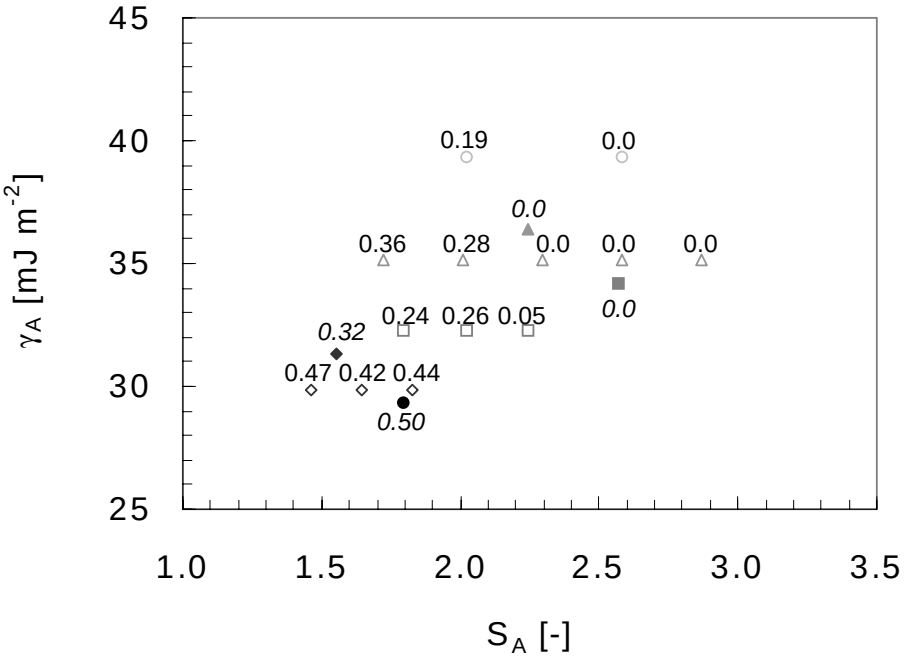

Figure 5.6 Fraction X_A of the stable polymorph A as a function of the supersaturation ratio S_A for $x_{v,EtOH}$=0.3, 0.4, 0.5 and 0.6 at 298K shown as open markers (this work) and for $x_{v,EtOH}$=0.2, 0.3, 0.4 and 0.5 at 293K shown as filled markers [Kitamura 1994].

In figure 5.7 crystals are shown from the experiments carried out at an ethanol fraction of $x_{v,EtOH}$=0.5 and a supersaturation ratio of respectively S_A=2.2 and S_A=2.8.

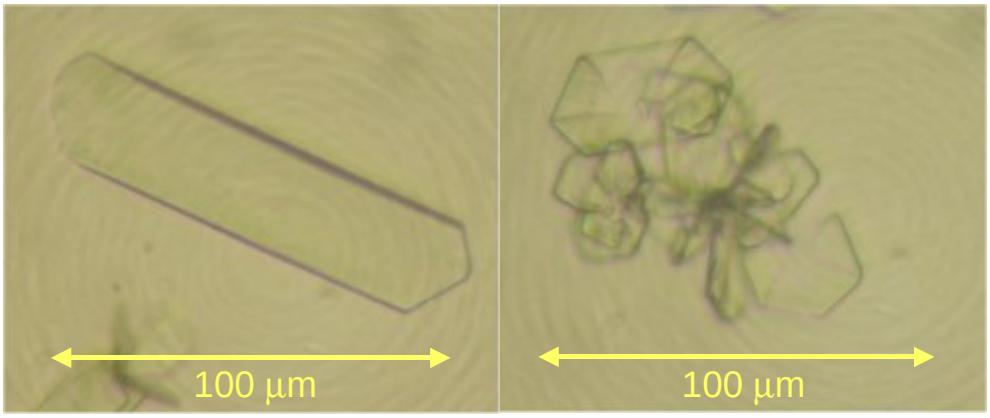

Figure 5.7. Left: crystals obtained for S_A=2.2 with $x_{v,EtOH}$=0.5 and X_A=0.25. Right: crystals obtained for S_A=2.8 with $x_{v,EtOH}$=0.5 and X_A=0.0.

5.5 Discussion

It can be estimated which of the two polymorphs of L-His will form as a function of the ethanol volume fraction by calculating the competitive nucleation and growth rates as a function of supersaturation ratio and interfacial energy. In figure 5.8 theoretical rates for homogeneous nucleation (HON) and for heterogeneous nucleation (HEN) are plotted for L-His form A as a function of the dimensionless solubility c_e/c_c [-] and dimensionless supersaturation $(c_0-c_e)/c_c$ [-] with $c_c=1/v_0$ [m^{-3}] being the crystal density according to Mersmann (2001). Equation (5.1) and the physical properties of the stable L-His polymorph A were used to calculate the supersaturation ratio to achieve a certain HON-rate. To calculate the HEN–rate a reasonable value for the kinetic parameter A_{HEN} of $1 \cdot 10^{20}$ [$m^{-3}s^{-1}$] was assumed and different values of the effective interfacial energy $\gamma_{eff}=\psi\gamma$ with efficiency factor ψ=0.3, 0.4 and 0.5 are shown.

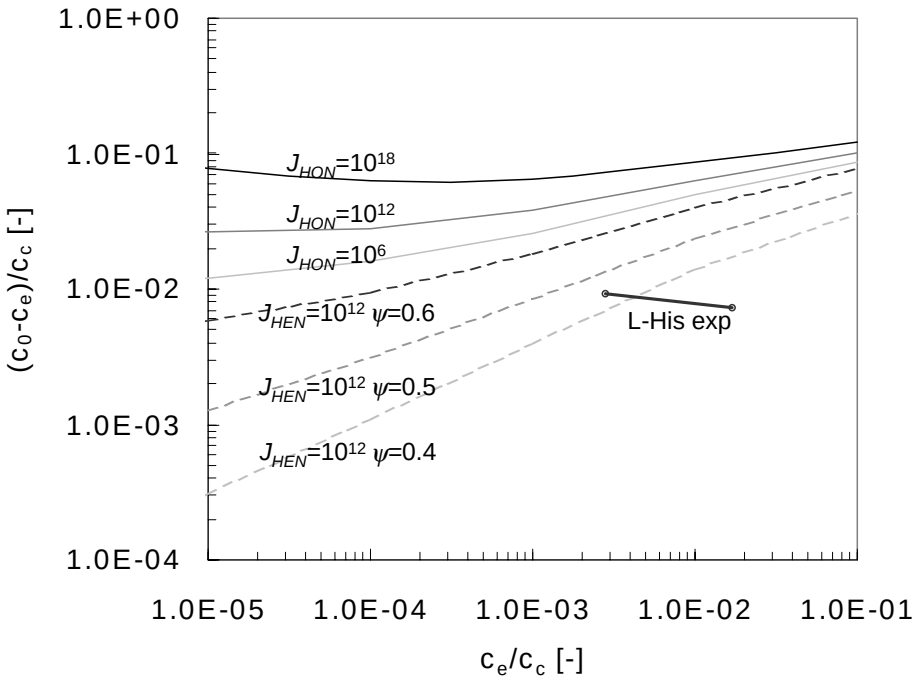

Figure 5.8 Theoretical rates for J_{HON} and for J_{HEN} as a function of the dimensionless solubility c_e/c_c [-] and dimensionless supersaturation $(c_0-c_e)/c_c$ [-] calculated according to equation (5.1). J_{HEN} for a value for the kinetic parameter A_{HEN} of $1 \cdot 10^{20}$ [$m^{-3}s^{-1}$] and value for the interfacial energy ψ=0.4, 0.5 and 0.6. Experimental conditions are shown for L-His form A.

In figure 5.8 the experimental conditions for supersaturation and solubility in a dimensionless form are included. With increasing ethanol volume fraction, the solubility c_e/c_c decreases by one order of magnitude while the superaturation $(c_0-c_e)/c_c$ increases only slightly. From this figure it was concluded that under these experimental conditions nucleation takes place according to a HEN mechanism.

The nucleation work for the two polymorphs was calculated using equation (5.2). The supersaturation ratio $S_A>S_B$ because bulk solubility of the stable polymorph A is slightly smaller than that of the metastable polymorph B: in pure water at 298K $c_{A,e}=0.28<c_{B,e}=0.30$ [kmol m^{-3}]. The two polymorphs also have slightly different molecular volumes $\nu_{0,A}=0.178\cdot10^{-27}<\nu_{0,B}=0.180\cdot10^{-27}$ [m^3]. From the equilibrium solubility in pure water and the molecular volume the interfacial energy can be calculated according to equation (5.4): $\gamma_A=23.5>\gamma_B=22.7$ [mJ m^{-2}] with ratio $\gamma_B/\gamma_A=0.97$. The resulting nucleation work $W^*_A<W^*_B$ results in a theoretically higher nucleation rate for the stable polymorph A.

A lower nucleation work for the stable phase compared to that of the metastable phase was also calculated using the CNT and equation (5.4) by Kabasci (1996) for Calcium Carbonate polymorphs Vaterite and Calcite. Kolar (1986) used an equation similar to equation (5.4) for the two polymorphs of Barium Fluoride. In both cases experimentally, however, the formation of the metastable phase was observed before that of the more stable phase. By using equation (5.4) a fixed relationship between interfacial energy and bulk solubility is introduced. However, this equation may be not sufficiently accurate to calculate the interfacial energy for polymorphs with almost identical solubility.

Experimentally, for L-Histidine for low S_A both form A and B were obtained while for increasing S_A only metastable form B was found. The observed polymorphic fraction is the result of both nucleation and growth. Kitamura (1994) experimentally determined the growth rates for L-His polymorphs A and B as a function of their supersaturation ratio S_A and S_B for $x_{v,EtOH}=0.0$, 0.2 and 0.4 by measuring the increase of crystal slurry mass with time. For low ethanol fraction: $G_A\approx G_B$ while for high ethanol fraction: $G_B\approx2G_A$ while a 2D nucleation mechanism was suggested. This indicated that with increasing ethanol fraction the ratio of the step free energy κ_B/κ_A and maybe also the ratio of the interfacial energy γ_B/γ_A, is lowered, lowering the relative nucleation work of metastable form B (both 3D HEN and 2D HEN) compared to that of stable form A hence favoring the formation of form B. It can, however, not be excluded that other factors like impurities influence the ratio of the step free energy κ_B/κ_A and the ratio of the interfacial energy γ_B/γ_A of

the polymorphs and hence selectively promote nucleation of one phase or inhibit growth of one phase.

5.6 Process simulations of polymorph crystallization

Process simulations were done to simulate a typical batch anti-solvent crystallization experiment producing L-His crystals. The process model is implemented in gPROMS (Process Systems Enterprise Ltd), a commercial modeling and optimization tool. A modular framework has been developed which enables the easy implementation of multi-component systems including multiple crystal phases, different supersaturation generation methods, operation modes, crystallizer types (DTB, FC, stirred vessel) as well as multi zonal models to account for non ideal mixing in the crystallizer (Bermingham 2002).

In this work the heterogeneous nucleation rate is calculated using the activity factor ψ to account for the change in the interfacial energy γ_{eff} and a constant, equal number of nucleation sites for both polymorphs. For the relatively high experimental supersaturation ratio it is not expected that growth takes place according to the spiral growth mechanism. Because well-faceted crystals were observed rough growth is neither likely. Crystal growth measurements on suspensions by Kitamura (1994) indicated a poly-nuclear growth mechanism. In the process model size independent poly-nuclear growth was relatively easily implemented.

In four simulations the activity factor ψ_i and the shape factor $k_{s,i}$ will be used to vary the ratio between γ_{eff} and κ of the polymorphs, effectively varying the competitive nucleation and growth rates. The experimental and simulation settings are given in table 5.2, together with the simulated mass fraction X_A at the end of the batch (80s).

Table 5.2 Experiment and simulation settings and simulated mass fraction X_A: batch experiments were simulated done at T=298K, Initial supersaturations S_A=2.2, S_B=2.0 and S_A=2.8, S_B=2.5 Initial volume 2 litre, volume fraction ethanol $x_{v,EtOH}$=0.5; Simulation settings: ψ_A=0.3; $k_{s,A}$=0.67, k_g=0.1·10^{-3} [m s^{-1}]; A_{HEN}=1·10^{20} [m^{-3} s^{-1}].

Simulation nr	Sim1	Sim2	Sim3	Sim4
ψ_B/ψ_A $k_{s,B}/k_{s,A}$	1 1	1 0.85	0.85 1	0.9 0.9
S_A=2.2: X_A at t=80s	1.00	0.50	0.47	0.07
S_A=2.8: X_A at t=80s	0.98	0.16	0.47	0.08

The simulated trends in the nucleation and growth rates and the mass fraction A for Sim1 are given in figures 5.9a and 5.9b. The settings in Sim1 are such that in fact the classical nucleation theory is used. The interfacial energy γ is calculated by equation (5.4) to estimate the step free energy κ using a shape factor k_s=2/3 for both polymorphs. The simulation predicts a mass fraction $X_A \approx 1$ due to the much higher nucleation and growth rates for the stable polymorph A, whereas in the experiment, a mass fraction A of around 0.3 is found for S_A=2.2 while for the experiments at S_A=2.8 only form B is observed.

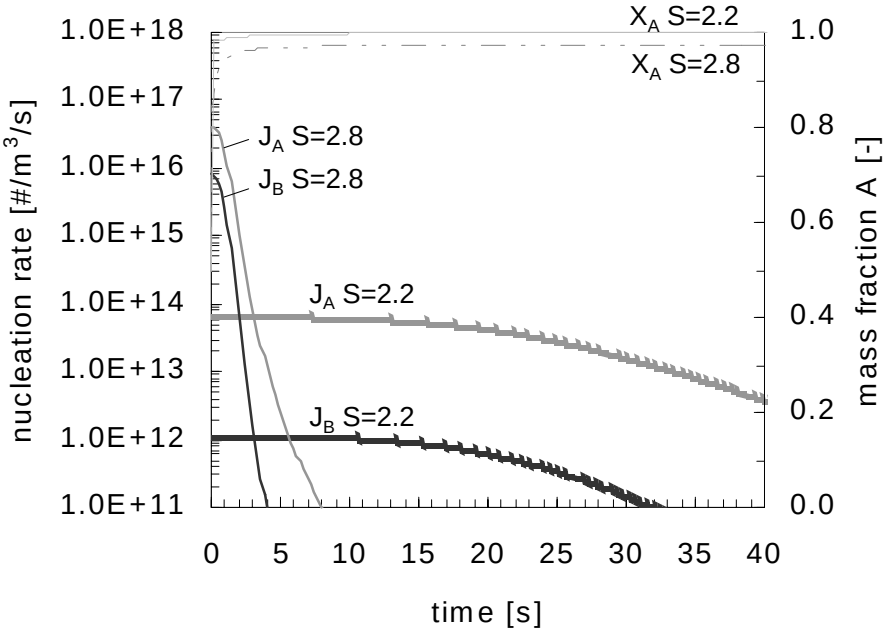

Figure 5.9a Sim1: dynamic simulation of the nucleation rates of the L-His polymorphs A and B at low S_A=2.2 and high S_A=2.8 both for x_{vEtOH}=0.5. Furthermore the fraction of L-His polymorph A is depicted. For the base case the following values were assumed: kinetic parameter $A_{HEN}=1\cdot10^{20}$ [$m^{-3}s^{-1}$], ψ=0.3 with ψ_A/ψ_B=1 and growth constant $k_G=0.1\cdot10^{-3}$ with $k_{s,A}/k_{s,B}$=1.

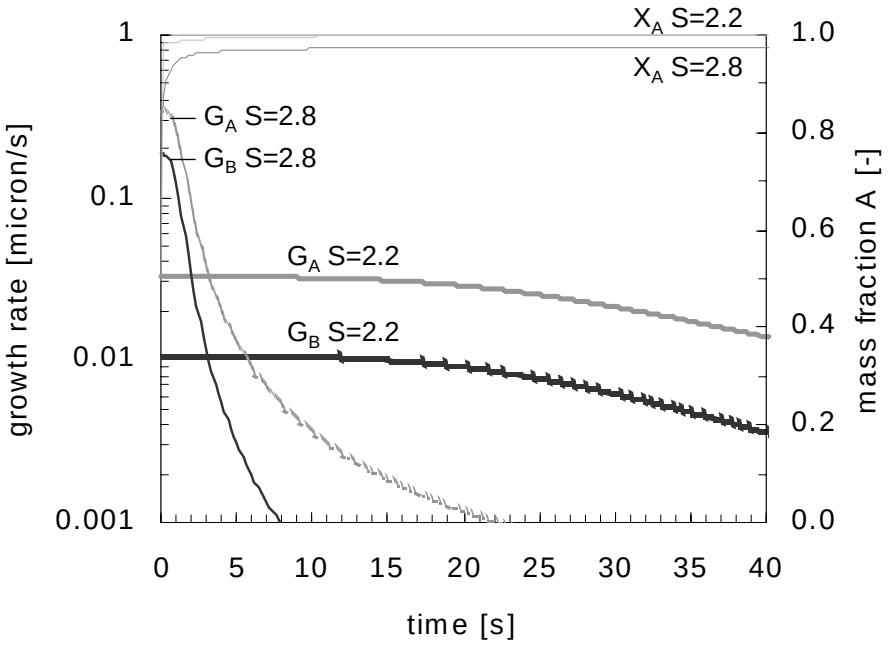

Figure 5.9b Sim1: dynamic simulation of the growth rates of the L-His polymorphs A and B at low S_A=2.2 and high S_A=2.8 both for x_{vEtOH}=0.5. Furthermore the fraction of L-His polymorph A is depicted. For the base case the following values were assumed: kinetic parameter $A_{HEN}=1\cdot10^{20}$ [$m^{-3}s^{-1}$], ψ=0.3 with ψ_A/ψ_B=1 and growth constant $k_G=0.1\cdot10^{-3}$ with $k_{s,A}/k_{s,B}$=1.

However if the ratio of $k_{s,B}/k_{s,A}$ is decreased the calculations predict a lower mass fraction (Sim2) for both S_A=2.2 and for S_A=2.8. For the ratio $k_{s,B}/k_{s,A}$=0.85 the calculated mass fractions are approximately equal to the observed mass fractions. If the ratio ψ_B/ψ_A for the two polymorphs is decreased (Sim3) the calculated mass fractions become lower as well, but for ψ_B/ψ_A=0.85 the calculated mass fraction for S_A=2.2 fits better with the observed value than that for S_A=2.8. The simulated trends in the growth rates and the mass fraction A for Sim2 are given in figure 5.10 while the simulated trends in the nucleation rates and the mass fraction A for Sim3 are given in figure 5.11.

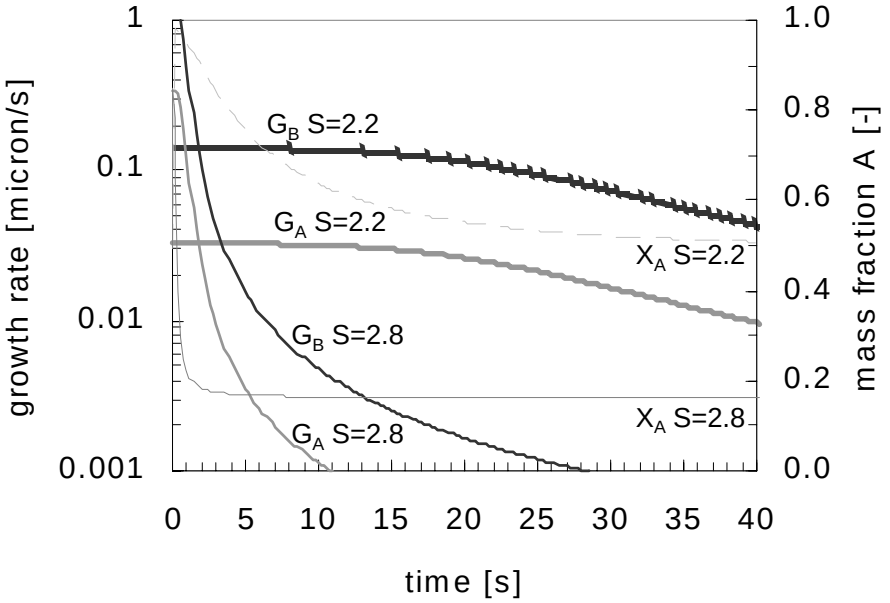

Figure 5.10 Sim2: dynamic simulation of the growth rates of the L-His polymorphs A and B at low S_A=2.2 and high S_A=2.8 both for x_{vEtOH}=0.5. Furthermore the fraction of L-His polymorph A is depicted. The following values were assumed: kinetic parameter $A_{HEN}=1\cdot10^{20}$ [$m^{-3}s^{-1}$], ψ=0.3 with ψ_A/ψ_B=1 and growth constant $k_G=0.1\cdot10^{-3}$ with $k_{s,A}/k_{s,B}$=0.85.

If in the simulations the ratios between interfacial energy γ_B/γ_A and the step-free energy κ_B/κ_A of the metastable polymorph B and stable polymorph A are further lowered, the nucleation and growth rates of metastable polymorph B are increased. Finally, if both ratios are decreased simultaneously to $k_{s,B}/k_{s,A}=\psi_B/\psi_A$=0.9 (Sim4) both the nucleation rate and the growth rate of polymorph B are higher than the those of polymorph A, resulting in a calculated mass fraction X_A<0.1 for both S_A=2.2 and S_A=2.8. Experimentally for high supersaturation ratio and for high ethanol volume fraction an increase of the polymorphic fraction of the metastable B polymorph was observed.

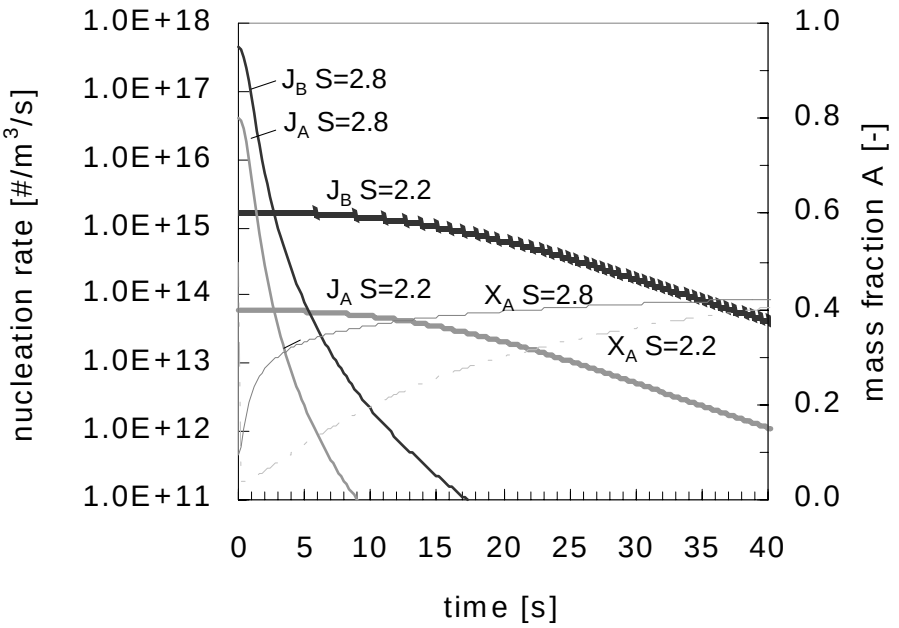

Figure 5.11 Sim3: dynamic simulation of the nucleation rates of the L-His polymorphs A and B at low S_A=2.2 and high S_A=2.8 both for x_{vEtOH}=0.5. Furthermore the fraction of L-His polymorph A is depicted. The following values were assumed: kinetic parameter $A_{HEN}=1\cdot10^{20}$ [$m^{-3}s^{-1}$], ψ=0.3 with ψ_A/ψ_B=0.85 and growth constant $k_G=0.1\cdot10^{-3}$ with $k_{s,A}/k_{s,B}$=1.

The appearance of concomitant polymorphs of L-His may be explained by the mechanism of competitive nucleation and growth rates. By varying the ratios between interfacial energy γ_B/γ_A and the step-free energy κ_B/κ_A of the two polymorphs, either simultaneously or independently, the competitive nucleation and growth rates and hence the polymorphic fraction could be manipulated in the simulations. It is not unlikely that with an increasing ethanol volume fraction in the mixed solvent the ratios γ_B/γ_A and κ_B/κ_A actually are changed. It is also not impossible that an additive or impurity acts selectively on only one of the polymorphs. For example an additive may selectively inhibit the growth of the metastable polymorph B, resulting in a relative increase of the growth rate of stable form A. In this case the formation of form A is promoted over that of form B. However, it is noted that other mechanisms are possible as well, for instance the pre-exponential factor A in the nucleation rate equation (5.1) may be different for the two polymorphs due to different values of the impingement factor.

5.7 Conclusions

During anti-solvent crystallization of L-Histidine from aqueous solution with ethanol as anti-solvent the polymorphic fraction of the metastable polymorph B increased with increasing supersaturation ratio. For $S_A \geq 2.3$ only polymorph B was observed while for $S_A \leq 2.0$ a mixture of metastable polymorph B and stable polymorph A was obtained. The polymorphic fraction of the crystals was measured by Raman-spectroscopy using a method for quantitative analysis that was newly developed for this compound.

Rate-equations for heterogeneous nucleation and polynuclear growth were introduced in a process simulation model of the batch anti-solvent crystallization of L-His. When the classical nucleation theory was applied with the apparent interfacial energy derived from solubility data, the formation of the stable polymorph A was erroneously predicted. The predicted polymorphic fraction changed when the relative interfacial energy and step free energy in the nucleation and growth rate equations were modified. The modification of the relative growth rates seemed the most effective way to approach the observed polymorphic fraction.

Experimental induction times were one to several orders of magnitude smaller than the transformation times. This is a strong indication that directly after mixing both polymorphs nucleated and grew simultaneously.

Measurements of the L-His solubility versus ethanol volume fraction were used to estimate the change in supersaturation ratio for both polymorphs. The calculated activity coefficient for L-His was found to be approximately equal for both actual and equilibrium conditions, allowing the use of the concentration based supersaturation ratio.

5.8 Acknowledgements

The authors thank Akzo Nobel, BASF, Bayer and DSM for their support to this project. Furthermore, the COSMOTHERM calculations performed by dr R.M. Geertman were highly appreciated.

5.9 References

Beckmann, W., J. Cryst. Growth 198/199 (1999) 1307

Bermingham, S., A design procedure and predictive models for solution crystallization processes, PhD thesis, Delft University of Technology (2002)

Eckert F.; A. Klamt, AIChE J. 48 (2002) 369
Kashchiev, D., Nucleation, basic theory with applications, Butterworth, Oxford, (2001)
Klamt, A.; F. Eckert, COSMOtherm, Version C2.1, Release 0104, COSMOlogic GmbH and Co. GG., Leverkusen, Germany (2004)
Kitamura, M., J. Chem. Eng. Japan, 26 (1993) 303
Kitamura, M.; H. Furukawa, M. Asaeda, J. Cryst. Growth 141 (1994) 193
Kitamura, M.; S. Ueno, K. Sato, in Crystallization processes, H. Ohtaki (editor), Wiley, Chichester (1998)
Madden, J.J.; E.L. McGandy, N.C. Seeman, Acta Cryst. B28 (1972) 2377
Madden, J.J.; E.L. McGandy, N.C. Seeman, Acta Cryst. B28 (1972) 2382
Mersmann, A., J. Cryst. Growth 102 (1990) 841
Mersmann, A., Crystallization Technology Handbook 2nd ed., Marcel Dekker, New York (2001)
Ono, T.; H.J.M. Kramer, J.H. ter Horst, P.J. Jansens, Cryst. Growth Des. 4 (2004) 1161
Toth, J; A. Kardos-Fodor, S. Halasz-Peterfi, Chem. Eng. Processing 44 (2004) 193

Chapter 6

The precipitation of both stable and metastable polymorphs of L-Glutamic Acid as a function of supersaturation and of agitation

Results partially published in J. Cryst. Growth 275 (2005) e1389-e1395

Polymorphs are of considerable interest to industry because they have different properties, for example, solubility and hence bioavailability for pharmaceuticals. Control over the formation of polymorphs during production is desired and starts with control over nucleation of the desired crystal form. This is especially the case for precipitation processes that are characterised by large variation in the spatial and temporal distribution of supersaturation and hence of the nucleation rate.

The precipitation of model compound L-Glutamic acid was performed using a pre-mixer to create instantaneously a homogeneous supersaturation from aqueous solutions of Sodium L-Glutamate and diluted Sulphuric Acid. Samples of the supersaturated pre-mixed solution were either subjected to vigorous post-stirring or left under quiescent conditions. For low supersaturation ($S \leq 13$), without post-stirring clustered platelet-shaped crystals of the stable beta polymorph were formed while with post-stirring large prismatic crystals of the metastable alpha polymorph were obtained. For high supersaturation ($S \geq 17$) the formation of rough spherulitic crystals of the beta phase was preceded by smooth spheres.

For high supersaturation it is proposed that the spheres are in fact a metastable phase that consists of droplets formed by liquid-liquid separation. Subsequently from these spheres crystals of the more stable beta phase nucleate by a heterogeneous mechanism. For low supersaturation, without post-stirring clustered platelets of the stable beta phase are formed according to the same mechanism, while during

post-stirring the metastable alpha phase nucleates, possibly from the stirre surface by a heterogeneous mechanism.

6.1 Introduction

Polymorphism is of great interest to industry because polymorphs have different physical properties, e.g. the solubility of pharmaceuticals. Control of the formation of the different polymorphic structures during production is desired, especially in the case of concomitant polymorphs. The relative stability of the polymorphs is defined by thermodynamics but the structure that will actually form, depends also on the kinetics, i.e. competitive nucleation and growth rates. In precipitation the supersaturation is high and therefore formation of a metastable phase is likely to occur, followed by transformation into a more stable phase.

L-Glutamic acid (L-Glu) was chosen because it is a relatively well-studied model compound that has two polymorphs with contrasting morphologies, the metastable alpha form having a rather compact prismatic shape and the stable beta form producing elongated plate-like crystallites. Both polymorphs crystallize in the orthorhombic space group $P2_12_12_1$ structure with $Z=4$ molecules in the unit cell but with different axis lengths (Hirokawa 1955, Lehmann et al 1972, Bernstein 1991). In the crystal lattices the L-Glu molecules are in the zwitter-ionic form and adopt different conformations with different torsion angles (Kitamura 1998). Kitamura (2002) measured a 20% higher solubility of the metastable alpha form compared to that of the stable beta form. Ishizu and Kitamura (2000) measured the growth rates of single crystals of both polymorphs from continuously flowing aqueous solution. With increasing (but still low) supersaturation the growth rate of the metastable alpha phase increased more compared to that of the stable beta phase while in both cases a birth-and-spread growth mechanism was indicated.

When cooling crystallization is applied in a stirred crystallizer, generally first the metastable alpha phase forms that subsequently transforms to the stable beta phase, according to Ostwald's rule of stages, as was described by Kitamura (1989), Garti and Zour (1997), Ferrari and Davey (2004) and Ono (2004). Kitamura observed that without agitation and for low supersaturation the stable beta phase formed directly. Liang et al (2004) found evidence that during cooling crystallization the rough surface of the stirrer acted as the main source of nuclei by a heterogeneous nucleation mechanism but the polymorphic form was not reported. Both Kitamura (1989) and Ono (2004) found that the transformation rate of the alpha form to the beta form increased with

crystallization temperature. Hiramatsu (1977), Sugita (1988), Kitamura and Funahara (1994), Garti and Zour (1997), Davey et al (1997) and Cashell (2005) reported the inhibition of the transformation by the use of additives.

Furthermore, nucleation of beta phase needles on the surface of the alpha phase prisms was observed by Ferrari and Davey (2004) and by Cashell (2003a and 2003b). Ferrari and Davey (2004) assumed that increased attrition of the metastable alpha polymorph due to intensified mixing would result in more surface area available for nucleation of the stable beta polymorph. Interestingly, the opposite was found by Cashell (2004): stirring a suspension of metastable alpha crystals would inhibit the transformation process. Disruption of the alpha surfaces was believed to prevent nucleation of the beta phase.

In cooling crystallization the maximum driving force that can be created is limited by the solubility of L-Glutamic acid in water. The starting point of nucleation during cooling from 80°C to the desired end temperature (usually between 25 and 45°C) is ill-defined. The formation of L-Glutamic acid by pH-shift precipitation from a solution of Sodium L-Glutamate and diluted acid may have the advantage of a well-defined high initial supersaturation, provided the solutions are instantaneously mixed.

Industrially L-Glutamic acid is generally produced by fermentation. When the broth is acidified precipitation of prismatic alpha crystals is preferred because these are easier to filter compared to the beta crystals (Sugita 1988). For the pH-shift precipitation with agitation Sugita observed a decrease in the purity of alpha crystals from 98 tot 92% by increasing the concentration of the Na-L-Glutamate solution from 0.3 to 0.4 M. Garti and Zour (1997) reported that pure alpha crystals were obtained from a Na-L-Glutamate solution of 0.6 M with Hydrochloric acid. Following this procedure Cashell (2003b) observed beta-phase crystals inside alpha crystals. It was concluded that beta crystals had nucleated in an earlier stage from the surface of alpha crystals and that these were later overgrown by the faster growing alpha crystals. Borissova et al (2005) obtained alpha crystals in a stirred crystallizer when a solution of Sodium L-Glutamate was slowly (>1hr) acidified using concentrated Hydrochloric acid.

Quayle (2002) investigated the precipitation in a stopped-flow cell without further agitation using Synchrotron X-ray diffraction. A mixture of alpha and beta crystals of L-Glutamic acid precipitated when an aqueous solution of 1.8 M Sodium L-Glutamate was mixed with 99.7% Acetic Acid in a 1:1 ratio.

The objective of this work is to study the pH-shift precipitation of the polymorphs of L-Glutamic acid as a function of high supersaturation. The formation of L-Glutamic acid seems to depend on the initial concentration but experimental conditions like agitation may as well play a role and they have to be taken into account.

6.2 Nucleation theory

In this study the classical nucleation theory (CNT) was followed as described and adapted by Kashchiev (1999). Solute molecules collide with each other at a certain frequency due to Brownian motion. After the creation of a driving force for precipitation, these collisions lead with certain efficiency to the formation of clusters of solute molecules. This is a dynamic process and molecules will attach and detach successively. The driving force for the creation of clusters is the decrease in chemical potential by molecules leaving the solution while forming a cluster due to the decrease in Gibbs free energy between the two bulk phases. However, a penalty has to be paid for creating an interface between the cluster and its surrounding solution.

The work of formation of an n-sized cluster W [J] can be approximated by:

$$W(n) = -nkTlnS + \gamma A_c(n) \tag{6.1}$$

with interfacial energy γ [J m^{-2}] and cluster surface area $A_c(n)$ [m^2]. The work of formation of a cluster will at first increase with increasing number of molecules until a maximum is reached. At this point the flux of solute molecules attaching to the cluster f^* equals the flux of molecules detaching from the cluster g^*. Up from this size, the cluster size will increase with every molecule that attaches and the work of formation will decrease with n. The cluster with the maximum work of formation also called nucleation work W^* is called the nucleus n^*.

For spherical clusters the surface area $A_c(n)=(36\pi v_0^2)^{1/3}n^{2/3}$ with $v_0=M/\rho_c N_a$ [m^3] the molecular volume with M [kg mol^{-1}] molecular weight, ρ_c [kg m^{-3}] crystal density and N_a [mol^{-1}] Avogadro's number. The interfacial energy γ [J m^{-2}] is a weighed average over all crystal faces. Mersmann (1990) derived the following relationship between the interfacial energy and the natural logarithm of the bulk solubility of the compound c_e [mol m^{-3}]:

$$\gamma = \beta kT \frac{1}{v_0^{2/3}} \ln \frac{1}{v_0 c_e} \tag{6.2}$$

For spherical clusters the shape factor β=0.514.

For spheres the nucleus size n^* and the nucleation work W^* can be derived from the condition $dW/dn=0$ for $n=n^*$ using equation (6.1):

$$n^* = \frac{32\pi v_0^{\,2}\gamma^3}{3(kT)^3 \ln^3 S} \qquad (6.3)$$

$$W^* = \frac{16\pi v_0^{\,2}\gamma^3}{3(kT)^2 \ln^2 S} = \tfrac{1}{2} n^* kT \ln S$$

The nucleus size and the nucleation work depend on two main parameters: the externally controlled supersaturation and the interfacial energy that is controlled by crystal-solution interaction.

6.3 Experimental procedure

In this study an aqueous solution of Sodium L-Glutamate was mixed with diluted Sulphuric acid. First L-Glutamic acid is formed in solution by the fast shift in the speciation equilibrium followed by relatively slow precipitation:

Na-L-Glu.H_2O (aq)+½ H_2SO_4 (aq) ⇔
H-L-Glu (aq)+½ Na_2SO_4 (aq) ⇔
H-L-Glu (s)+½ Na_2SO_4 (aq)

Solutions were prepared from Sodium L-Glutamate monohydrate (Orsan-Ajinomoto), from Sulphuric acid (Baker) and from ultra pure water made by reverse osmosis. The solutions were filtered over a 0.22 μm filter when they were introduced in the set-up. In our work the actual concentration after mixing the flows varied from c_0=0.25, 0.375, 0.5, 0.75, 1.0 tot 1.25 molal with corresponding supersaturation ratio S=4, 6, 8, 13, 17 to 22. Most experiments were carried out in duplo except for the experiments at S=8 and 22. All experiments were carried out at room temperature.

The solutions were pre-mixed in a set-up that was built to achieve complete mixing within milliseconds in order to create instantaneously a high supersaturation (Roelands 2003, 2004). The two flows pre-mixed in a Y-shaped mixing-tee with a static mixer inserted in the outflow tube. After the system had reached steady state samples of about 100 ml of the mixture were collected at the end of the tube in a beaker. The samples were treated in two ways: either the beaker was covered with

foil and left without agitation or a magnetic stirrer or an overhead impeller was used for post-stirring. In figure 6.1 the experimental set-up is schematically depicted.

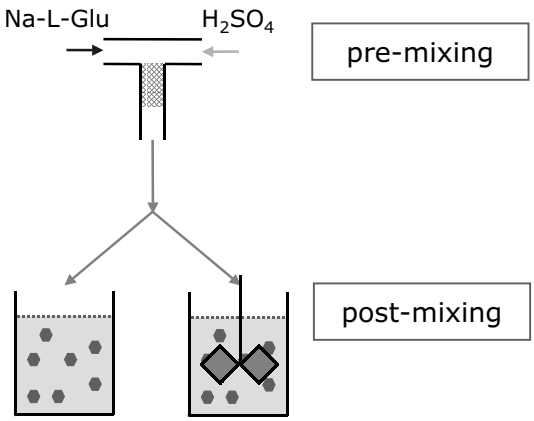

Figure 6.1 Schematic depiction of the experimental set-up.

Suspensions were filtered to collect the crystals and washed with ultra pure water. Raman spectra of the filtered wet cake were acquired using a Kaiser instrument for dispersive Raman with a 732 nm laser. For each cake three different samples were measured. The percentage of each polymorph present in the samples was determined using a method for quantitative analysis (Ono 2004). Furthermore, microscopic images of the crystals in the suspension were obtained and some samples were dried for scanning electron microscopy (SEM), focussed ion beam (FIB) imaging (Hodnett 2005) and powder diffraction (pXRD).

A suspension of alpha crystals made by pH-shift precipitation with post-stirring was kept overnight while being stirred in order to follow the transformation of the alpha crystals to beta crystals by a solution mediated mechanism.

6.4 Results precipitation experiments

L-Glutamic acid was precipitated from a solution at a supersaturation ratio of S=4, 6, 8, 13, 17 and 22. The flow that left the tube of the pre-mixing device was visibly clear. The induction time to observe crystals in the beaker decreased with increasing supersaturation. In the non-agitated samples crystals could be observed first at the bottom of the beaker. The induction time period varied from a few seconds for S=22 to 2 hours for S=4. It also depended on sample post-stirring: samples

agitated with the magnetic stirrer became turbid first, next the sample agitated with the overhead impeller. Even for low supersaturation, with post-stirring the solutions became turbid within minutes.

In figure 6.2 the fraction of the alpha polymorph in the wet filter cake of the precipitate is shown as function of supersaturation ratio. Furthermore, it is shown whether or not the mixture was post-mixed. Without post-stirring always the beta form was observed. With post-stirring for $S \leq 13$ the alpha form was obtained, while for $S \geq 17$ predominantly the beta form was obtained for both agitated and non-agitated mixtures.

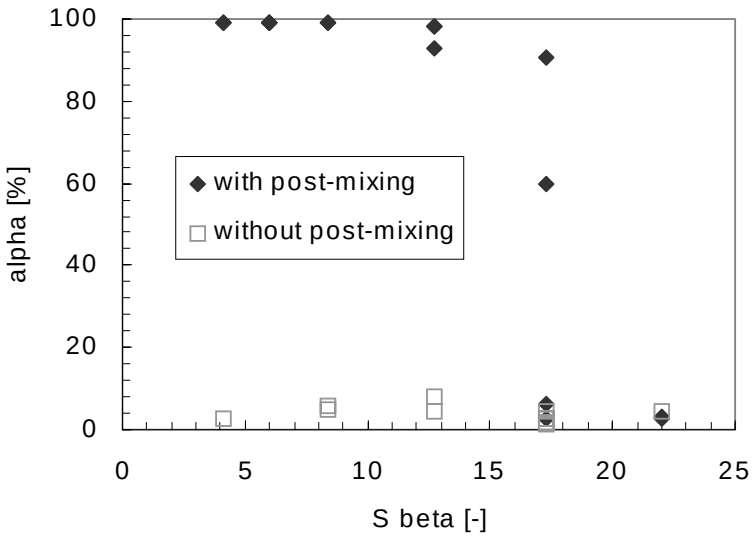

Figure 6.2 Alpha polymorph fraction in the wet filter cake as a function of supersaturation S and of post-stirring conditions. Quantitative analysis based on Raman measurements.

To illustrate the effect of post-stirring of the polymorphic form that was obtained microscopic and SEM images of the samples are shown in figure 6.3 for increasing supersaturation $S=6$, 13 and 17. For low supersaturation $S=6$ and 13 with post-stirring only prismatic alpha crystals were obtained while without post-stirring only clustered beta platelets could be observed (figures 6.3a and 6.3b). For high supersaturation $S=17$ both with and without post-stirring beta spherulites were observed, while with post-stirring also a number of alpha prisms was found (figure 6.3c).

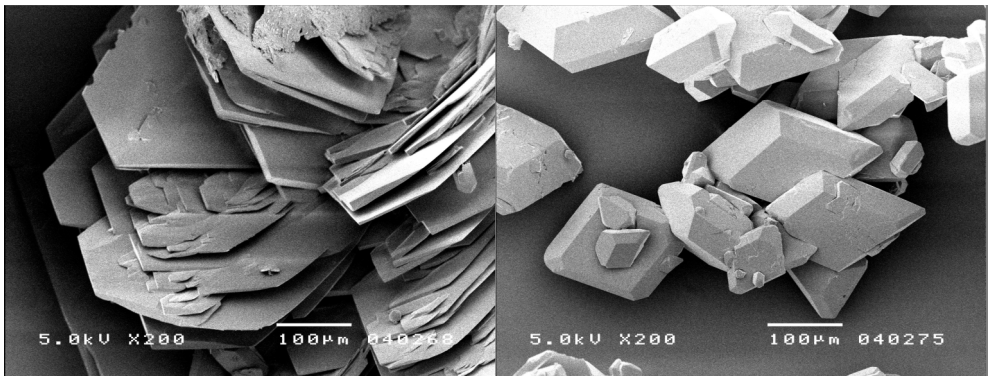

Figure 6.3a SEM images of L-Glutamic acid crystals precipitated at S=6. Left: without post-stirring, beta platelets. Right: without post-stirring, alpha prisms.

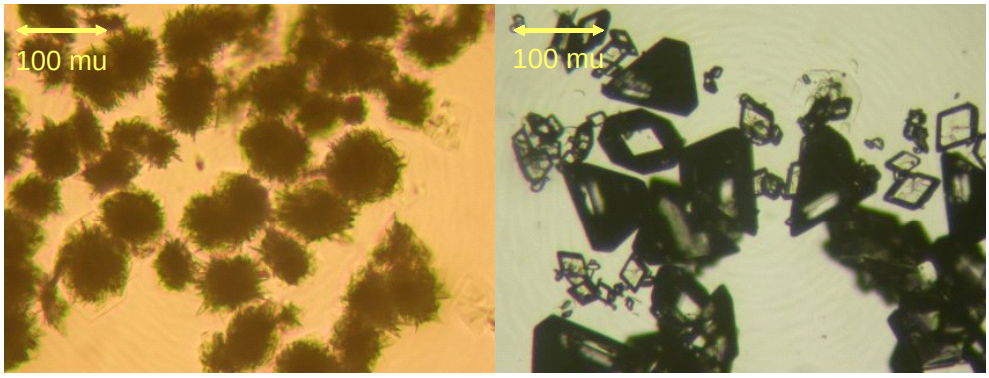

Figure 6.3b Microscopic images of L-Glutamic acid crystals precipitated at S=13. Left: without post-stirring, beta platelets. Right: without post-stirring, alpha prisms.

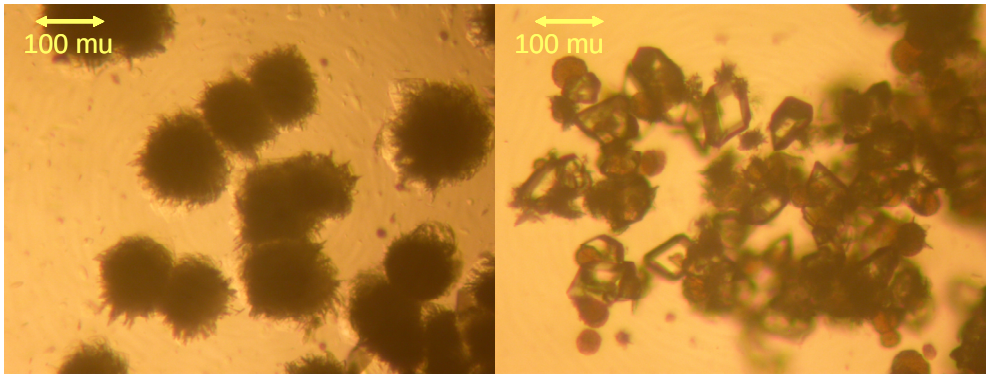

Figure 6.3c Microscopic images of L-Glutamic acid crystals precipitated at S=17. Left: without post-stirring, beta spherulites. Right: without post-stirring, beta spherulites and alpha prisms.

For the beta crystals obtained without post-stirring it was found that with increasing supersaturation ratio S=6, 13, 17 and 22 the mean size of the platelets decreased while the clusters turned into a more

spherulitic shape. A detailed SEM image of a spherulite obtained without post-stirring for high supersaturation S=22 is shown in figure 6.4. The surface of the spherulitic crystal consists solely of small beta platelets.

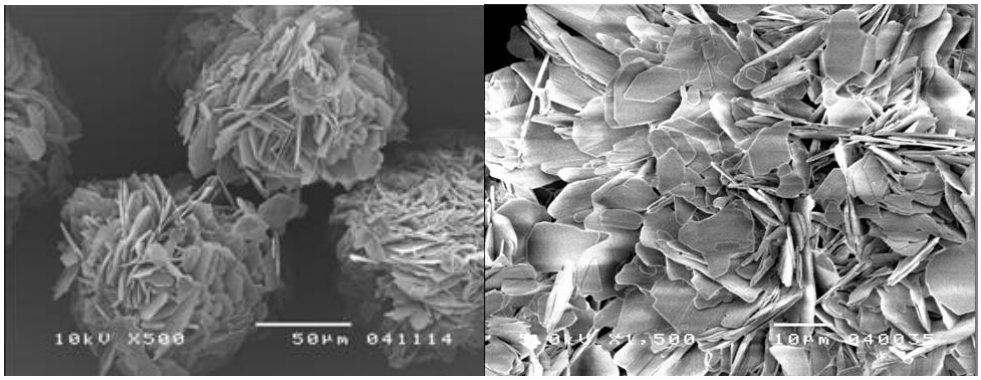

Figure 6.4 SEM images of details of L-Glutamic acid crystal precipitated at S=22.

To explain these findings additional measurements were carried out. The spherulites obtained at high supersaturation were examined in detail. In figure 6.5 microscopic images are shown of a sample taken from a beaker without post-stirring at high S=17. The first image was made within seconds after pre-mixing while the second image was obtained approximately one minute later. On the first image smooth spheres can be observed while on the second image the previously shown rough spherulites are visible.

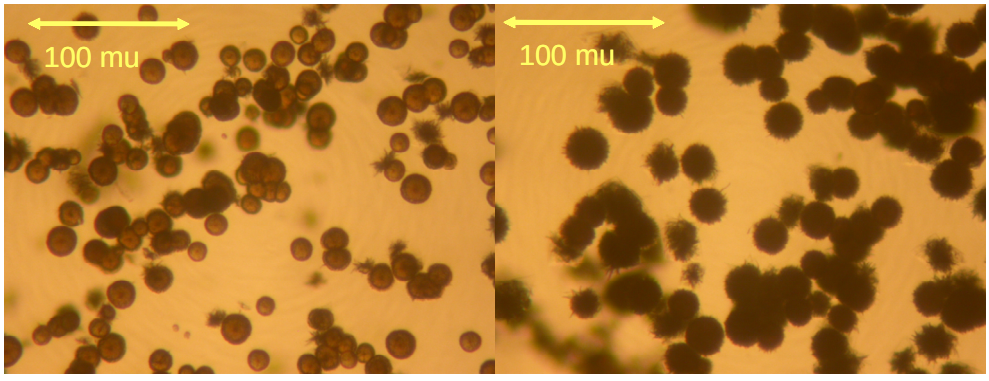

Figure 6.5 Microscopic images of L-Glutamic acid crystals precipitated at S=17 without spherulites. Left: spheres. Right: beta spherulites.

Unfortunately the lifetime of the smooth spheres was short, usually smaller than a minute, and it was not possible to isolate them by filtration due to crystallization on the filter of the beta form. To study the internal structure of the spherulitic crystals, dried samples were further analysed using FIB and pXRD. It was investigated whether the structure of the spheres could be maintained inside these spherulites. In

figure 6.6 the powder diffractogram of a spherulitic crystal sample is shown obtained for S=17 without post-stirring. The sample consisted completely of the stable beta phase, with no indication of peak broadening due to the presence of an amorphous phase inside the spherulites. Furthermore, characteristic peaks can be observed of Sodium Sulphate, crystallized from adhering solution during drying.

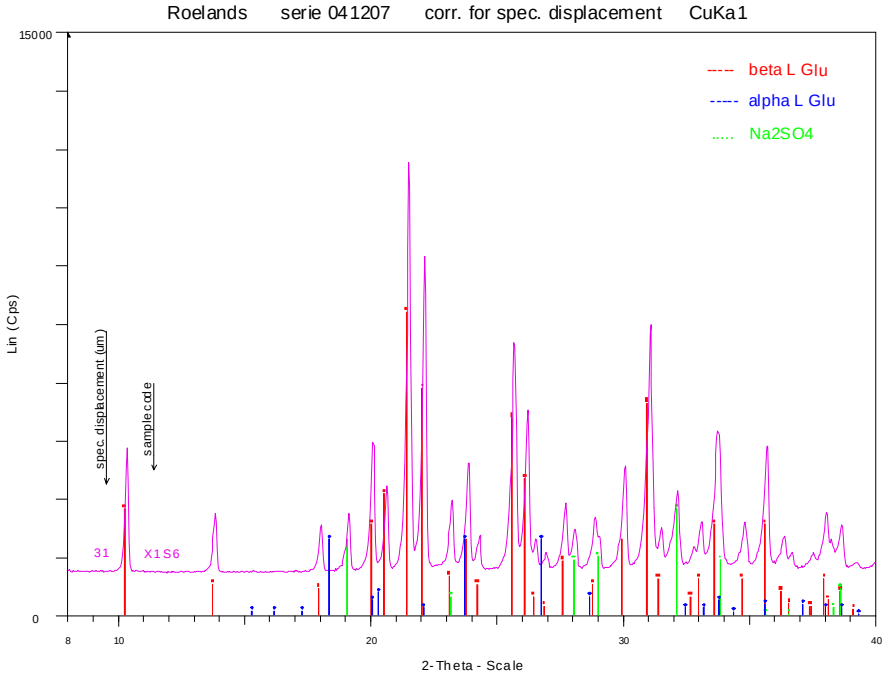

Figure 6.6 Powder diffractogram of L-Glutamic acid crystals precipitated at S=17 for spherulites obtained without post-stirring.

Using FIB single spherulitic crystals were examined. Half of the crystal was cut away to gain access to the interior. In figure 6.7 images are shown of the crystal before and after cutting. The structure inside the crystal is difficult to discern but seems to be homogeneous. The platelets at the exterior appear to be radially oriented, indicating that the spherulites were not formed by random agglomeration.

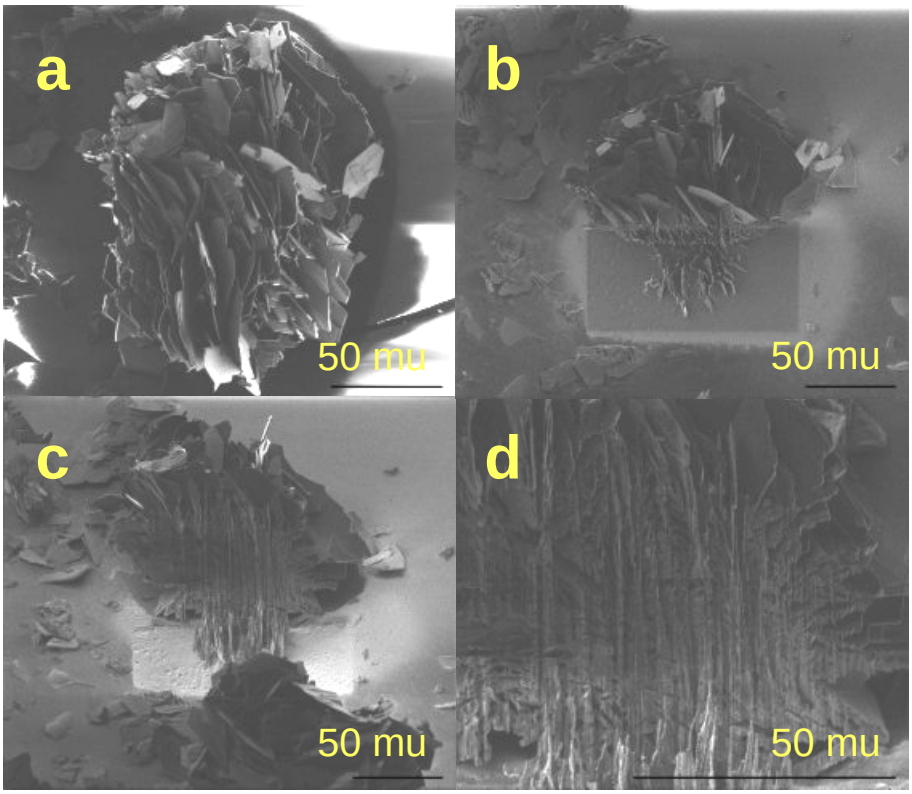

Figure 6.7a-d FIB images of a spherulitic L-Glutamic acid crystal precipitated at S=17, (a) before cutting, (b) after cutting, (c) tilted, (d) in detail.

In another experiment the two reactant solutions were poured directly in a stirred crystallizer so pre-mixing and post-stirring were not separated. In figure 6.8 a series microscopic images are shown of a sample taken within seconds after the solution in the crystallizer became turbid. Under the microscope, under stagnant conditions, spheres, spherulites and prisms can be observed to co-exist and to grow simultaneously for S=17 without transformation taking place. The time period between the images is in the order of seconds. This is an indication that without post-stirring growth of spheres and both crystal forms of L-Glu is not limited by transport by diffusion.

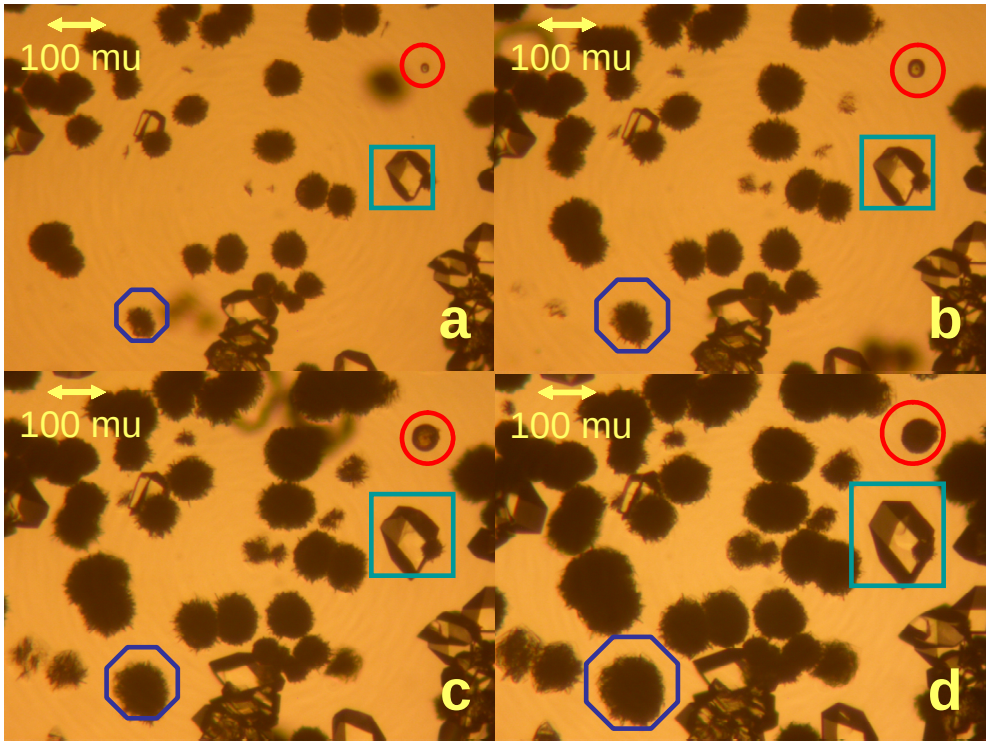

Figure 6.8 Time series of microscopic images of growing L-Glutamic acid crystals precipitated at S=17. Framed particles: sphere (circle), alpha prism (square), beta spherulite (octagon).

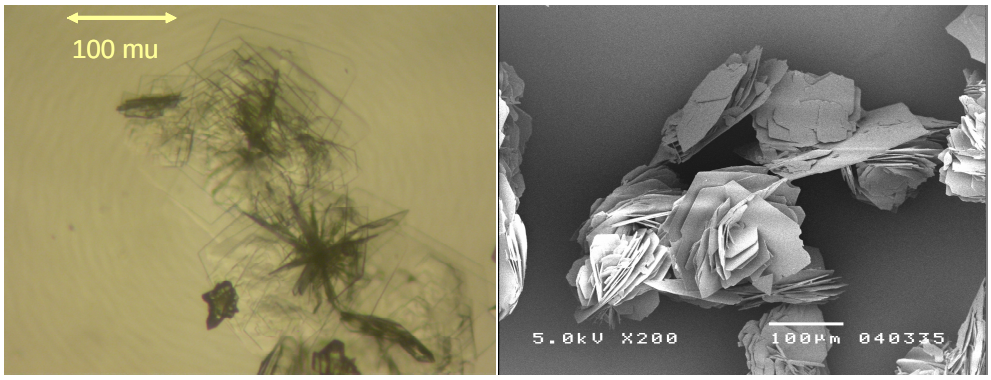

Figure 6.9 Left: microscopic image of clustered beta platelets of L-Glutamic acid precipitated at S=6. Right: image clustered beta platelets of L-Glutamic acid precipitated at S=8.

Furthermore, some images are shown of samples that were precipitated for low supersaturation S=6 and 8. Figure 6.9 shows microscopic and SEM images of clusters of beta platelets obtained by precipitation without post-stirring. It can be observed that the centered platelets are

very similar to the spherulites shown before, although the number of platelets is smaller and the size of the platelets is larger for the crystals obtained for low supersaturation. This is an indication that the beta platelets and spherulites that are obtained without post-stirring for both low and high supersaturation are formed according to the same mechanism.

For comparison, the microscopic image in figure 6.10 shows more needle-like beta crystals obtained by solution mediated transformation from prismatic alpha crystals in a stirred crystallizer over 24 hours. In this figure the prismatic alpha crystals can be observed as well. The shape of the needle-like beta crystals obtained by slow recrystallization differs significantly from the shape of the clustered beta platelets obtained by precipitation. This indicated that the beta platelets were not obtained by recrystallization from alpha prisms.

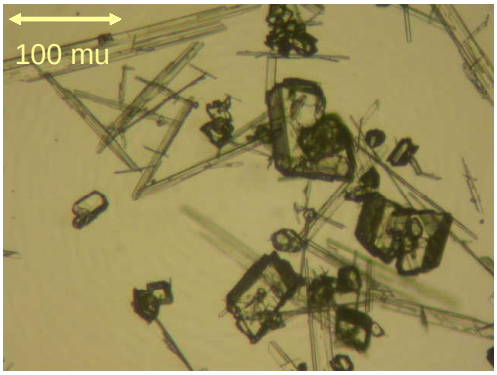

Figure 6.10 Microscopic image of needle-like beta crystals and of prismatic alpha crystals of L-Glutamic acid during transformation in solution.

In figure 6.11 the effect of post-stirring is shown on the alpha prisms for low supersaturation $S=6$ for samples taken from the suspension at $t=3$ and 17 minutes. With increasing residence time the mean size of the alpha prisms seems to increase while at the same time especially the larger prisms (>100 μm) become damaged at the corners, probably by attrition. The formation appeared to be faster when a magnetic stirrer was used compared to the use of steel or Teflon-lined overhead stirrers.

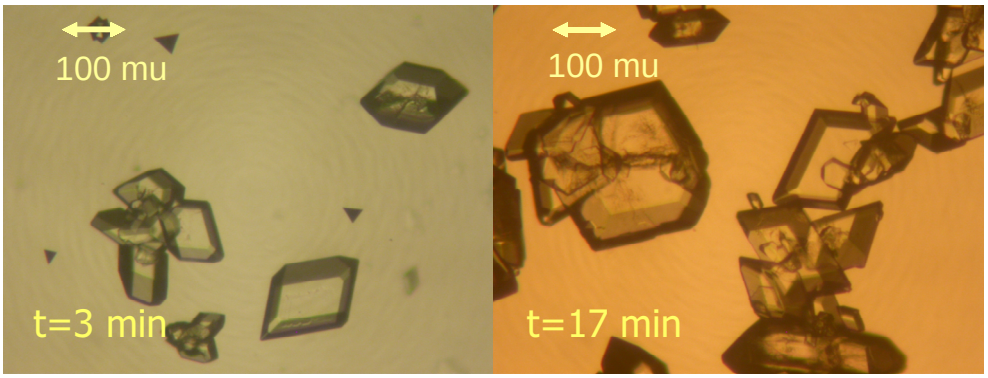

Figure 6.11 Microscopic image of prismatic alpha crystals of L-Glutamic acid for samples taken at t=3 min (left) and t=17 min (right) from stirred suspension.

6.5 Postulation of a formation mechanism

The experimental formation of the metastable alpha phase and of the stable beta phase of L-Glu can be divided between high ($S \geq 17$) and low ($S \leq 13$) supersaturation. A mechanism will be proposed to explain the experimental results as a function of supersaturation and of post-stirring.

For the experiments carried out for high supersaturation ($S \geq 17$) the observations can be summarized as follows:

a. Without post-stirring:
- Spherulites consisting of many small beta platelets are formed within seconds.
- Spheres are preceding the spherulites, spheres could not be isolated.
- pXRD: spherulites pure beta form, no amorphous phase.
- FIB: platelets at exterior spherulite are radially oriented, spherulites are not agglomerates.

b. With post-stirring:
- Many spherulites, also few alpha prisms.

c. Quiescent sample taken from a stirred crystallizer:
- Spheres, spherulites and prisms grow simultaneously.

From these observations it is proposed that the observed spheres consist of a metastable, short-living L-Glu rich phase created by a liquid-liquid separation. It is further proposed that crystals of the stable beta phase of L-Glu nucleate from the spheres by a heterogeneous nucleation mechanism and subsequently grow into spherulites while consuming the remaining supersaturation. The observations by FIB and pXRD of the spherulites and the impossibility to isolate the spheres by filtration

suggest that the spheres do not consist of a solid, possibly amorphous, phase.

The liquid-liquid separation occurs after supersaturation is created by instantaneous pre-mixing. The two liquid phases are assumed to be thermodynamically metastable with respect to the formation of a crystalline phase from the supersaturated solution but their formation may be kinetically favoured. The liquid phases, one rich in solute and one poor, co-exist in equilibrium with each other, so the chemical potential and hence the supersaturation of the solute would be equal in each phase. From the droplets the stable beta phase nucleates, either from the bulk or at the interface between droplet and surrounding solution. In figure 6.12 the possible mechanism is depicted schematically.

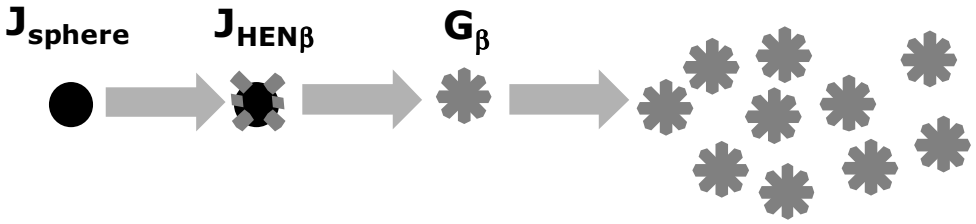

Figure 6.12 Schematic depiction of the possible precipitation mechanism for high supersaturation ($S \geq 17$).

For the experiments carried out for low supersaturation ($S \leq 13$) the observations can be summarized as follows:

a. Without post-stirring:
- Clustered beta platelets are formed within minutes (slow).
- Centered platelets resemble spherulites obtained for high S.
- Shape distinctively different form needle-like crystals obtained by transformation.

b. With post-stirring:
- Alpha prisms are formed within seconds (fast).
- Prisms grow within minutes to size >50 μm, attrition takes place.
- Prisms form independent of mixer type, magnetic stirrer or overhead impeller.

From the observations without post-stirring it is concluded that the formation of the clustered and centered beta platelets takes place according to the same mechanism as was observed for high supersaturation: beta crystals nucleate heterogeneously from metastable droplets. Because of the lower supersaturation the number

of droplets is small and their size remains small as well so these are not visible.

It is proposed that with post-stirring the metastable alpha phase nucleates directly from the mixed solution, probably favoured by the stirrer surface due to a heterogeneous mechanism. High shear rates around the stirrer blades and collisions between magnetic stirrer and crystallizer bottom may favour fragmentation and dispersion of alpha crystals within the bulk of the solution. When the alpha crystals have grown to a sufficiently large size to become subject to attrition (>50 μm), this mechanism may additionally contribute to the formation of the alpha phase. In figure 6.13 the possible mechanism is depicted schematically.

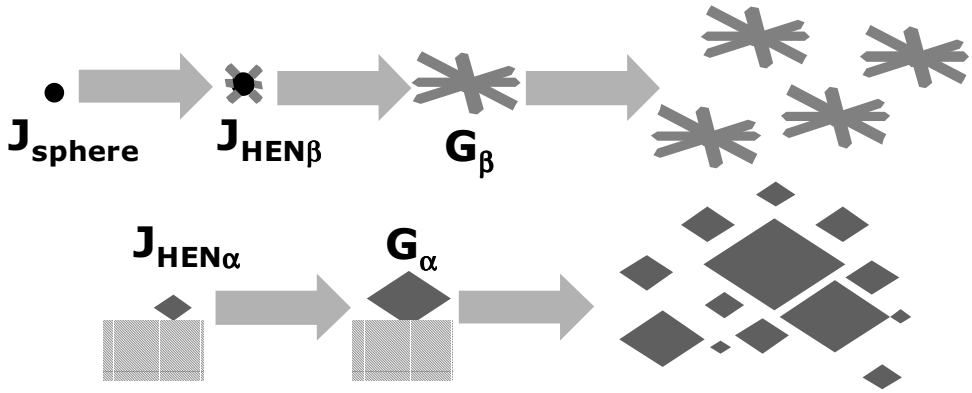

Figure 6.13 Schematic depiction of the possible precipitation mechanism for low supersaturation (S≤13), without post-stirring (top) and with post-stirring (bottom).

6.6 Discussion

Precipitation processes are generally taking place at high supersaturation levels and the occurrence of metastable phases that are sometimes amorphous is commonly observed. Subsequently metastable phases often recrystallize into more stable crystalline phases by a solution-mediated mechanism. Some examples of ionic compounds able to form both amorphous and crystalline phases are Calcium Carbonate (Sawada 1999), Calcium Phosphate (Brecevic 1987) and Alumina (Sato 1984). The number of publications on the formation of amorphous phases of molecular compounds from solution is surprisingly small. Stagner and Guillory (1979) reported the preparation of an amorphous form of Iopanoic Acid by precipitation from an aqueous solution of Sodium Iopanate with diluted acid.

Furthermore, the occurrence of a liquid-liquid separation (oiling-out) resulting in the formation of droplets of a solute-rich phase in a dispersed solute-poor phase was reported for both large molecules (Galkin and Vekilov 2000, Vekilov 2004 and Drenth 1999, 2005) and relatively small molecules (Lafferrère et al 2003, 2004a, 2004b, Bonnett 2003, Kim 2003, Grön 2001 and Chattopadyay and Myerson 2005). These phases are thermodynamically metastable compared to the formation of a solid phase from solution. This phenomenon took generally place in highly supersaturated solutions while for small molecules these solutions were concentrated as well.

The concentration of the solutions used in the experiments described in this work varied from approximately 5-20 wt% for L-Glu with 2-7 wt% Sodium Sulphate. This relatively high concentration agrees well with the concentration ranges given in the studies on liquid-liquid separation supporting the proposed mechanism.

The possible relationship between the nucleation rate of the stable beta phase from the droplets and the nucleation rate of the metastable alpha phase under the influence of the stirrer is schematically plotted in figure 6.14 as a function of supersaturation. The nucleation rate of the beta phase increases with increasing supersaturation ratio, indifferent whether post-stirring is applied. With post-stirring alpha crystals nucleate faster for low supersaturation ratio and slower for high supersaturation ratio.

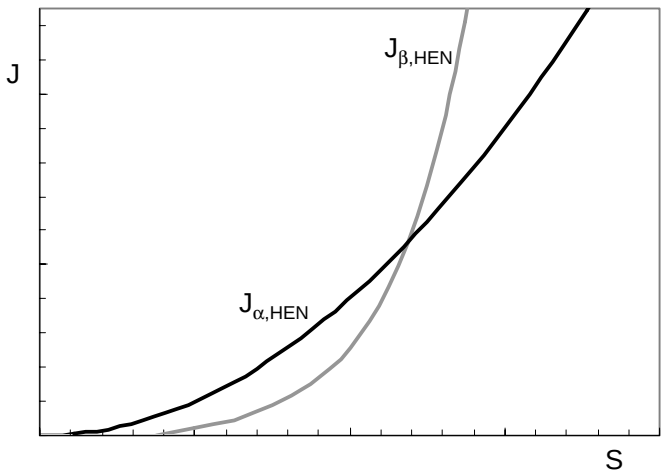

Figure 6.14 Schematic depiction of the relative nucleation rates as a function of supersaturation of the stable beta phase from droplets and of the metastable alpha phase during post-stirring.

At first sight, the experimental results on the pH-shift precipitation of L-Glutamic acid without post-stirring do not seem to follow Ostwald's rule of stages because the stable beta polymorph is directly precipitated and not the metastable alpha polymorph. The Ostwald rule of stages, however, is an observation rule and not a physical law. Furthermore, according to the proposed mechanism, the formation of the stable beta phase could be preceded by the formation of a less stable liquid phase. With post-stirring, Ostwald's rule is followed as well because the less stable alpha phase nucleates first. When a suspension of alpha crystals was kept overnight while being stirred, these prismatic crystals transformed to needle shaped crystals of the more stable beta phase.

The proposed relative stability of the phases according to the postulated mechanism is shown in figure 6.15 for low supersaturation (left) and for high supersaturation (right). Least stable is the supersaturated solution created by instantaneous mixing, followed by the two liquid phases obtained by the liquid-liquid separation, the metastable alpha phase and finally the stable beta phase.

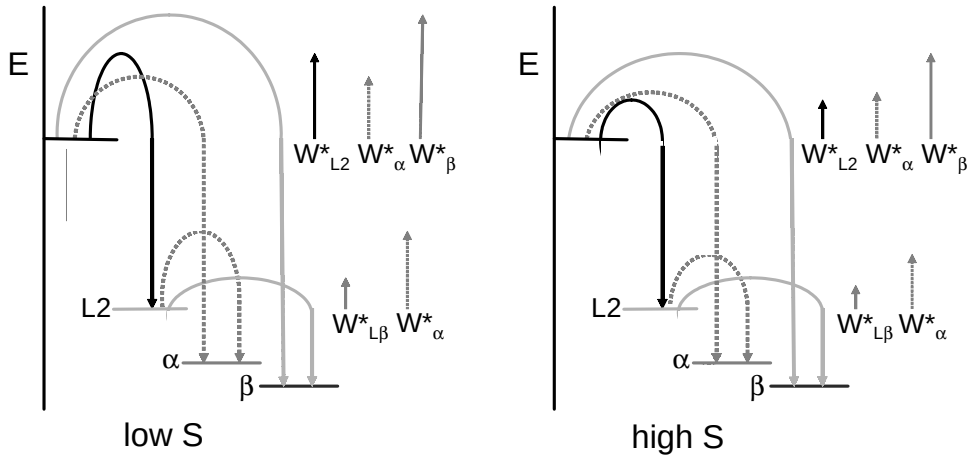

Figure 6.15 Schematic depiction of the relative stability and of the nucleation work of the different phases according to the postulated precipitation mechanism for low supersaturation (left) and for high supersaturation (right).

In this figure relative values of the nucleation work of the phases are presented as well. Bernstein et al (1999) suggested that the polymorphic phase that has the lowest nucleation work, is actually formed. For low supersaturation (left), starting from the supersaturated solution, the nucleation work of the droplets is higher than that of the

metastable alpha phase, but to nucleate the alpha crystals the presence of a stirrer is required. The stable beta phase does not nucleate directly from the supersaturated solution because of the higher nucleation work of this phase compared to that of both droplets and alpha phase. In the absence of a stirrer the liquid-liquid separation takes place. Next from the droplets the nucleation work for the stable beta phase is lower compared to that of the metastable alpha phase.

For high supersaturation (right) the nucleation work is lowered for all phases. From the supersaturated solution the nucleation work of the droplets is approximately the same as hat for the alpha phase in the presence of a stirrer. Without post-stirring only droplets can be observed while with post-stirring both droplets and alpha crystal are formed. From the droplets the nucleation work is lower for the stable beta phase again compared to that of the metastable alpha phase.

Finally, in figure 6.16 the phase diagram is shown. Three phases can be observed in equilibrium with the solution: a highly metastable liquid phase (denoted by c for the concentrated phase and d for the dispersed phase), the metastable crystalline alpha phase and the stable crystalline beta phase. It is noted that the solution contains apart from L-Glutamic acid also a considerable amount of sodium sulphate. In the case of precipitation without post-stirring, first a liquid-liquid-separation occurs, followed by a transformation of the droplets into the stable beta phase. In the case with post-stirring first the metastable alpha phase crystallizes, followed by a solution mediated transformation towards the stable beta phase.

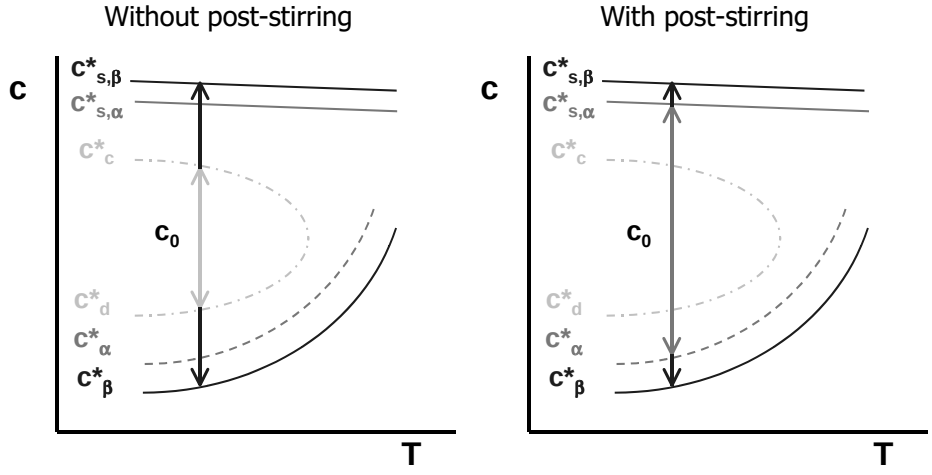

Figure 6.16 Schematic phase diagram for L-Glutamic acid for the case without post-stirring (left) and with post-stirring (right).

6.7 Conclusions

L-Glutamic Acid was precipitated from solutions of Sodium L-Glutamate and diluted Sulphuric acid that were continuously pre-mixed in a Y-mixer to create instantaneously a homogeneous supersaturation. Using this set-up the formation of the L-Glu crystals was studied as a function of increasing supersaturation ratio by increasing the concentrations in the reacting solutions. Samples of the pre-mixed supersaturated solution were collected in beakers that were either subjected to post-stirring or left under quiescent conditions.

For relatively low supersaturation ($S \leq 13$), with post-stirring prismatic crystals of the metastable alpha phase were formed while without post-stirring clustered platelets of the stable beta phase were obtained. The induction time in post-stirred samples was smaller, usually less than a minute, compared to up to one hour for non-agitated samples. For high supersaturation ($S \geq 17$), within seconds spherulites of the stable beta phase were observed both with and without post-stirring. With post-stirring apart from beta spherulites also alpha prisms were formed.

A mechanism was postulated to explain the formation of the polymorphs of L-Glu as a function of supersaturation and of agitation. It is proposed that a liquid-liquid separation can take place resulting in the formation of droplets of metastable phase, preceding nucleation of crystals of the stable beta phase from the droplets. Growth of the platelet-shaped beta crystals results in the formation of spherulites. For low supersaturation, without post-stirring the beta phase formed slowly according to the same mechanism, forming clustered platelets. With post-stirring prismatic crystals of the alpha phase nucleated directly, possibly by a heterogeneous mechanism from the stirrer surface. The fragmentation and dispersion of the alpha crystals in the solution may be facilitated by a high shear rate near the stirrer.

On microscopic images of samples taken at high supersaturation, smooth spheres were observed that over a time scale of seconds to minutes turned into rough spherulites. However, these spheres could not be isolated for analysis. Powder diffraction of the spherulites revealed that these consisted solely of the beta phase without any indication of peak broadening due to the presence of an amorphous phase. By analysis of a spherulitic crystal by focused ion beam it was observed that the beta platelets at the exterior had a radial orientation, indicating that the spherulites were not formed by agglomeration.

On microscopic images of a suspension sample from a stirred crystallizer spheres, alpha prisms and beta spherulites grew simultaneously without tranformation.

For the experiments carried out at low superaturation, the clustered and centered beta platelets that formed without post-stirring resembled the spherulites obtained for high supersaturation. The shape differed from needle-like crystals obtained by transformation. Large alpha prisms (>50 μm) that were obtained when post-stirring was applied became damaged due to attrition.

6.8 Acknowledgements

The authors thank Akzo Nobel, BASF, Bayer and DSM for their support to this project. Furthermore, the help of Serguei Belochapkine and Mitch Loan (FIB) of the University of Limerick, Niek van der Pers (pXRD), Paul Durville (SEM), Takuya Ono and Luo Lin was highly appreciated.

6.9 References

Bernstein J.; R.J. Davey, J.-O. Henck, Angew. Chem. Int. Ed. 38 (1999) 3440
Bonnett, P.E.; K.J. Carpenter, S. Dawson, R.J. Davey, Chem. Commun. (2003) 698
Brecevic, Lj.; V. Hlady, H. Füredi-Milhofer, Colloids and Surfaces 28 (1987) 301
Cardew, P.T.; R.J. Davey, Proc. R. Soc. Lond. A 398 (1985) 415
Cashell, C.; D. Corcoran, B.K. Hodnett, Chem. Comm. (2003) 374
Cashell, C.; D. Sutton, D. Corcoran, B.K. Hodnett, Cryst. Growth Des. 3 (2003) 869
Cashell, C.; D. Corcoran, B.K. Hodnett, J. Cryst. Growth 273 (2004) 258
Cashell, C.; D. Corcoran, B.K. Hodnett, Cryst. Growth Des. 5 (2005)
Chattopadhyay, S.; D. Erdemir, J.M.B. Evans, J. Ilavsky, H. Amenitsch, C.U. Segre, A.S. Myerson, Cryst. Growth Des. 5 (2005) 523
Davey, R.J.; N. Blagden, G.D. Potts, R. Docherty, J. Am. Chem. Soc 119 (1997) 1767
Drenth, J., Cryst. Growth Des., accepted for publication (2005)
Ferrari, E.S.; R.J. Davey, Cryst. Growth Des. 4 (2004) 1061
Garti, N.; H. Zour, J. Cryst. Growth 172 (1997) 486
Galkin, O.; P.G. Vekilov, J.Am. Chem. Soc. 122 (2000) 156
Grön, H.; K.J. Roberts, J. Phys. Chem. B 105 (2001) 10723
Haas, C.; J. Drenth, J. Cryst. Growth 196 (1999) 388
Hirokawa, S., Acta Cryst. 8 (1955) 637
Ishizu, T J.; M. Kitamura, J. Cryst Growth 209 (2000) 138

Kashchiev, D., Nucleation Basic Theory with Applications, Butterworth Oxford (1999)
Kim, S.; C. Wei, S. Kiang, Organic Process Research & Development 7 (2003) 997
Kitamura, M., J. Cryst. Growth 96 (1989) 541
Kitamura, M.; H. Funahara, J. Chem. Eng. Japan 27 (1994) 124
Kitamura, M.; S. Ueno, K. Sato, in Crystallization processes, H. Ohtaki (editor), Wiley, Chichester (1998)
Kitamura, M., J. Cryst. Growth 237-239 (2002) 2205
Lafferrère, L.; C. Hoff, S. Veesler, Eng. Life Sci. 3 (2003) 127
Lafferrère, L.; C. Hoff, S. Veesler, Cryst. Growth Des. 4 (2004a) 1175
Lafferrère, L.; C. Hoff, S. Veesler, J. Cryst. Growth, 269 (2004b) 550
Lehmann, M.S.; T.F. Koetzle, W.C. Hamilton, J. Cryst. Mol. Struct. 2 (1972) 225 (1972)
Liang, K.; G. White, D. Wilkinson, L.J. Ford, K.J. Roberts, Cryst. Growth Des. 4 (2004) 1039
Mersmann, A., J. Cryst. Growth 102 (1990) 841
Ono, T.; H.J.M. Kramer, J.H. ter Horst, P.J. Jansens, Cryst. Growth Des. 4 (2004) 1161
Quayle, M.J. et al, Phys. Chem. Chem. Phys. 4 (2002) 416
Sato, T., Ind. Crystallization 84 (1984) 385
Sawada, K., Mechanism of Crystal Growth of Ionic Crystals in Solution, Chapter 3 in Crystallization Processes, H. Ohtaki (ed.) Wiley, New York (1998)
Stagner, W.C.; J.K. Guillory, J. Pharm. Sci. 68 (1979) 1005
Sugita, Y., Agric. Biol. Chem. 52 (1988) 3081
Vekilov, P.G., Cryst. Growth Des. 4 (2004) 671

Dankwoord

De kiem voor mijn promotie-onderzoek werd gelegd toen ik in 1995/1996 mijn afstudeerwerk uitvoerde op het lab Apparatenbouw. Hier wisten Gerda van Rosmalen en Mantijn van Leeuwen bij mij een wetenschappelijk vlammetje te ontsteken. Dit vuurtje werd in de daaropvolgende jaren, toen ik voor Akzo Nobel werkte, aangewakkerd door mijn collega's, in het bijzonder door Rob Geertman en Jan Meijer. In 2000 hakte ik eindelijk de knoop door en van Peter Jansens, die toen net hoogleraar was geworden, kreeg ik het vertrouwen om een promotie-onderzoek op te starten. In de jaren daarna hielpen Peter, Joop, Herman en tot mijn grote vreugde af en toe ook Gerda het vuur brandend te houden. Bedankt voor de vonken!

Een goed vuur stoken doe je niet alleen. De afgelopen jaren heb ik het plezier en voorrecht gehad de volgende studenten tijdens het afstuderen te begeleiden: Shanfeng, Lorianne, Raoul, Aimee, Martijn, Tuong, Amir. Ik hoop dat ik bij jullie af en toe ook een vlammetje heb kunnen ontsteken.

De brandstof werd geleverd door de vaste staf van de afdeling: Paul, Michel, Gerard, Andre, Martijn, Stefan, Jan en Jan. Bedankt voor de brandstof! Bijzonder veel waardering heb ik voor het lassen en assembleren van de opstelling door Gerard en voor het maken van de vele SEM-foto's door Paul. Het thema van dit dankwoord is overigens ontleend aan de gezamenlijk gevolgde BHV-les van brandweerman Krijn.

Om het vuur gaande te houden, is zuurstof nodig. Enkele wetenschappers die geholpen hebben het vuur aan te blazen wil ik in het bijzonder noemen: Dimo Kashchiev, Donald Kirwan, Mitsutaka Kitamura, Jos Derksen, Marcelo Seckler, Dolf Bruinsma, Joachim Gross, Geert-Jan Witkamp en Hugo Meekes. Daarnaast wil ik de contactpersonen van de industriële partners Akzo Nobel, Bayer, Basf en DSM bedanken voor hun interesse en adviezen.

Wie een vuurtje stookt, geniet niet alleen van de vlammen, maar brandt zich ook wel eens. Gelukkig zat ik niet alleen op de blaren: Yohana, Gerrit, Marcel, Robert, Maaike, Gerard, Raymond, Cristiana, Abilash, Shanfeng, Christof, Crismono, Aris, Adreanne, Pieter, Dima, Perize, Elif, Daniela, Frans, Paolo, Takuya, Haruo, Kazu, Frank, Hubert, bedankt voor het bluswater!

Brandstof, zuurstof en een vonk moeten natuurlijk wel in een goede mengverhouding aanwezig zijn. Dit kan alleen wanneer er een goede work-life balance is. Om het evenwicht tijdens een promotie te behouden zijn er gelukkig familie en vrienden en niet in de laatste plaats kinderen: Ruben en Veerle. In het bijzonder mijn ouders, schoonouders, broer René en vriendin Roeby wil ik bedanken voor hun belangstelling. Prilly, dankjewel voor de mooie kaft van dit proefschrift!

Eén persoon ben ik in het bijzonder dankbaar: Marloes, jij bent altijd de grootste drijvende kracht voor me geweest!

About the author

Resume

Mark Roelands was born November 4th, 1970 in 's-Hertogenbosch. After completing secondary school (Gymnasium β) at the Jacob Roelands Lyceum in Boxtel he started studying Chemical Technology at the Delft University of Technology. In 1996 he received his degree after completing a graduation project on precipitation at the Laboratory for Process Equipment in the group of professor Gerda van Rosmalen.

After his graduation Mark Roelands worked for several years in the Process Technology Department of Akzo Nobel Chemicals Research in Arnhem. His main task was to give process support on industrial crystallization of soda ash, vacuum salt, sea salt and EDTA-products.

In 2000 he returned to the Laboratory for Process Equipment of the Delft University of Technology to start this PhD-project. During these years Mark and his wife Marloes became the proud parents of a son, Ruben, and a daughter, Veerle.

On May 1st, 2005 he joined the Separation Technology group of the Dutch Organization for Applied Scientific Research TNO in Apeldoorn applying his knowledge and experience on particle engineering, bio-separations and melt crystallization.

Papers

1. The unexpected formation of the stable beta phase of L-Glutamic Acid during pH-shift precipitation, Journal of Crystal Growth, 275 (2005) e1389-e1395.
2. Development of an experimental method to measure nucleation rates in reactive precipitation, Crystal Growth & Design, 4 (2004) 921-928.
3. An analysis of mixing in a typical experimental set-up to measure nucleation rates of precipitation processes, 2003, Chemical Engineering & Technology 26 (3), 296-302.
4. Pathways for polymorphism in precipitation processes, 2005, Proceedings of the 12th International Workshop on Industrial Crystallization (BIWIC12), September 2005, Halle, Germany.
5. Nucleation kinetics of polymorphic precipitation, 2001, Proceedings of the 8th International Workshop on Industrial Crystallization (BIWIC8), September 2001, Delft, Netherlands, 39-45.

Presentations

1. Pathways for polymorphism in precipitation processes, 2005, 12th International Workshop on Industrial Crystallization (BIWIC12), September 2005, Halle, Germany.
2. Nucleation in precipitation processes to achieve control over structure, shape and size distribution, 4th Netherlands Process Symposium (NPS4), October 2004, Veldhoven, Netherlands.
3. The unexpected formation of the stable beta phase of L-Glutamic Acid during pH-shift precipitation, 14th International Conference on Crystal Growth (ICCG14), August 2004, Grenoble, France.
4. Controlled mixing and reaction as a prerequisite for process intensification in precipitation, 3rd Netherlands Process Symposium (NPS3), October 2003, Veldhoven, Netherlands.
5. Nucleation rate measurements for reactive precipitation, 6th conference on Crystal Growth of Organic Materials (CGOM6), August 2003, Glasgow, Scotland.
6. Measurement of concomitant nucleation rates of polymorphs, 15th International Symposium on Industrial Crystallization (ISIC15), September 2002, Sorrento, Italy.
7. Polymorphism in precipitation, Crysopt thematic network, February 2001, Barcelona, Spain.